UNIVERSITÄT DUISBURG ESSEN

Open-Minded

From supramolecular networks to a pH-switchable Dendrimer as a potential Drug Carrier

Dissertation

zur Erlangung des akademischen Grades eines Doktors der Naturwissenschaft

- Dr. rer. nat. -

vorgelegt von Diplom Chemikerin

Julia Schulz

geboren in Wuppertal

Institut für Organische Chemie der Universität Duisburg-Essen

Essen 2017

From supramolecular networks to a pH switchable Dendrimer as a potential Drug Carrier

Gutachter	**Prof. Dr. Carsten Schmuck**
	Prof. Dr. Thomas Schrader
Prüfungsvorsitzender	**Privatdozent Dr. Holger Somnitz**

Tag der Disputation 24.03.2017

Eidesstattliche Erklärung

Die vorliegende Arbeit wurde von Oktober 2010 bis Januar 2017 im Institut für Organische Chemie der Universität Duisburg–Essen unter der Anleitung von Herrn Prof. Dr. Carsten Schmuck angefertigt.

Ich erkläre hiermit des Eides statt, dass ich die vorliegende Arbeit selbst verfasst und mich dabei keiner anderen als der von mir bezeichneten Quellen und Hilfen bedient habe.

Ich erkläre hiermit, dass ich an keiner anderen Stelle ein Prüfungsverfahren beantragt beziehungsweise die Dissertation in dieser oder anderer Form bereits anderweitig als Prüfungsarbeit verwendet oder einer anderen Fakultät als Dissertation vorgelegt habe.

Essen, den

Julia Schulz

Curriculum Vitae

In der elektronischen Version aus Datenschutzgründen nicht enthalten.

Danksagung

Als ich beschlossen hatte, Chemie zu studieren, war mir eigentlich schon klar, dass ich auch promovieren möchte. Jetzt, wo die Dissertation fertig ist, ist es an der Zeit, den vielen Menschen, die mich in dieser Zeit beruflich und privat begleitet haben endlich Danke zu sagen. Anfangen möchte ich mit meinem Doktorvater Professor Dr. Carsten Schmuck. Danke, dass du mir die Möglichkeit gegeben hast, in diesem spannenden Themenfeld zu promovieren und dafür, dass du mich bei meiner Arbeit stets unterstützt hast, auch wenn es zwischendurch mal nicht so rund lief. Das Arbeiten in deiner Arbeitsgruppe hat mir immer sehr viel Spaß bereitet. Das lag nicht zuletzt an den vielen tollen Menschen in dieser Gruppe und der Fakultät, die mich bei der Anfertigung dieser Arbeit praktisch, wissenschaftlich und seelisch unterstützt haben. Für die praktische Hilfe danken möchte ich Dr. Heinz Bandmann und Dr. Torsten Schaller für die Unterstützung bei der Aufnahme der NMR-Spektren, Herrn Werner Karow und Frau Gudrun Heinrich für die Aufnahme der Massenspektren, Dr. Wilhelm Sicking für die große Hilfe bei den Kraftfeldberechnungen, Herr Manfred Zähres für die Messung des DOSY-NMRs und Elio Zellermann für die Messung der TEM Bilder.

Bei der Synthesearbeit konnte ich mich immer auf die Hilfe und gute Tipps von Elisabeth Verheggen verlassen. Außerdem habe ich bei dir immer ein offenes Ohr und guten Rat gefunden, nicht nur wenn es um die Synthese ging. Danke dafür! Nicht vergessen möchte ich natürlich Pia Mereu, eine weitere gute Seele der Arbeitsgruppe, die uns alle mit der Synthese von Grundbausteinen und an der HPLC unterstützt hat. Ein weiteres Dankeschön geht an meine Azubis, die ich während meiner Promotionzeit betreuen durfte. Im Labor wart ihr eine große Hilfe und mit der alljährlichen Inventur wär ich ohne euch wahrscheinlich nie fertig geworden ;-)!

Ein weiterer Dank gebührt Prof. Dr. Michael Giese, Prof. Dr. Jens Voskuhl und (demnächst Dr.) Lina Bartsch für das Korrekturlesen dieser Arbeit. Dr. Hannes Korth möchte ich für die gute Zusammenarbeit im allgemeinen Danken. Auch bei dir habe ich immer ein offenes Ohr gefunden. Selbstverständlich möchte ich weiteren Kollegen für die gute Zusammenarbeit danken. Dazu zählen Dr. Monika Seifert, Ulla Nüchter, Dr. Christoph Hirschäuser, mein späterer Labornachbar Dr. Mao Li und natürlich Christine Cangemi, du hast mit deinem tollen Organisationstalent den AK am Laufen gehalten. Für eine tolle Zeit und eine super Arbeitsatmosphäre danke ich auch Anja Heimann, Christian Schlütting, Dr. Supratim Banerjee, Marcel Mertel, Elio Zellermann, Dr. Alba Gigante und allen anderen im AK Schmuck.

Und dann sind da noch die Menschen, die über die Zeit wesentlich mehr als nur Kollegen oder gute Bekannte geworden sind, Menschen, die ich im Leben nicht wieder missen will. Danke an (bald Dr.) Sandra Junghänel, Dr. Ina van Kamp, Dr. Ute Schlund, Dr. Kerstin Grossert und (bald Dr.) Lina Bartsch,

dass es euch gibt! Ohne euch wäre die Zeit nicht ansatzweise so schön gewesen. Ich hätte nicht so schöne Hochzeiten besucht, hätte nicht so viel Spaß auf Achterbahnen gehabt und mein Kleiderschrank wäre wohl fast leer ;-)!

Für die tolle mentale und im Studium sehr Tatkräftige Unterstützung und langjährige Freundschaft möchte ich selbstverständlich auch meinen Freunden aus Studienzeiten danken. Danke Steffi, Yassin und Jenny. Ihr seid toll!

Und dann sind da noch meine längsten Wegbegleiter, auf die ich mich schon zum Teil seit 28 Jahren verlassen kann. Und ich so unglaublich froh dass wir immer noch so ein toller Kreis sind. Konfetti, Sekt und Bier gehen Anna, Hanna, Stephie, Joanna, Eva, Ralle, David, Wunni, Carsten, Dominic und Patric. Patric, ich hoffe du schaust uns allen von da oben zu! Hier unten vermissen wir dich… Und dann ist da noch mein Thomas. Um es mit deinen Worten zu sagen, danke Ray Tomlinson für die Erfindung der E-Mail, der Rest ist eine wunderbare Geschichte, jetzt schon seit fast 8 Jahren. Danke für deine großartige Unterstützung. Ohne dich hätte ich das nicht geschafft. Ein großer Dank geht selbstverständlich auch an meine Familie. Danke an Tante Ekka, ja ich pass auf mich auf und gehe mit keinem mit ;-)! Danke an meine Eltern dafür, dass ihr immer für mich da seid und mich immer emotional und finanziell aufgefangen habt. Ohne euch wär das alles gar nicht möglich gewesen!

Danke!!!

Table of content

1 INTRODUCTION

Dendrimers present a unique and versatile class of macromolecules. They are characterized by their nearly perfectly branched structure resulting in a monodisperse, highly symmetrical spherical architecture. Since the first synthesis of dendrimers by *Vögtle et al.* in the late 1970s a great variety of different dendrimers have been developed.[1,2] In the early years of dendrimer research the main focus was on the synthesis of different dendrimers and the development of new synthetic strategies. Later the research focus turned more toward potential application of dendrimers and dendritic macromolecules.

Dendrimer applications have been under development in various fields, one of them biomedical chemistry.[3] One key feature of dendrimers is the multivalency especially in combination with the globular shape. The number of surface groups is increasing exponentially with every generation. This can result in enhanced solubility of dendrimers compared to classic linear polymers.[4] Another key feature is the possibility to encapsulate guest molecules within the interior of the dendrimer, allowing applications like solubility enhancement of poorly water-soluble molecules and drug delivery. Potential applications for drug delivery were already proposed in the mid-1980s. Newkome went as far as calling dendrimers with a hydrophobic interior/core and hydrophilic shell unimolecular micelles.[5,6] Drug delivery is an important research field especially for cancer treatment, because many established and novel cancer drugs are poorly water-soluble. Moreover, with the right design of a carrier system it might be possible to control the release of the drug and thus target tumor tissue in a controlled and selective manner, reducing negative side effects these drugs usually come along with.[7]

There are different approaches for the development of drug carrier systems; but dendrimers are particularly promising candidates, due to their unique, branched and spherical architecture. Combination of this unique architecture of dendrimers with a supramolecular approach allows the development of self-assembled dendrimers, which can be triggered by external stimuli. This concept might be beneficial for finding suitable drug carrier systems for cancer therapy, tailored for a targeted and selective release. Since tumor cells exhibit a slightly more acidic pH value compared to healthy tissue[7], pH value changes can be a useful trigger mechanism for payload release. Already a lot of research has been done in the field of supramolecular dendrimers and is still ongoing, resulting in the design of many promising smart supramolecular polymeric materials and functional supramolecular devices.[8] A challenge however, is the binding stability of those systems in aqueous solution, which is a crucial requirement for the use of supramolecular dendrimers in biomedical

applications, such as drug delivery. The aim of this work was to develop a supramolecular templated dendrimer using a supramolecular binding motif, which is able to form stable self-assemblies in aqueous media and to study its characteristics concerning the encapsulation and controlled release of poorly water-soluble guest molecules.

2 BACKGROUND INFORMATION

2.1 Supramolecular chemistry

In materials science new functional materials such as polymers, dendrimers and hydrogels are continually developed and refined. These materials have various potential applications either in the actual field of materials science e.g. as surface coatings[9], polymers[10,11] or in biomedical science for example as sensors[12] or drug carriers.[13] The design of new smart materials can considerably benefit from the use of supramolecular chemistry. Through the combination of covalently bound building blocks with noncovalent reversible bonds self-assembled nanostructures can be formed.[14] The advantages of this approach are for instance the possibility to control the material by changing external parameters and hence switch the aggregates between different states. Moreover, the reversibility of the noncovalent bond allows a minimization of structure defects or even self-healing properties for supramolecular polymers. However, the use of supramolecular chemistry can be challenging. Since most applications especially biomedical ones require aqueous solutions the noncovalent binding motifs used to form supramolecular aggregates need to be stable in water.

Most supramolecular noncovalent binding motifs, except for metal coordination, rely on weak interactions. These interactions include hydrogen bonds, ion pairs, hydrophobic interactions and π-π stacking. Although a great variety of binding motifs used for supramolecular chemistry based on those interactions exists, major drawbacks are well known. For example supramolecular structures based on weak interactions can be formed and studied in organic solvents, such as chloroform, but show no stability in highly polar solvents let alone water. Only binding motifs utilizing multiple weak interactions might be reasonably stable in competitive solvents.[15]

2.1.1 Guanidiniocarbonylpyrrole carboxylate zwitterion

A suitable binding motif for the formation of supramolecular nano-assemblies in polar solvents such as DMSO or water is the guanidiniocarbonylpyrrole carboxylate zwitterion developed by Schmuck *et al.*in the late 1900s. Originally the development of the GCP-zwitterion started with the design of an artificial arginine analogue for enhanced oxo anion binding. [16,17]

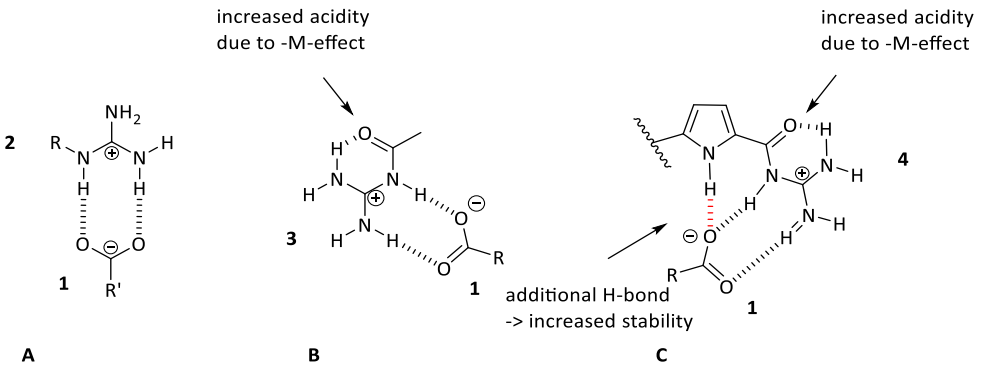

Figure 1: Carboxylate binding by a simple guanidinium cation (A), an acyl guanidinium cation (B) and the guanidiniocarbonyl pyrrole cation (C)

Oxo-anion binding to simple guanidinium cations (Figure 1) is rather weak especially in competitive solvents, such as water or DMSO. Introducing an acyl group increases the acidity of the NHs due to a-M-effect, which is even amplified by the additional hydrogen bond of the acyl group. This increased acidity of the NHs leads to favored H-bond formation and hence improves the binding. Using the guanidiniocarbonyl pyrroles as a binding motif enhances the binding to oxo anions even further. The additional H-bond and the ideally preorientated rigid scaffold increases the complex stability significantly by several orders of magnitude compared to the acyl guanidinium cation (in DMSO : water; 6 : 4).[16,17]

Based on this efficient oxo anion binding motif the GCP-zwitterion was developed.[15] This zwitterion is self-complimentary and forms highly stable head to tail dimers even in polar solvents. The estimated binding constant K_{ass} in DMSO is about 10^{10} to 10^{12} M^{-1}.[15]

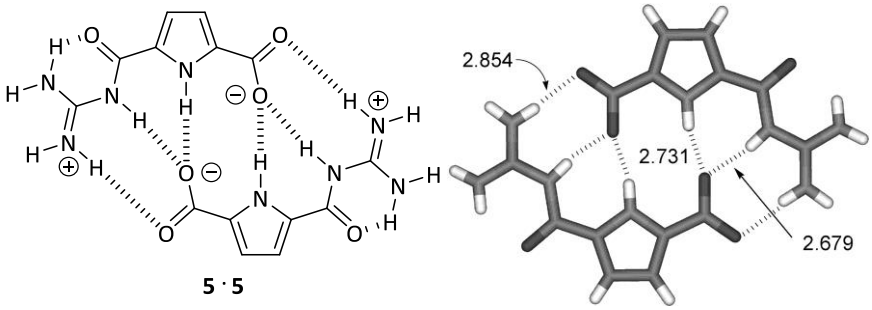

Figure 2: 5-(Guanidiniocarbonyl)-1*H*-pyrrole-2-carboxylate dimer (left) and the- X-ray crystal structure with hydrogen bond lengths in Å[18] (right); X-ray crystal structure reprinted with permission from Schmuck C, Wienand W., *J Am Chem Soc* 2003, 125(2): 452-459. Copyright © 2003 American Chemical Society

The dimer formation was confirmed in gas phase via ESI-MS and in solution by ^{1}H-NMR. A characteristic downfield shift of the amide NH signal and the split of the guanidinium NH signal into two peaks were observed in comparison to the normal expected signals for an acylguanidinium

cation.[15] Moreover, the GCP-zwitterion dimer could be detected with the help of an X-ray crystal structure. The X-ray crystal structure revealed the dimers to be planar and symmetric. The length of the amide N-O (2.679 Å), guanidinium N-O (2.854 Å) and the pyrrole N-O (2.731 Å) hydrogen-bonds are rather short indicating strong intermolecular interactions.[18] In all measurements no larger aggregates could be observed.

A water-soluble analogue (Figure 3) was synthesized by the incorporation of two triethylene glycol chains to the molecule allowing the determination of the binding constant of the guanidiniocarbonylpyrrole carboxylate zwitterion dimers in water. The measurement revealed a binding constant of 170 M^{-1}, which is still a notably high value and significantly more stable than two simple Coulomb interactions.[18 19]

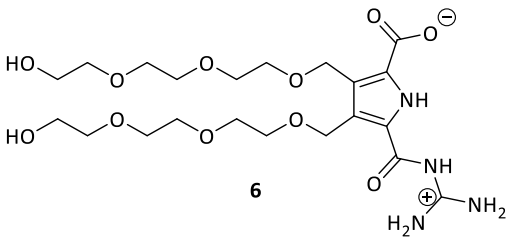

Figure 3: Water-soluble analogue of 5-(Guanidiniocarbonyl)-1*H*-pyrrole-2-carboxylate zwitterion. The water-solubility is ensured by two PEG chains at the backbone of the pyrrole[18,20]

The high stability of the dimers results from the perfect combination of hydrogen bonds network and the two mutual interacting ion pairs. Moreover the rigidity and the resulting planarity of the zwitterions favor the dimerization and prevent intramolecular interactions of the carboxylate and the guanidinio moiety. The synthesis of a neutral knock-out analogue further proofed, that the ion pairs are crucial for a stable dimerization in polar solvents.[17,18]

Since the zwitterionic state, similar to natural amino acids, only occurs in a narrow and specific range around neutral pH (around 6), it is possible to reversibly switch the self-association on and off by changing the pH value either to acidic or basic conditions and back to 6.

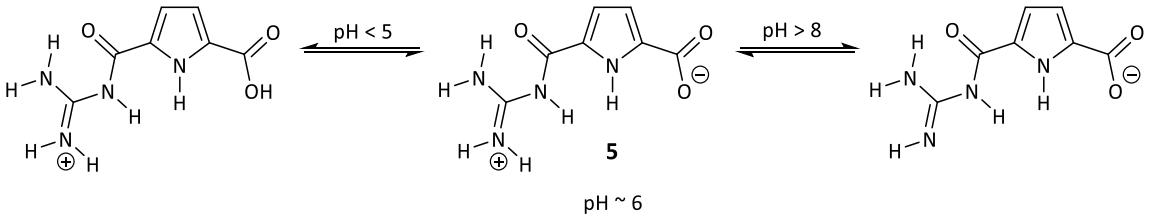

Figure 4: pH dependence of the 5-(Guanidiniocarbonyl)-1*H*-pyrrole-2-carboxylate zwitterion; at pH values below 5 the cationic form is present, while at pH above 8 the anionic form exists[15]

The high stability of the guanidiniocarbonylpyrrole carboxylate zwitterion dimers even in aqueous solution, the pH dependent reversible switchability between monomer and dimer, a facile synthesis[20-22] and the uncomplicated possibility to functionalize the methyl group in position 4 make the guanidiniocarbonylpyrrole carboxylate zwitterion a suitable binding motif to design more complex supramolecular structures. There are basically two pathways to obtain higher supramolecular structures with the GCP-zwitterion. First, it is possible to add further functionalities to rearward periphery of the pyrrole ring. Those functionalities include metal-binding sides[23], dendrons[24] and secondary amines[25]. Another possibility is the linkage of two or more GCP-zwitterions by a molecule of physical/chemical interest, such as perylenes[26], or a suitable linker. One example is the self-assembly of a triple zwitterion (Figure 5), in which three functionalized guanidiniocarbonylpyrrole carboxylate zwitterions are linked via a flexible *tren* linker.[27] As expected, the self-assembly behavior of a triple zwitterion is more complex than the single zwitterion. Intramolecular and intermolecular self-assembly compete whereas the intramolecular assembly depends on the length and flexibility of the linker.[27] It was found that a highly hierarchical self-assembly takes place. In low concentrations the triple zwitterion forms dimers in DMSO solution, whereas two binding sides of each molecule form intramolecular loops and the third guanidiniocarbonylpyrrole carboxylate moieties assemble intermolecularly to form the dimer[28] as illustrated in Figure 5 (top-right).

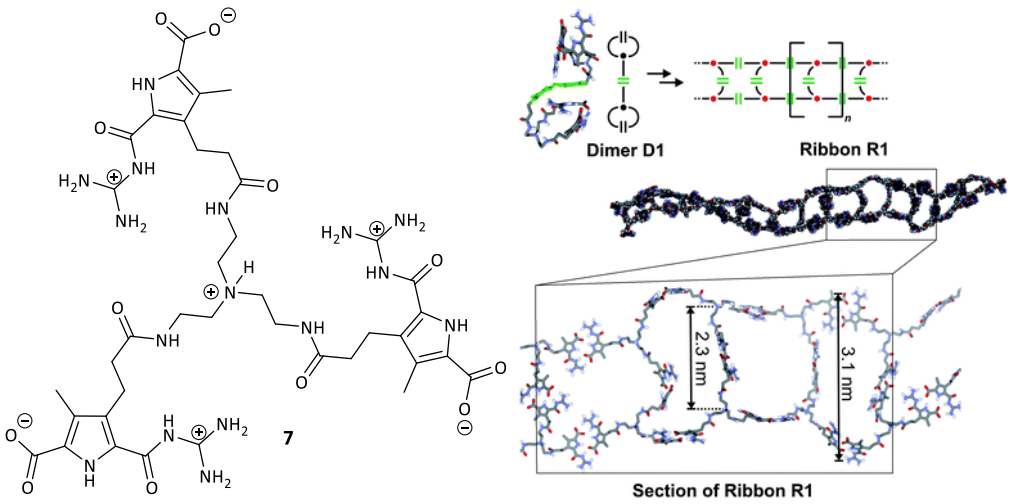

Figure 5: Chemical structure of the triple zwitterion (left); structure of the dimer obtained with force field calculations and schematic illustration of the dimer and the 2-dimensional ribbons (top-right); force field calculation of the structure of the 2-dimensional ribbons (bottom-right); reprinted with permission from Rehm TH, Gröhn F, Schmuck C. *Soft Matter* 2012, 8(11): 3154-3162 Copyright © 2012, Royal Society of Chemistry

With increasing concentration those dimers rearrange into 2-dimensional ribbons (Figure 5; bottom right), which further aggregate to form supramolecular nanospheres in solution. Figure 6 shows AFM measurements of the nanospheres (A,B,C) and the ribbon networks (D) on a mica surface.[28]

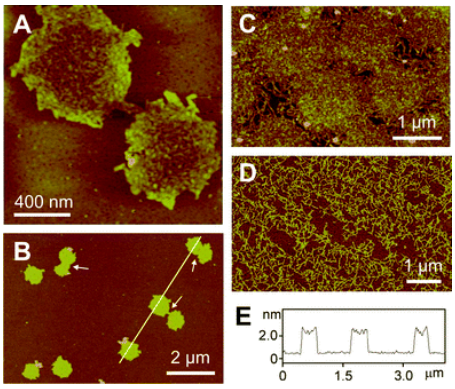

Figure 6: AFM image of the nanospheres deposited on a mica surface and analyzed with tapping mode AFM (A, B, C), section plot of the 3 plates in B, revealing a uniformly height of 2.5 nm and diameter of 450 nm (E), AFM image of the ribbon network (D); reprinted with permission from Rehm TH, Gröhn F, Schmuck C. *Soft Matter* 2012, 8(11): 3154-3162

Another example for the self-assembly of multiple guanidiniocarbonylpyrrole carboxylate zwitterions connected by a linker is a quadruple zwitterion.[29] Four guanidiniocarbonyl pyrrole carboxylate zwitterions are arranged in a tetrahedral fashion around a pentaerythritol core via click reaction as illustrated in Figure 7. Since the linker is reasonably flexible, intramolecular assemblies of the zwitterions are possible. Indeed, at low concentrations (0.5 mM) the zwitterions solely assemble into intramolecular loops. With increasing concentration the molecules start to self-assemble intermolecularly resulting in vesicle like structures (1 mM), network-like structures and eventually a transparent gel in DMSO (45-50 mM) is formed. This gel undergoes a completely reversible gel-sol transition upon the addition of either acid or base and upon heating (100 °C) and cooling (Figure 7). The pH switchability of the smaller aggregates at lower concentrations could be confirmed by dynamic light scattering, DOSY-NMR and atomic force microscopy (Figure 7).[29]

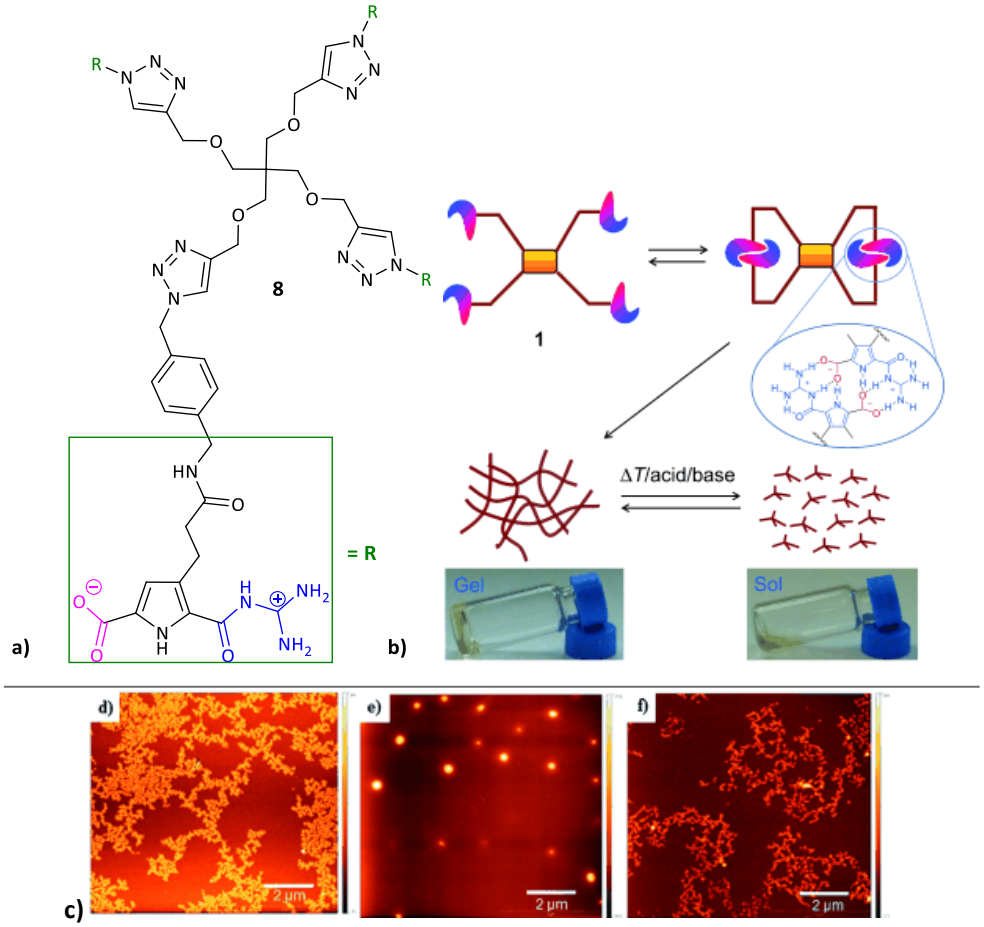

Figure 7: a) Chemical structure of the quadruple zwitterion ; b) Schematic illustration of the formation of intramolecular loops (top); reversible sol-gel transition (bottom); c) Images of 5 mM samples in DMSO spin-coated on a mica surface and analyzed with tapping mode AFM, left 5 mM DMSO, middle 5 mM DMSO + TFA and right 5 mM + TFA + Et_3N; pictures reprinted with permission from Hisamatsu Y, Banerjee S, Avinash MB, Govindaraju T, Schmuck C. *Angew Chem-Int Edit* 2013, 52(48): 12550-12554, Copyright © 2013 WILEY-VCH Verlag GmbH & Co. KGaA, Weinheim [29]

Further examples of higher supramolecular structures, realized by using the guanidiniocarbonyl pyrrole carboxylate zwitterion and derivatives thereof, do include supramolecular pH switchable polymers[23], hydrogels[30], rod-like nano-assemblies[25], vesicles[31,32] and untemplated dendrimers[24].

2.2 Dendrimers

2.2.1 Introduction

Dendrimers are highly branched, well defined, monodisperse, radially symmetric nano-sized macromolecules.[33] Their name derives from the Greek words *dendron* and *meros*, translating to *tree* and *part*, due to their branched, tree like architecture.[34]

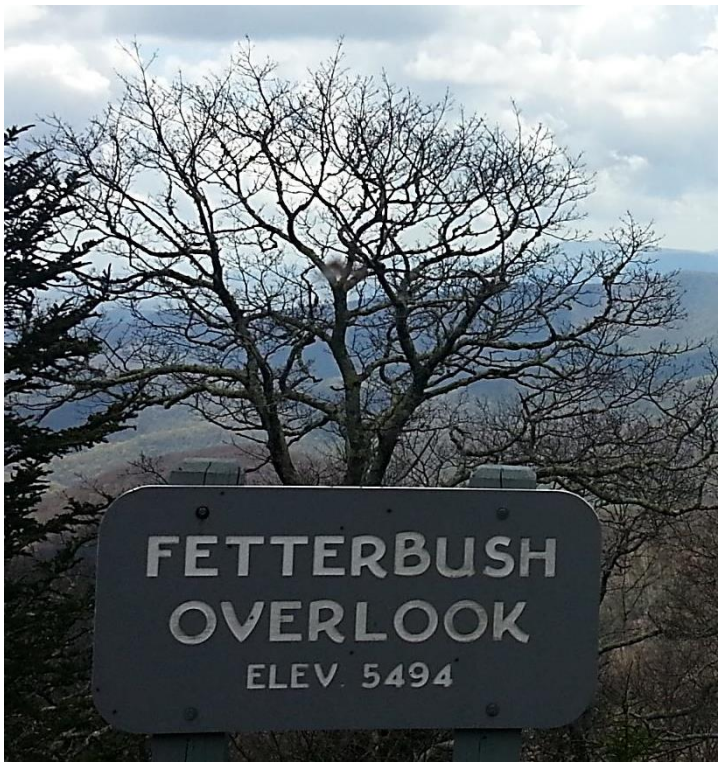

Figure 8: Tree near Ashville, North Carolina USA (Photo taken by Julia Schulz); Comparing the branched architecture of trees and dendrimers, it is obvious why the Greek and Latin terms for tree were chosen to name this class of macromolecules.

Dendrimers differ from regular linear polymers in their extraordinary symmetry, high branching, monodispersity and their maximized density of terminal functional groups.[35] Early research in this field started in the late 1970s by Vögtle *et al.*, calling this class of macromolecules cascade molecules.[1] In the early 1980s Newkome *et al.* developed symmetrically branched globular macromolecules with a tree-like architecture choosing the Latin term *arborols* (tree) as a name for this class of macromolecules.[6] However, Tomalia *et al.* coined the term dendrimer also in the early 1980s by developing the polyamidoamine (PAMAM) dendrimers and the Starburst polymers, which are formed by the linkage of these dendrimers.[35] In the last 30 years a vast number of different dendrimer structures have been realized.[2] Figure 9 gives an overview of some popular dendrimer

classes including the polyamidoamine (PAMAM) dendrimers, polylysine (PLL) dendrimers and polypropylenimine (PPI) dendrimers.

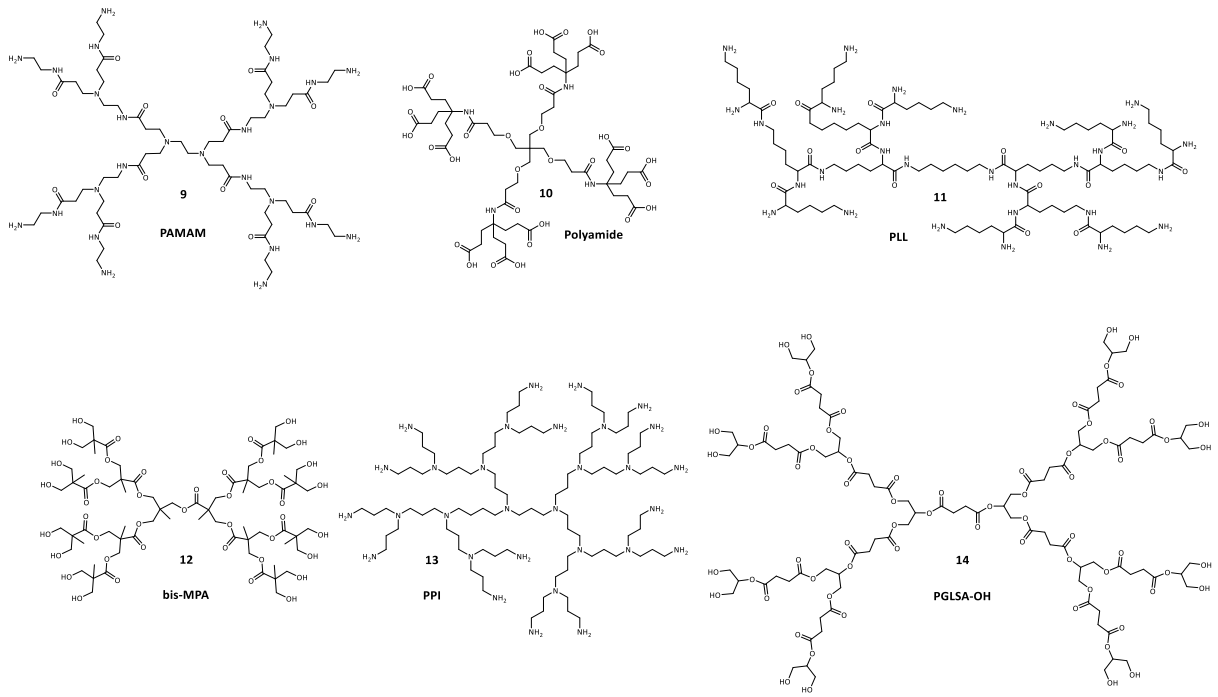

Figure 9: Overview of popular dendrimer classes[7]

2.2.2 Structure and properties of dendrimers

Hyperbranched polymers and dendrimers are the only two classes of polymers that consist entirely of branched units. But unlike hyperbranched polymers, which exhibit an irregular architecture, dendrimers are highly ordered and regularly branched which is achieved by a stepwise iterative synthesis approach.[36] A schematic dendrimer is illustrated in Figure 10. Dendrimers basically consist of three regions, starting with an internal core from where repeating, symmetrically branched units originate. These units constitute the interior layers, called generations. The outer shell is the terminal functionalization of the outermost generation.[35] The properties of the terminal functionalization can significantly affect the dendrimers characteristics such as the shape, the stability, the solubility, the viscosity and the conformational flexibility or rigidity, respectively.[37] In sharp contrast to traditional linear polymers, which only have two end groups, the number of terminal groups of dendrimers grows exponentially with generations. With increasing molecular weight of the dendrimer the properties are increasingly dominated by the nature of the end groups. Thus, the modification of the outer shell allows a facile modification of the characteristics of dendrimers as well as tailoring them for potential applications[38]. While the number of the branched repeating units, the generations, alternatingly highlighted and labeled with generation (G) number in Figure 10, defines the size of the

dendrimer due to its linear increase with increasing number of generations. The form of the interior plays a key role concerning the density within the dendrimer. Hence the modification of the generations allows the tailoring of the size and the shape of internal cavities which can be important for applications relying on host-guest complexes of smaller molecules within the dendrimer. Moreover, the number of terminal functionalities depends on the number of generations since the number of generations indirectly affects the properties of the outer shell and in particular, the resulting rigidity, occurring for higher generations, due to steric crowding on the surface, or flexibility, at lower generations, of the structure.[33] Also the multivalent core affects the size and the shape of the dendrimer to a certain extent, depending on the size, form and multivalency of the core. A wedge-like branch of a dendrimer is called a dendron as highlighted in light blue in Figure 10.

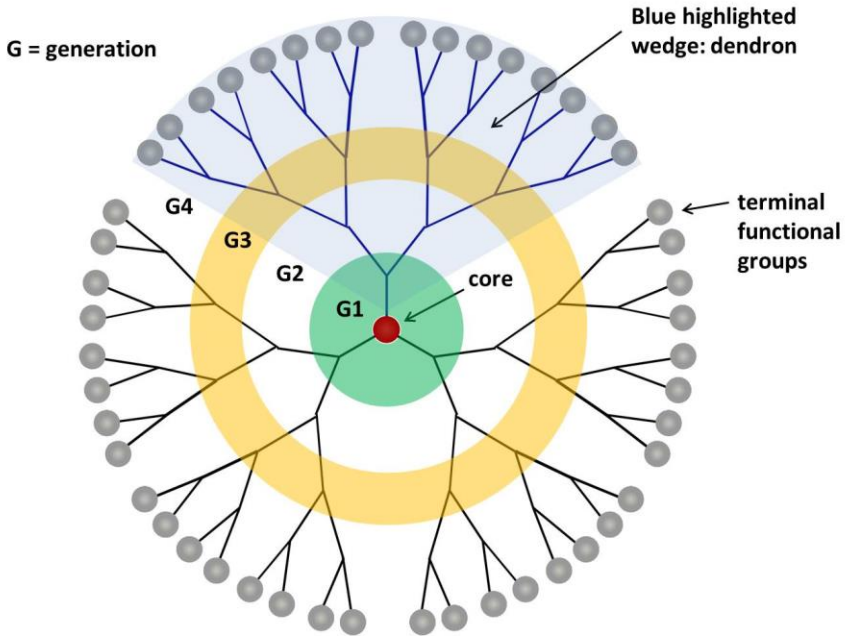

Figure 10: Schematic illustration of a dendrimer

However, the assumption that dendrimers are perfectly globular shaped macromolecules oversimplifies the behavior of most dendrimers, since a backfolding of the terminal groups into the interior is possible.[39] This results in dense interior of the dendrimers opposed to a dense shell, as illustrated in Figure 11.

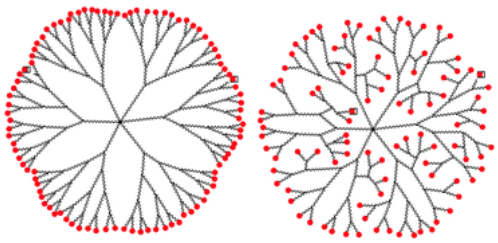

Figure 11: Schematic illustration of a dendrimer with all terminal groups facing outward (left) and the possible backfolding of the terminal groups into the interior of the dendrimer.[7] Illustration reprinted with permission from Mintzer MA, Grinstaff MW, *Chem Soc Rev* 2011, 40(1): 173-190; Copyright © 2010, Royal Society of Chemistry

In contrast to linear polymer growth that theoretically can infinitely continue, the synthesis of dendrimers is sterically limited to a certain size. This limit is called the DeGennes dense packing. After reaching the DeGennes dense packing only irregular growth of the dendrimer is possible resulting in major defects. Defects of the dendrimers structure can also occur before the DeGennes dense packing is reached, due to steric hindrance or incomplete reactions during synthesis, especially for dendrimers larger than generation 4. There have been tremendous synthetic efforts that have yielded elegant methodologies to construct a large repertoire of dendritic macromolecules, which will be briefly introduced in the next chapter.

2.2.3 Dendrimer synthesis

There are two complementary general approaches for the synthesis of dendrimers.[36] The divergent method starts at the core and diverts outward from there in iterative steps. The convergent method however, starts at what will later be the outer shell and converts inward to the core. A schematic illustration of both general synthetic routes leading to dendrimers is depicted in Figure 12.

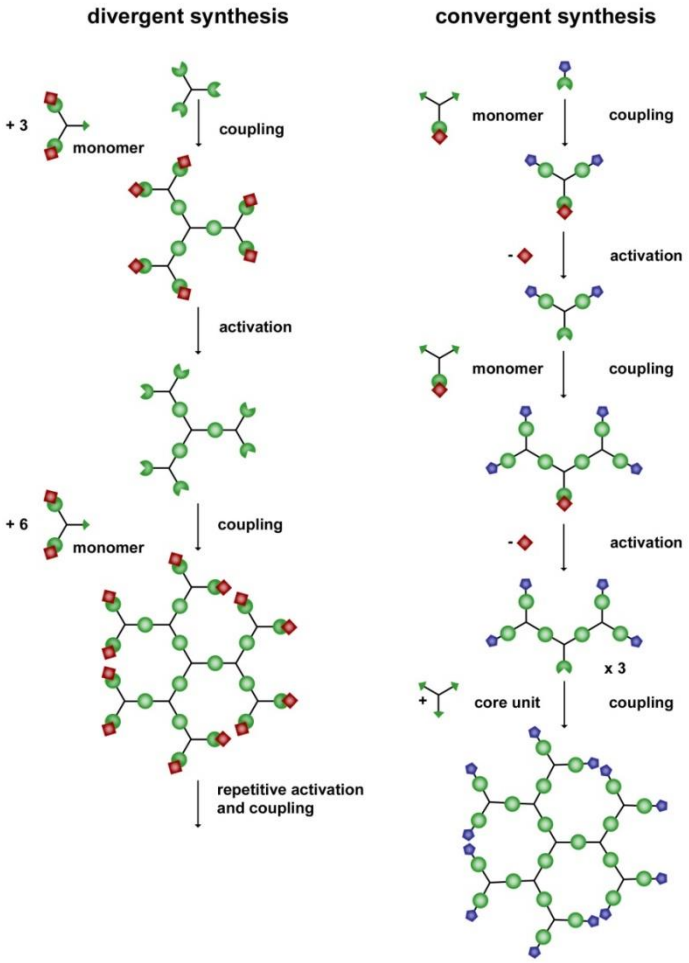

Figure 12: Schematic illustration of the divergent (left) and the convergent (right) synthesis approaches of dendrimers[36]

2.2.3.1 Divergent synthesis

The divergent approach was the initial synthesis route when Vögtle *et al.*[1], Newkome *et al.*[6] and Tomalia *et al.*[35] first developed the cascade molecules, arborols and dendrimers, respectively. This synthesis route starts at a multifunctional core with monomer units bearing one complementary reactive site and multiple protected or unreactive sites. Following the first coupling with the core, the terminal groups can be activated and subsequently react again with monomer units. This way the dendrimer will be synthesized in an exhaustive, step-wise and iterative manner. The synthesis of a [G1]-PAMAM dendrimer, as shown in Figure 13, should exemplarily be discussed in more detail. The reaction sequence starts with a suitable core, which can be e.g. ethylenediamine or, as used in this example, ammonia, which undergoes an exhaustive Michael addition with methylacrylate. This is followed by activation for the next generation step, which is in this case an amidation with a vast excess of ethylenediamine.

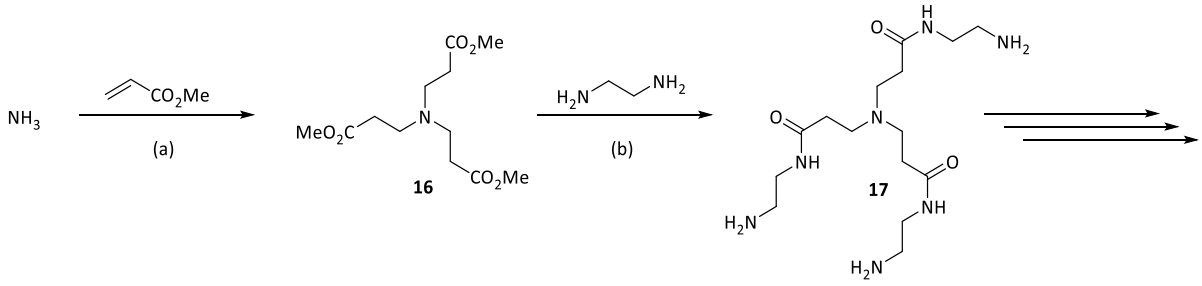

Figure 13: Iterative synthesis strategy to obtain PAMAM dendrimers, consisting of a Michael-addition (a) and an amidation (b), developed by Tomalia *et al.*[35,40]

These steps can be repeated to obtain PAMAM dendrimers of higher generations. The divergent synthesis is applicable for a broad spectrum of different dendrimers and is suited for the large scale synthesis. However, this method has some limitations as the number of terminal functional groups increases exponentially with every generation and hence the number of coupling reactions as well. In addition, the possibility of incomplete reactions or side reactions is exponentially increased and the formation of defects becomes more likely with higher generation dendrimers. 4th generation PAMAM has only 8 % defect free dendrimers.[7] Moreover, the monomers are used in a vast excess to ensure a complete reaction, which has to be removed after each reaction step. Even more important is the removal of the activating agent as long as it is capable of initiating new growth by itself, e.g. like the ethylenediamine in PAMAM synthesis, in order to avoid the formation of new smaller unwanted dendritic structures. While the removal of the monomers may be straightforward, the purification of the dendrimers is challenging since flawed molecules are structurally very similar to the intended dendrimer. Because of this divergently prepared dendrimer samples are generally mixtures of several closely related compounds with an extremely low overall polydispersity.[36]

One option to improve the divergent synthesis, by minimizing the purification effort, is the use of click chemistry. The Cu(I) catalyzed alkyne-azide "click" cycloaddition[41], which is an enhancement of the Huisgen 1,3-dipolar cycloaddition was first used by Wooley *et al.* to divergently grow dendrimers up to generation three.[42] Hereby the core (1,2-bis(2-azidoethoxy)ethane) is functionalized with azide groups, while the branching units (1-propargylbenzene-3,5-dimethanol) contain one alkyne group and two hydroxyl groups, which can be activated for the further growth of the dendrimer. A 2nd generation dendrimer, synthesized by using this approach, is illustrated in Figure 14. Because of the high yields and lack of byproducts provided by the Cu(I) catalyzed alkyne-azide 1,3-dipolar cycloaddition click strategy, the dendrimer purification can be minimized and the disadvantages from the increasing number of reactions for each generation are diminished, thus improving the divergent synthesis route to obtain dendrimers.

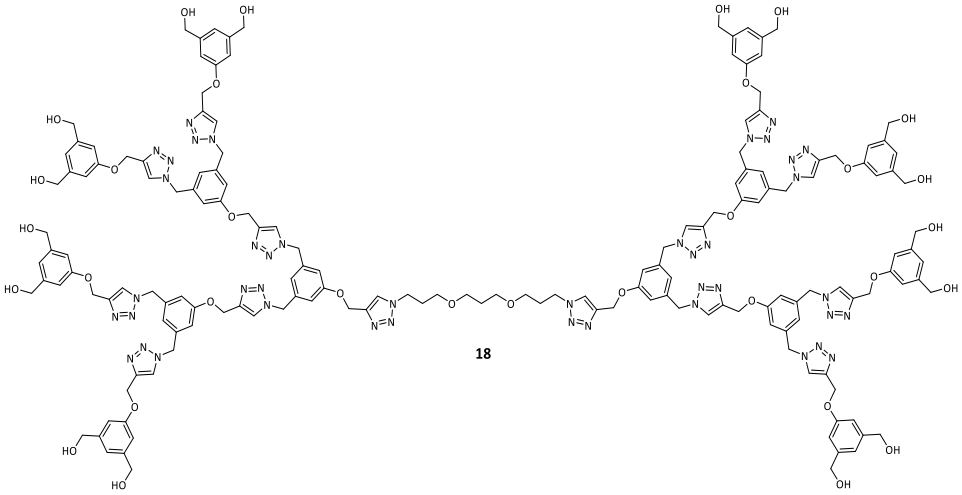

Figure 14: Second generation dendrimer obtained by a divergent click chemistry approach, using the Cu(I) mediated alkyne-azide 1,3-dipolar cycloaddition click reaction [42]

The combination of two different click reactions, in this case the Cu(I) mediated alkyne-azide 1,3-dipolar cycloaddition and a Diels-Alder reaction of a furan with a maleimide, was also successfully used to divergently develop a dendrimer, reported by Kakkar *et al.* in 2010.[38] The synthesis of a second generation dendrimer, using this approach, is illustrated in Figure 15. Three different building blocks are used to build up the dendritic structure in a step-wise manner. A trivalent alkyne functionalized core can be "clicked" to three building blocks carrying each one azide functionalization and two furan rings ($AzFu_2$) via the copper(I) promoted alkyne-azide cycloaddition. The resulting molecule **xy** has six furan rings as terminal groups. The next step consist of a Diels-Alder reaction of the terminal furan rings with six building blocks, carrying each one maleimide and two alkyne functionalities ($MaAc_2$).

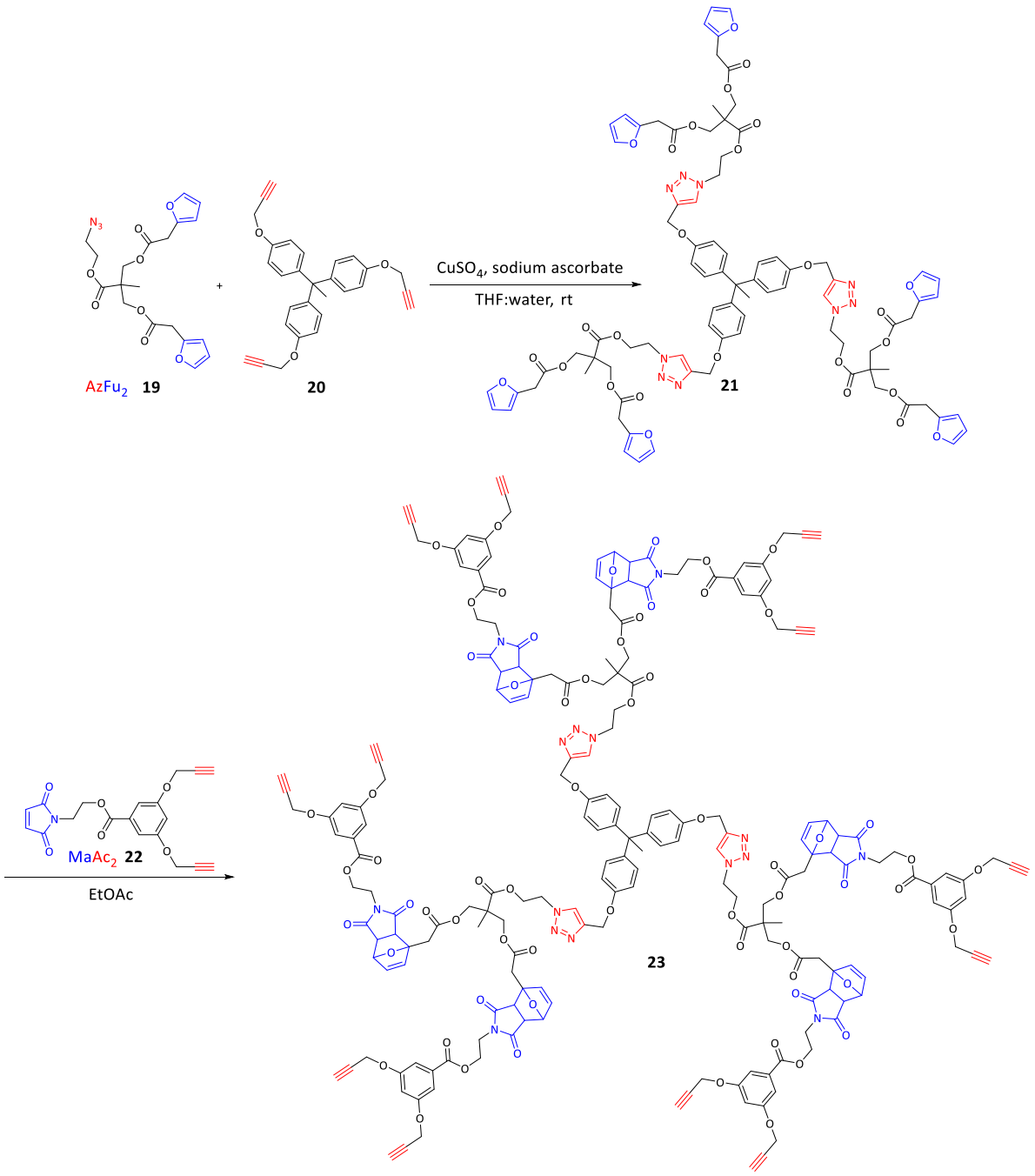

Figure 15: Divergent synthesis of a dendrimer utilizing two kinds of click reactions; red representing the 1,3-dipololar cycloaddition and blue represents the Diels-Alder reaction.[38]

These dendrimers exhibit thermo-responsiveness, due to the retro-Diels-Alder disassembly upon higher temperatures.

2.2.3.2 Convergent synthesis

The convergent synthesis of dendrimers starts with what eventually will be the outer shell and proceeds inward to form a wedge like dendron, which can be attached to a suitable core by a functionalization at the focal point of the dendron, to complete the synthesis (Figure 12). The convergent synthesis is generally limited to the synthesis of smaller dendrimers, normally up to 4th generation due to steric hindrance during the attachment of bigger dendrons to the core. The biggest advantage however is that the dendrimers can be obtained in a very high purity via convergent synthesis. For each generation step, only a small number of coupling reactions take place per molecule, opposed to the divergent synthesis approach. This lowers the likelihood of structure defects significantly.[36] The purification after each step is easier because the coupling steps only require a slight excess of monomers and the structural differences between the intended product and flawed byproducts is generally bigger than the differences between dendrimers and flawed dendrimers during the divergent synthesis route. This enables the effective use of chromatographic purification, ensuring the isolation of essentially single molecular species of precise molecular weight and structure.[36]

The convergent synthesis approach for dendrimers was pioneered by Fréchet et al. in 1990[43], by developing the synthesis of a poly(aryl ether) dendrimer, illustrated in Figure 16.

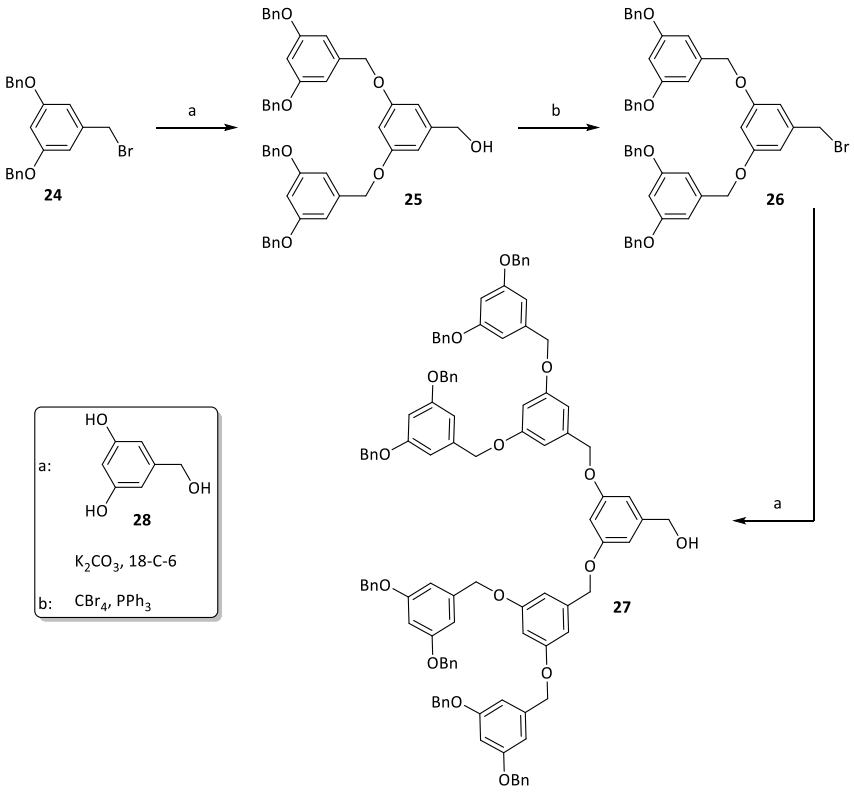

Figure 16: Convergent synthesis of a poly(aryl ether) dendron shown for the [G3]-Br by Fréchet *et al.*[36,43]

The dendron synthesis starts with a Williamson-coupling of two benzylic bromide monomers **24** to both phenolic groups of 3,5-dihydroxybenzyl alcohol in the presence of potassium carbonate and 18-crown-6 resulting in two new ether linkages and therefore the 2nd generation dendron with a focal benzylic alcohol functionality. The next step is the activation of the focal point by bromination with carbon tetrabromide and triphenyl phospine to enable the next coupling with 3,5-dihydroxybenzyl alcohol. Subsequent repetitions of the Williamson coupling and bromination steps allow the synthesis of dendrons up to generation 6. Although the Williamson coupling of the highly nucleophilic phenolate and a highly activated benzylic bromide exhibits very good yields, the coupling reactions show decreasing yields with increasing generations, as steric constraints begin to hinder the coupling step.

All of the dendrons from generation one through six can also be effectively coupled to a tris(phenolic) core **29** to form tridendron dendrimers **30**, though an analogous steric effect causes a slight reduction in yields for the larger dendrimers

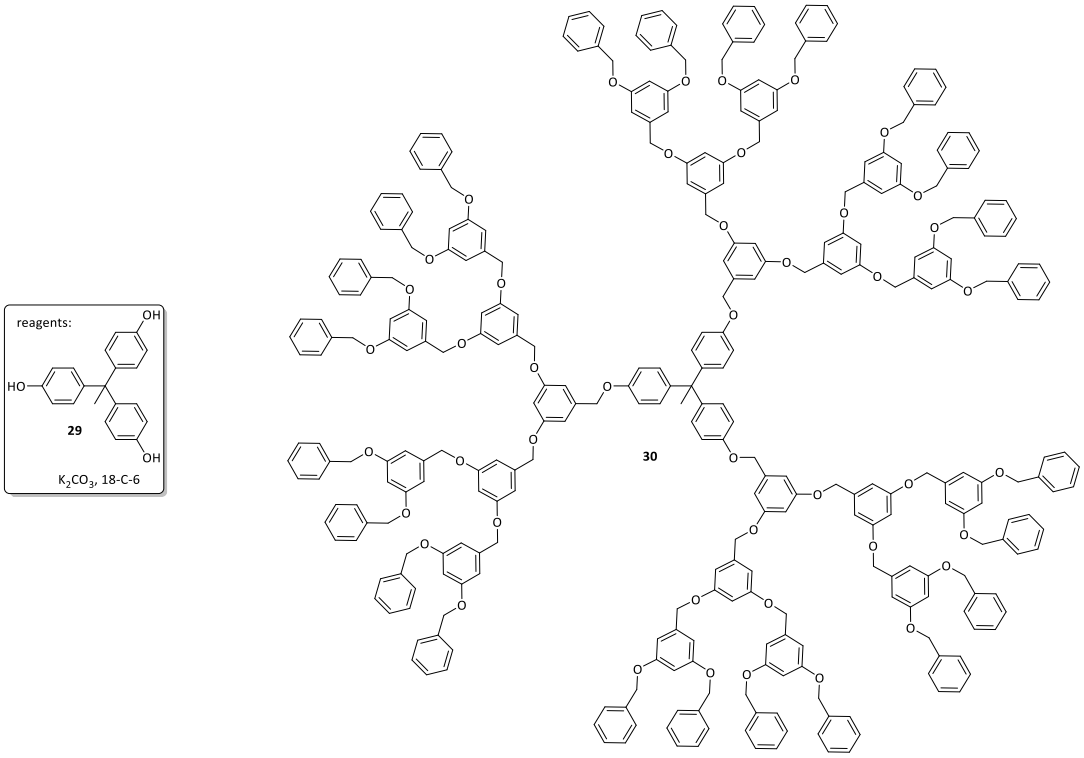

Figure 17: 3rd generation poly(aryl ether) dendrimer 30 with a tris(phenolic) core [45]

The poly(benzyl ether) dendrimer synthesis is one of only a few convergent syntheses that can produce dendrons and dendrimers in reasonable yields up to the 6th generation.

A similar synthesis approach was used to synthesize poly(alkyl ether) dendrimers, which are aliphatic analogues of the poly(benzyl ether) dendrimers. Based on methallyl dichloride as the monomer the

synthesis was initiated by the Williamson ether coupling of the branching unit, which is a di-protected triol (ketal or benzyl ether protection groups), with the allylic chloride functionalities of the monomer.[44] The double bond of the methallyl dichloride serves several functions. Firstly, it activates the allylic halide moieties for the Williamson coupling and it prevents elimination side reactions. Later it serves as a latent hydroxyl group at the focal point of the dendron for growth of the next generation. This "ene" functionality could readily be converted to the corresponding primary alcohol via hydroboration/oxidation, allowing further Williamson ether coupling. This procedure was repeated in high yields to obtain dendron of the 5th generation. These dendrons were attached to a triallyl chloride core moiety to form the respective dendrimers.[45] The peripheral ketal or benzyl ether protecting groups can be quantitatively removed by acid-catalyzed hydrolysis or palladium-catalyzed hydrogenolysis. Thus, the periphery of the resulting dendron consists of numerous hydroxyl groups, which are capable of further modification by alkylation or esterification. Additionally, these hydroxyl groups and the polar backbone of the dendron ensure good water-solubility, which makes these dendrons similar to poly(ethylene glycol), which may prove useful in macromolecular catalysts or in biomedical applications in particular.

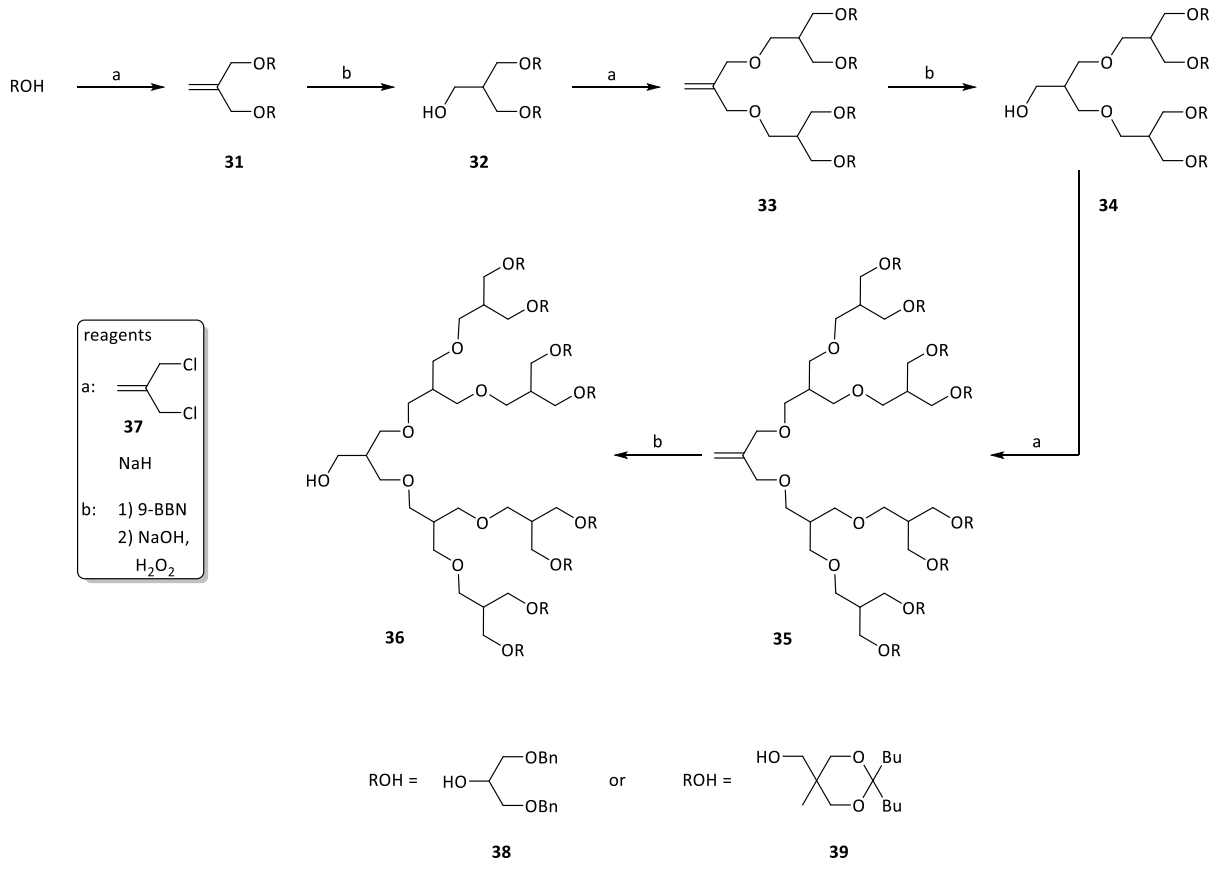

Figure 18: Synthesis of poly(alkyl ether) dendrons[44]

Moreover, the convergent synthesis approach allows the synthesis of unsymmetrical co-dendrimers by the attachment of two or more different types of dendrons to one core.[46,47]

2.2.4 Supramolecular dendrimers

Classical supramolecular polymers are an interesting and important field of research since many years. The use of non-covalent interactions, such as multiple hydrogen bonds, metal-ligand coordination, host-guest interactions and π-π stacking endow the polymers with several interesting physical and chemical properties based on the reversible nature of these interactions, which are usually lacking in traditional covalently bound polymers. They can undergo dynamic switching of their structure, morphology and function in response to outer stimuli like pH value, temperature, light and redox agents. That allows a wide range of applications in the biomedical field, in nanotechnology and as functional smart materials. [48-50] Transferring this concept of the combination of supramolecular chemistry and polymer chemistry to dendrimers, the field of supramolecular dendritic polymers opens a vast array of possibilities of self-assemblies formed either from functionalized dendritic subunits or by small well designed monomers to form dendritic structures. Already a lot of research has been done in this field and is still ongoing, resulting in the design of many promising smart supramolecular polymeric materials and functional supramolecular devices.[8] Figure 19 illustrates different possibilities for the self-assembly of supramolecular dendritic polymers, ranging from supramolecular spherical dendrimers, supramolecular dendronized linear polymers, supramolecular dendritic-linear and dendritic-dendritic copolymers to supramolecular dendritic multiarm copolymers. Those supramolecular dendritic polymers can further self-assemble into a variety of higher hierarchical supramolecular structures such as micelles, vesicles, fibers, nanorings and helical tubes.

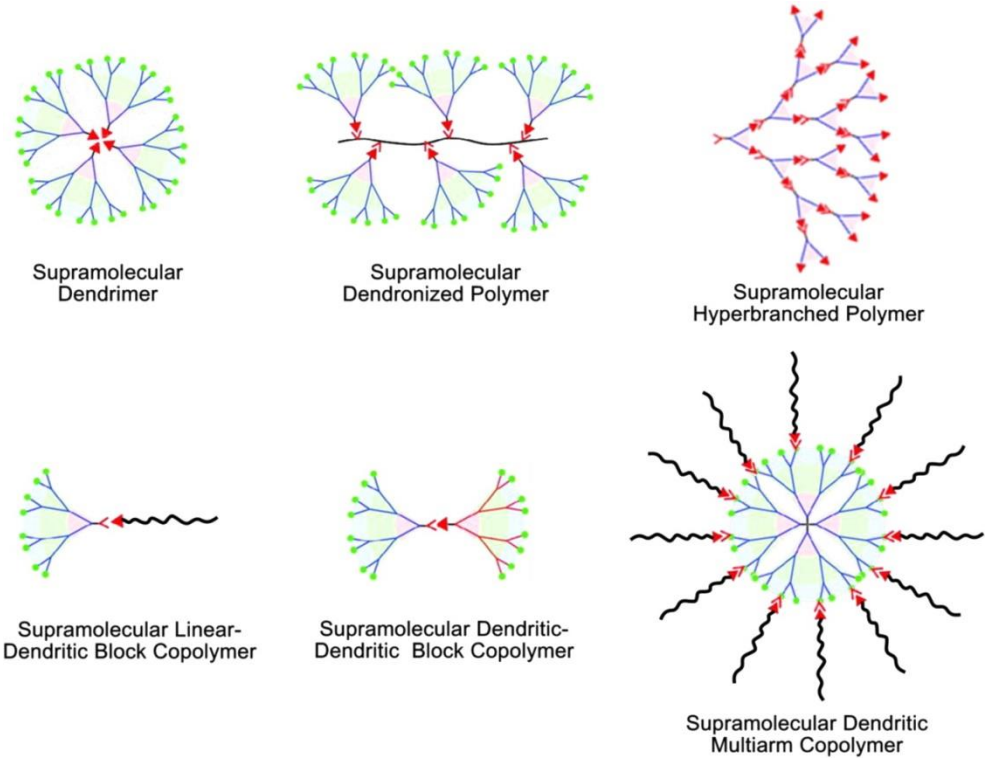

Figure 19: Illustration of different possibilities for the self-assembly of supramolecular dendritic polymers, ranging from supramolecular spherical dendrimers, supramolecular dendronized linear polymers, supramolecular hyperbranched polymers, supramolecular dendritic-linear and dendritic-dendritic copolymers to supramolecular dendritic multiarm copolymers[8]. Reprinted with permission from R. Dong, Y. Zhou, X. Zhu, *Accounts of Chemical Research* 2014, *47*, 2006-2016; Copyright (2014) American Chemical Society.

The overview on supramolecular dendritic polymers given in this thesis is limited on some striking examples of the formation of supramolecular dendrimers.

The use of supramolecular binding motifs to form dendritic structures and dendrimers has several advantages over classical entirely covalently bound dendrimers. For one it can simplify the synthesis process, because larger dendrimers can self-assemble from smaller covalently bound substructures, which are more easily synthetically accessible. Moreover the implementation of supramolecular reversible non-covalent bonds adds interesting properties such as responsiveness to external stimuli to an already unique structure that is a dendrimer, which can lead to new promising applications.[8] However, many applications especially biomedical applications require smart materials which are stable in aqueous media, so the choice of a suitable supramolecular binding motif is crucial.

There are basically two ways to design self-assembled dendrimers. The first option is to use a template as a core unit around which dendrons assemble and form a dendrimer. This template can be a specially designed molecule, metal ion or a nano-particle. It is also possible to design and

functionalize a dendron or branching monomers in a way that they can form untemplated dendrimers. Both options are illustrated in Figure 20.

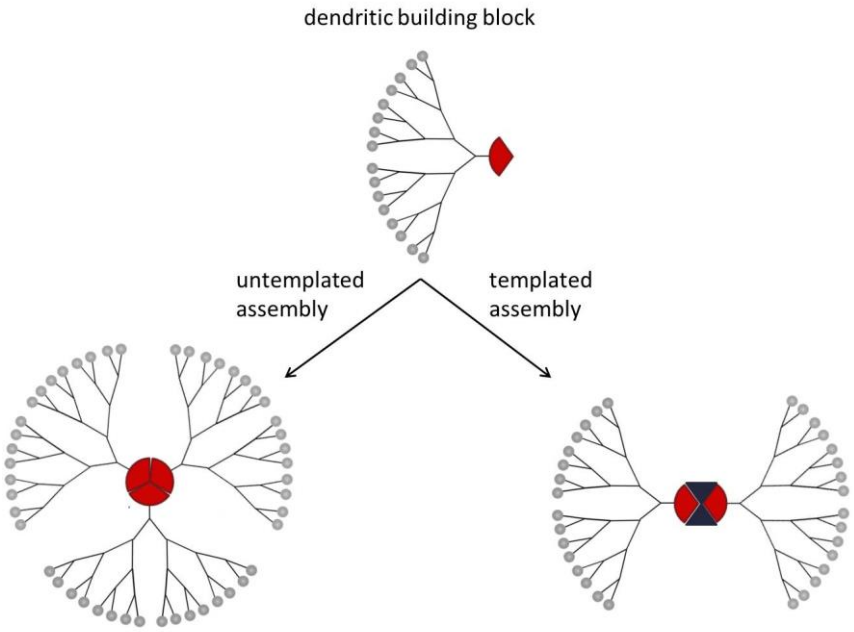

Figure 20: Schematic illustration of the untemplated and templated self-assembly of functionalized dendritic building blocks[51]

2.2.4.1 Untemplated supramolecular dendrimers

The untemplated formation of supramolecular dendrimers is a powerful strategy for generating well-defined dendrimers from mono-functionalized dendrons with self-complementary units, which guarantees structural accuracy while eliminating steps from the conventional multistep synthesis approach.[8]

A typical example for supramolecular untemplated dendrimers are the hexameric dendritic structures developed by Zimmerman *et al.* as shown in Figure 21.[52] They developed a hexameric disk shaped dendrimer using two isophthalic acid units attached to a rigid aromatic spacer as the binding motif. This binding side could then be connected with Fréchet-type dendrons of different generations (generation 1 to 4). While the self-assembly of smaller dendron resulted in a linear architecture, it was observed that the self-assembly of higher generation dendrons form hexameric structures. However, this kind of supramolecular dendrimers had a major drawback as they showed a low stability even in moderately competitive solvents such as THF.[53]

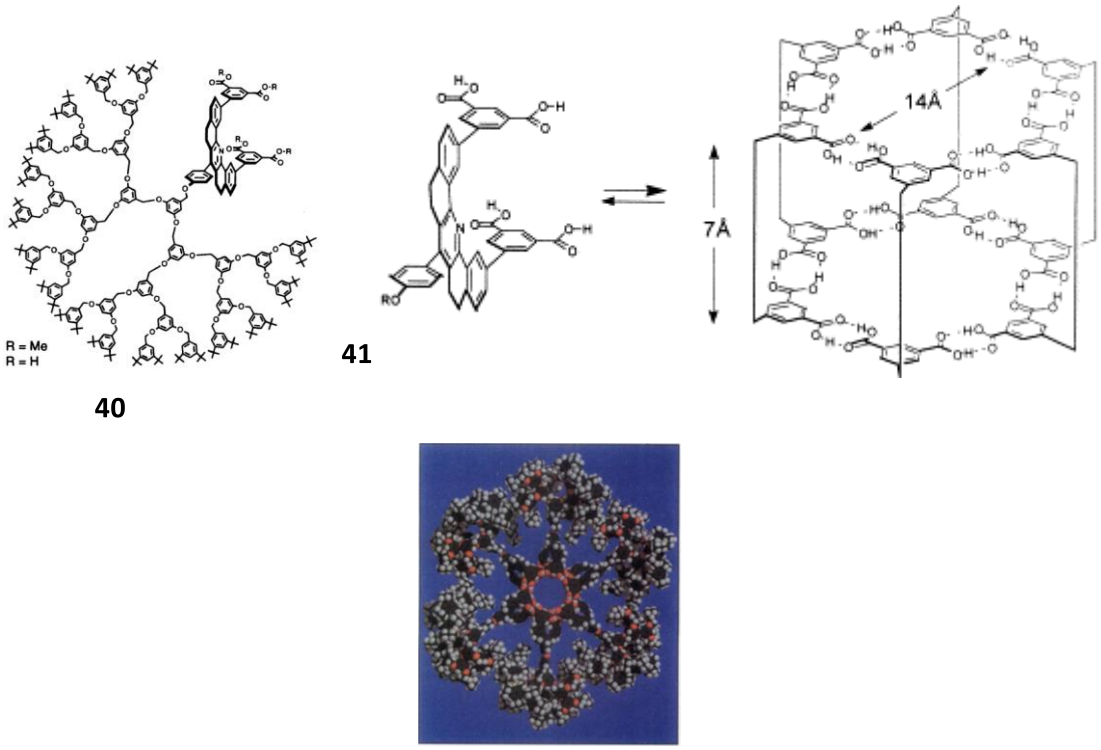

Figure 21: Fréchet-type dendrimer functionalized with a binding motif consisting of two isophthalic acid units attached to a rigid aromatic spacer (top, left); formation of hexameric disk shaped dendrimer by the binding motif (top, right); molecular modeling of a disc shaped 4th generation dendrimer(bottom).[53] Picture reprinted with permission from Zeng FW, Zimmerman SC, Kolotuchin SV, Reichert DEC, Ma YG, *Tetrahedron* 2002, 58(4): 825-843; Copyright © 2002 Elsevier Science Ltd, all rights reserved and Zimmerman SC, Zeng FW, Reichert DEC, Kolotuchin S, *Science* 1996, 271(5252): 1095-1098; Copyright © 1996, American Association for the Advancement of Science.

To achieve a better stability of the aggregates the binding site was replaced by a self-complementary multiple hydrogen bonding motif based on the H-bond pattern of the guanine-cytosine base pair (Figure 22).[54] This binding motif allowed the hexamer formation even in a 15 % aqueous THF solution and could be confirmed by studies using ^{1}H-NMR, size exclusion chromatography and dynamic light scattering. The stability of the hexamer is dependent on the size of the dendron, increasing with the size of the dendron whereas the biggest dendron used was the third generation.[54]

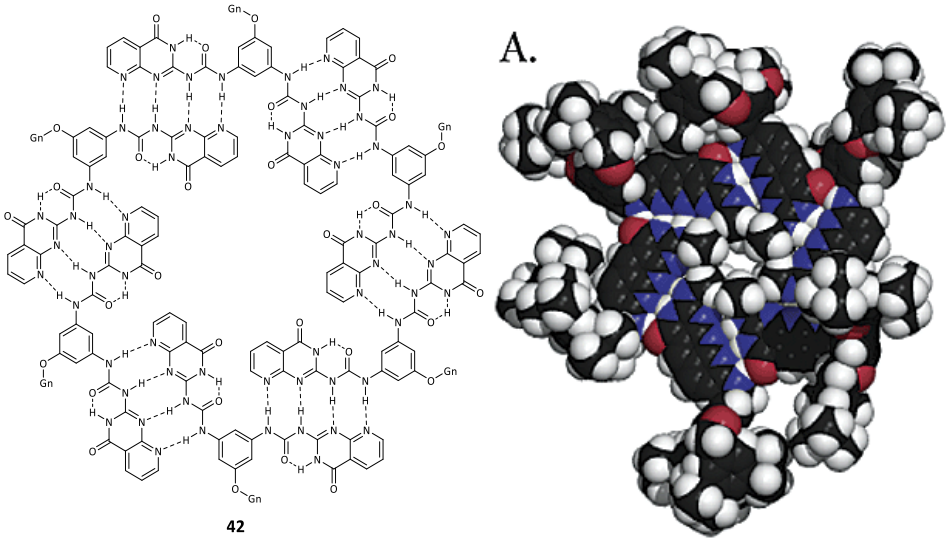

Figure 22: Hexameric dendrimer based on the assembly of a self-complementary multiple hydrogen bonding motif based on the H-bond pattern of the guanine-cytosine base pair; Left: chemical structure of the self-complementary binding motif; right molecular modeling of the 1st generation dendrimer; molecular modeling reprinted with permission from Ma Y, Kolotuchin SV, Zimmerman SC., *J Am Chem Soc* 2002, 124(46): 13757-13769. Copyright 2002 American Chemical Society.[54]

Another example for an untemplated supramolecular dendrimer is illustrated in Figure 23. Fréchet-type dendrons are functionalized at the focal point with complementary derivatives of melamine and cyanuric acid to form a reversibly self-assembled dendrimers based on hydrogen bonds.[55] However, the dendrimer formation is again limited to dendrons of lower generations, due to steric reasons.

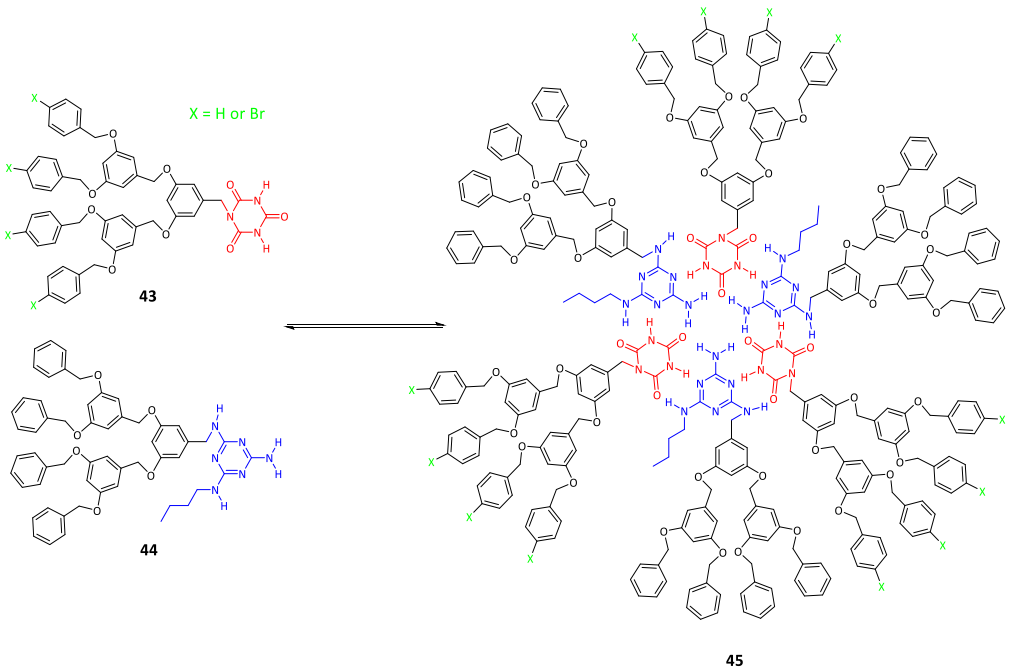

Figure 23: Unsymmetrically self-assembled Fréchet-type dendrimer using complementary derivatives of melamine and cyanuric acid as binding motif[55]

A more recent example of the formation of untemplated supramolecular dendrimers was reported by Schmuck and Merschky *et al.* in 2010. By functionalizing the focal point of polyglycerol dendrons (1st to 3rd generation) with the 5-(guanidiniocarbonyl)-1*H*-pyrrole-2-carboxylate zwitterion as the binding motif, it was possible to form highly stable supramolecular dendrimers in water. The dendrimer formation and the pH-switchability of these dendrimers were confirmed by ^{1}H-NMR, DOSY-NMR, GCP and dynamic light scattering.

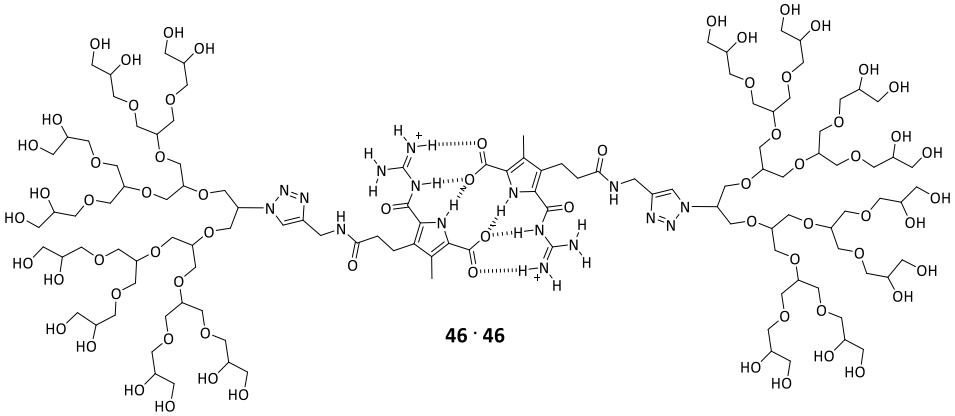

Figure 24: A supramolecular and pH switchable 3rd generation polyglycerol dendrimer stable in aqueous media using the 5-(guanidiniocarbonyl)-*1H*-pyrrole-2-carboxylate zwitterion as a self-complementary binding motif[24]

Calculations showed that the dendrons shield the 5-(guanidiniocarbonyl)-*1H*-pyrrole-2-carboxylate dimer from the solvent, creating a less polar micro-environment, resulting in an even stronger binding of the zwitterions compared to the 170 M^{-1} in water for the parent zwitterion.

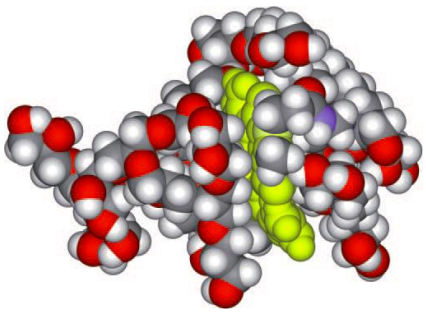

Figure 25: Energy minimized structure of the 3rd generation dendrimer showing that the 5-(guanidiniocarbonyl)-*1H*-pyrrole-2-carboxylate dimer is (highlighted in yellow) shielded by the polyglycerol dendrons, creating a slightly less polar microenvironment.[24] Picture reprinted with permission from Merschky M, Wyszogrodzka M, Haag R, Schmuck C, *Chem-Eur J* 2010, 16(48): 14242-14246. Copyright © 2010 WILEY-VCH Verlag GmbH & Co. KGaA, Weinheim

2.2.4.2 Templated supramolecular dendrimers

The templated design of supramolecular dendrimers allows a predesigned control over the aggregation of the dendrimers, because the choice of the template determines the number and the layout of the dendrons. The templates can be metal ions, nano-particles or specially designed core molecules functionalized with a suitable binding motif.

A prominent example for a metallo-supramolecular dendrimer is the photoactive ruthenium bipyridine $[Ru(bpy)_3]^{2+}$ complex developed by Vögtle et al. in the late 1990s.[56] The bipyridine moieties are functionalized with Fréchet-type dendron up to 3rd generation with either 4'-*tert*-butylphenyloxy or phenyl units in the periphery, shown in Figure 26. The trisbipyridine-type ruthenium complexes lose their salt character with increasing size of the dendron and are soluble in organic solvents only, depending on their peripheral group in THF (4'-*tert*-butylphenyloxy) or acetonitrile (phenyl).

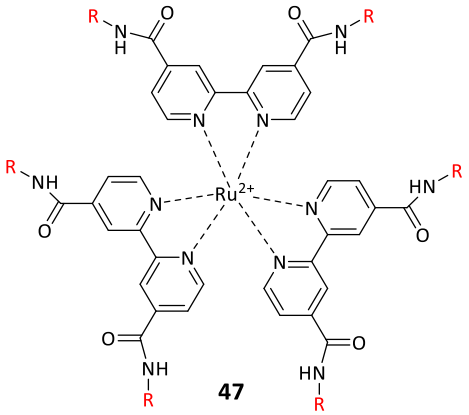

Figure 26: Bipyridine moieties are functionalized with Fréchet-type dendrons up to the 3rd generation and forming supramolecular dendrimers by the formation of trisbipyridine-type ruthenium complexes.[56]

The formation of supramolecular dendrimers is also possible by utilizing host-guest interactions. Gibson *et al.* synthesized pseudorotaxanes by self-organization based on the host-guest interactions of ammonium salt and a dibenzo[24]crown-8 ether. The crown ether is functionalized with Fréchet-type dendron of 1st-3rd generation, while the ammonium groups are located at a tritopic trisphenylbenzene core molecule. These two building blocks self-assemble into discrete supramolecular dendrimers.[57]

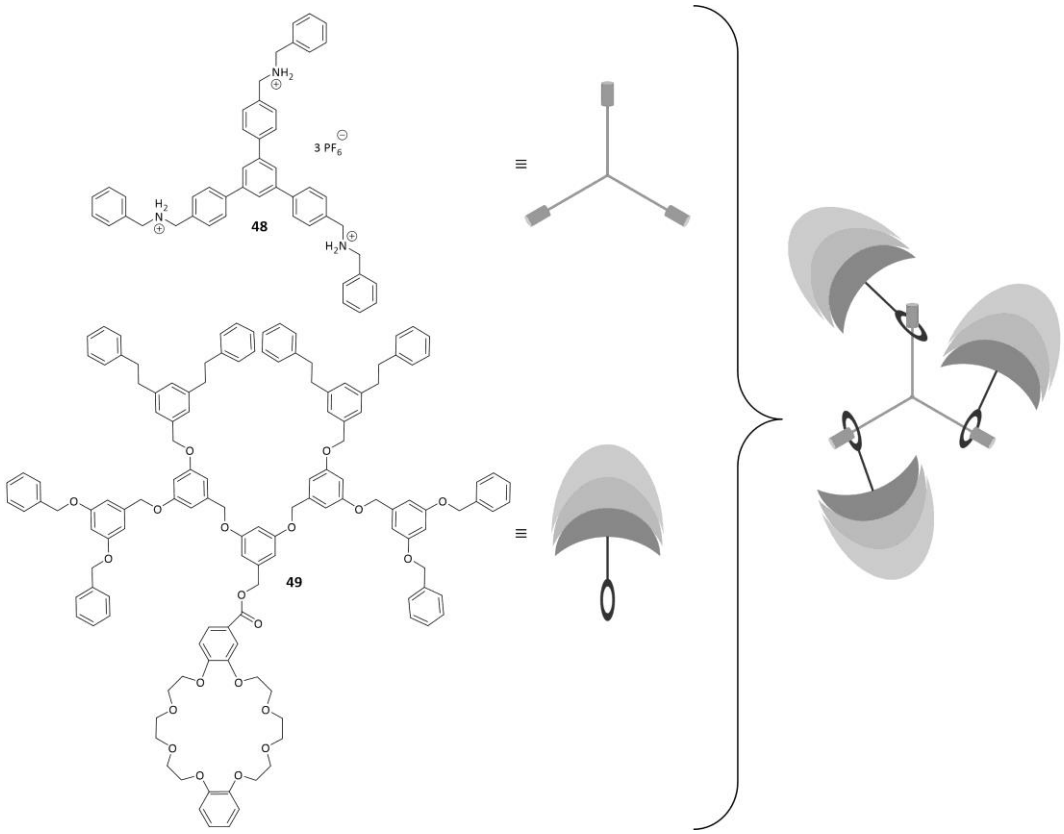

Figure 27: Schematic illustration of the self-organization of pseudorotaxanes based on the host-guest interactions of ammonium salts and dibenzo[24]crown-8 ethers[57]

Another more recent example for a supramolecular dendrimer based on host-guest interactions was developed by *Wu, Zhang, et al.* in 2012. This supramolecular dendrimer is formed based on the interactions of adamantyl functionalized oligo(ethylene glycol) dendrons and a tritopic cyclodextrin functionalized core unit. These dendrimers exhibit thermoresponsive properties at elevated temperatures and are stable in aqueous solution.[58]

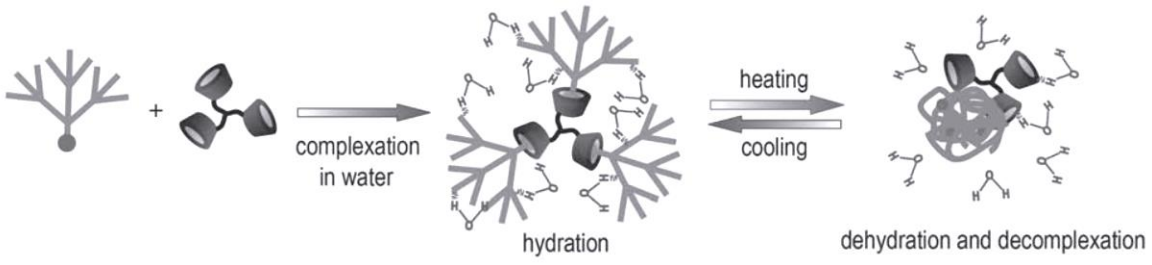

Figure 28:Schematic illustration of the formation of a thermoresponsive supramolecular dendrimer based on the interactions of adamantyl functionalized oligo(ethylene glycol) dendrons and a tritopic cyclodextrin functionalized core unit.[58] Picture reprinted with permission from Yan J, Zhang X, Zhang X, Liu K, Li W, Wu P*, et al., Macromolecular Chemistry and Physics* 2012, 213(19): 2003-2010. Copyright © 2012 WILEY-VCH Verlag GmbH & Co. KGaA, Weinheim

Most designs of supramolecular dendrimers use pre-synthesized dendritic subunits as building blocks. The first supramolecular dendrimers formed by non-dendritic small molecule subunits were developed by *Hirsch et al.*[59] in 2005. The self-assembly is based on the aggregation of a homotritopic core, a heterotopic AB_2 functionalized branching unit and terminal end capping groups, using a combination of the Hamilton receptor and a cyanuric acid derivative as a complementary binding motif based on multiple hydrogen bonding. Simply mixing a core with defined amounts of branching units and end caps leads to completely self-assembled supramolecular dendrimers. This way dendrimers could be obtained in different generations and they exhibit a uniform size and perfect globular shape.

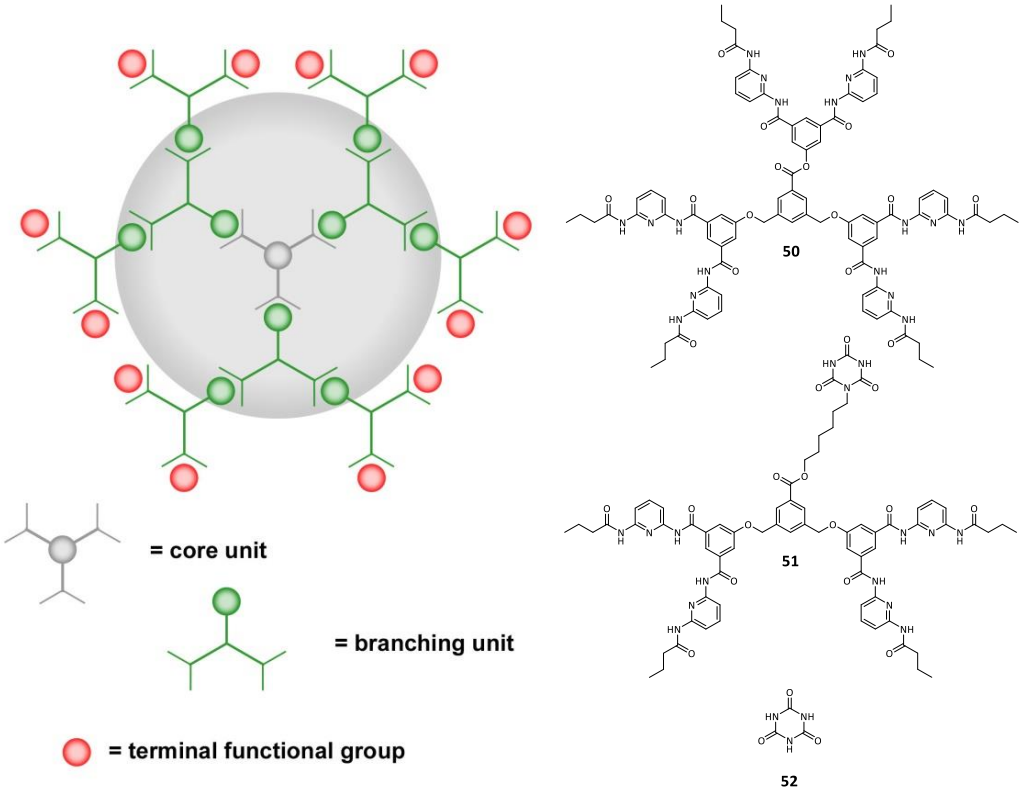

Figure 29: By Hirsch et *al.* developed supramolecular dendrimer based on the self-assembly of a homotritopic core 50, a heterotopic AB_2 functionalized branching unit 51 and terminal end capping groups 52[59]

Since the formation of these dendrimers is not controllable, dendrons with defects can form as well. To avoid the formation of defects, new approaches with orthogonal binding motifs were developed. In these approaches the combination of the Hamilton receptor/ cyanuric acid system with either a metal-coordination[60] or a complementary ADDA/DAAD hydrogen bond pattern[61] was used.

Because of their well-defined, unique architecture, dendrimers are interesting and promising scaffolds for a variety of applications particularly in the biomedical field, which will be discussed in the next chapter.

2.2.5 Applications of Dendrimers

The enhanced solubility compared to a linear polymer of analogous molecular weight is only one example of how the highly and regularly branched, almost globular structure of dendrimers results in numerous interesting and advantageous properties contrasting those of linear polymers. These properties can be utilized for many applications.[36] The controlled stepwise synthesis of dendrimers allows controlling details of the core, interior and periphery and to specifically tailor the physical, chemical or biological properties. This way the resulting monodisperse macromolecules can function as synthetic analogues of peptides or polynucleotides. Monodispersity and the controlled composition of dendrimers has been one of the key factors which made dendrimers interesting for biomedical research. They allow the investigation of structure activity relationships. Since the actual composition of the macromolecule is known it is possible to relate the biological activity to specific aspects of the structure. This is a powerful tool for fundamental research in drug and medical device development.[7]

Another important key feature of dendrimers is the multivalency especially in combination with the globular shape. As described before, the number of surface groups is increasing exponentially with every generation. This is not only important for the enhanced solubility but also the modification of those surface functional groups can add interesting properties to the dendrimer. For example the attachment of ligands for certain receptors onto the surface of a dendrimer, makes the dendrimer a potent targeting molecule for biologic targets that shows enhanced binding.[7,62,63] Another key feature is the possibility to encapsulate guest molecules within the interior of the dendrimer, allowing applications like solubility enhancement of poorly water-soluble molecules and drug delivery.

Dendrimer applications have been under development in various fields[3], for example metallo-dendrimers in catalysis[64-66] and dendrimers in organocatalysis[67-69] or in photophysical applications e.g. as highly efficient dendritic OLEDs[70]. Yet, most applications of dendrimers lie within the biomedical field. Dendrimers are current subject of research in the development of novel antimicrobial or antiviral drugs.[71-74] Furthermore dendrimers found their way into tissue engineering[7,75-77], as molecular glues, into magnetic resonance imaging[3,78-81] and as vectors in gene transfection[82-84]. Moreover dendrimers are utilized as bio sensors[3] and in drug delivery. The last one is a major field of research and substantial part of this work. Dendrimers as drug carriers and drug delivery in general will be discussed in detail in the following chapter.

2.3 Drug Carrier

2.3.1 Introduction

Many potential as well as established drugs in particular chemotherapeutic agents are poorly water-soluble, hydrophobic small molecules. This implicates not only the obvious limitations caused by the solubility issues but also degradation and fast metabolism of these drugs are factors that have to be taken under consideration. Moreover, the drugs can circulate to most tissues in the body including healthy cells, which is in particular problematic concerning chemotherapeutics, as they are designed to kill (cancer) cells. This can lead to severe side effects. A suitable drug carrier system could overcome those problems by encapsulating a drug and deliver it to specific regions in the body and hence reduce the systemic toxicity of drugs. This drug carrier should also be able to prevent the fast metabolism of a drug. Free drugs incorporated in the blood stream are quickly filtered and removed by the kidneys. A carrier system with a size larger than 5 nm is above the renal threshold and will likely remain longer in the bloodstream.[7]

In case of the delivery of anti-cancer agents the enhanced permeation and retention effect can be used as passive targeting method for tumor tissue as a three-dimensional target for the drug delivery. Fast growth of cancer cells leads to disordered cell barriers and hence hyper permeability of tumor vasculature. Additionally, tumor tissue shows only poor lymphatic drainage. This results in passive accumulation and increased retention of macromolecules in the tumor.[7,85,86]

So the development of suitable drug carriers systems capable of solubilizing a drug, protecting it from fast metabolism and delivery of the drug to a specific side and a subsequent controlled release is a matter of biomedical research for many years. There is a variety of different drug carriers, starting from inorganic nano-particles e.g. gold nano-particles[87-89] or nano-porous nano-particles like zeolites[90-92] to a broad spectrum of organic carrier systems. Organic carrier systems include micelles[93,94], emulsions[94,95], nanogels[96], hydrogels[94,97] and vesicles[94,98,99] formed by polymers, surfactants or lipids.

Because polymers have shown great promise in the development of anticancer drug delivery systems,[100] the application of dendrimers, with their unique architecture and properties, in this area is particularly interesting.

2.3.2 Dendrimers in Drug Delivery

Dendrimers are promising scaffolds for drug delivery[101] due to their architecture, both the core region and the shell can be utilized for drug delivery, either by encapsulation of the drug guest molecule in the interior of the dendrimer or by the covalent formation of dendrimer drug conjugates at the outer shell (dendrimers as pro-drugs).[7,101]

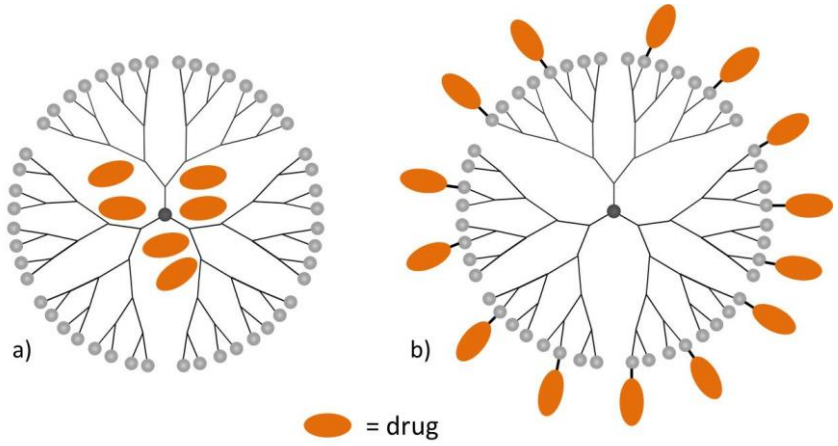

Figure 30: a) Encapsulation of small guest molecules within the interior of a dendrimer; b) Dendrimer-drug conjugate[4]

The leading principles for the use of dendrimers as delivery vehicles involve the charge of the terminal groups which should be neutral or negative in order to avoid or minimize toxicity, the design of the molecular architecture to optimize the pharmacokinetics and very good water solubility. Moreover variability in the size and architecture toward optimization of cellular internalization and passive accumulation in damage tissues or the possible use of targeting groups such as folic acid, peptides, monoclonal antibodies or glycosides, that can bind specifically to the receptor targets overexpressed on cancer cells.

The most commonly used dendrimers are PAMAM[102] dendrimers, but also other dendrimers including PPI dendrimers, polyarylether dendrimers, polylysine dendrimers, polyester dendrimers and polyglycerol dendrimers are widely used. For the right choice of a suitable dendrimer the biocompatibility, toxicity and the water solubility of a dendrimer with the given terminal functionalization has to be taken under consideration.

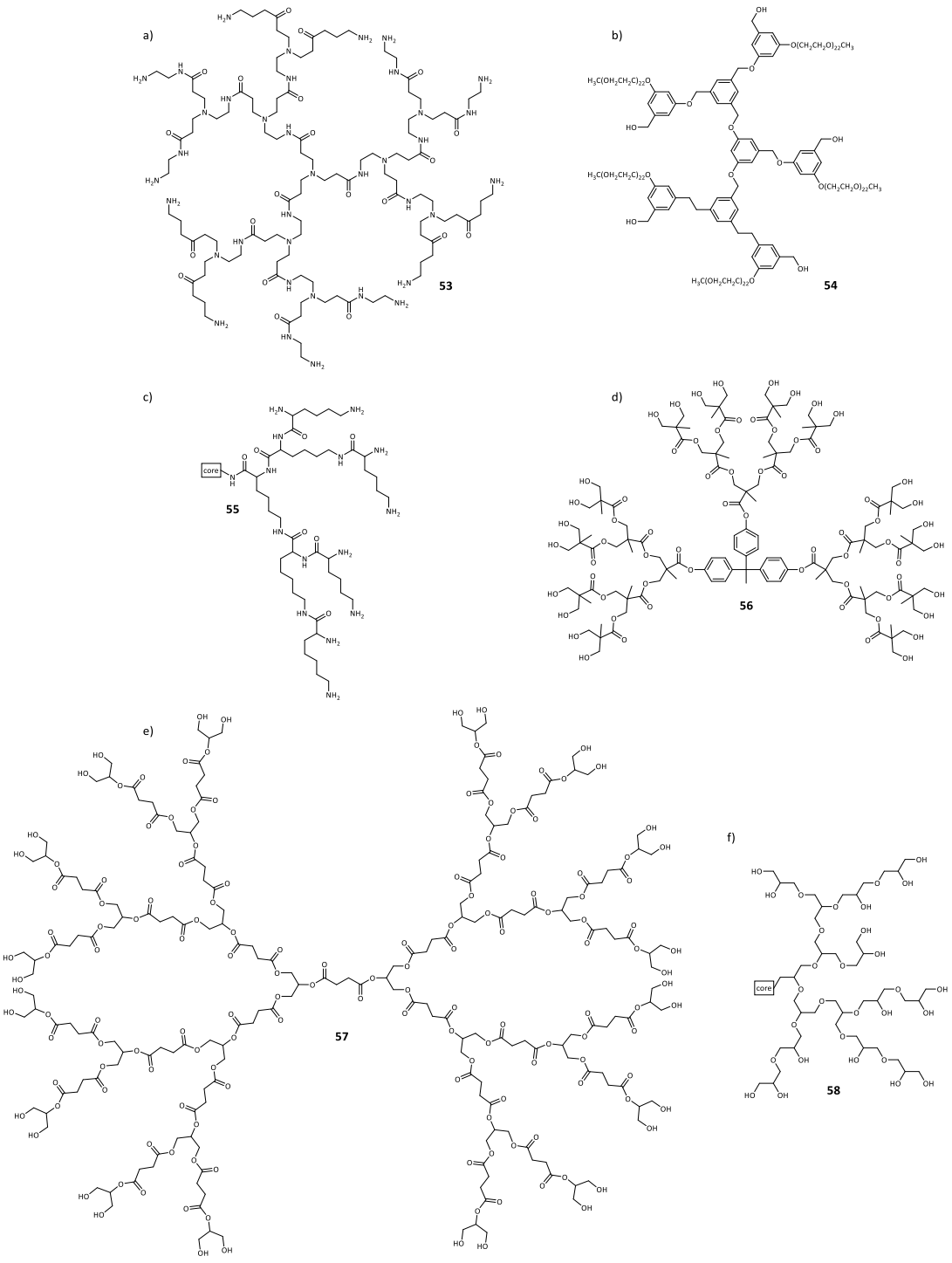

Figure 31: Structures of biocompatible dendrimers that have been tested for drug delivery applications. (a) PAMAM dendrimer. (b) Polyaryl ether dendrimer. (c) Polylysine dendron. (d) Polyester dendrimer based on 2,2-bis(hydroxymethyl)propionic acid. (e) Polyester dendrimer based on glycerol and succinic acid. (f) Dendritic polyglycerol.[101]

Generally, amino-terminated (cationic) dendrimers like PAMAM or PPI dendrimers induce more cytotoxicity, based on cell viability measurements, compared with PEGylated dendrimers and species with OH or anionic (e.g., carboxyl) functionality of the same generation and concentration.[4] The functionalization of dendrimers with PEG is a commonly used approach to avoid toxicity and improve

the water solubility of a dendrimer.[3,103] Another possibility is the use of polyglycerol dendrimers, which are basically branched PEG. These polyglycerol dendrimers are highly water-soluble and several studies have demonstrated the biocompatibility of dendritic Polyglycerols and a potentially safe profile for *in vitro* and *in vivo* applications.[104] Compared to PEG, which is one of the most studied biocompatible polymers, as a benchmark material, polyglycerol dendrimers show very similar properties with respect to the biocompatibility. In preliminary cell culture experiments, hyperbranched polyglycerol with a molecular weight of 5 kDa showed absolutely no toxicity on the cellular level.[104] Moreover dendritic polyglyerols are able to improve the pharmacokinetics and thus the bioavailability by increasing the plasma halftime of the transported active agent, due to low interactions with plasma proteins.[85] The plasma halftime of dendritic polyglycerol is particularly high and increases with molecular weight ranging between 32-57 hours.[105] Low toxicity, high stability and the unique architectural and chemical surface tuneability make polyglycerol dendrimers especially promising candidates as vehicles for solubilization, encapsulation, complexation, delivery, and site-specific targeting of small-molecule drugs, biopharmaceuticals, and contrast agents.

2.3.2.1 Dendrimer-drug conjugates

The conjugation of drugs and dendrimers can be achieved by different approaches. However, the coupling of amines with carboxylic acids is the most commonly used. PAMAM, PPI and lysine dendrimers with amine terminal functionalities are widely used for drug conjugation, making the amide-formation the obvious method. Moreover several further options have been utilized to covalently form dendrimer drug conjugates including the formation of thiourea bonds, reductive amination, alkyne-azide click chemistry, thiol-ene reactions and the formation of degradable linker such as disulfide bridges. Moreover not only the attachment of drugs to the outer functional groups of the dendrimer is possible but also the attachment of targeting groups (folic acid, peptides, monoclonal antibodies, and glycosides) which bind specifically to the receptor targets overexpressed on cancer cells is possible. Dendrimer-drug conjugation has some major drawbacks because it may complicate manufacturing due to additional synthetic steps to connect drug and dendrimer covalently, which can also influence economics, and more importantly complicate regulatory issues. Within the scope of this thesis guest encapsulation of dendrimers will be in focus.

2.3.2.2 Guest encapsulation

Guest encapsulation by dendrimers is one of the key features of dendrimer properties. For drug delivery, the interior pockets of dendrimers can encapsulate drug molecules via noncovalent

interactions such as electrostatic, hydrophobic, and hydrogen-bond interactions. Potential applications for drug delivery were already proposed in the mid-1980s. Newkome went as far as calling dendrimers with a hydrophobic interior/core and hydrophilic shell unimolecular micelles.[5,6] The guest-encapsulating property of dendrimers goes together with their solubilizing properties. Poor or non-water-soluble molecules can be encapsulated by water-soluble dendrimers and hence solubilized in aqueous media. These solubilization properties are dependent on the number of generations of the dendrimer, increasing with higher generations.[4] Moreover, dendrimers with their regular and well-defined architecture can not only be chemically modified at the shell, but also the interior can be tuned to tailor the required properties for successful guest-molecule encapsulation.

Many studies concerning guest encapsulation for solubilization and drug delivery have been done with PAMAM dendrimers, since they are commercially available and water-soluble. Moreover the terminal functional groups can easily be modified. Other suitable and widely used dendrimers for encapsulation studies include PPI, polyether, and polyglycerol dendrimers.[3]

A well-known example is Meijer's so called dendritic box, a PPI dendrimer for which the dendrimer-guest complex is capped by reaction of the terminal amino groups with Boc- or Fmoc protected amino acids for permanent guest encapsulation or subsequent release upon deprotection using formic acid.[106,107]

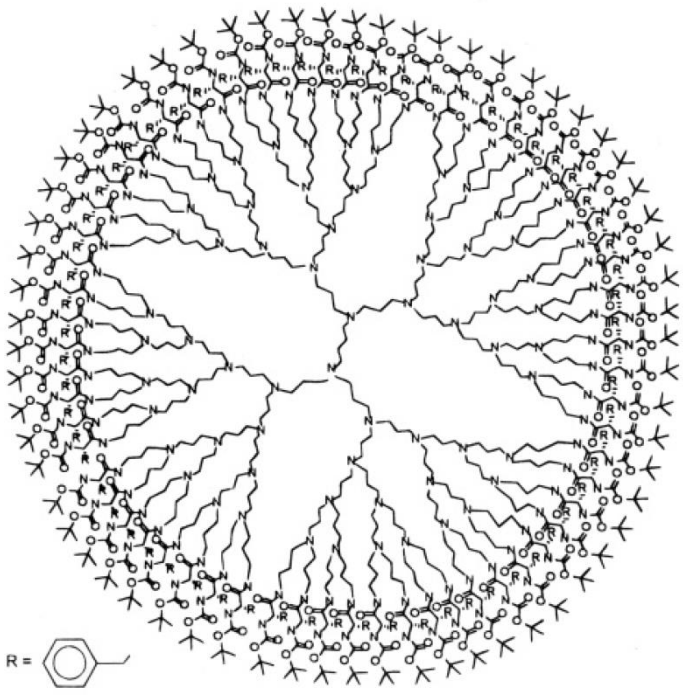

Figure 32: The so called dendritic box, a PPI dendrimer with terminal boc-protected amino acids developed by Meijer *et al.* reprinted with permission from Jansen J, Meijer EW, Debrabandervandenberg EMM., *J Am Chem Soc* 1995, 117(15): 4417-4418. Copyright © 1995 American Chemical Society

Several authors reported studies of guest-molecule encapsulation by different kind of dendrimers. Used guest molecules include small hydrophobic molecules such as salicylic acid and benzoic acid[108], a variety of dyes such as Reichart's dye[109], Bengal Rose[110,111], 4,5,6,7-tetrachlorofluorescein[111] or Nile Red[112] and wide range of drugs[3,113]. One example for a successful drug delivery by encapsulation is a dendrimer based on glycerol and succinic acid, shown in Figure 33. The poorly water-soluble anticancer drug 10-hydroxycamptothecin (10HCPT) was tested for encapsulation by the dendrimer and delivery to various cancer cell lines. The solubilization of 10HCPT in an aqueous solution of the [G4.5]-PGLSA-COONa dendrimer (1.4 $mmol \cdot L^{-1}$) resulted in a 10HCPT concentration of 240 $\mu mol \cdot L^{-1}$. This equates to a 10-fold increase of the 10HCPT concentration compared to the free 10HCPT concentration of less than 25 $\mu mol \cdot L^{-1}$. Using this dendrimer as a vehicle did not only increase the solubility of the active agent but also increased drug uptake by human breast adenocarcinoma (MCF-7) cells by 16-fold compared with the free drug and improved cellular retention of 10HCPT within the cell.[114]

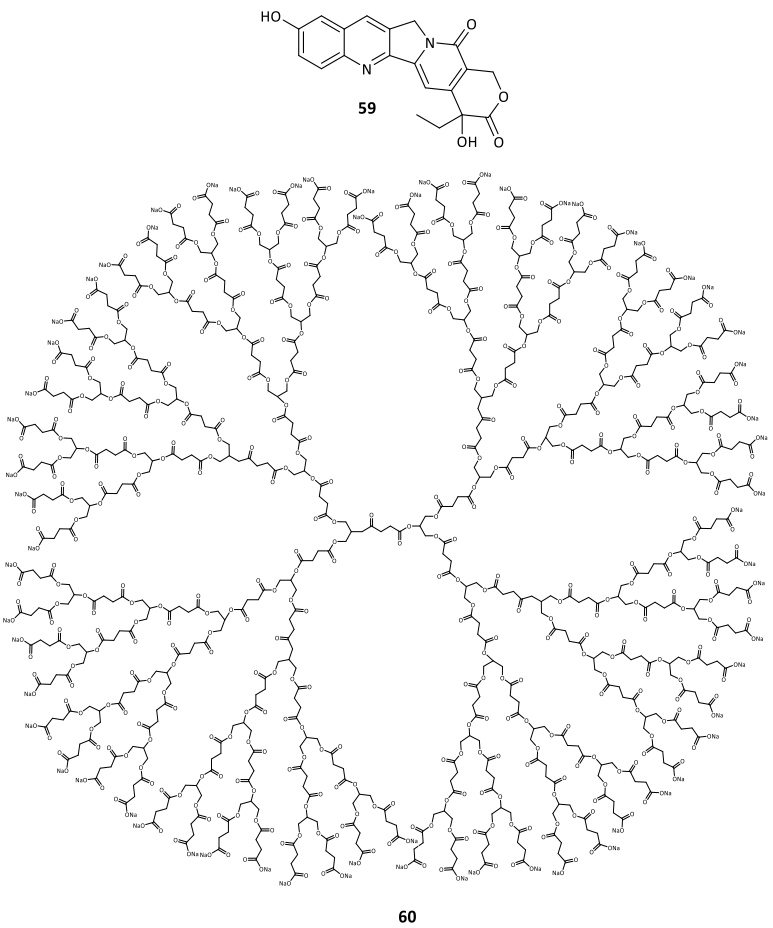

Figure 33: Chemical structure of 10-hydroxycamptothecin (top) and a [G4.5]-PGLSA-COONa dendrimer (bottom)[114]

As already exemplified before dendritic polyglycerols are particularly promising candidates for drug delivery, due to their exceptional biocompatibility. The aqueous solubilization of paclitaxel, a poorly

water-soluble drug widely used for cancer chemotherapy, by perfect dendritic architectures was studied by Park *et al.* in the early 2000s. During the studies the solubilization capacity of generation 3-5 polyglycerol dendrimers was compared to the ability of star-shaped PEGs to solubilize the drug. Results showed higher drug solubilization for the polyglycerol dendrimers, whereas a generation and concentration dependent enhancement of paclitaxel solubility was observed. [G.3], [G.4], and [G.5] polyglycerol dendrimers increased paclitaxel solubility by 270, 370, and 434-fold, respectively, for 10 wt % solutions. Polyglycerol dendrimers, at a concentration level of 80 wt % in water, increased the solubility of paclitaxel by 10000-fold.[115,116] The use of polyglycerol dendrimers for the encapsulation of hydrophobic guest molecules requires the modification of the interior of the dendrimer. Making the interior of the dendrimer more apolar, results in a core-shell architecture, which promises a better encapsulation of the hydrophobic guest molecule.

An example for this approach is the use of dendritic polyglycerols for the encapsulation of different hydrophobic guest molecules as unimolecular micelles based on hyperbranched polyglycerols. These hyperbranched and hence not perfectly shaped polyglycerols are hydrophobically derivatized by the attachment of alkyl chains within the interior of the hyperbranched polymer.[105] The binding capacity for hydrophobic molecules such as palmitic acid depends on the alkyl content in the polymers, which can be easily manipulated by tuning the polymer composition. The synthetic strategy employed for the preparation of these copolymers is flexible; the hydrophobic core can be made bigger by using a larger molecular weight hyperbranched polyglycerol polymer core and attaching more alkyl groups. Kainthan *et al.* tested their suitability as a drug delivery vehicle.[105]

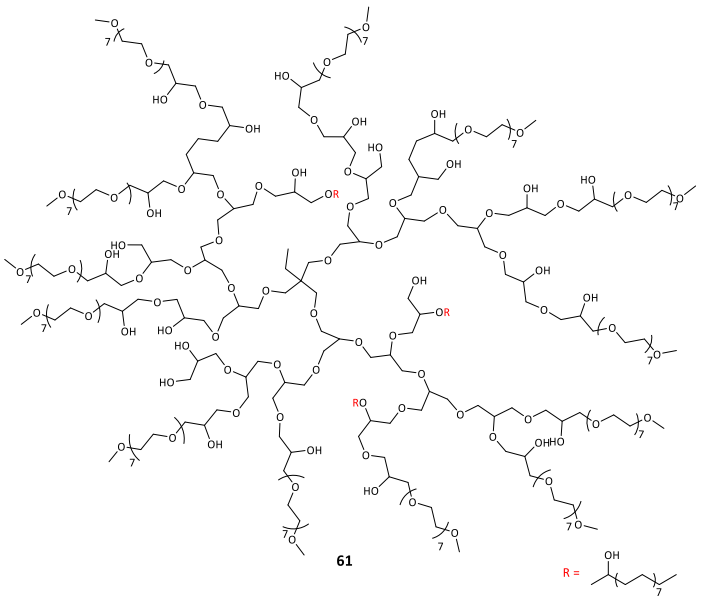

Figure 34: Hydrophobically derivatized place hyperbranched polyglycerol[105]

Further example of dendritic polyglycerols with a more hydrophobic core is a library of several polyglycerol dendrimers with different generations and aromatic cores of different size and shape developed in the working group of Haag. Those core shell architectures were evaluated as solubilizing agents for the hydrophobic dye nile red. First a dendritic triblock amphiphile (Figure 35) consisting of two polyglycerol dendrons coupled to a biphenyl core via amide bonds were studied for their aqueous solubilization abilities of Nile red. Generally one expects the solubilization capacity to increase with higher dendrimer generation, as it could be observed for multiple dendritic solubilization agents. However, a reversed correlation between encapsulation and dendron generation was found in this case. This is due to aggregation of the triblock amphiphiles, rather than a unimolecular encapsulation of Nile red. While the use of larger dendrons would normally enhance the solubilization of Nile red, in this case, an increasing size of the dendrons results in steric hindrance of the formation of higher complexes.[117]

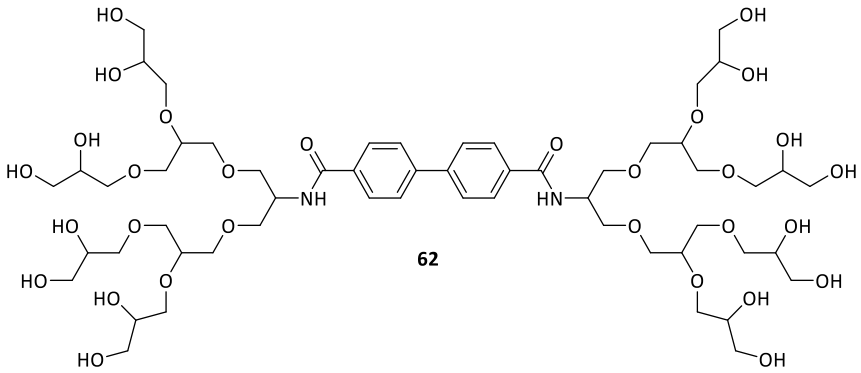

Figure 35: Dendritic triblock amphiphile consisting of two polyglycerol dendrons [G2] coupled to a biphenyl core via amide bonds[117]

A usable property of Nile Red is its solvatochromic behavior, which allows the determination of the polarity of the environment of the dye by measuring the UV-Vis absorption. The results of these UV-Vis measurements revealed a strong redshift of the absorption band for Nile Red with the [G1] dendron complex, with λ_{max} = 620 nm, and a strong blueshift for it in the [G2] dendron complex, with λ_{max} = 462 nm (Figure 36). The first shift corresponds to a highly polar environment, such as the polyglycerol groups, surrounding the Nile Red when solubilized by the [G1]-dendron complex. The latter value for Nile Red absorption indicates a highly nonpolar environment of the dye, such as the biphenyl core, when solubilized by the [G2]-dendron complex. One could assume that the aggregation of the triblock amphiphiles is driven by π-π-stacking of the biphenyl cores, making them unavailable for the Nile red molecules in case of the [G1]-dendron. With increasing size of the dendron the steric hindrance of the formation of higher complexes increases as well, meaning the biphenyl core are better available for the Nile red molecules leading to the observed strong blueshift in case of the [G2]-dendrons.

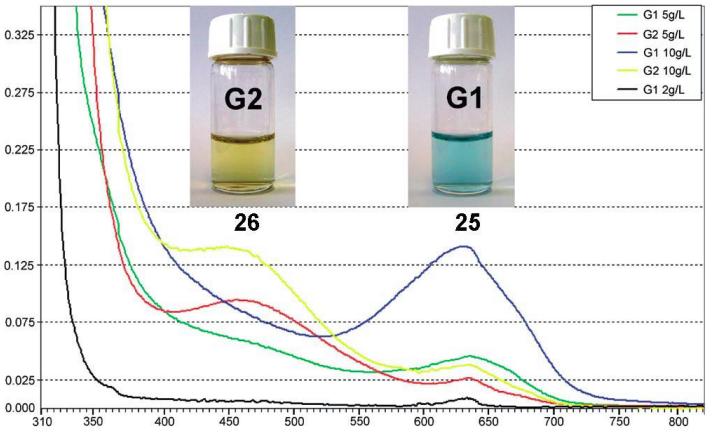

Figure 36: UV-Vis measurements of Nile Red solubilized by [G1]- and [G2]-polyglycerol dendrimers with a biphenyl core; strong redshift of the absorption band for Nile Red with the [G1]-dendrimer complex (λ_{max} = 620 nm) and a strong blueshift for the [G2]-dendrimer complex (λ_{max} = 462 nm).[117] Reprinted with permission from Wyszogrodzka M, Mows K, Kamlage S, Wodzifiska J, Plietker B, Haag R, *Eur J Org Chem* 2008(1): 53-63. Copyright © 2008 WILEY-VCH Verlag GmbH & Co. KGaA, Weinheim

More core-shell architectures were obtained by a click chemistry approach, using the alkyne-azide 1,3-dipolar cycloaddition. Those core-shell architectures consist of differently substituted benzene cores or a 1,3,5-trisphenyl benzene core and polyglycerol dendrons of different generations, illustrated in Figure 37. The studies concerning the solubilization ability of these dendrimers have shown a clear dependency of the size of the dendrons as well as the size of the chosen core. The transport capacity of the dye was significantly improved by expanding the core size which indicates that an extended aromatic core is necessary for efficient encapsulation and transport of hydrophobic compounds. The encapsulation of Nile red was significantly improved by a factor of 200 compared to the previous work using a biphenyl core by enlarging both core and dendrimer size.

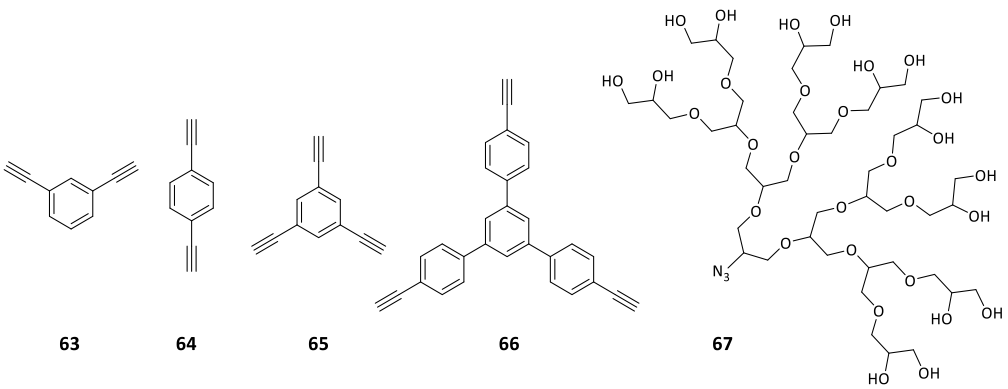

Figure 37: Chemical structures of the used aromatic cores and an exemplary 3rd generation polyglycerol dendron[112]

The dendrimer with 1,3,5-trisphenylbenzene core and [G3]-dendron (Figure 38) showed the best encapsulation properties within this library.[112,118]

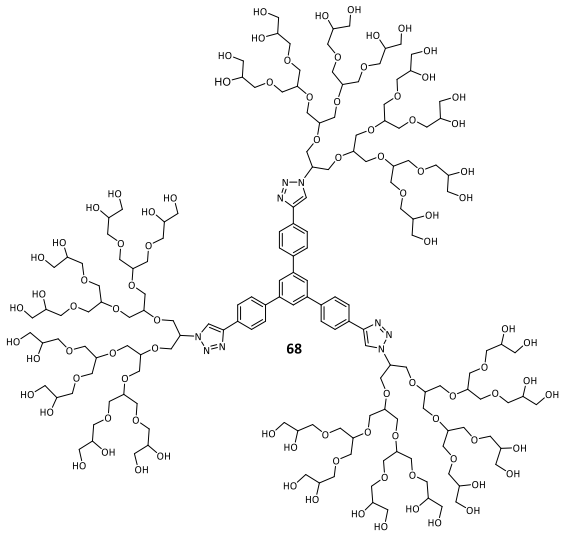

Figure 38: Polyglycerol dendrimer consisting of three [G3]-polyglycerol dendron and the 1,3,5-trisphenylbenzene core showed the best solubilization properties of Nile Red compared to dendrimers with smaller core entities and dendrons of lower generations[112]

The UV–Vis absorption spectra revealed a strong red shift of the absorption band of Nile red with [G.1]-dendrimer complex which suggests the presence of Nile red in a very polar environment, e.g., when it is surrounded by glycerol units. In higher generations, where the maximum absorption was shifted to lower wavelengths, Nile red was likely to be located in the hydrophobic core, resulting in the observed improved solubilization capacities.

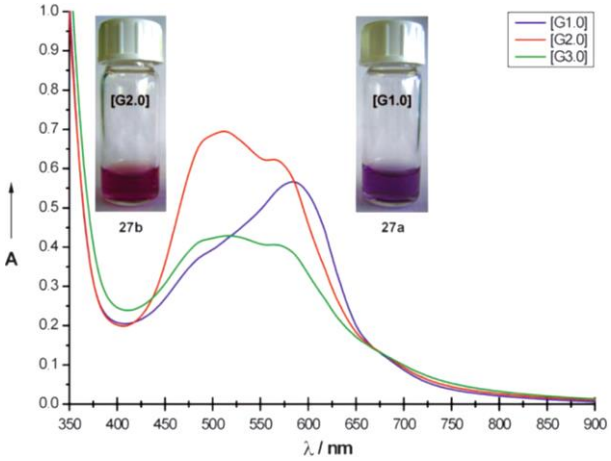

Figure 39: UV-Vis measurements of Nile Red solubilized by the[G1], [G2] and [G3]- dendrimers with the 1,3,5-trisphenylbenzene core; strong red shift of the absorption band of Nile red with [G.1] dendrimer was observed, while the maximum absorption for [G2] and [G3]- dendrimers dye complexes were shifted to lower wavelengths.[112] Reprinted with permission from Wyszogrodzka M, Haag R, *Chem-Eur J* 2008, 14(30): 9202-9214. Copyright © 2008 WILEY-VCH Verlag GmbH & Co. KGaA, Weinheim

There are already several approaches for the successful encapsulation of guest molecules within dendrimers, but the encapsulation of active agents in dendrimers is the first step towards drug delivery. Poorly water-soluble drugs can be solubilized and transported into aqueous media. However, it is mandatory to take release mechanisms into account when designing a vehicle for drug delivery.

2.3.2.3 Controlled release

The encapsulation of active agents in dendrimers is the first step towards drug delivery. Equally or even more important is the release of the guest molecules in a controlled manner. The drug-loading capacity of dendrimers as well as drug release from dendrimers may be controlled by adjusting the physicochemical properties of the dendrons as well as dendrimer generation. One way to influence the release of an encapsulated guest is the modification of the shell by PEGylation. Studies of the influence of different degrees of PEGylation of [G4]-PAMAM dendrimers revealed no significant differences between drug release rates in native and PEGylated PAMAM-G4 systems with 28 % and 34 % of PEGylation, although all systems contribute to delayed release of the drug compared to a non-complexed reference state. In systems with higher PEGylation degrees, the rate of drug release decreases noticeably, which can be attributed to the formation of a conformational cloud by more external PEG chains that mask external charges and lessen internal dendrimer swelling. In systems under study, the release of 60 % of the drug occurs within 2 h of dialysis, whereas 80 % of the drug is released within approximately 4 h.[119] This approach of controlled drug release only allows temporal control, which is beneficial for the administration of e.g. pain killers, because the drug delivery happens constantly and keeps the drug concentration constant and within the therapeutic window over a certain amount of time ensuring the maximum possible benefit derived from the drug.[13]

The precise control of side specific payload release from a dendrimer presents a challenge. To achieve a side specific release, as it is necessary for drug delivery in cancer therapy, stimuli responsive dendrimers can be of great use. These smart polymers are designed to specifically release their guest molecules at targeted regions. They could offer distinct clinical advantages over those dendrimers that release payloads passively. A wide range of stimuli, which can be either endogenous (acid, enzyme, and redox potentials) or exogenous (light, ultrasound, and temperature change) allow great flexibility in the design of stimuli-responsive dendrimers.[120] Acid-responsive delivery systems are the most widely investigated stimuli-responsive systems and well suited especially in cancer therapy, since tumor cells exhibit a more acidic environment compared to healthy tissue. Several strategies exist for the design of stimuli-responsive dendrimers[121] including the preparation of responsive micelles consisting of amphiphilic dendrimers[122] or dendritic polymers for payload

encapsulation, synthesis of self-immolative dendrimers[123] that degrade into small molecules upon exposure to a specific trigger or the attachment of bulky terminal groups like PEG via acid labile linkers. Several approaches use a modified dense shell like Meijer's dendritic box. The dense outer shell is connected to the dendrimer via acid labile bonds and using this pH responsiveness to trigger the release. This principle is illustrated in Figure 40.

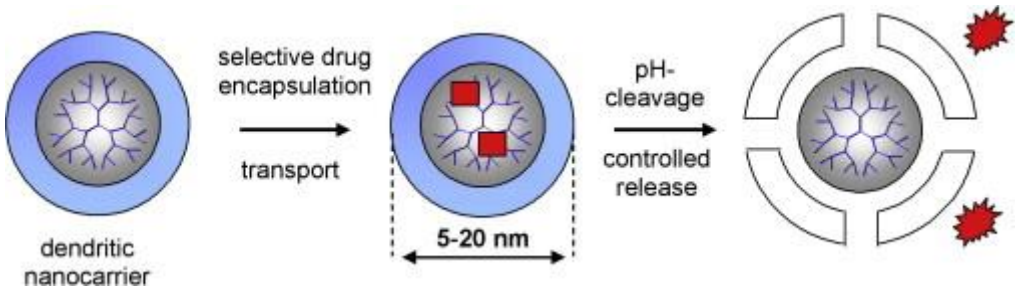

Figure 40: Illustration of the concept to use a dense shell of a dendrimer to obtain a controlled release of the dendrimers payload by pH controlled cleavage of the shell[124]. Reprinted with permission from Haag R, *Angew Chem-Int Edit* 2004, 43(3): 278-282. Copyright © 2004 WILEY-VCH Verlag GmbH & Co. KGaA, Weinheim

As shown in Figure 32 Meijer's dendritic box has a high density at the shell due to Boc-protecting groups as the terminal functionalities, preventing the release of guest molecules from the dendrimer. The cleavage of these Boc-groups by using formic acid or TFA can trigger the release, but requires rather harsh conditions inapplicable for biomedical applications.[107]

Another example for the approach of using a dense shell to control the release of the guest molecule is a core-shell structure where a PEG shell was attached to hyperbranched polyglycerol with a pH-labile linker. The dendritic nanocarriers were prepared by attaching tri-PEGylated benzaldehydes of varying lengths to the hyperbranched PG amine by using pH-labile imine bonds as shown in Figure 41. The designed structures were able to encapsulate the anticancer agent doxorubicin and indotricarbocyanine, a near-infrared imaging dye. It was found that nanocarriers with the shortest PEG chain (n = 4) and a denser shell showed the best encapsulation efficiency (up to 5 molecules/PEGylated polyglycerol). In an early study in nude mice, the doxorubicin nanocarrier could be dosed up to 24 mg kg^{-1} free doxorubicin equivalents as an intravenous administration which was a significant increase in the maximum tolerated dose (MTD) compared to free doxorubicin MTD. Although the pH-triggered cleavage of the PEG shell was confirmed by IR, the high IC_{50} values obtained for three cancer cell lines (3.3–31 mM) may be due to an insufficient release.[125,126]

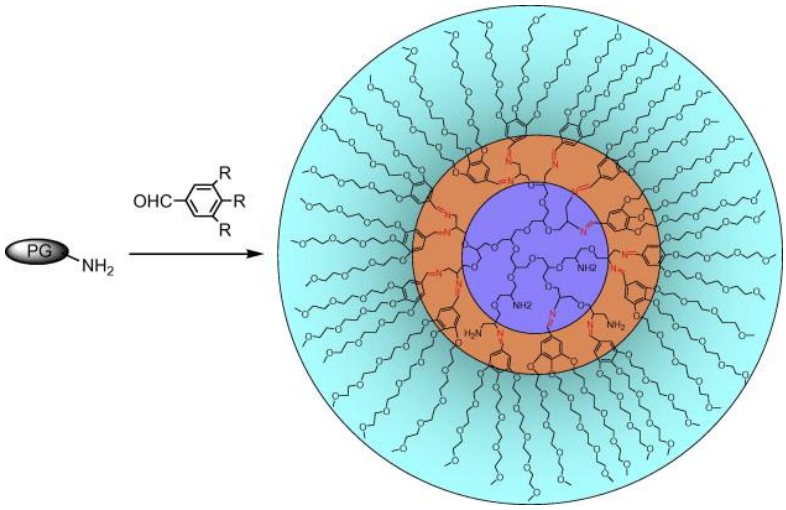

Figure 41: Core-shell architecture consisting of a PEG shell attached to hyperbranched polyglycerol via pH-labile imine bonds[126]. Reprinted with permission from Xu SJ, Luo Y, Graeser R, Warnecke A, Kratz F, Hauff P, *et al.*, *Bioorg Med Chem Lett* 2009, 19(3): 1030-1034. Copyright © 2008 Elsevier Ltd. All rights reserved.

The controlled payload release from a dendritic drug carrier is still greatly challenging. The use of non-covalent supramolecular dendrimers might offer a next step towards controlled payload release, due to the non-covalent and hence stimuli responsive nature of used binding motifs. Since the combination of covalent bound building blocks with non-covalent binding motifs resulting in various nano-assemblies proofed to be highly successful in the development interesting smart materials with promising applications, this approach is highly promising for the development of smart dendrimers in drug delivery. We want to present here a pH-switchable dendrimer for guest encapsulation based on a templated supramolecular polyglycerol dendrimer/core-shell architecture using the guanidinio-carbonyl carboxylate zwitterion as a non-covalent binding motif.

3 PROJECT AND OBJECTIVES

The objective of this work is to synthesize a templated supramolecular dendrimer that is stable in aqueous solution and hence can be investigated regarding its ability to be used as nano transporters in biomedical applications. Classical dendrimers already proved to be a promising class of polymers for applications such as nano-carriers among many others. A supramolecular dendrimer however can be specifically tailored to react on certain external stimuli to obtain a controlled release, whereas the stability in water is challenging using the supramolecular approach.

The concept is a core-shell architecture consisting of both a hydrophobic core entity and a water-soluble dendritic shell, as illustrated in Figure 42. Those entities will be connected via non-covalent interactions formed by a suitable binding motif to allow responsiveness to outer stimuli.

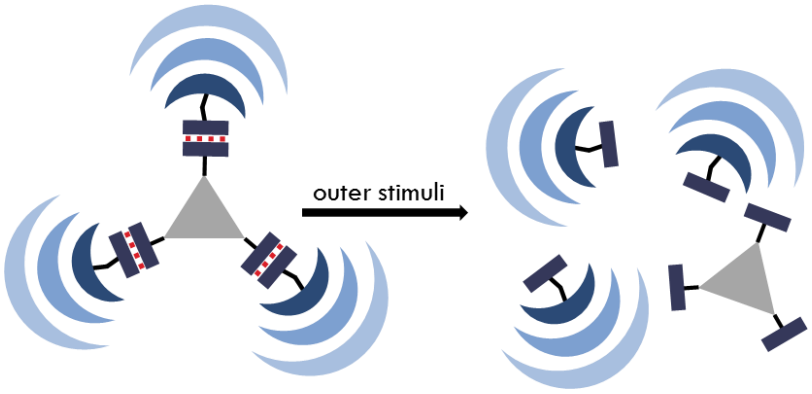

Figure 42: Schematic illustration of the concept to form a supramolecular templated dendrimer consisting of tritopic hydrophobic core and water-soluble dendrons connected via a noncovalent binding motif, allowing responsiveness upon outer stimuli

The key advantage of the setup compared to classical dendrimers is the possibility to embed a hydrophobic core in the center of the dendrimer to improve the encapsulation of hydrophobic, non-water soluble guest-molecules while the dendritic shell can provide the required water solubility. This can be readily achieved in a supramolecular fashion, since the core and the shell components will be functionalized with complementary non-covalent binding motifs, which can be triggered to assemble and disassemble by outer stimuli. So not only the assembly of those core-shell architectures and thus the encapsulation of a guest can be controlled, but also the release of this guest molecule can be triggered by using outer stimuli.

A reasonably sized aromatic entity should be chosen as the template, big enough to provide a hydrophobic center for non-water soluble molecules to non-covalently bind within the core-shell-architecture. However, to retain the overall water solubility of the core-shell-architecture the size of the core should be reasonable. Inspired by the core-shell architectures developed by Haag *et al.* a 1,3,5-trisphenylbenzene entity was chosen as the core. During an investigation of covalently bound core-shell architectures with different aromatic cores for the solubilization of the non-water-soluble dye Nile Red, this core molecule showed the best solubility enhancing properties.[112] The 1,3,5-trisphenylbenzene molecule (Figure 43) offers four benzene rings and three positions that can be easily functionalized for further modification during the synthesis.

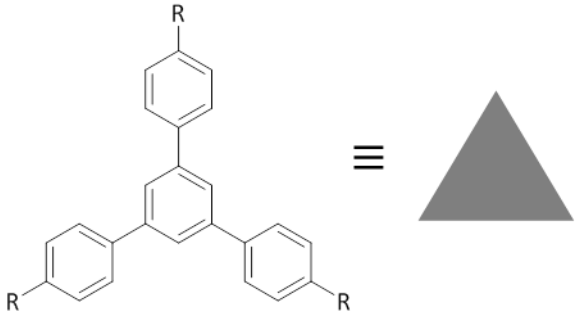

Figure 43: Chemical structure of the 1,3,5-trisphenylbenzene core molecule and the schematic illustration representing this moiety.

The shell of the supramolecular dendrimer should provide the required water solubility and is supposed to shield the core and guest molecule from the aqueous environment. Therefore, it needs to have a certain size, shape and has to be highly water soluble. Moreover it is crucial for the shell molecules to be non-toxic and biocompatible, if the core-shell architecture went into application. An aliphatic analogue of the poly(benzyl ether) dendrimers, the poly(alkyl ether) dendrimers[43,44,127] developed by Fréchet and co-workers in the late 1990s can be a suitable choice as the dendritic water-soluble shell. These architectures are a dendritic analogue of the highly biocompatible poly(ethylene glycol) (PEG), which is a highly promising well studied structural skeleton for many biological applications. Polyglycerol dendrons are also known to be biocompatible and exhibit low toxicity, high plasma halftime and stability.[98,105]

Haag *et al.* modified the synthesis of these polyglycerol dendrons.[112] Successful studies concerning the encapsulation and solubilization of hydrophobic guest molecules have been carried out with Nile Red[105], doxorubicin[120] and palmitic acid[105]. Thus, the shell entity will be consisting of three polyglycerol dendrons, illustrated in Figure 44.

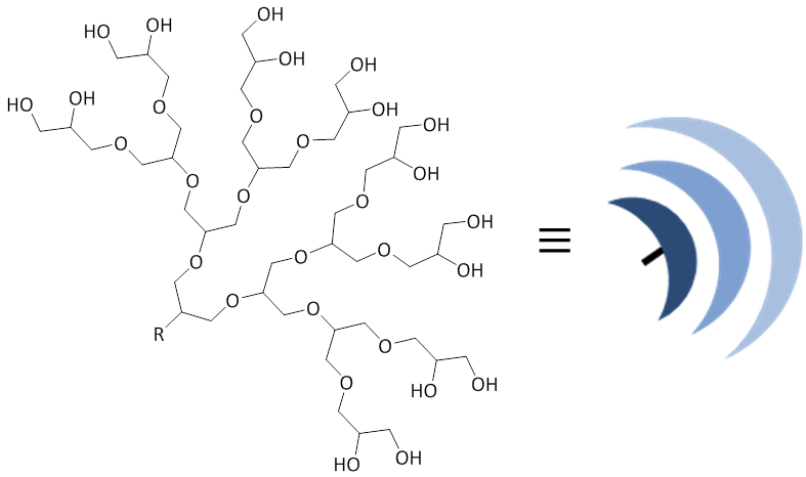

Figure 44: Polyglycerol dendron of the 3rd generation and its schematic illustration

The connection between core and shell is accomplished by non-covalent bonds. As a suitable building block the guanidiniocarbonylpyrrole zwitterion was chosen. It is a self-complimentary binding motif which forms pH-switchable dimers due to the combination of six hydrogen bonds and two ion pairs. The 5-(guanidiniocarbonyl)-1*H*-pyrrole-2-carboxylate zwitterion was developed by Schmuck *et al.* as an evolvement from the 2-(guanidiniocarbonyl)-1*H*-pyrroles[15], which were known for improved oxo-anion binding compared to simple acyl guanidine. By the addition of the carboxylate group in position 5 of the pyrrole ring, a zwitterionic state was possible and these zwitterions could self-assemble into dimers. NMR studies of the zwitterion showed that this particular setup indeed forms discrete dimers.

The major advantage of this binding motif is that the formed dimers are highly stable even in polar solvents such as DMSO ($K = 10^{12}\ M^{-1}$) and water ($K = 170\ M^{-1}$).[18]

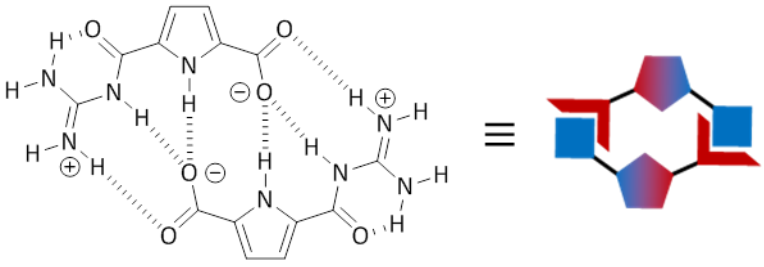

Figure 45: 5-(Guanidiniocarbonyl)-1*H*-pyrrole-2-carboxylate dimer (left) and its schematic illustration

The dimer formation is pH switchable since the zwitterion is only stable at around neutral to slightly acidic pH (pH value around 6). At pH values higher than approximately 8 the zwitterion will be deprotonated thus the anion will be formed. The protonated, cationic form will be present at a pH value below approx. 4 respectively.[15]

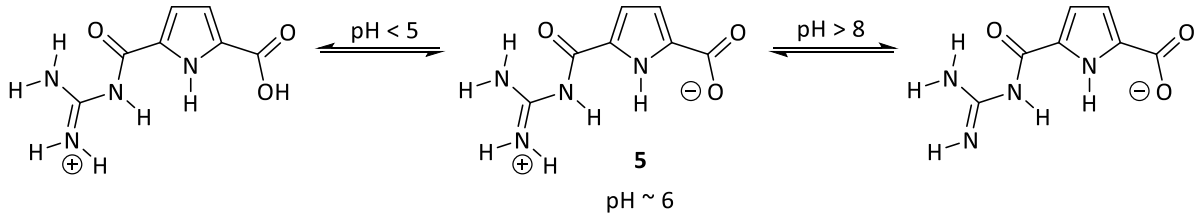

Figure 46: pH dependence of the protonation state of the 5-(guanidiniocarbonyl)-1*H*-pyrrole-2-carboxylate zwitterion; at pH values below 5 the cationic form is present, while at pH above 8 the anionic form exists[15]

The extraordinary stability of the dimer, its pH switchability, in a physiological relevant pH range (around pH 7.4) and the feasible functionalization of the pyrrole ring, allows the formation of higher supramolecular structures and smart materials with possible biomedical applications.

Both the dendritic shell entities and the core have to be functionalized with the 5-(guanidiniocarbonyl)-1*H*-pyrrole-2-carboxylate zwitterion. A suitable method is the Cu(I) mediated alkyne-azide click reaction, which is an easy and convenient reaction requiring very mild conditions and an azido and an alkyne functionality. The combination of the pyrrole zwitterion and polyglycerol dendrons was already synthesized by *Merschky et al.* and their dimer formation was studied.[24] The same synthesis pathway as used by *Merschky et al.* should be used to synthesize the zwitterionic polyglycerol dendrons. Therefore the pyrrole building block will be functionalized with the alkyne moiety by utilizing the carboxylic acid in position 3 of the pyrrole ring for a coupling reaction and the focal point of the dendron will be the azide functionality (Figure 47).[24]

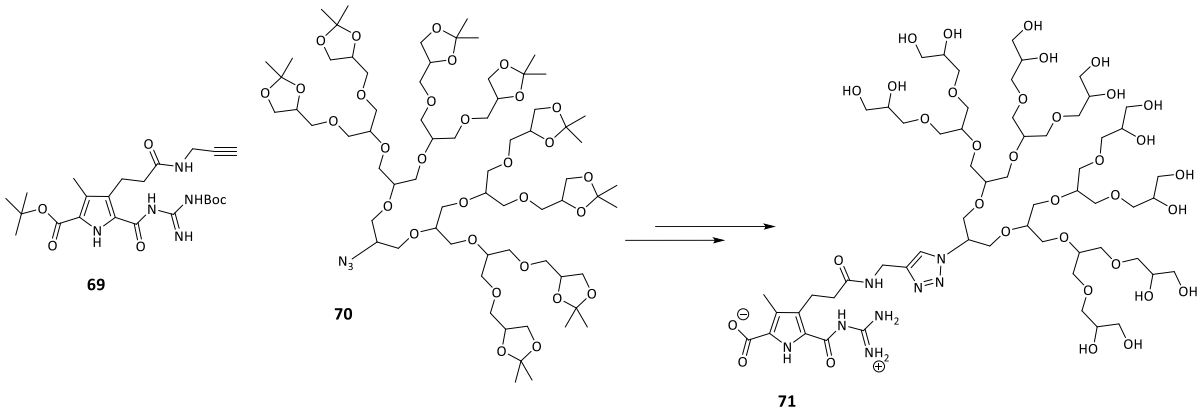

Figure 47: The zwitterionic polyglycerol dendron can be synthesized using the alkyne functionalized pyrrole building block 69 and a polyglycerol dendron (here G3) with a focal azide group ([G3]-N_3)[24]

The azide functionalization on the 1,3,5-trisphenylbenzene core should be easily possible at the three *para* positions. The pyrrole building block will again be functionalized with the alkyne moiety, but the design of the linker needs some modification to shorten its length, as shown in Figure 48.

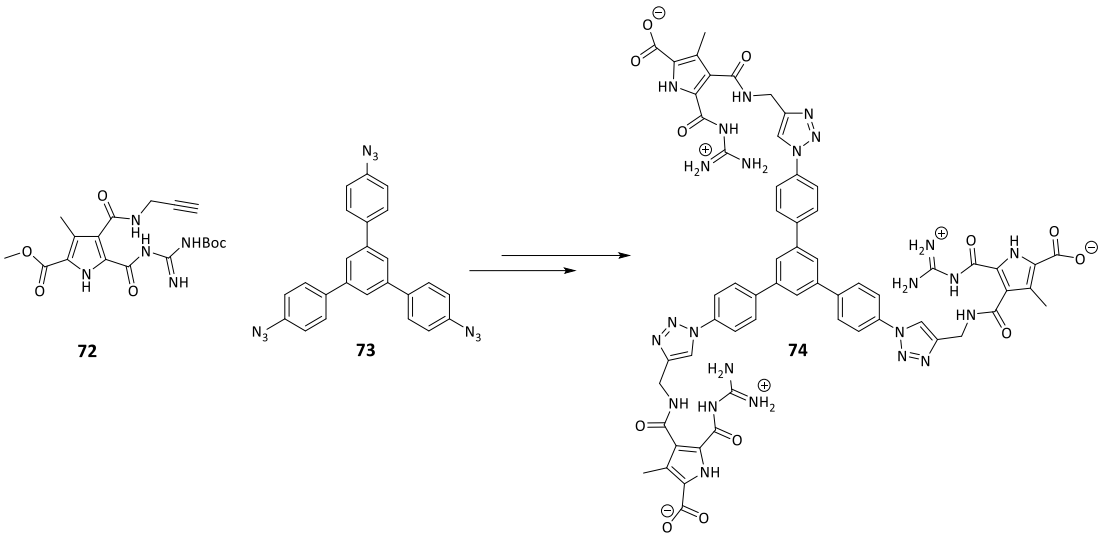

Figure 48: Synthetic setup for the tritopic zwitterionic core molecule 74. The pyrrole moiety is alkyne functionalized whereby the linker between the pyrrole ring and the alkyne group has to be as short as possible. The 1,3,5-trisphenylbenzene core 74 is azide functionalized at the three para positions of the benzene rings

The zwitterionic tritopic core needs to be as rigid as possible to avoid intramolecular interactions between the pyrrole binding motifs, otherwise the formation of intramolecular loops will occur, as has been observed for similar but flexible tris- or quadruple 5-(guanidiniocarbonyl)-1*H*-pyrrole-2-carboxylate zwitterions[28,29]. This intramolecular loop could complicate the formation of core-shell assemblies of the core and the dendrons and can lead to defect structures. The required rigidity can be achieved by choosing a preferably short linker between the pyrrole and the alkyne functionalization. A force field calculation for the chosen setup of this molecule is illustrated in Figure 49 and shows that no intramolecular interactions can occur between the zwitterions.

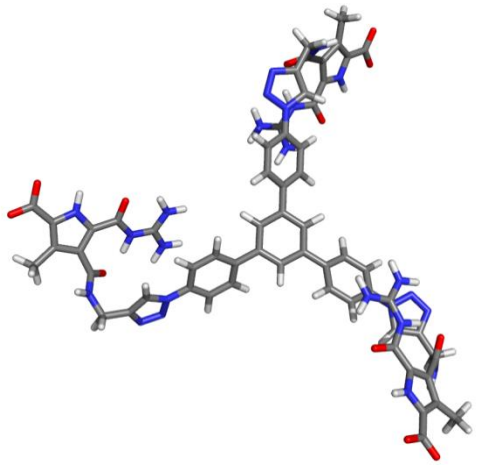

Figure 49: Force field calculations (Maestro) of the tritopic zwitterionic core indication that no intramolecular loops of the zwitterions can be formed due to the rigidity of the chosen linker

Thus the tritopic zwitterionic core molecules are expected to form three-dimensional network like structures (Figure 50) similar to structures observed for the tris- or quadruple-zwitterions.[28,29] However, due to the rigid structure of the tritopic zwitterionic core molecule the formation of network-like structures should already take place at low concentrations as no formation of intramolecular loops is possible.

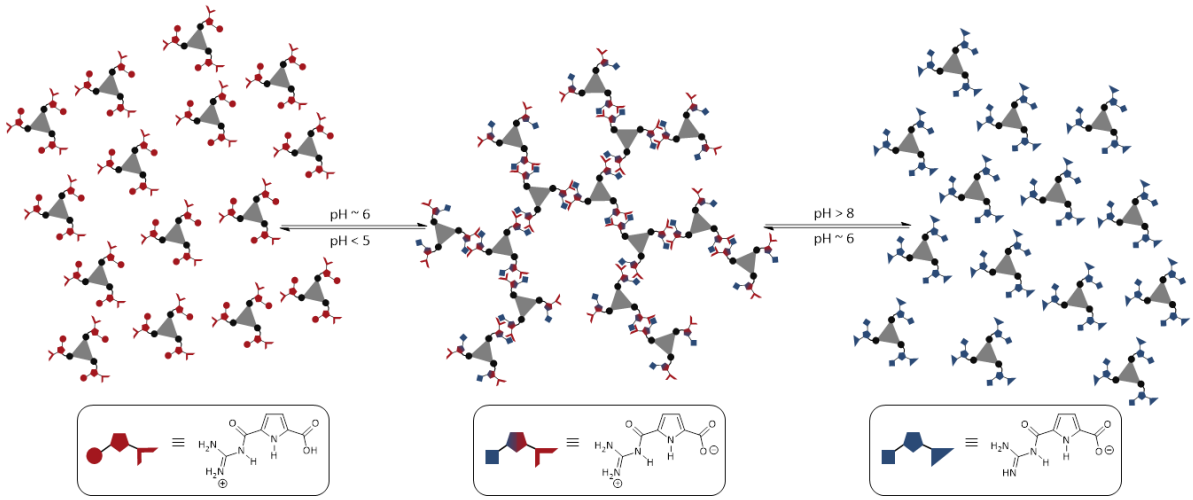

Figure 50: Simplified illustration of the expected three-dimensional networks formed by the trivalent zwitterionic 1,3,5-trisphenylbenzene core (middle) and the reversible destruction of the assembly induced by a pH change below a pH value of 5 or above a pH value of 8

After the addition of the zwitterionic dendrons one tritopic zwitterionic core and three zwitterionic dendrons can assemble into core-shell architectures at around neutral pH, which can be disassembled via changing the pH value above 8 or below 5. This supramolecular templated dendrimer and its pH switchability is schematically illustrated in Figure 51.

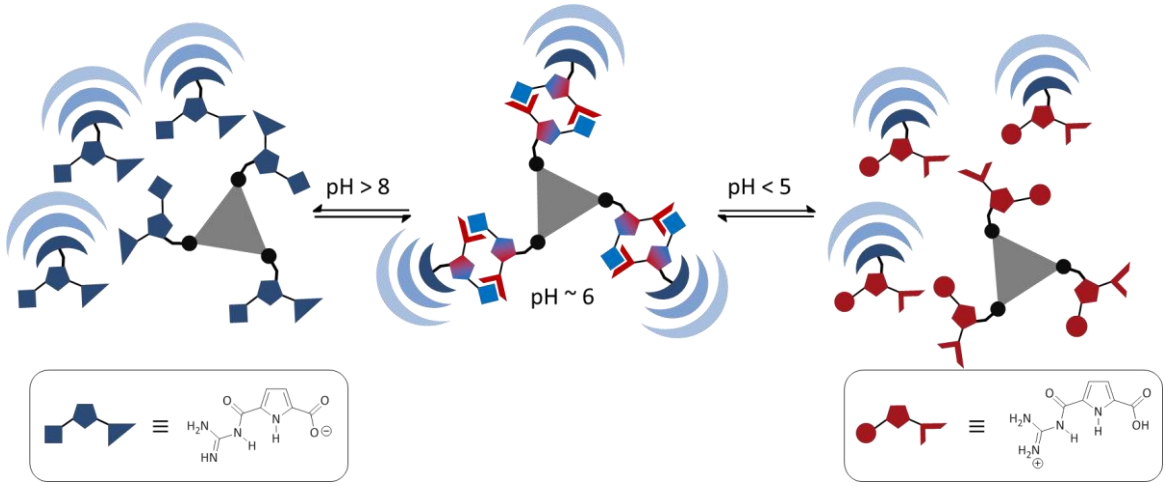

Figure 51: Schematic illustration of the pH switchable templated dendrimer with a hydrophobic core and a highly water-soluble dendritic shell.

The idea behind this project is to study this pH switchable core-shell architecture as a nano-carrier with controlled release for non-water soluble molecules such as cancer drugs. As long as the core-shell architecture does not disassemble it provides a hydrophobic center to attract other hydrophobic guest molecules, whereas the hydrophilic shell provides good water solubility and biocompatibility. As soon as the pH value is changing below 5 or above 8, the ion pairs will fall apart and the whole core-shell architecture will disaggregate resulting in the release of the encapsulated molecule.

4 RESULTS AND DISCUSSION

4.1 Synthesis

The synthesis of the templated supramolecular dendrimer comprises of the synthesis of the zwitterionic template core molecule and the zwitterionic polyglycerol dendrons. For both entities the synthesis of different precursors is necessary, which have to be combined to form these two building blocks. These precursors are the polyglycerol dendrons, the functionalized aromatic 1,3,5-trisphenylbenzene core and the respective pyrrole building blocks. The synthesis of the zwitterionic core and the tritopic zwitterionic core molecule will be discussed in two separate subchapters starting with the dendrons.

4.1.1 Dendron

The following chapter describes the synthesis of the zwitterionic dendron, which was generally performed according to literature protocols from *Haag et al.* (dendron synthesis)[112] and *Merschky et al.* (Synthesis of the zwitterionic dendrons)[24,128], but due to several difficulties during the synthesis and purification, some modifications have been done. Since this synthesis utilized click chemistry, two precursors with both, azide and alkyne functionalization were necessary. The dendron is supposed to carry the azide functionalization at the focal point (Figure 52, **70**), while the guanidiniocarbonylpyrrole carboxylate zwitterion should be functionalized with an alkyne moiety at the carboxylic acid in position 4 of the pyrrole (Figure 52, **69**).[24,128] Figure 52 shows the retrosynthesis of the zwitterionic [G3]-polyglycerol dendron **46**, to give a short overview of the required precursor molecules.

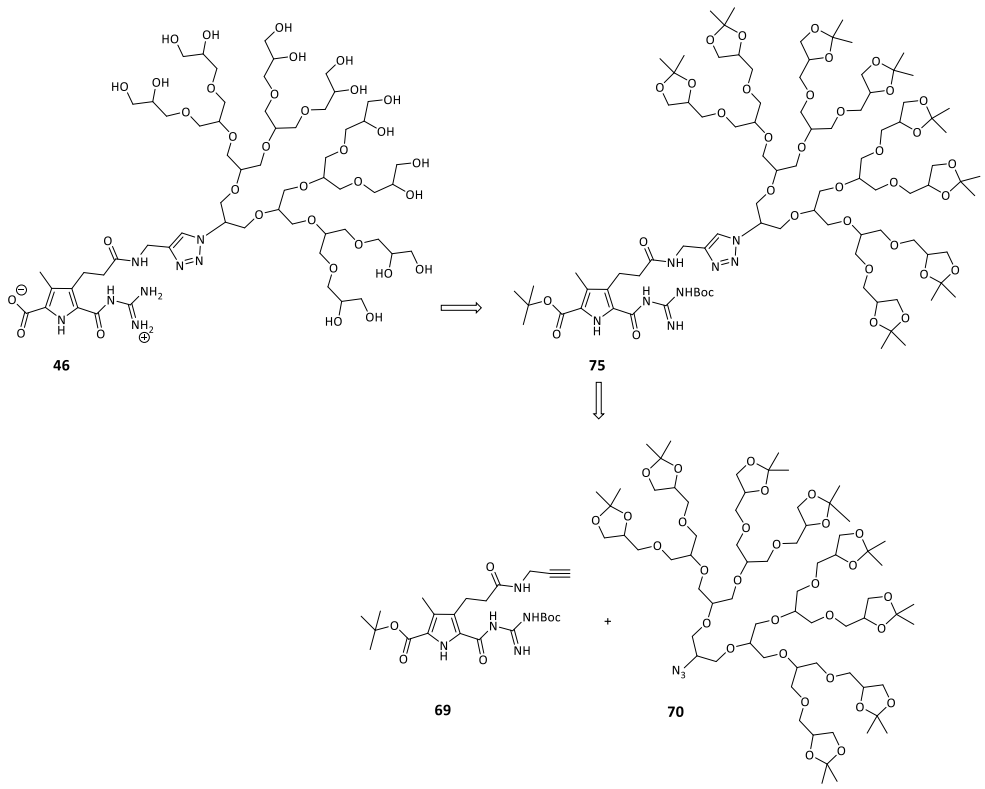

Figure 52: Retrosynthetic illustration of the synthesis of the zwitterionic [G3]-polyglycerol dendron

The first precursor to synthesize was an azide functionalized 3rd generation dendron.[112] The synthesis of the azide functionalized [G3]-dendron **70** was performed in a convergent manner. Figure 53 shows the retrosynthetic pathway of this dendron synthesis.

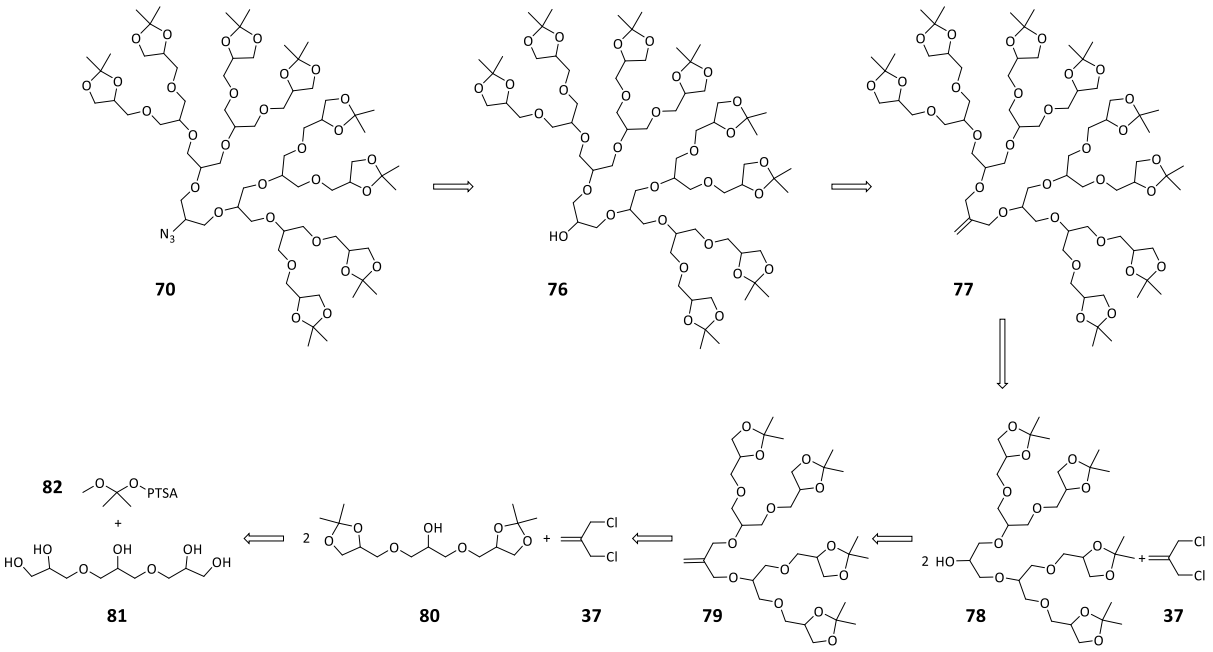

Figure 53: Retrosynthetic illustration of the synthesis of the azide functionalized 3rd generation polyglycerol dendron ([G3]-N_3)[112]

The first step was the introduction of the acetal groups to triglycerol (**81**) to protect the diols. Therefore the synthesis of the dendron started with the commercial available triglycerol and 2,2-dimethoxy-propane as the protective agent in the presence of *p*-toluenesulfonic acid (PTSA). The purification of the crude product in the literature protocol[112] was done via column chromatography with ethyl acetate and *n*-hexane or by HPLC with 15 % 2-propanol in n-hexane. The reaction was done on a 150 g (625 mmol triglycerol) scale. Purification by column chromatography of larger amounts does require large amounts of solvent, which is especially unfavorable when working with *n*-hexane, and can be quite time consuming. Since the product is an oily substance, the purification of the crude product could be done via a fractionalizing distillation (0.2 mbar, 140 °C) instead of column chromatography. The [G1]-OH dendron **80** was obtained with a yield of 65 %, which is within a similar range as the literature value (70-78 %) and is depending on the purity of the commercially available triglycerol, which generally contains 20-30 % other oligomers.[112]

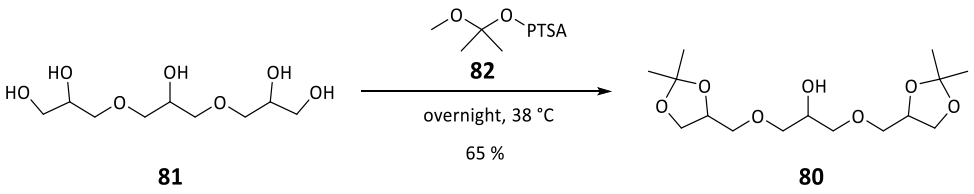

Figure 54: Attachment of the acetal protecting groups to triglycerol yields the [G1]-OH dendron 80

The first generation "jump" followed, in which two [G1]-OH dendrons **80** were attached to methallyl dichloride **37** in a S_N2 reaction, yielding the 2nd generation dendron with a C-C double bond at the focal point ([G2]-ene). This reaction is shown in Figure 55. Pursuing literature protocol, this synthesis step required extensive column chromatography to purify the resulting product. Again the synthesis was done on a multi gram scale (100 g) and chromatography was done with 25 % 2-propanol in *n*-hexane as eluent. For the column chromatography a 50 x 500 mm glass column with SiO_2 and a flow of 60 mL per minute was used. In order to get a decent separation, a maximum of 4 g of crude product per chromatography sequence could be purified, while one sequence lasted 50 minutes. In order to simplify the purification again a distillation of the oily crude product was tested which proved to be an easier and less time and solvent consuming method to obtain a clean 2nd generation polyglycerol dendron ([G2]-ene). The fractionating distillation was carried out under reduced pressure (0.2 mbar; oil pump vacuum) at 160 -185 °C. However, the distillation residue still contained a significant amount of product, meaning that at least a purification of the residue by column chromatography is necessary. The [G2]-ene **79** could be obtained as a colorless oil with a yield of only 60 % after both purification steps. In literature protocol the yield with 94 % is somewhat higher. A possible reason for this could be that *Haag et al.* used HPLC for the purification instead of MPLC. This

might allow a sharper and better separation of the [G2]-ene from any starting material or byproducts especially because the separation was already challenging, due to the similar elution characteristics of the involved molecules. However, purification *via* HPLC in such a multi-gram scale was not applicable with the available preparative HPLC. None the less, the [G2]-ene **79** could be obtained in moderate yields and decent amounts of several grams.

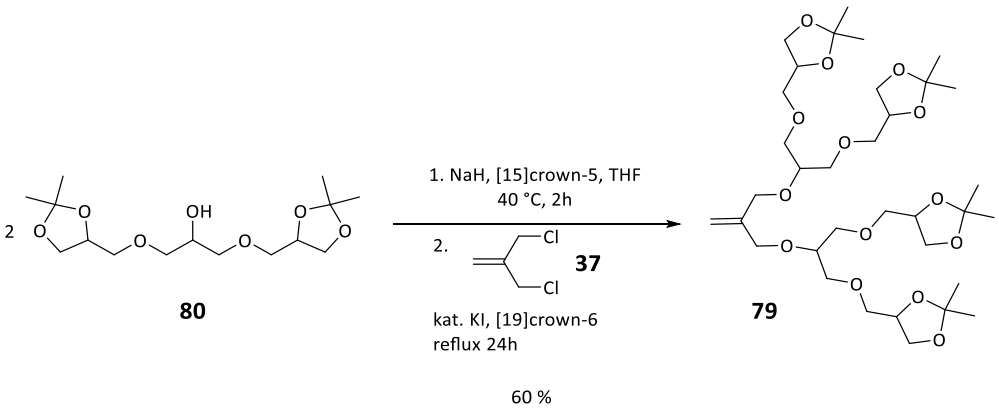

Figure 55: Generation "jump" from the [G1]-OH to [G2]-ene, using methallyl dichloride

The next generation step again requires a hydroxyl group at the focal point of the dendron. The transformation of the "ene" at the focal point of molecule **79** into a hydroxyl group (**78**) was managed according to the protocol by an ozonolysis with a yield of 96 % (Figure 56).

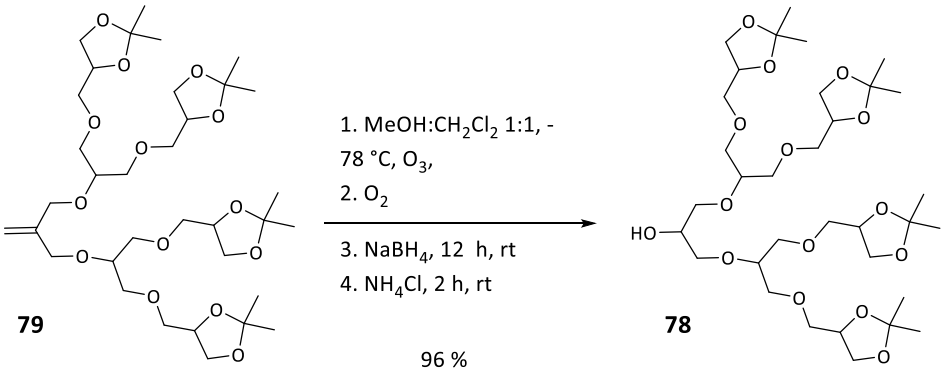

Figure 56: Synthesis of [G2]-OH by ozonolysis

The next generation "jump" to the [G3]-ene **77** was carried out analogous to the synthesis of the [G2]-ene **79**. Two [G2]-OH dendrons **78** were attached to methallyl dichloride **37** as shown in Figure 57. A distillation of the crude product was not successful due to the high boiling point of the [G3]-ene **77**. Thus the purification had to be done by column chromatography according to literature protocol using *n*-hexane and 2-propanol in a 1 : 1 ratio. Again, the column chromatography was performed with a 50 x 500 mm glass column with SiO_2 with a flow of 60 mL per minute. In order to get a decent

separation a maximum of 4 g of crude product per chromatography sequence could be purified. One purification sequence ran for 60 minutes and the retention time of the product was between 17 and 31 minutes. The [G3]-ene **77** dendron was obtained with 84 % yield as colorless oil. Again, the obtained yield is lower than in literature protocol (92 %), likely also due to the different used liquid chromatography method. Reaction and purity control was performed using mass spectroscopy. The mass spectrum, which was measured after the purification showed only one peak representing the [G3]-ene. Further peaks could only be found at the level of the baseline noise, indicating a high purity of the [G3]-dendron **77**.

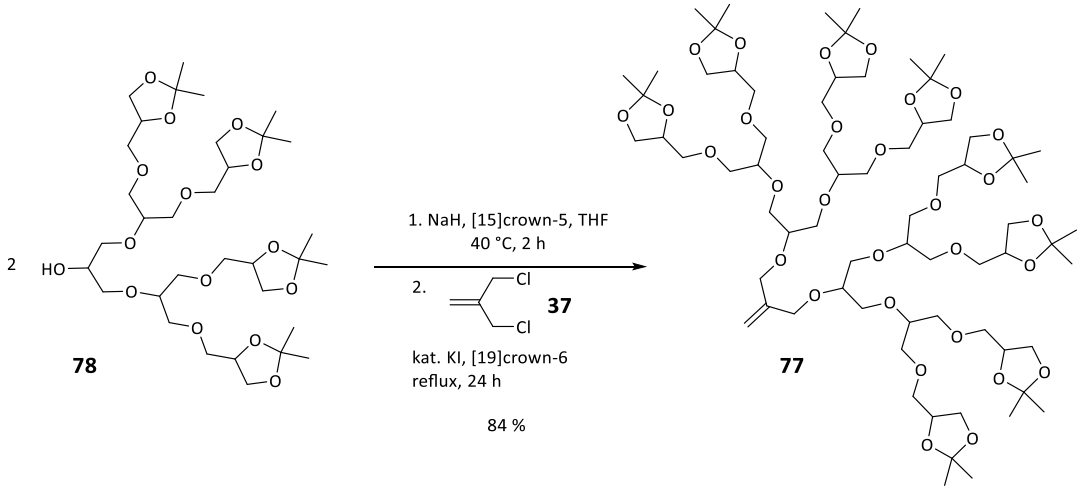

Figure 57: Generation "jump" from the [G2]-OH to [G3]-ene, using methallyl dichloride

The next step was again an ozonolysis to convert the [G3]-ene **77** into the [G3]-OH **76** (Figure 58). The reaction was done analogous to the previous ozonolysis and yielded the [G3]-OH **76** nearly quantitatively. Subsequently the focal point was functionalized with an azide group using methanesulfonyl chloride and sodium azide according to literature protocol. The [G3]-N_3 **70** was obtained with a yield of 86 % as a light yellow and viscous oil.

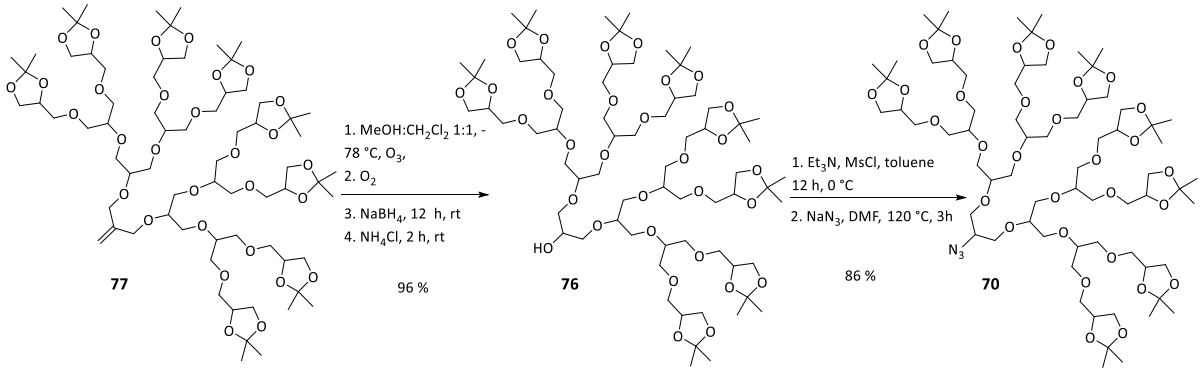

Figure 58: Synthesis of the [G3]-OH 76 by ozonolysis and the following azide functionalization using methanesulfonylchloride and sodium azide

The [G2]-N_3 dendron **129** (expermental part) was not synthesized in the course of this thesis, but was provided by coutesy of Elisabeth Verheggen, who is a lab technichian in the *Schmuck* group.

The alkyne functionalized pyrrole building block **69** was synthesized by coupling propargylamine to the triester building block **91**[24], which can be synthesised via a standart procedure developed in the Schmuck group.[22] The reaction scheme is depicted in Figure 59.

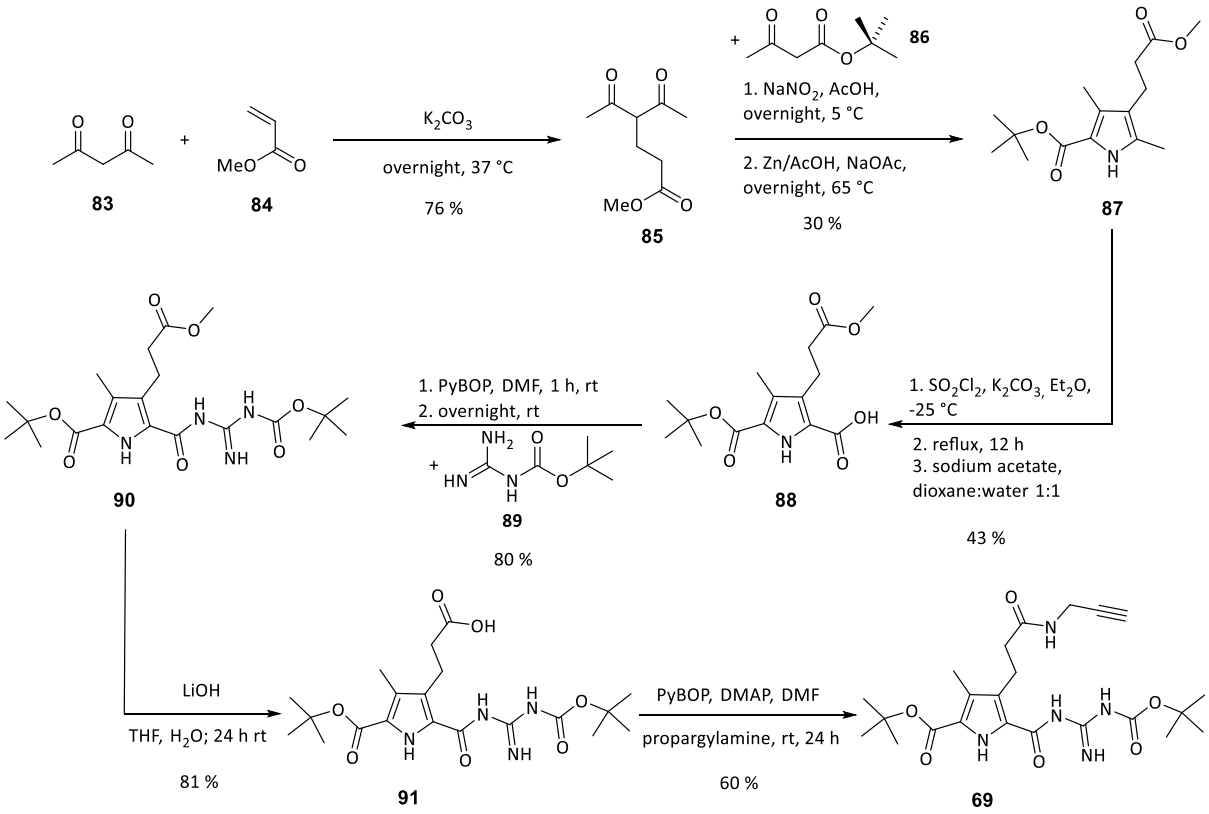

Figure 59: Synthesis scheme of the alkyne functionalized "triester" pyrrole building block 69 according to literature[22,24]

The first reaction step is the formation of the methyl-4-acetyl-5-oxohexanoate (**85**) followed by a Knorr pyrrole synthesis with *tert*-butyl acetoacetate, forming the pyrrole ring **87**. The third step is the oxidation of the methyl group at position 4 with sulfuryl chloride to obtain the carboxylic acid **88**. The implementation of this step requires special diligence due to the high sensibility of the reaction against moisture and deviations of the temperature. In the following step the pyrrole building block **88** was coupled to boc-guanidine with standard coupling conditions using PyBOP. The methyl ester was cleaved with lithium hydroxide to allow the later coupling of the free carboxylic acid **91** with propargylamine. These reaction steps could be realized with moderate to good yields.

Both building blocks **69** and **70** were combined via click chemistry. A suitable reaction type was the 1,3-dipolar cycloaddition of an alkyne and azide functionality, the so called Huisgen reaction. But opposed to the classical Huisgen reaction, which is thermally induced, a Cu(I) mediated alkyne-azide click reaction was performed. This is an easy and convenient reaction requiring very mild conditions The required copper(I)-catalyst was generated *in situ* by the reduction of copper(II) sulfate by sodium ascorbate, and DIPEA was added as a ligand to stabilize Cu(I).

Both the [G2]-zwitterionic dendron **131** and the [G3]-zwitterionic dendron **46** were synthesized, but only the synthesis of the [G3]-dendron will be discussed, since the synthesis are largely analogous and literature known ([G2]-dendron in experimental part). The click reaction and the deprotection including the subsequent purification were planned according to the literature known synthesis by *Merschky*[24]*,* but was carried out with some modifications in particular during the purification, due some difficulties during the implementation of the literature protocol. The click reaction (Figure 60) was carried out in a water : THF solvent mixture in a 1 : 1 ratio. Only small equivalents of sodium ascorbate (0.3 eq), copper sulfate (0.15 eq) and DIPEA (0.3 eq) were added to the mixture. Both salts were added as an aqueous solution with a subsequent addition of THF to readjust the 1 : 1 ratio. The reaction was monitored by TLC. When TLC indicated no further reaction progress after approximately 24 h, but also not a complete reaction, the addition of sodium ascorbate (0.3 eq), copper sulfate (0.15 eq) and the respective amount of THF was repeated. This way three portions of sodium ascorbate (0.3 eq) and copper sulfate (0.15 eq) were added to the reaction in total to sustain the required Cu(I) concentration.

In a second attempt of the click reaction, the reaction was carried out under argon atmosphere. This led to shorter reaction times of approximately four hours, which was determined by monitoring the reaction by TLC. Moreover only one addition of sodium ascorbate (0.3 eq) and copper sulfate (0.15 eq) was necessary. So the click reaction could be simplified and the reaction time was significantly shortened by performing it under argon atmosphere. The purification of the [G3]-pyrrole building block **75** was tested with literature known conditions with MPLC (SiO_2, step gradient ethyl

acetate : n-hexane 0.1 : 9.9 to methanol : *n*-hexane0.5 : 9.5)[128], but could not be realized this way, due to poor elution of the crude product on the chromatography column. New conditions for the liquid chromatography with eluents of higher polarity were tested. The most efficient way for purification proved to be MPLC with a step gradient of isopropanol : *n*-hexane 7 : 3 to 100 % isopropanol to obtain the purified product **75** with a yield of 51 %.

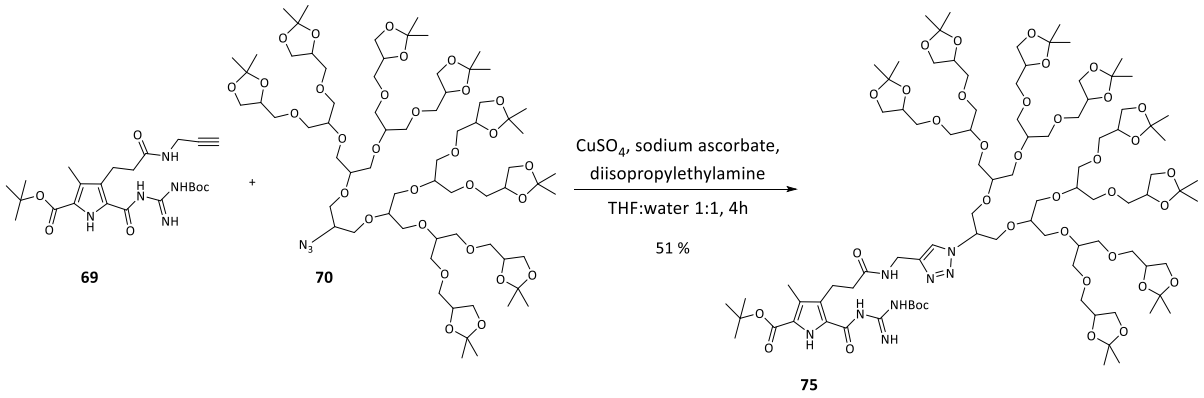

Figure 60: Copper(I) promoted click-reaction of the alkyne functionalized pyrrole building block 69 and the [G3]-N3

The deprotection of the eight acetal groups (Figure 71), the *tert*-butyl ester and the boc-group was done in one step. However, the cleavage of the acetal groups turned out to be more challenging than expected. In literature protocol by *Merschky et al.*[24,128] the deprotection reaction was performed with TFA in acetonitrile at 40 °C. These conditions were also used for this deprotection during this work, but the deprotection of the acetal groups was not successful. Admittedly, the used conditions are not suitable for cleaving acetal groups, because a certain amount H_2O is mechanistically required. Due to this discrepancy between the mechanistic requirements of the reaction and the literature protocol, the experimental implementation of the deprotection of the smaller dendrons ([G1] and [G2]) were compared to the protocol of the [G3]-dendron deprotection. And indeed, up to 5 equivalents of 5 % aqueous hydrochloric acid were added to the reaction mixture. This lead to the assumption, that the lack of aqueous hydrochloric acid in literature protocol was simply a lapse by the author to mention this fact. Thus, the reaction was eventually performed in a TFA : acetonitrile (1 : 1 ratio) mixture with a reasonable amount of aqueous hydrochloric acid (5 %) at 45 °C.

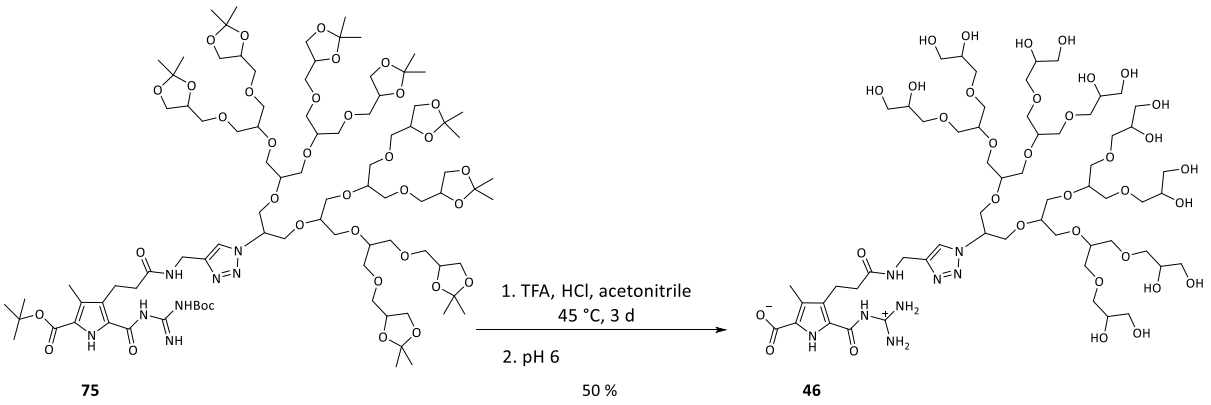

Figure 61: The deprotection of the Pyrrole-[G3]-dendron includes the cleavage of eight acetal groups, tert-butyl ester and the boc-group. The reaction was done using a mixture of TFA and aqueous HCl

The reaction was monitored via HPLC (gradient H_2O : Methanol 80 : 20 to 100 % MeOH in 15 minutes, retention time 11 min). For this gradient the reaction had to be in an advanced stadium to ensure the solubility in the required solvent mixture, since the water-solubility increases with a decreasing number of acetal groups and thus with the advancing reaction process. So the solubility of the taken sample from the reaction mixture is a first indication for the progress of the deprotection reaction. The resulting crude product was purified via reversed phase chromatography (MPLC) according to literature protocol. Subsequently the pH value was set to 5.8 to obtain the zwitterion **46**, which was again purified from any salts using MPLC. The zwitterionic [G3]-dendron was obtained as a colorless and highly viscous oil with a yield of 50 % and good purity of 95 %, which was determined via HPLC.

4.1.2 Core

In the following the synthesis of the trivalent zwitterionic core molecule will be discussed. As the schematic illustration shown in Figure 62 reveals, this molecule basically consists of two individual building blocks, which are the aromatic template molecule and the guanidinocarbonyl pyrrole building block. Both building blocks need to be equipped with functional groups allowing the linkage between both molecules. Again, the alkyne-azide 1,3-dipolar cycloaddition was chosen as a suitable approach for making this linkage.

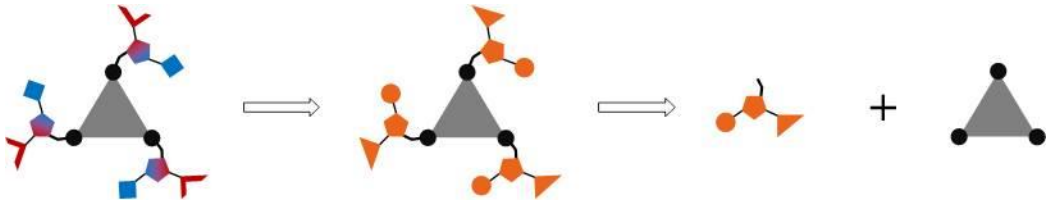

Figure 62: Schematic illustration of the retrosynthetic approach of the tritopic zwitterionic core molecule

In principal two different synthetic pathways are possible, depending on the functionalization of each building block. The aromatic core (**73)** could be azide functionalized, if the pyrrole building block would carry the alkyne functionalization (**72**), as displayed in Figure 63 (top; pathway A).

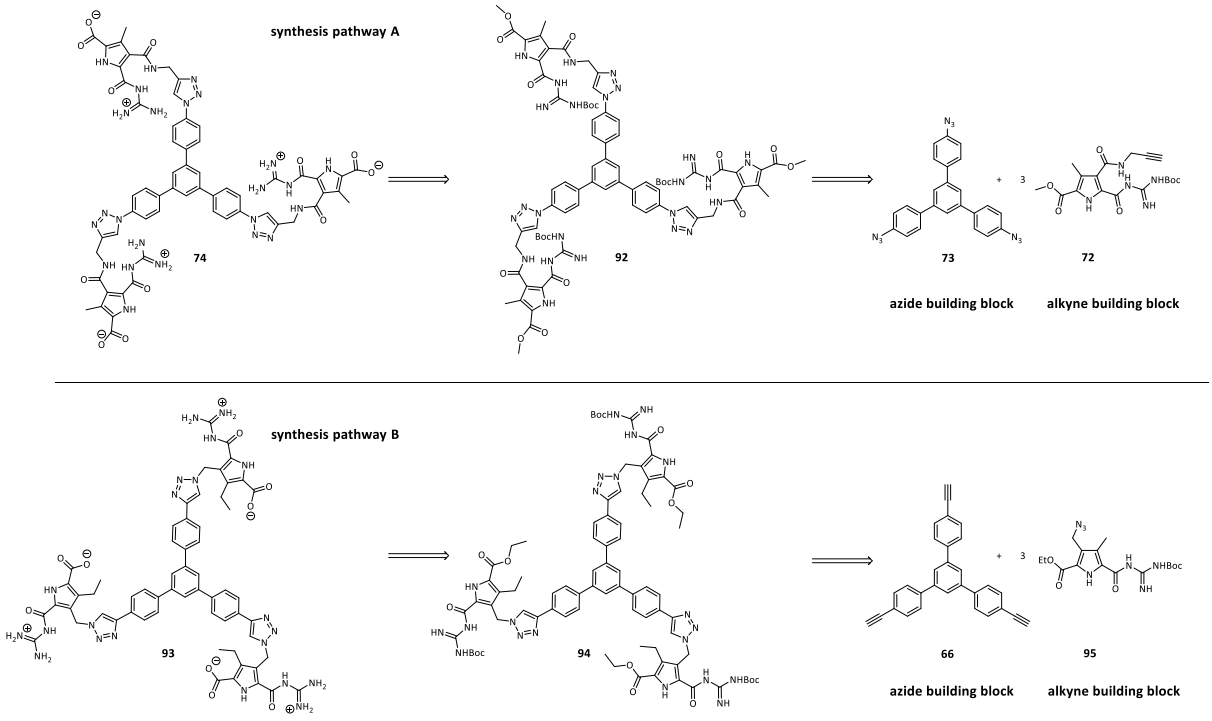

Figure 63: Retrosynthetic approach towards a trivalent zwitterionic core molecule with two possible synthesis pathways A (top) and B (bottom)

On the other hand it is just as well conceivable to functionalize the aromatic core with the alkyne groups (**66**) and the pyrrole building block with one azide functionality (**95**), also shown in Figure 63 (bottom; pathway B).

Both synthesis pathways were pursued during this work, but only pathway A eventually proofed to be successful. The reasons for the failure of the synthesis pathway B were issues during the synthesis of the pyrrole building block; particularly the mono bromination did not work out as hoped before. Also an alternative route, using the dibromide and thus the diazide building block failed, mainly because the deprotection of the ester groups was not possible.

However, the synthesis of the alkyne functionalized aromatic core **66**, which was required for synthesis pathway B, did work well and in good yields as shown in Figure 64 (diploma thesis; Sonogashira reaction).

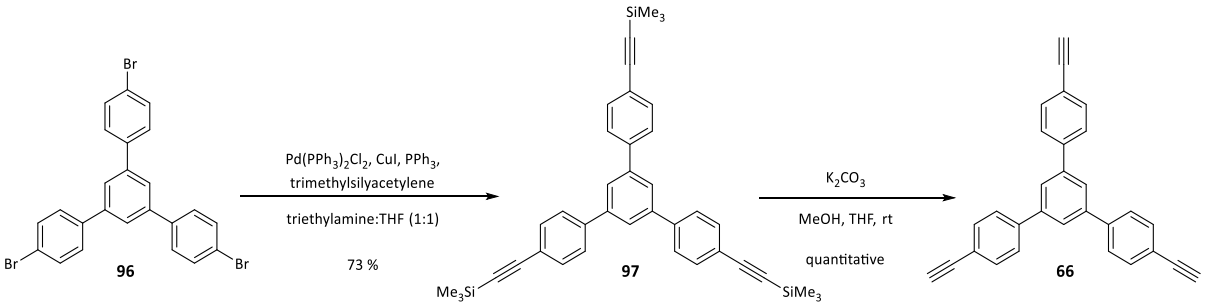

Figure 64: Synthesis of the alkyne functionalized aromatic core 66 (diploma thesis; Sonogashira reaction)

As mentioned before, the synthesis of a required suitable azide functionalized pyrrole building block was not possible. Figure 65 shows the retrosynthesis of the originally planned synthesis approach to obtain this azide functionalized pyrrole building block **98**.

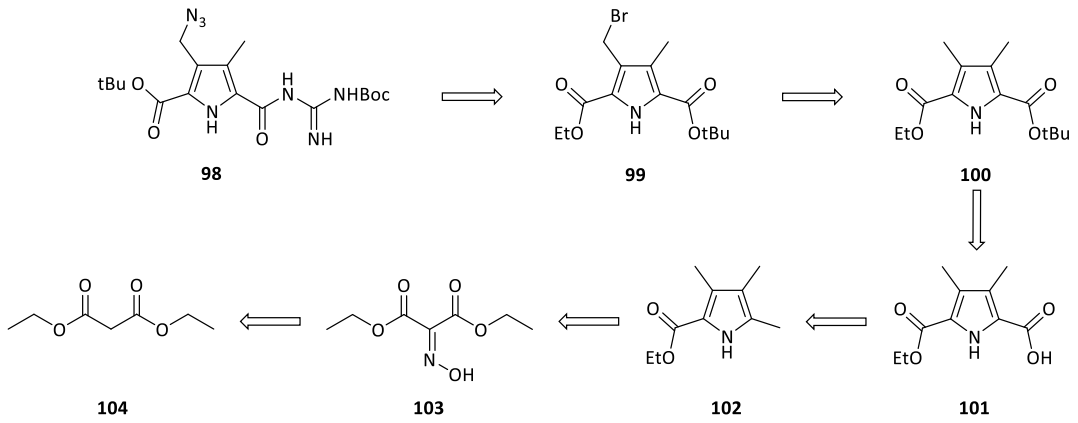

Figure 65: Retrosynthesis of the originally planned route to obtain the azide functionalized pyrrole building block 98

The first four steps of this synthesis, which are yielding pyrrole building block **100**, worked well and with good to moderate yields according to literature protocol from the *Schmuck* group[20,129]. These synthesis steps are illustrated in Figure 66.

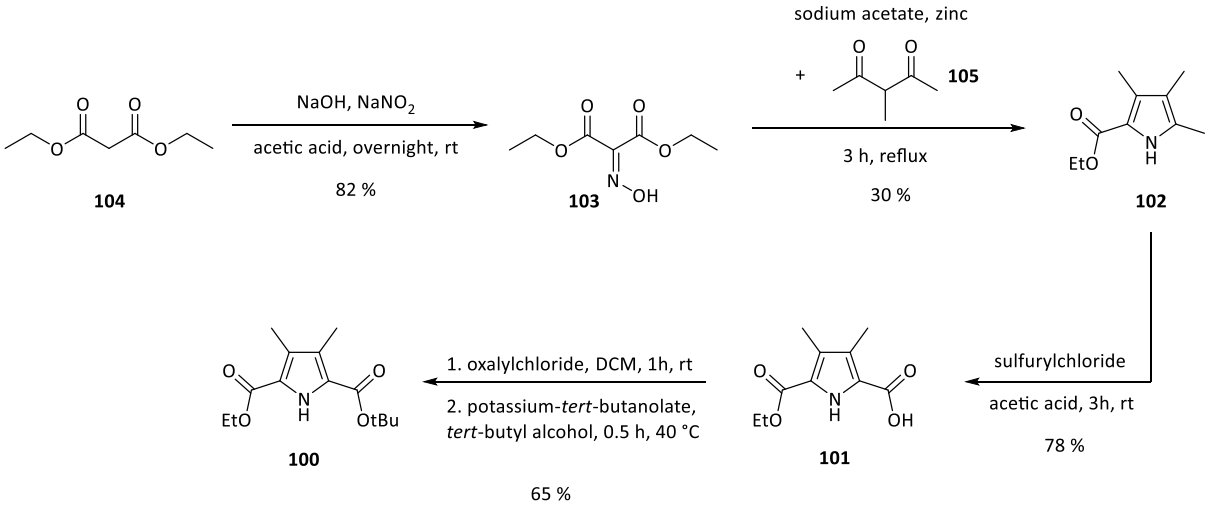

Figure 66: Synthesis of the "dimethyl" pyrrole building block 100 according to literature[20]

However, the attempt of a Lewis acid catalyzed selective bromination using zirconium tetrachloride and one equivalent of *N*-bromosuccinimide at low temperatures (0-5 °C), as shown in Figure 67, was not successful. The ^{1}H-NMR showed that the reaction yielded a mixture of different bromination states, probably including the wanted product **99**. Unfortunately the mixture could not be separated by using chromatographic methods, since the elution characteristics of the resulting products were too similar.

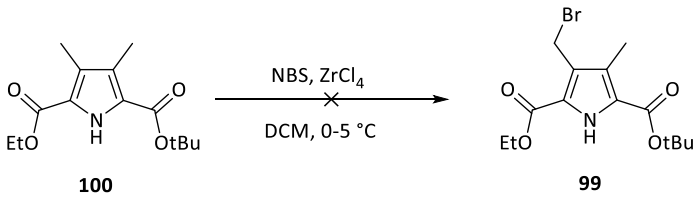

Figure 67: Unsuccessful attempt of a Lewis acid catalyzed selective bromination using Zirconium tetrachloride and *N*-bromosuccinimide

Instead, the dibromide **106** was synthesized in a classical Wohl-Ziegler bromination, also by using a literature known synthesis protocol established in the *Schmuck* group[20,129], with quantitative yield. Subsequently both bromines were substituted with sodium azide in an acetone : water mixture in a 3 : 1 ratio at room temperature obtaining the diazide **107** in very good yield (Figure 68).

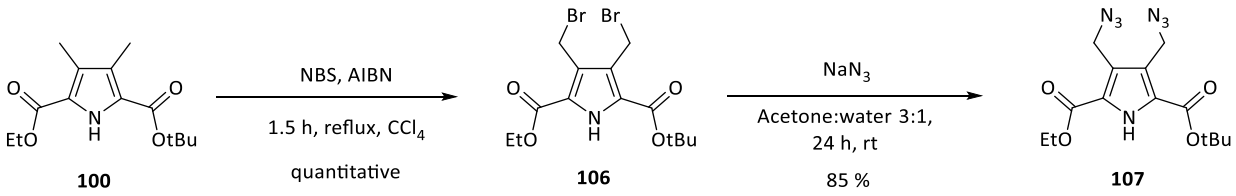

Figure 68: Wohl-Ziegler bromination of pyrrole building block 100 and the substitution reaction with sodium azide yielding the pyrrole building block 107

The following synthesis step was the deprotection of one ester group, to be able to couple the guanidine moiety later on. The cleavage of the ethyl ester as well as the *tert*-butyl ester was not successful in terms of obtaining the required molecule **108** or **109**. It might be possible, that the azide groups are not stable enough to endure the harsh conditions required for the ester cleavage.

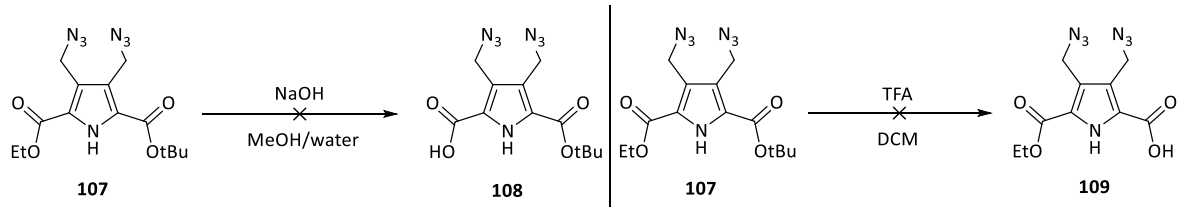

Figure 69: Attempted deprotection reactions of either the ethyl ester or the *tert*-butyl ester in basic or acidic conditions respectively

Parallel to the attempts of the deprotection of one of the carboxyl groups, a click reaction of the diazide and the alkyne functionalized aromatic core was performed.

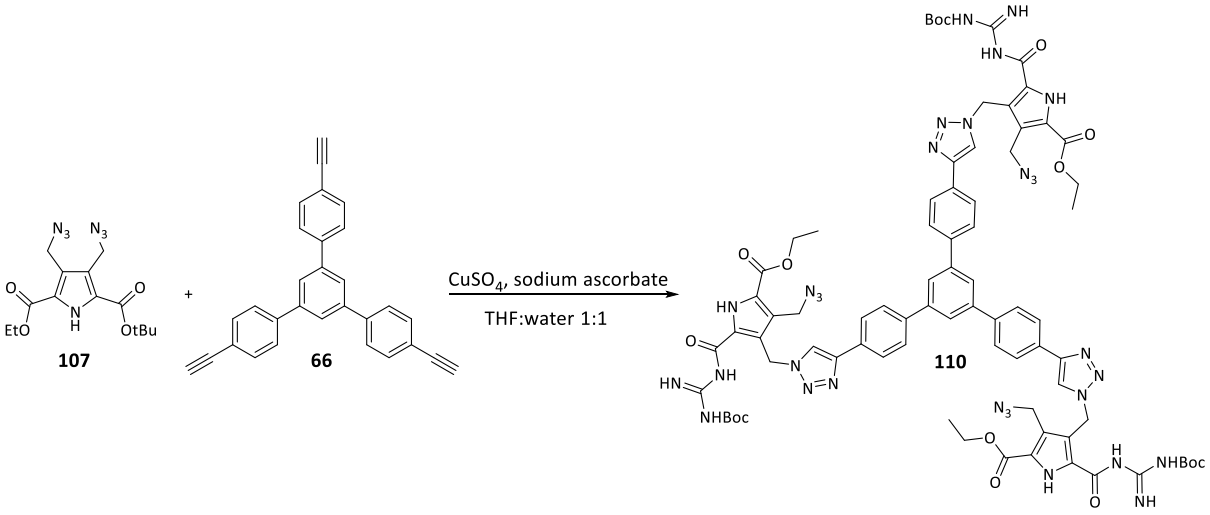

Figure 70: Test click reaction of the di-azide pyrrole building block 107 and the alkyne functionalized aromatic core 66

This should clarify, if it is expedient to further pursue this synthesis route, or if the second azide functionality on the pyrrole building block has an interfering influence on the reaction. The result of this test reaction was not entirely clear, since the reaction product precipitated and was not soluble in any solvent anymore. So either the molecule **110** could be synthesized, but is just insoluble itself, or due to the second azide available on the pyrrole building block, a random "polymer"-like structure was formed. The later assumption is more likely the case. Owing to these difficulties during the implementation of synthesis pathway B, all further attempts to synthesize molecule **110** were canceled. As a result, the sole focus lied with synthesis pathway A, which showed more promising results.

The azide functionalized aromatic template **73** was already synthesized during my diploma thesis. A short overview of this synthesis is shown here nonetheless. There are two ways to obtain the azide functionalized 1,3,5-trisphenylbenzene. One way is to start with the commercially available 1,3,5-tris-(4-bromophenyl)-benzene, where one can substitute the bromines with sodium azide.

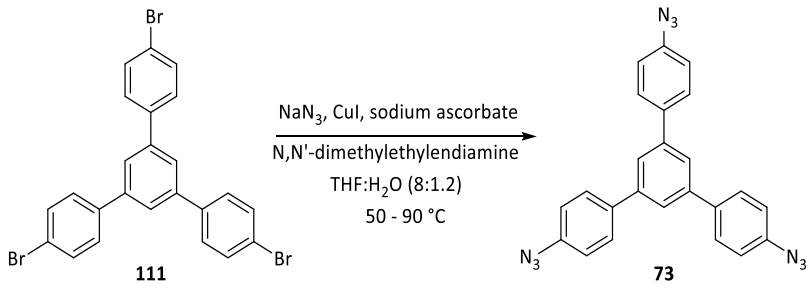

Figure 71: Synthesis of 1,3,5-Tris(4-azidophenyl)-benzene using 1,3,5-Tris-(4-bromophenyl)-benzene as starting material

This method however results in a mixture of the wanted molecule **73** with three azide functionalities, with molecules with two or only one azide functionality. Those molecules have all very similar R_f-values, so the purification was very difficult.

The better synthesis pathway starts from the commercially available 4-iodoacetophenone in which the critical step is a ring formation.

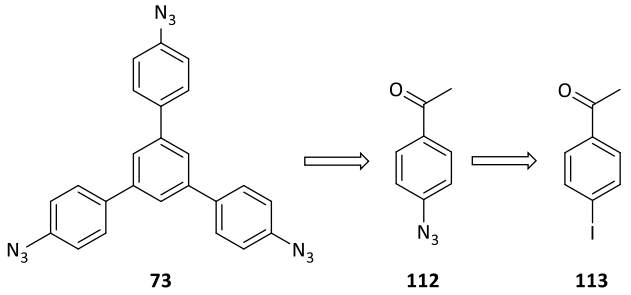

Figure 72: Retrosynthesis of the of 1,3,5-tris(4-azidophenyl)-benzene 73

The azide functionality can be attached via a substitution reaction of the Iodine of 4-iodoacetophenone (**113**) with sodium azide and Cu(I) as catalyst. A trimerization of 4-azidoacetophenepne (**112**) with silicon tetrachloride follows in dry ethanol to obtain the 1,3,5-tris(4-azidophenyl)-benzene (**73**) in good yield and with an effortless purification via a short column chromatography (filtration over SiO_2).

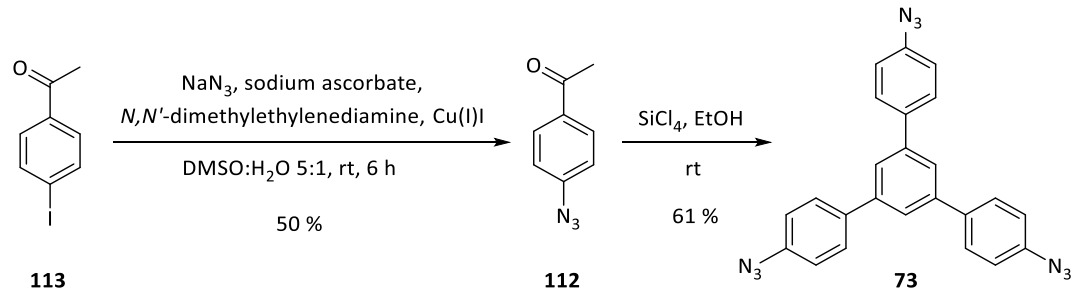

Figure 73: Synthesis of 4-azidoacetophenone and subsequent trimerization of 4-azidoacetophenone yielding 1,3,5-tris(4-azidophenyl)-benzene 73

The synthesis of the alkyne functionalized pyrrole building block **72** with the short linker was the next step for the making of the trivalent zwitterionic core entity. The linker between the pyrrole ring and the alkyne functionalization needs to be as short as possible to gain the necessary rigidity in the tritopic zwitterionic core molecule (**74**, Figure 49 in chapter 3) to avoid intramolecular dimerization. The retrosynthesis in Figure 74 shows the initially planned synthesis approach for the alkyne functionalized pyrrole building block.

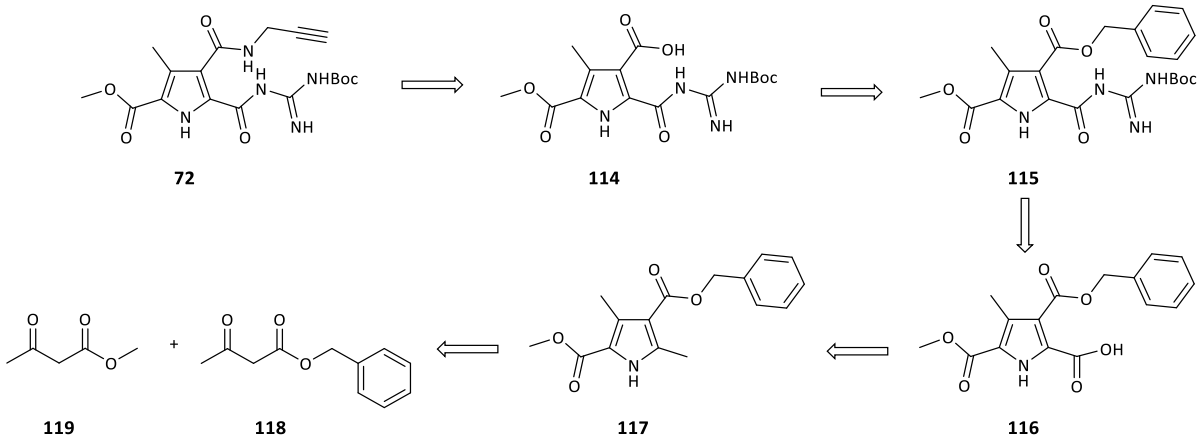

Figure 74: Retrosynthetic illustration of the originally planned synthesis of the pyrrole building block 72

The implementation of the synthesis during my diploma thesis revealed however, that the last synthesis step featured only a very poor yield of 11 %. This step was the coupling reaction of propargylamine with the free carboxylic acid of the pyrrole building block **114**. PyBOP was used as the coupling reagent; the reaction mixture was stirred for 48 hours at room temperature and was monitored by TLC.

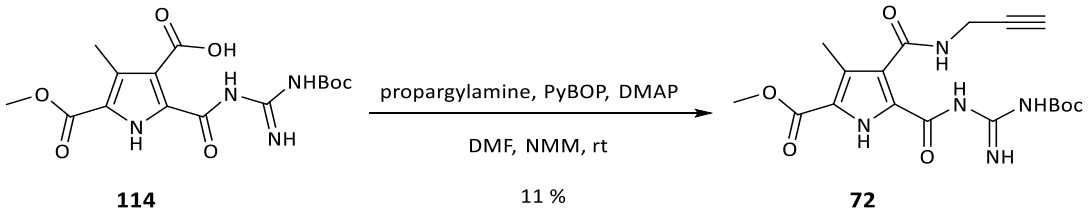

Figure 75: Coupling reaction of pyrrole building block 114 with propargylamine

A possible reason for the bad yield is probably an intramolecular ring formation between the guanidine moiety and the carboxylic acid as shown in Figure 76.

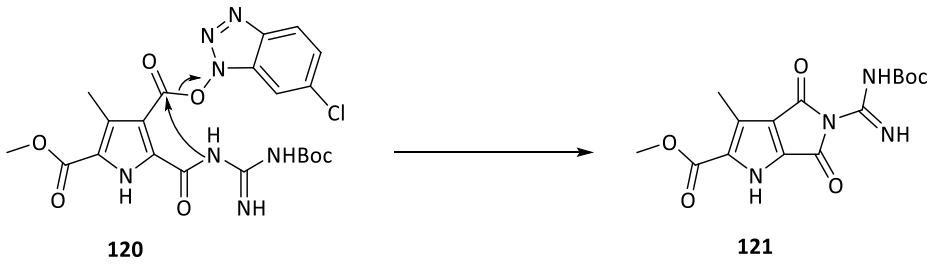

Figure 76: Possible ring formation between the guanidine moiety and the carboxylic acid.

The yields of the previous steps of this 5 step synthesis route are rather moderate to good, but mainly due to the poor yield of this last coupling step the resulting overall yield is only 0.08 %. Hence, this synthesis rout did not present an appropriate way to synthesize a reasonable amount of the alkyne functionalized pyrrole building block **72** to allow further synthesis steps towards the tritopic zwitterionic core **74**.

Consequently this synthesis route was optimized to a more appropriate synthesis pathway to obtain a reasonable amount of the alkyne functionalized pyrrole building block. The retrosynthetic synthesis pathway of the optimized route is illustrated in Figure 77.

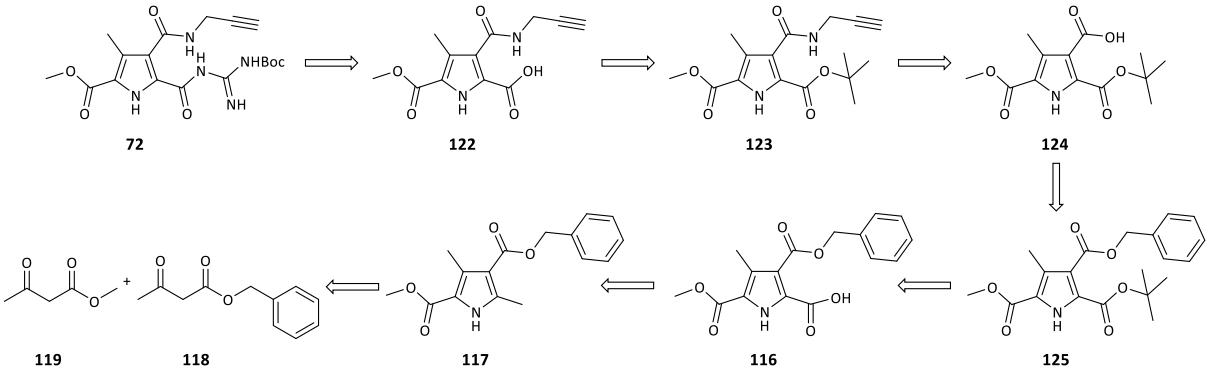

Figure 77: Retrosynthesis of the modified synthesis of the alkyne functionalized building block 72

This pathway incorporates an additional step by protecting the carboxylic acid in position 4 with a *tert*-butyl ester (**125**). This way it is possible to couple the propargylamine to the pyrrole first and later attach the guanidine moiety. Therefore it was possible to avoid the intramolecular ring formation.

The first step of this synthesis route is a Knorr like pyrrole synthesis starting from the commercial available methyl acetoacetate and benzyl acetoacetate yielding molecule **117** with 39 %. The ring formation is followed by the oxidation of the methyl group in position 4 with sulfuryl chloride yielding the carboxylic acid **116** with 45 %.

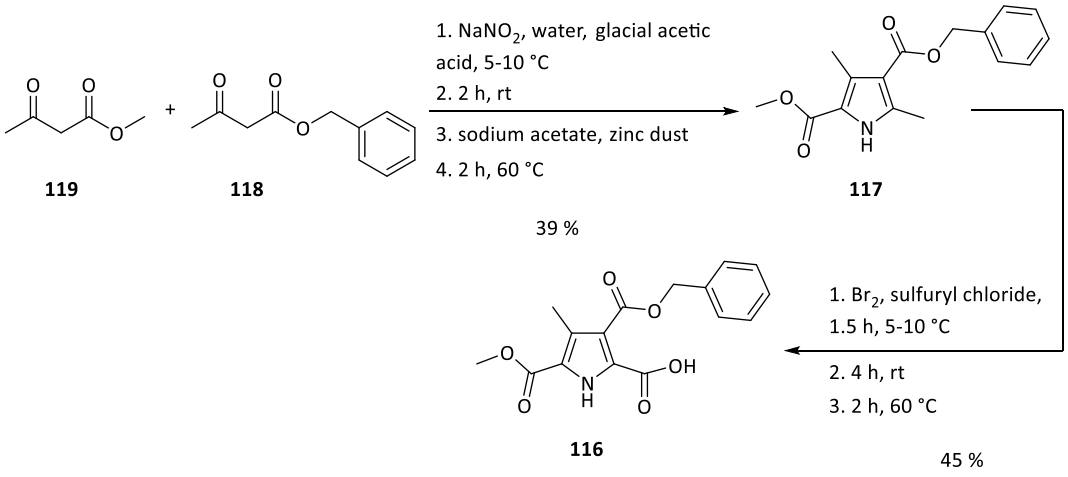

Figure 78: Synthesis of the pyrrole building block 117 with a Knorr like pyrrole synthesis and the additional oxidation of the methyl group in position 5 of the pyrrole ring using sulfuryl chloride, yielding the carboxylic acid 116

The resulting carboxylic acid **116** was converted into a *tert*-butyl ester using tert-butanol and DCC as a coupling reagent yielding the tert-butyl ester **125** with 64 % (Figure 79). This step was necessary to protect the carboxylic acid for the later coupling reaction with propargylamine. To allow this coupling reaction the benzyl ester was cleaved with palladium on charcoal under hydrogen atmosphere with nearly quantitative yield (molecule **124**). Subsequently the coupling reaction of the carboxyl group with propargylamine worked with a reasonably good yield of 53 %. DIC and Cl-HOBt were used as the coupling reagents. The reaction was performed at 70-80 °C for four hours and stirred at room temperature for another 48 hours while the reaction was monitored by TLC. The subsequent purification was done via MPLC.

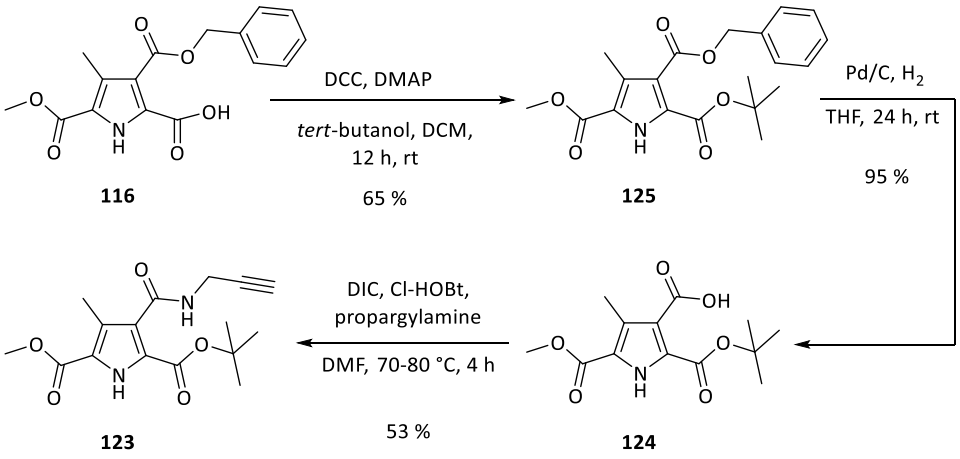

Figure 79: Coupling of the *tert*-butyl ester using DCC and *tert*-butanol, followed by the hydrogenolysis of the benzyl ester and the coupling of propargylamine using DIC and Cl-HOBt as coupling reagents

After the successful coupling of propargylamine the *tert*-butyl ester was cleaved using TFA in dichloromethane, as shown in Figure 80. The reaction was performed at ambient temperature. After 24 hours TLC indicated complete reaction, so solvent and acid were removed under reduced pressure. The pyrrole building block **122** with the free carboxylic acid could be obtained in quantitative yield. The following step was the coupling of boc-guanidine to the carboxylic acid of molecule **122**. For a first attempt of this coupling reaction PyBOP was used as a coupling reagent. However, the reaction was not successful under these conditions since the wanted product **72** could only be obtained with a yield of 5 %. Instead of PyBOP as the coupling reagent Cl-HOBt and DIC were used in the second attempt of this reaction. Moreover, the reaction was heated to 80 °C for two hours. Subsequently the mixture was stirred for another 48 hours until TLC monitoring indicated that the reaction was complete. This way it was possible to obtain the alkyne functionalized pyrrole building block **72** with a yield of 66 %.

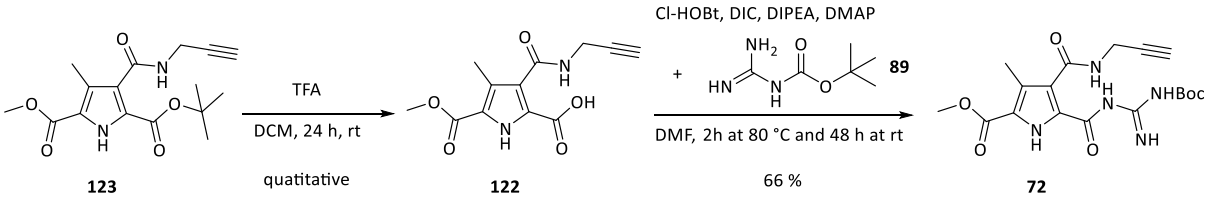

Figure 80: Cleavage of the *tert*-butyl ester followed by the coupling with boc-guanidine

Due to the change of the synthesis route the overall yield of the synthesis of the alkyne functionalized pyrrole building block **72** could be improved from 0.08 % in 5 steps to 4 % in 7 steps, which allowed the synthesis of this molecule in reasonable amounts and thus the following click reaction with 1,3,5-tris(4-azidophenyl)-benzene.

After the successful syntheses of both building blocks, 3.3 equivalents of the alkyne functionalized pyrrole building block **72** were “clicked” to the azide functionalized aromatic template **73** (1,3,5-tris-(4-azidophenyl)-benzene) *via* an 1,3-dipolar cycloaddition (Figure 81).

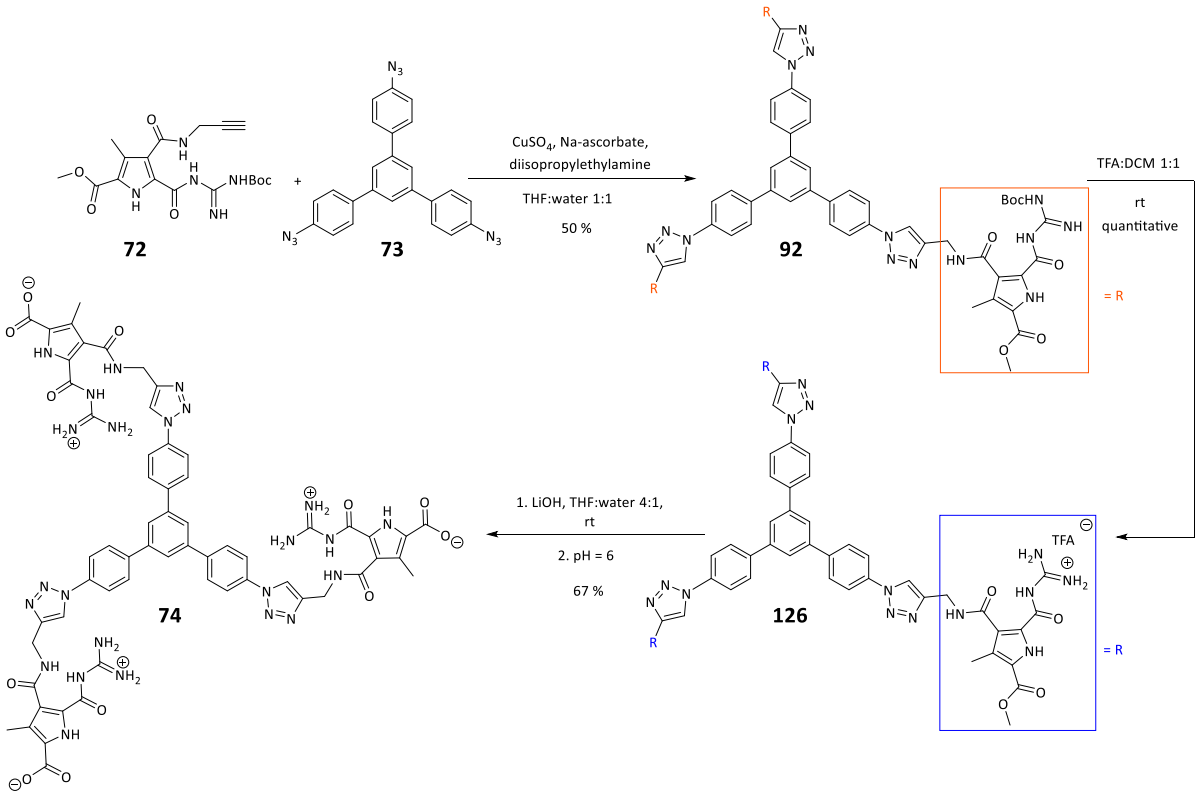

Figure 81: Click reaction of the alkyne functionalized pyrrole building bock 72 and the azide functionalized 1,3,5-trisphenylbenze with subsequent Boc-group and methyl ester cleavage yields the tritopic zwitterionic core molecule 74

The click reaction was carried out in a water : THF mixture in a 1 : 1 ratio. Diisopropylethylamine served as a ligand for copper(I), which was *in situ* generated from copper sulfate (pentahydrate) and sodium ascorbate. DIPEA, sodium ascorbate and $CuSO_4$ were only added in small equivalents which were 0.6 equivalents for DIPEA and sodium ascorbate and 0.3 equivalents for $CuSO_4$ respectively. Theoretically, since Cu(I) is acting as catalyst, a small amount should suffice. However, Cu(I) can oxidize to Cu(II) due to atmospheric oxygen, so the addition of both sodium ascorbate and $CuSO_4$ was repeated after the reaction did not show any progress after stirring the reaction mixture at ambient temperature seven days. Moreover the temperature was raised from ambient temperature to 40 °C. The reaction was constantly monitored by TLC and HPLC. The addition of sodium ascorbate and $CuSO_4$ was further repeated for another three times in a time range of another ten days. The addition of higher amounts of both salts is rather unfavorable since high salt concentrations lead to a phase separation of the THF : water mixture. In this case the click reaction hardly takes place. So the reaction mixture needed to be diluted, which means the concentration of the actual reactants (alkyne and azide building blocks) decreased significantly. In this case four further additions of sodium ascorbate and $CuSO_4$ were done which were accompanied by the addition of 4 mL solvent each time. After a time range of 20 days in total HPLC showed no 1,3,5-tris(4-azidophenyl)-benzene starting material anymore. However, the product **92** did not show up on the chromatogram, since it

precipitated from the reaction mixture. The reaction was terminated and water and dichloromethane were added in hopes to be able to extract the product from the reaction mixture, since the precipitate was extremely fine. However, the product did not dissolve in DCM, instead the precipitation became more distinct allowing it to be filtered off. The product was washed with DCM and dried. The product **92** was obtained as a light brown solid substance with a yield of 50 %. Solubility tests with the product **92** showed that the substance was only soluble in DMSO and DMF. In hindsight, it would probably have been better to conduct the reaction under argon atmosphere, as it was later done with the alkyne-azide click reaction of the [G3]-dendron (in the timeline of this work this reaction was done before the click reaction of the dendron). By working under argon atmosphere any further addition of sodium ascorbate and $CuSO_4$ might not have been necessary. Moreover the reaction time could have been drastically reduced. None the less, it was possible to obtain the protected core molecule **92** in a moderate yield and in a reasonable amount of 119 mg, which allowed proceeding with the synthesis of the tritopic zwitterionic core **74**.

After the click reaction both protection groups were cleaved. The boc-group was cleaved quantitatively using a mixture of dichloromethane and trifluoroacetic acid in a 1 : 1 ratio, whereas the core molecule **92** first had to be dissolved in pure TFA due to solubility issues. The mixture was stirred at room temperature for 24 hours. Dichloromethane and TFA were removed under reduced pressure, the residue was resolved in 5 % aqueous HCl and subsequently freeze dried for anion exchange. The cationic core molecule **126** could be obtained as a brown solid substance in quantitative yield. The methyl ester was cleaved using lithium hydroxide in a water and tetrahydrofuran mixture. The mixture was stirred at room temperature for 72 hours (over the weekend). At first, the methyl ester protected core molecule **126** formed a suspension with the water : THF mixture. During the reaction the mixture became a solution, because the anionic form of the core molecule **74** is indeed water soluble. THF was removed under reduced pressure and the pH value of the remaining aqueous solution was set to 5.8 and the zwitterion precipitated from the solution. The precipitate was filtered using a nylon membrane and was washed with several solvents.

Table 1: Solubility of the tritopic zwitterion core molecule 74

DCM	x	Chloroform	x	MTBE	x	Acetonitile	x
Methanol	x	1,4-Dioxane	x	Isopropanol	x	THF	x
Toluene	x	Ethyl acetate	x	DMF	x	DMSO	yes

The tritopic zwitterionic core molecule **74** could be obtained with a moderate yield of 67 %. The obtained product was a dark, nearly black solid and only soluble in DMSO (Figure 82 in Table 1).

Figure 82: Solid tritopic zwitterionic core 74

The dark color of the tritopic zwitterionic core building block is notable, as a lighter color like beige or light brown was expected. Other molecules with a trisphenylbenzene architectures like the 1,3,5-tris(4-bromophenyl)benzene and the 1,3,5-tris(4-azidophenyl)benzene show a slightly brownish color, also the protected molecule **92** is a beige/light brown substance. The dark color probably results from strong intermolecular aggregation.

4.1.3 Summary

The first step for the success of the project was the successful synthesis of the zwitterionic polyglycerol dendrons and even more importantly the synthesis of the novel tritopic zwitterionic trisphenylbenzene core molecule **74**. The zwitterionic polyglycerol dendrons were mainly synthesized according to literature protocols. Some alterations to this literature protocols were done to either simplify or improve purification processes, as it was done for the purification of the [G2]-ene and the protected [G3]-pyrrole building block **75**. Or the synthesis was optimized by some alterations, as it was done by performing the click reaction under argon atmosphere. Moreover, some alterations were necessary simply due to different technical equipment used during this work, so the purification of the “ene” dendrons by liquid chromatography was done using MPLC instead of HPLC.

For the development of a novel tritopic zwitterionic trisphenylbenzene core molecule, which will function as the template for the supramolecular dendrimers, two different synthesis pathways were thinkable and pursued, which are shown in Figure 83.

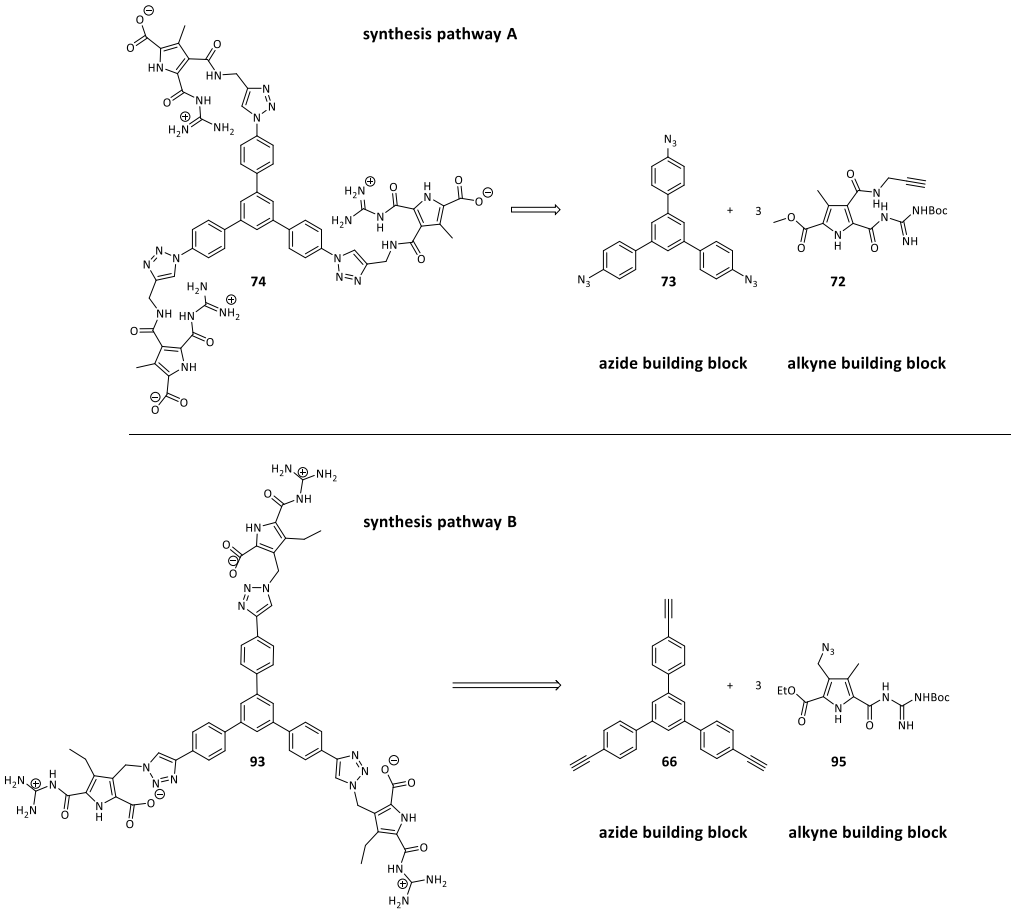

Figure 83: Short retrosynthetic illustration of synthesis pathway A and B

Both synthesis pathways were pursued, yet only synthesis pathway A proved to be successful. The synthesis of the zwitterionic core molecule **93** via pathway B failed with the synthesis of the required azide functionalized pyrrole building block. During the synthesis of the zwitterionic core molecule **74** via pathway A, some obstacles occurred while synthesizing the required alkyne functionalized pyrrole building block **72**. However, these obstacles were overcome by optimization of the synthesis route. Both building blocks were combined in an alkyne-azide click reaction. The click reaction was followed by two deprotection steps to generate the zwitterion. In the end it was possible to obtain the required zwitterionic template molecule **74** with moderate to good yields and in decent amount. This allowed further studies of this tritopic zwitterionic core molecule concerning the self-assembly behavior in solution and on surface. Also the formation of the templated supramolecular dendrimer after the addition of the zwitterionic dendrons and subsequently the solubilization properties of this dendrimer could be studied.

4.2 Characterization of the core

After the successful synthesis of both required building blocks, the properties of those molecules could be investigated. Since the investigation of the dimer-formation of the zwitterionic polyglycerol dendrons was already the subject of the PhD thesis of Merschky[24,128], the focus in this work is on the investigation of the trivalent zwitterionic core and the core-shell architectures formed by dendron and core. In this chapter the investigations of the zwitterionic 1,3,5-trisphenylbenzene core molecule will be discussed.

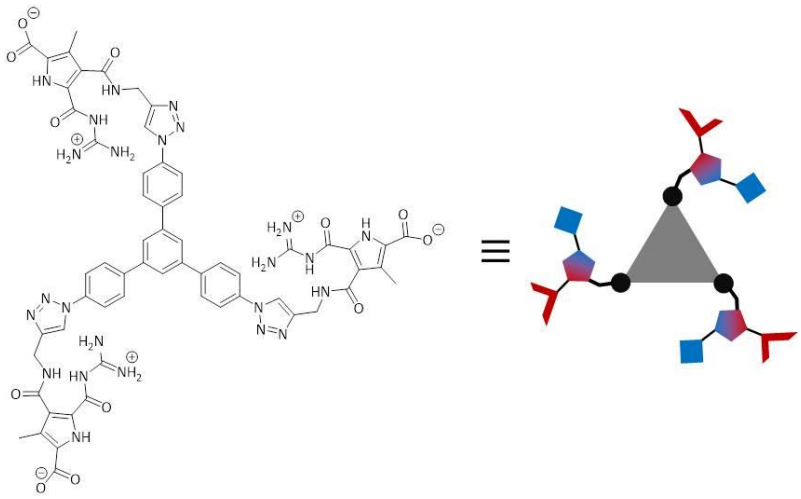

Figure 84: chemical structure of the trivalent zwitterionic 1,3,5-trisphenylbenzene core building block and the schematic illustration

The core molecule carries three guanidinocarbonyl pyrrole zwitterions, each on one end of the "triangular"-shaped 1,3,5-trisphenylbenzene core. Those zwitterions form intermolecular self-complimentary dimers at a pH of around 6.

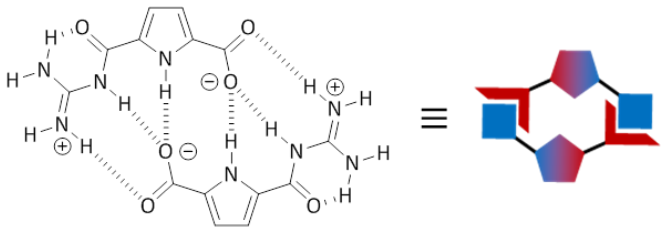

Figure 85: chemical structure of the guanidiniocarbonylpyrrole carboxylate zwitterion dimer and the schematic illustration

An important factor for the formation of intermolecular interactions between different zwitterionic 1,3,5-trisphenylbenzene core molecules or the zwitterionic 1,3,5-trisphenylbenzene core and the

zwitterionic dendrons is the lack of intramolecular interactions. This was taken into consideration during the design of the core molecule. As a consequence the linker between the aromatic system and the pyrrole building block was designed to be as short as possible. Modeling calculations of the synthesized core showed that no intermolecular interactions can occur.

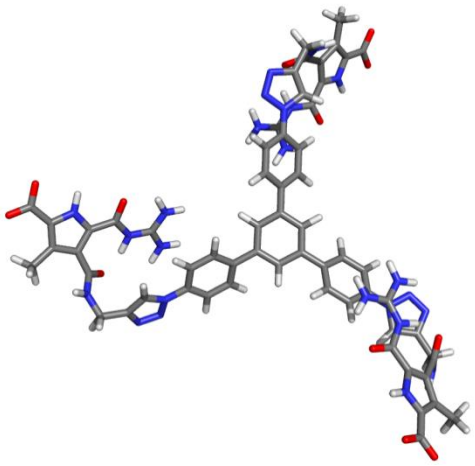

Figure 86: Modeling of the structure of the trivalent zwitterionic 1,3,5-trisphenylbenzene core building block

Therefore the architecture of the trivalent zwitterionic core molecule allows predicting the formation of pH switchable networks in solution, which are illustrated in the center part of the scheme below. Changes of the pH value either towards acidic or basic conditions will protonate or deprotonate the guanidiniocarbonyl pyrrole moieties, thus the formation of dimers and therefore any higher aggregates is no longer possible. This is illustrated on the left and right side respectively in Figure 87.

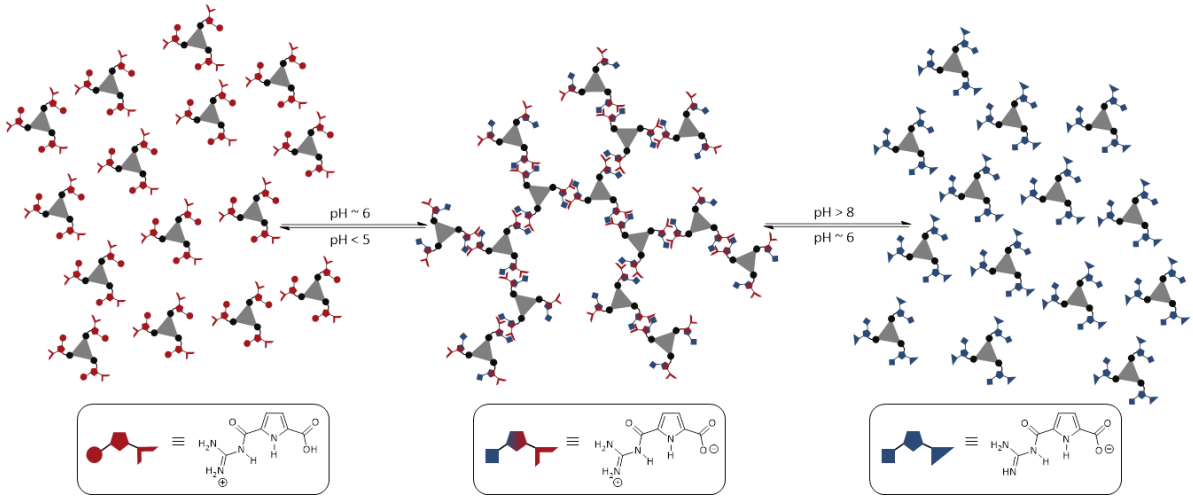

Figure 87: Simplified illustration of the expected three-dimensional networks formed by the trivalent zwitterionic 1,3,5-trisphenylbenzene core (middle) and the reversible destruction of the assembly induced by a pH chance below a pH value of 5 or above a pH value of 8

The ^{1}H-NMR spectrum measured after the synthesis gave a first hint for a strong aggregation. The signals representing the NH and aromatic protons shift into one big broad signal. Only after the addition of TFA and thus the disassembly, the individual signals could be seen in the spectrum. Figure 88 shows the ^{1}H-NMR spectra of the methyl ester protected building block **126** (top), the zwitterionic core **74** (middle) and the cationic form of the core after the addition of TFA to the NMR sample (bottom).

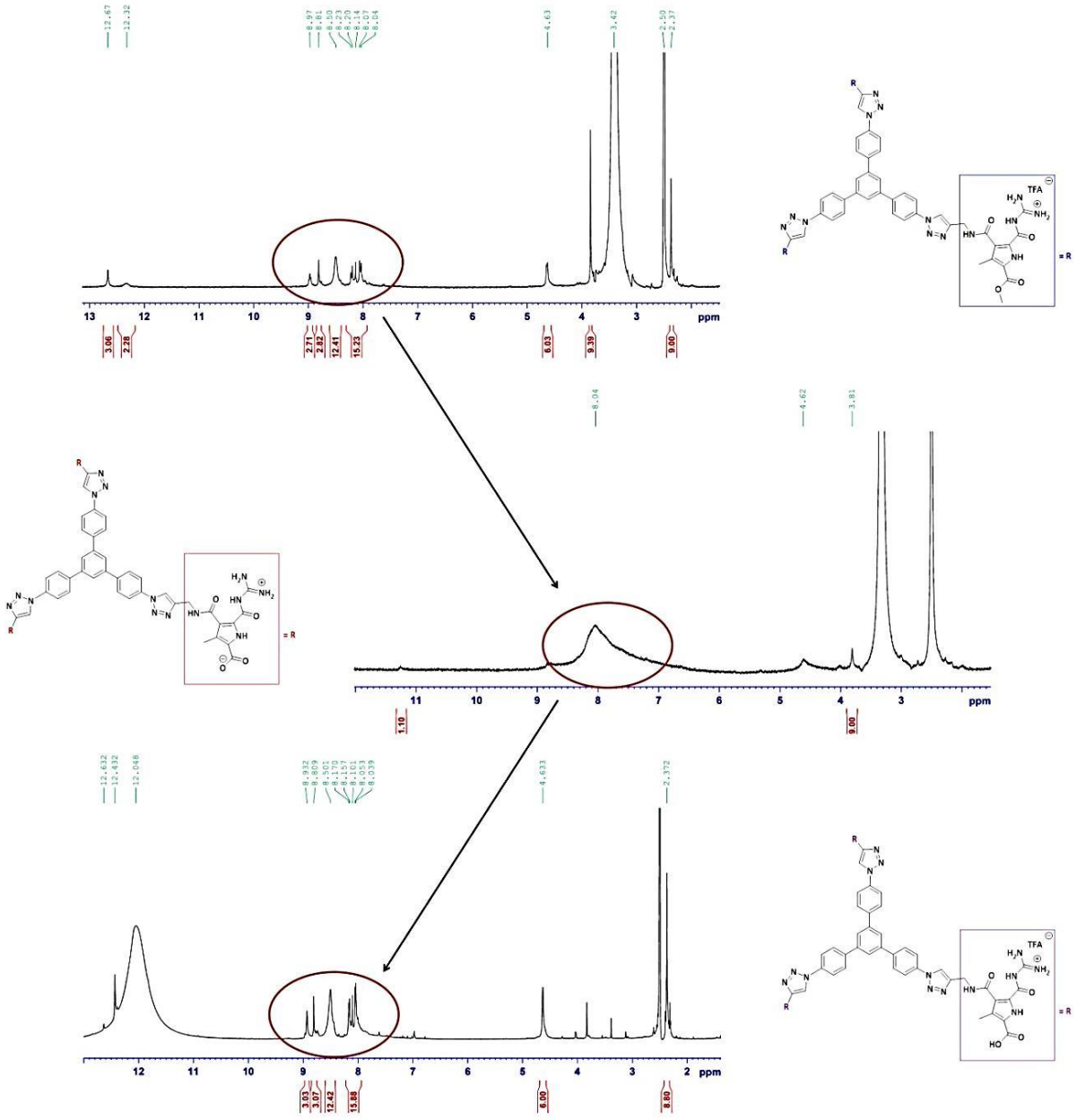

Figure 88: ^{1}H-NMR spectra of the methyl ester protected building block 126 (top), the zwitterionic core 74 (middle) and the cationic form of the core after the addition of TFA to the NMR sample (bottom). The crucial peaks are marked with a circle.

The aromatic CH signals, the NH signals and the CH signal from the triazole rings are all individual peaks in the ^{1}H-NMR spectrum of the methyl ester protected building block **126**. After the deprotection and pH value adjustment to 6 to obtain the zwitterion, these signals are indistinguishable and appear as one broad signal (middle spectrum). In hopes to obtain a ^{1}H-NMR spectrum with individual signals for the relevant protons a ^{1}H-NMR measurement at higher temperature (373 K, 100 °C) was done, but did not show the wanted effect. Only after the addition of TFA to this sample and hence the disaggregation of the assemblies the signals are again distinguishable as individual signals (bottom spectrum).

Since NMR spectroscopy confirmed the expected structure and the pH-dependent aggregation of the zwitterionic core molecule **74**, further experiments were conducted to learn more about the shape and size of the aggregates formed by the zwitterionic core molecule **74**.

4.2.1 Microscopy

A suitable method to study nano-assemblies on a surface is atomic force microscopy, short AFM. The AFM samples were prepared from a DMSO stock solution, since the trivalent zwitterionic core was only soluble in DMSO. The pictures were taken by using tapping mode on a freshly cleaved mica surface, on which 6 µL of the DMSO solution were dropped and subsequently spin coated (60 rps; 10 min). Indeed the anticipated network formation was observed in DMSO even at low concentrations down to 1 µM.

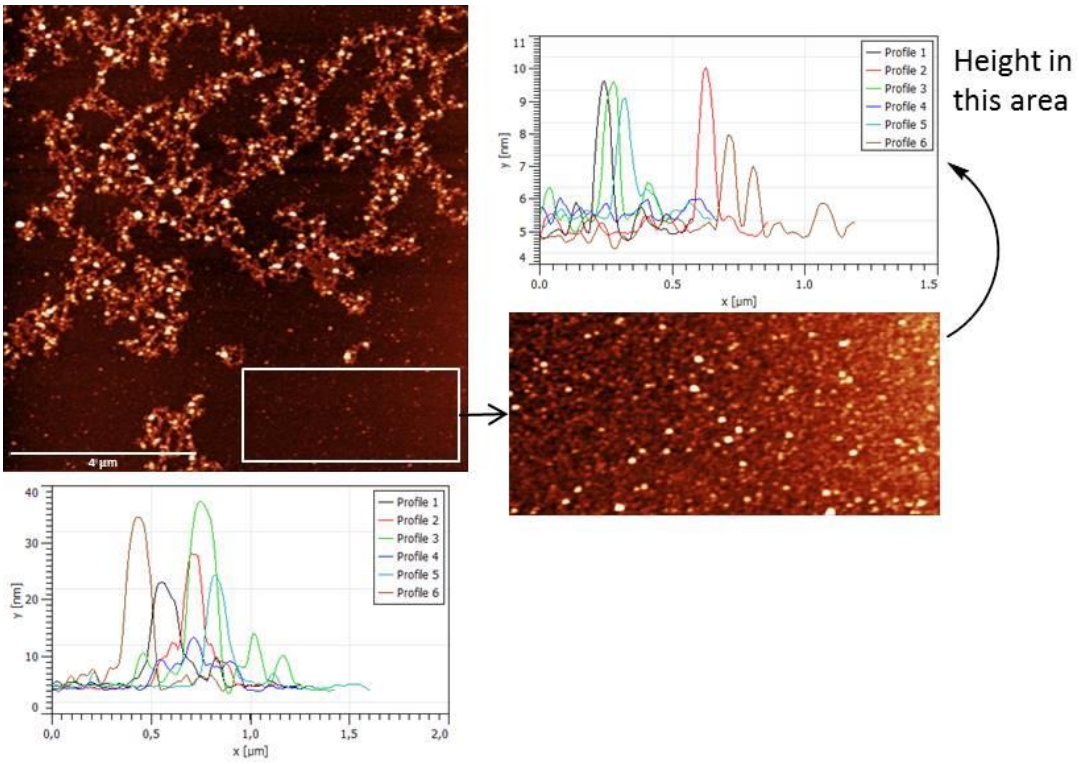

Figure 89: AFM images of the tritopic zwitterionic core molecule 74 (1 mM); picture was prepared by dropping a DMSO solution with a concentration of 1 mM on a mica surface with subsequent spin-coating (60rps, 10 min) and analyzed by AFM tapping mode; height up to 40 nm; Zoom: darker areas of the AFM pictures indicate that the mica surface might be empty in these areas. A zoom into one of these areas illustrates that the mica surface is indeed fully covered by aggregates with heights still up to 10 nm

Figure 89 shows an AFM picture of the trivalent zwitterionic building block measured on a mica surface prepared with a 1 mM zwitterionic core solution in DMSO. In the AFM image one can see a fully covered mica surface where a distinct 3-D network is noticeable on top of all. The height of these network structures is between 10 to 40 nm, indicating numberous layers of molecules are piling up. This picture proves the netwok formation of the trivalent zwitterionic core molecule. The darker areas of the AFM pictures might indicate that the mica surface might be empty in these areas. A zoom into one of these areas illustrates that the mica surface is indeed fully covered by aggregates with heights still up to 10 nm. The chosen concentration of 1 mM seems to be too high to image a distinct single network with optimally only a few layers of molecules. Subsequent measurements should acertain, if and to what extent this behavior changes with decreasing concentration and if it is possible to get a more detailed view of the actual nano-assembly.

An AFM measurement of the zwitterionic 1,3,5-trisphenylbenzene core with a ten times lower concentration (Figure 90) results in a picture which is very similar to Figure 89 a.

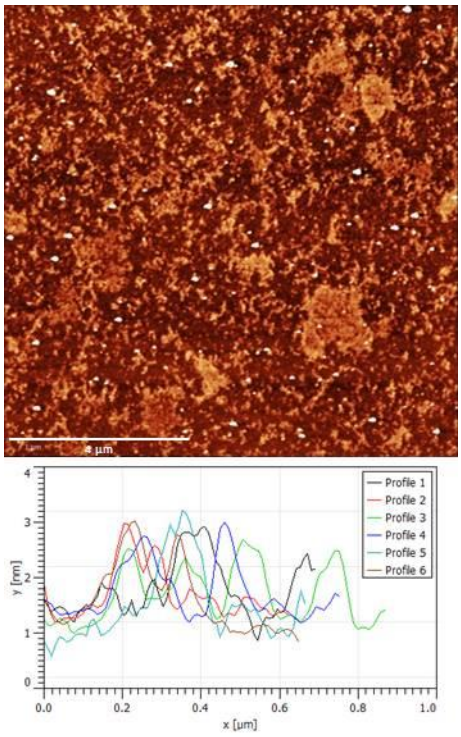

Figure 90: AFM image of the tritopic zwitterionic core molecule 74 (0.1 mM); picture was prepared by dropping a DMSO solution of 0.1 mM concentration on a mica surface with subsequent spin-coating (60rps, 10 min) and analyzed by AFM tapping, height around 2-3 nm

The whole surface is covered by aggregates. These aggregates are again branched and thus can be called 3-D networks. The height is however considerable lower with only 3-4 nm, meaning the lower concentration resulted in fewer molecular layers lying on top of each other.

An AFM picture of the core molecule with a concentration of 50 µM (Figure 91 a) clearly shows the network formation on the mica surface. The height of these structures is around 4-8 nm.

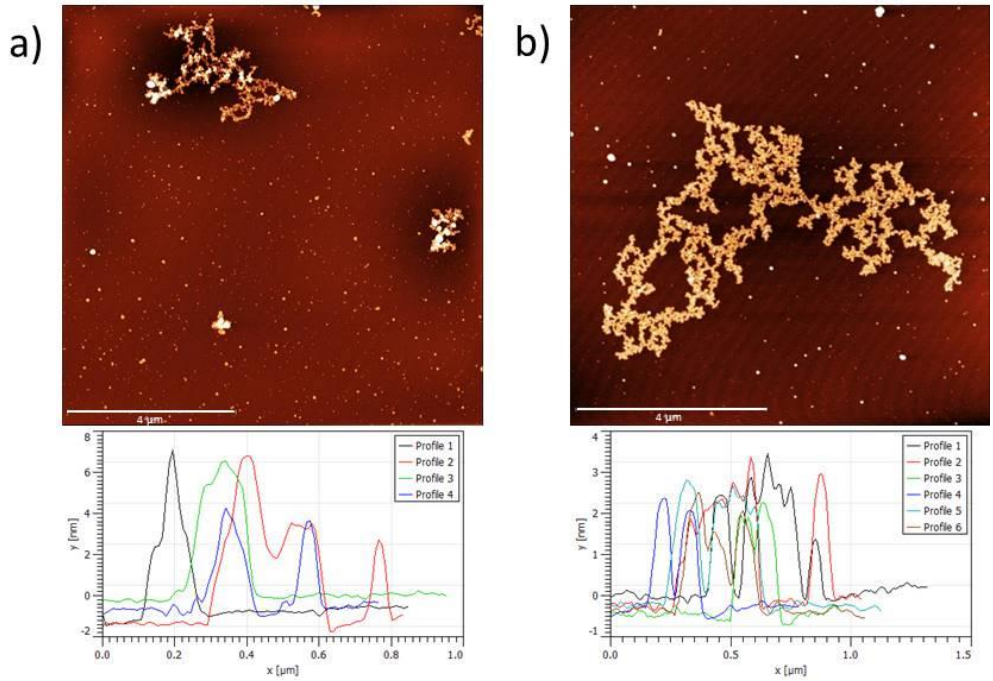

Figure 91: AFM images of the tritopic zwitterionic core molecule 74; pictures were prepared by dropping a DMSO solution of the respective concentration on a mica surface with subsequent spin-coating (60rps, 10 min) and analyzed by AFM tapping mode a) 0.05 mM sample; height up to 8 nm; b) 0.01 mM sample, height around 3 nm

Further dilution of the tritopic zwitterionic core **74** solution in DMSO to 0.01 mM still results in the formation of networks on the mica surface. The height of these networks is 3-4 nm. In this case however the network structure is more distinct and defined and the surrounding areas show the uncovered mica surface, recognizable by the visible, slightly darker crosslines in the picture. This picture depicts very nicely and detailed the networked formed by the zwitterionic 1,3,5-trisphenylbezene core **74**.

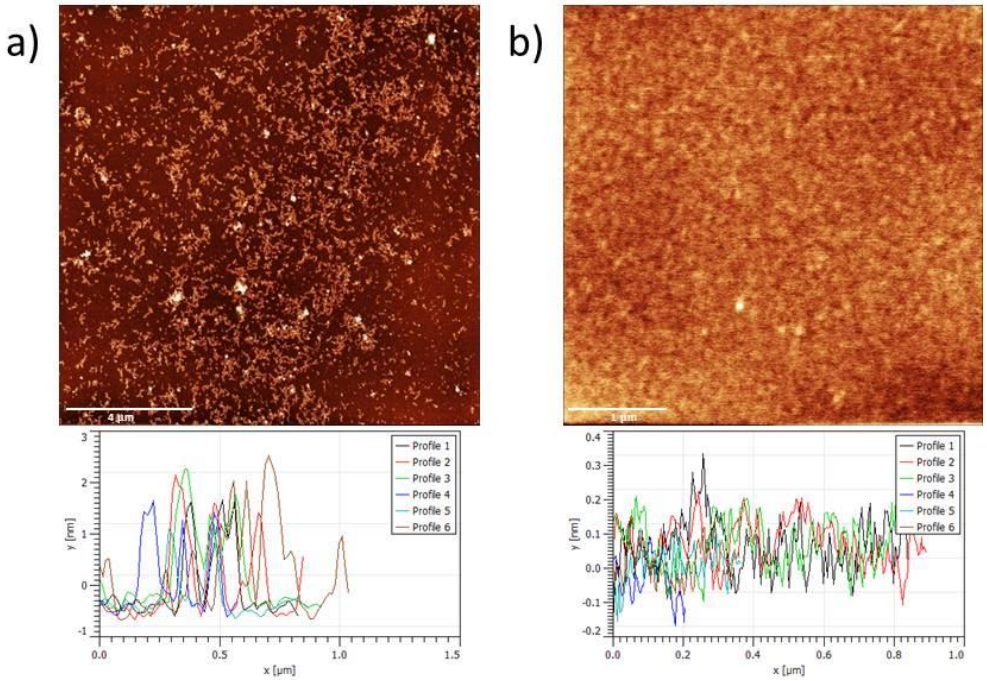

Figure 92: AFM images of the tritopic zwitterionic core molecule 74; pictures were prepared by dropping a DMSO solution of the respective concentration on a mica surface with subsequent spin-coating (60rps, 10 min) and analyzed by AFM tapping mode a) 0.001 mM sample; height up to 2-3 nm; b) 0.00001 mM sample, height around 0.3 nm

A concentration of only 1 µM 63 in DMSO still showed network like structures with a height of 2-3 nm. Here, these structures are smaller in it-self, but these small aggregates cover nearly the whole surface. Even the AFM measurement of a highly diluted sample with a concentration of 0.01 µM showed a very thinly (up to 0.5 nm) but completely covered mica surface. The visible patterns in this picture indicate that a network-like structure is still formed by the trivalent zwitterionic core. These results indicate a high stability of the aggregation of the zwitterionic core **74** and substantiates that the chosen design of the molecule indeed results in the required rigidity to avoid intramolecular interactions between the zwitterion and instead favors the intermolecular network formation, since this was observable even at extremely high dilution. Similar literature known systems like the *tren*-linked tris-zwitterion[28] or the quadruple zwitterion[29] in which the zwitterions are connected using flexible linkers do not show network-like structures at low concentrations. Instead the formation of smaller aggregates such as an intramolecular ring formation was observed.

Also the pH dependent switchability of the network formation by the guanidiniocarbonylpyrrole functionalized 1,3,5-trisphenylbenzene core was demonstrated with the use of AFM. Three samples were prepared in a DMSO solution. One sample only contained the zwitterionic core molecule. Trifluoroacetic acid was added to the second sample to obtain the cationic form of molecule **74**. The third sample was first treated with TFA and subsequently an equimolar amount of triethylamine was

added to readjust the pH value to regain the zwitterionic form. All three samples were measured by tapping mode AFM on mica surface.

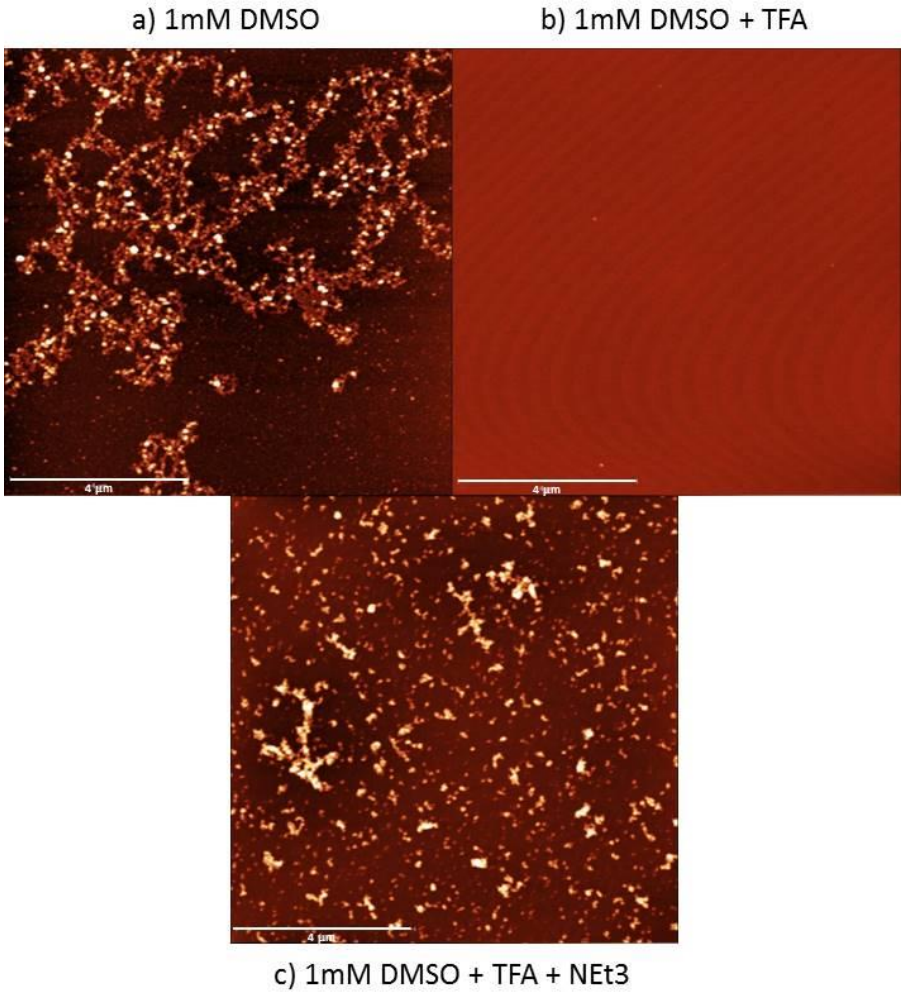

Figure 93: Tapping mode AFM measurement of the pH dependent switchability of network-like structures of core molecule 74; a) The image of a 1 mM 74 sample in DMSO (height 10-40 nm); b) The 1 mM sample after the addition of TFA (height 1-2 nm); c) The 1 mM sample of 74 after the addition of TFA and an equimolar amount of Triethylamine (height 10-30 nm)

Figure 93 a) shows the picture of an AFM measurement of a 1 mM sample in DMSO, where the network-like structures are prominent. In Figure 93 b) one can see the AFM picture after the addition of TFA. Due to the acid the carboxylate groups of the core molecule **74** were protonated and thus positively charged. Therefore the molecule **74** loses its capability to form any kind of aggregates, which is confirmed by the AFM measurement of this sample. The image shows only very few small assemblies with heights of 1-2 nm, but mostly an empty mica surface and no higher aggregates whatsoever are visible. This clearly illustrates that the formation of higher, network like structures is as expected not possible anymore after the protonation of the zwitterionic binding motif. By adding

an equimolar amount of triethylamine network-like structures should reform. Indeed, when the pH value is readjusted by the addition of an equivalent amount of triethylamine the formation of networks is occurring and was measured by AFM, shown in Figure 93 c). The aggregates visible in Figure 93 c) are branched structures and show heights of 10-30 nm, which is comparable to the heights of the original 1 mM sample. However, the network-like structures are not as distinct as the ones in a). Due to the sample preparation also a small amount of water is added to the DMSO solution together with the TFA and also the triethylamine. The addition of water interfered with the network formation, resulting in smaller and less defined structures.

AFM measurements in DMSO : water mixtures with a vast excess of water did not show the network formation at all but rather vesicle like aggregates. Since the zwitterionic core molecule is not soluble in pure water and rather hydrophobic it minimizes its surface in water and hence forms smaller vesicle like structures instead of three dimensional networks.

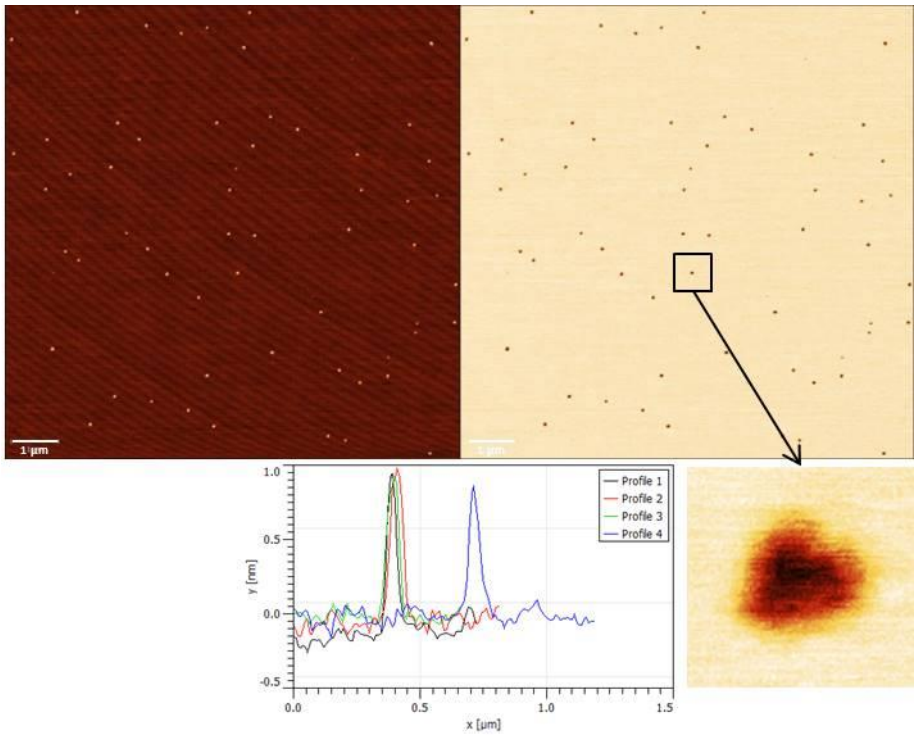

Figure 94: AFM measurement of the tritopic zwitterionic core molecule 74 on mica surface prepared from aqueous solution (0.5 % DMSO, 0.1 mM); left: Height image, showing small vesicle like structures with height around 1 nm; right: The respective phase image with an exemplary zoom on one particle to make the halo better visible; bottom: height profile

These vesicles can be seen in the AFM measurements in Figure 94. The left picture represents the height image, showing small dots with a height of around 1 nm on an otherwise empty mica surface. On the right side the phase image is depicted. The phase of an AFM measurement represents the

softness of a measured material or aggregate. The darker the color of a structure is imaged, the softer the material is. This phase picture indicates, that these dots are indeed a soft matter since they are darker (softer) than the mica surface. A slightly lighter rim visible in the zoom-in picture in Figure 94 b) around the dark particles is called halo and indicates vesicle-like aggregates.

Another microscopy method which was used to image the network-like structures formed by the tritopic zwitterionic core was transmission electron microscopy. The measured sample was prepared from a 0.001 mM solution of the tritopic zwitterionic core molecule **74** in DMSO and stained with uranyl acetate. The TEM image in Figure 95 shows a large aggregate with a length of approximately 400 nm, consisting of several smaller nano-assemblies with a size of around 20 nm.

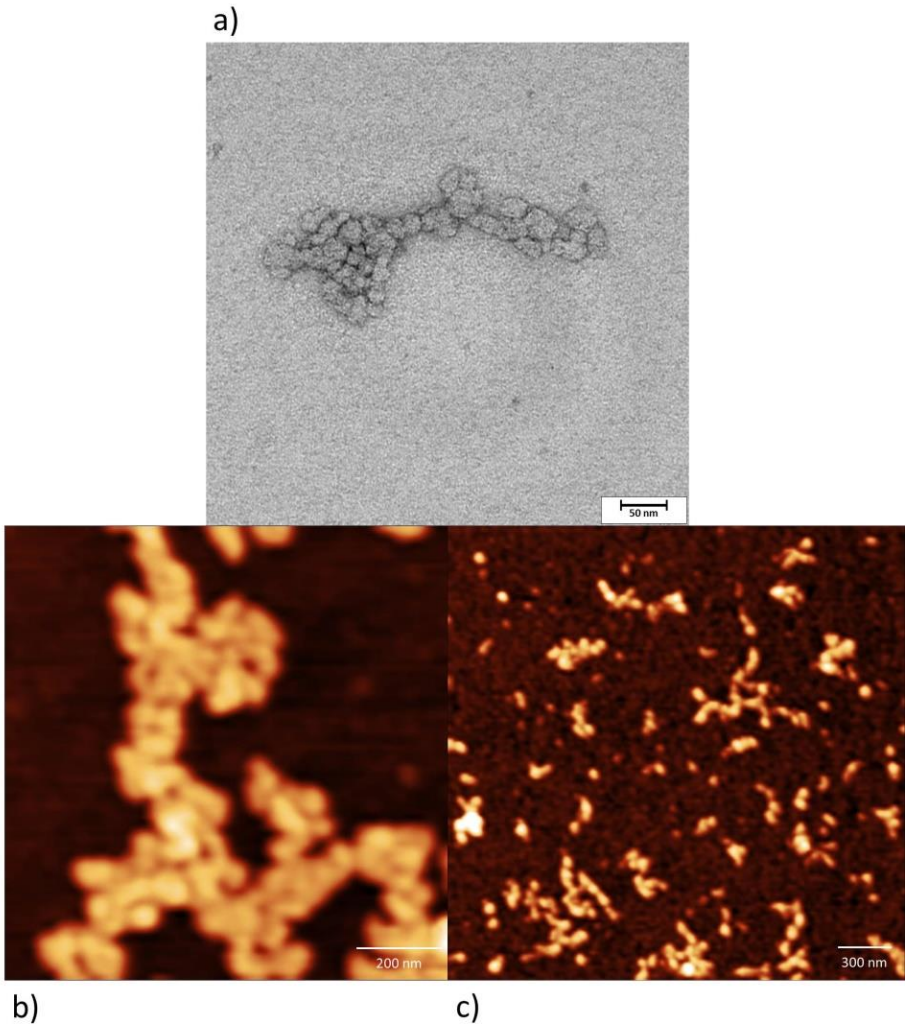

Figure 95: a) TEM image of the tritopic zwitterionic core molecule 74 (0.001 mM in DMSO/stained with uranyl acetate); b) zoom-in on the aggregate structures visualized by AFM (0.01 mM in DMSO); c) zoom-in on AFM picture (0.001 mM in DMSO)

Figure 95 b) is a zoom of an AFM picture taken from a 0.01 mM sample in DMSO. This close-up onto the zwitterionic core aggregate on the mica surface shows indeed the similarity and comparability of the aggregate structures visualized by AFM and TEM. The 0.01 mM AFM picture was chosen for the comparison solely due to reasons of the resolution of the AFM pictures. A close up of the same magnitude into the 0.001 mM AFM picture shows very similar structures yet the picture is less sharp. The AFM picture in Figure 95 c), prepared with a 0.001 mM sample in DMSO, shows that the overall size of the structures found on the mica surface for this concentration have the similar dimensions as the structures found via TEM, which lie approximately within 100-500 nm in length for the AFM picture and between 300-400 nm for the TEM pictures.

Unfortunately is was not possible to measure TEM images with a higher-resolution, due to the bad contrast of molecule **74**, even after staining the sample with uranyl acetate. But the resulting TEM image is still in good agreement with the expectation of the formation of higher, network-like structures by the tritopic zwitterionic core molecule **74**, which could already been proven by AFM measurements.

Overall, these TEM and especially AFM measurements helped to learn more about the shape of the aggregates formed by zwitterionic core molecule **74**. As expected, the observed aggregates showed a network like architecture, even at low concentrations down to 0.0001 mM. However, these experiments only reflect the aggregate formation on surfaces and not in solution.

4.2.2 Dynamic Light Scattering

To get further insight into the size and shape of the aggregates formed by the trivalent zwitterionic core molecule **74**, Dynamic Light Scattering (DLS) measurements were made to study the aggregation in solution as well and not only on a surface.

DLS allows measuring the hydrodynamic radius of particles based on the principle of the Brownian movement. A laser light is pulsed into the solution or dispersion and the back scattered light gets detected. Because of the movement of the particles the pattern of the backscattered light will change. That allows the calculation of the diffusion coefficient and then with the use of the Stokes-Einstein equation (1) the hydrodynamic radius of the given particles.

$$D = \frac{kT}{6\pi\eta r} \quad (1)$$

Equation 3: Stokes-Einstein equation for spherical objects in a constant medium of distinct viscosity; *D* = diffusion coefficient [$m^2 \cdot s^{-1}$], *k* = Boltzmann constant [$J \cdot K^{-1}$], *T* = temperature [K], , η = viscosity [$Ns \cdot m^{-2}$] and r as the hydrodynamic radius of spherical particle

However, the method has its drawbacks. The principle only delivers reliable and exact hydrodynamic radii values for spherical particles, due to the Stokes-Einstein equation. The more the given particles differ from the perfect spherical shape, the less accurate the determined hydrodynamic radius will be. Moreover larger particles will always give a stronger signal due to their larger surface resulting in a stronger backscattering of the light (scattering intensity is proportional to the sixth power of the particles radius r). That means that a few larger particles can give a stronger signal than a high number of small particles. It can even happen that the small particles cannot be detected anymore. Another problem can be the dynamic nature of supramolecular aggregates. Due to the equilibrium of their formation and disruption the particles are not shape and size consistent at all time. This can result in measurement errors. A solution for this problem is to make several measurements to find a good average value to work with. The results of the DLS measurements are given as a size distribution by number, since the number of particles with respective sizes (hydrodynamic radii) is the significant parameter, instead of the radius dependent intensity of the scattered light. To be able to obtain reliable data, it makes sense to make several measurements for each sample and thus verify the results. In general, if the curves are labeled with consecutively numbered and labeled with the letter M, representing measurement, each curve is an individual, non-time dependent measurement of the same sample, done in succession without any delay aside from the respective previous measurements.

Due to the poor solubility of the tritopic zwitterionic core molecule **74** the sample was treated with ultrasound to dissolve the molecule in DMSO. During the first attempt to get a good measurement of the solution it appeared that the measured size of the particles depend on the duration of time the sample was treated with ultrasound. After 155 consecutive minutes of ultrasound treatment the smallest particle size of only around 5 nm was measured, as shown in Figure 96.

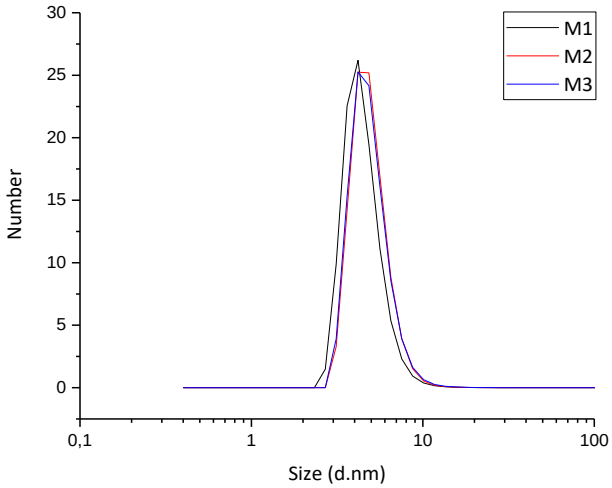

Figure 96: DLS measurement (size distribution by number) of a 1 mM sample of the tritopic zwitterionic core molecule 74 in DMSO after consecutive 155 min in ultrasonic bath; the measured curves range from hydrodynamic radii of 1.5-10 nm with a maximum at 5 nm

In the following the sample was kept at ambient conditions for several months to determine if the sample's aging influences the size of the aggregates and if at a certain size of the aggregates a thermodynamic equilibrium of the aggregation process exists. DLS measurements were done after 3, 4, 9 and 10 months of aging. After three months the size of the aggregates increased up to 12 nm, after four months to 14 nm and after 9 months up to 18 nm. After ten months a size of around 20 nm was measured (Figure 97).

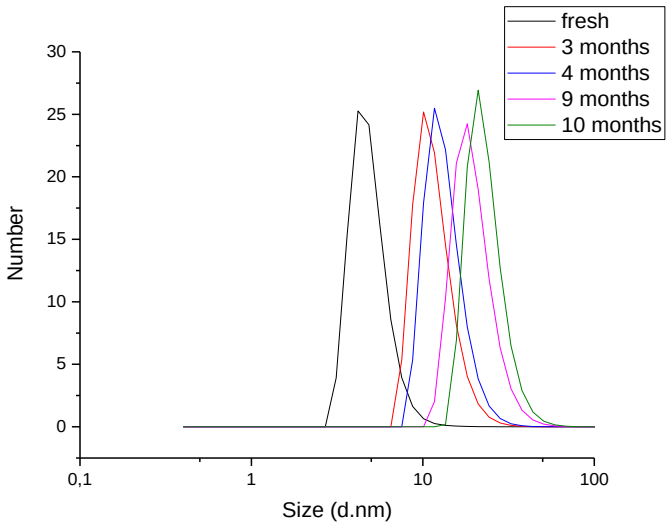

Figure 97: Sizes of the aggregates formed by the tritopic zwitterionic core molecule (1 mM) after ultrasonification (5 nm) and after aging for 3 months (12 nm), 4 months (14 nm), 9 months (18 nm) and 10 months (20 nm)

The ten-fold dilution of the aged sample did not affect the particle size, as shown in Figure 98.

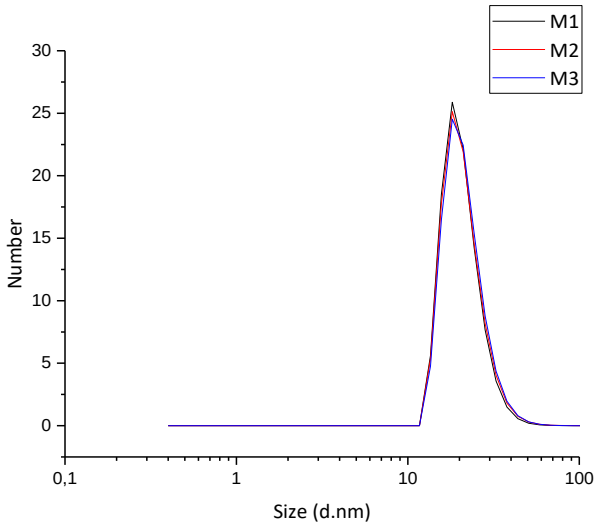

Figure 98: DLS measurement (size distribution by number) of a 0.1 mM sample of the tritopic zwitterionic core molecule 74; measured hydrodynamic radius 17-21 nm

These data suggest that thermodynamic equilibrium of the aggregation process exists at a size of around 20 nm at a concentration of 1 mM as well as 0.1 mM.

The DLS measurements were not only carried out in DMSO but also in water, since the overall goal is to work in pure water anyway. We used two different approaches to work in water. The zwitterionic molecule is not soluble in water, but it is possible to use a DMSO stock solution with a high concentration to prepare a solution in water with a low concentration and a small fraction of DMSO.

A sample with a fraction of 0.5 % DMSO in water and a concentration of 0.1 mM was prepared and measured with DLS (Figure 99). The determined sizes of 20-23 nm are in the same range as the 0.1 mM sample in pure DMSO.

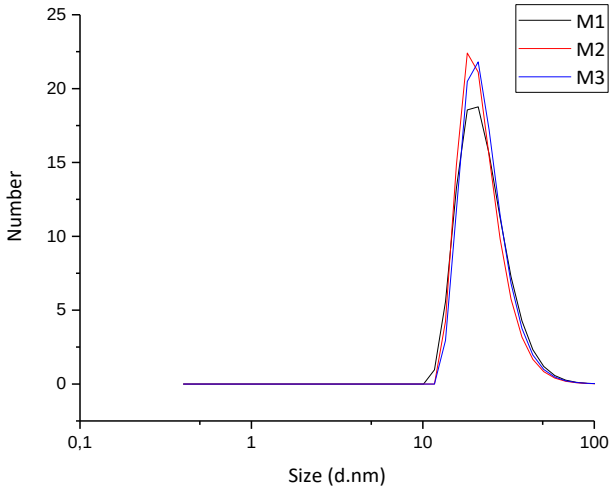

Figure 99: DLS measurement (size distribution by number) of a 0.1 mM sample of the tritopic zwitterionic core molecule 74 in water with 0.5 % DMSO; measured hydrodynamic radius 20-23 nm

The aggregates of the tritopic zwitterionic core molecule seem to reach an equilibrium at a certain size of around 20 nm, which is in the range of approximately 14 molecules per aggregate based on the surface of a spherical vesicle. Moreover, it is interesting to compare these sizes determined by DLS with the aggregate size found by the AFM measurements done from an aqueous solution.

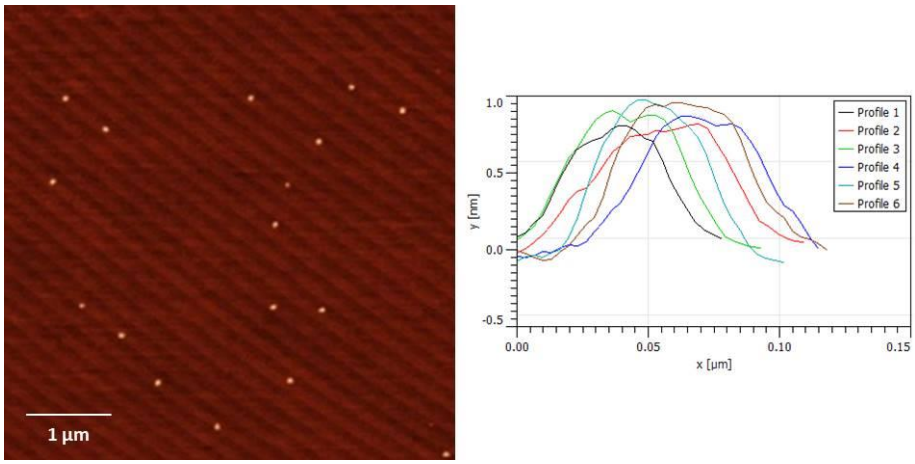

Figure 100: AFM measurement of the tritopic zwitterionic core molecule 74 on mica surface prepared from aqueous solution (0.5 % DMSO, 0.1 mM)

Assuming the aggregates sit on the mica surface in an ellipsoid shape, it is possible to estimate their volume by measuring the length (a), width (b) and height (c) of the aggregate on the surface and place the resulting values in following equation (2).

$$V = \frac{4}{3} \times \pi \times a \times b \times c \quad (2)$$

Equation 2: Equation to calculate the volume of an ellipsoid

The determined sizes of the particle on the mica surface were approximately 1 nm in height and around 70-80 nm in width and length. So the volume of these particles is 18.5 µm^3.

This volume can be used to calculate the radius of a sphere, which should be the idealized shape of the aggregates in solution, using equation (3).

$$V = \frac{4}{3} \times \pi \times r^3 \quad (3)$$

Equation 3: Equation to calculate the volume of a sphere

The resulting radius of these particles is 16 nm or a diameter of around 32 nm respectively. Given the fact, that the determination of particle sizes via AFM, aside from the height, are not very exact and these calculations are rather estimations, the sizes of the particles found on AFM compared to the sizes found with DLS are at least within the same magnitude.

The second option to prepare a sample in water is to dissolve the tritopic zwitterionic core molecule **74** in 0.1 M sodium hydroxide solution, since the anion is water-soluble. That allows the preparation of a 10 mM stock solution which can be diluted to the needed sample concentration with water and aqueous HCl to readjust the pH-value back to 6. This way the zwitterionic trivalent core building block is dissolved and stable in water at a concentration of 0.1 mM, which was used for DLS measurements (Figure 101). The sizes of the aggregates however show bigger variations when measured with DLS and lie within a range of 6 to 18 nm. A reason for this behavior can be the fresh formation of these aggregates after the complete disruption caused by the solving in aqueous sodium hydroxide. The aggregation process did not reach completely the thermodynamic equilibrium at this point and assemblies of all sizes between 6 and 18 nm do exist.

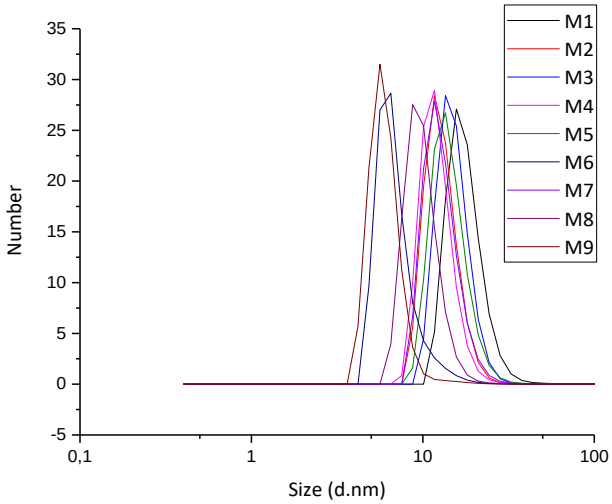

Figure 101: DLS measurement (size distribution by number) of a 0.1 mM sample of the tritopic zwitterionic core molecule 74 in water (prepared from 0.1 M NaOH stock solution); measured hydrodynamic radii between 6-18 nm

As a comparison a sample of the tritopic core at a pH value of 11.9 was measured (Figure 102). It shows a size distribution of 0.6-2.6 nm. These inconsistent sizes probably result from the non-spherical architecture of the molecule, which is rather flat and has an estimated length of approximately 3 nm. However, by means of this measurement it is possible to conclude that the core molecule does not form any aggregates at basic pH, but instead the monomers are present.

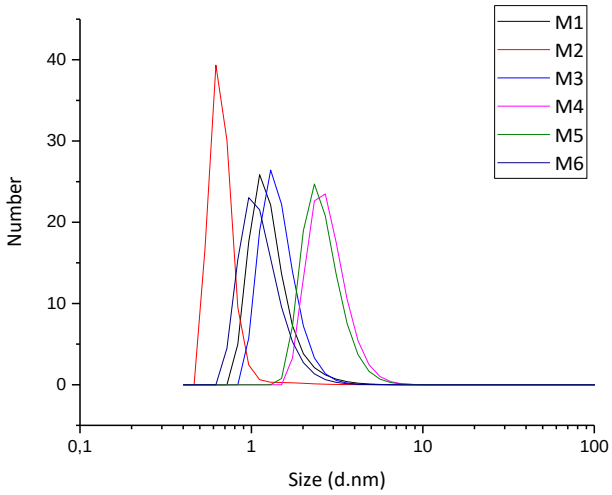

Figure 102: DLS measurement (size distribution by number) of a 0.07 mM sample of the tritopic zwitterionic core molecule 74 in water (prepared from 0.1 M NaOH stock solution) at a pH value of 11.90; measured hydrodynamic radii between 0.6-2.6 nm

4.2.3 Summary

The successful synthesis of the tritopic zwitterionic core in good yields allowed studies of the properties of the molecule **74** in surface using AFM and TEM and in solution using DLS. AFM measurements strikingly demonstrated the network-like aggregation of the molecule even in low concentrations. Also the pH switchability of these structures was confirmed using AFM. DLS studies revealed the size of the aggregates in DMSO and aqueous solution, allowing a comparison of the particle sizes between the aggregates formed by solely the core molecule and the aggregations formed after the addition of the zwitterionic dendrons. The addition of these dendrons and the formation of the templated supramolecular dendrimers will be discussed in the following chapter.

4.3 Addition of Dendron

As mentioned above the goal of this work is to form a templated supramolecular dendrimer. More precisely this supramolecular dendrimer is a pH switchable one-to-three core-shell architecture consisting of the core building block **74** and the zwitterionic dendrons. Figure 103 illustrates the breaking up of the 3-D networks of the self-assembled core due to the addition of the zwitterionic [G3]-dendron to the network-like structure of the tritopic zwitterionic core molecule **74** and the formation of the templated supramolecular dendrimer.

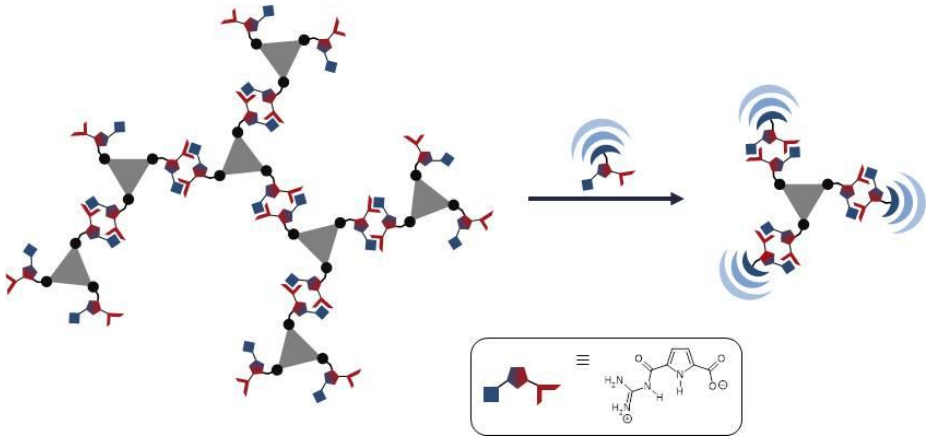

Figure 103: Simplified illustration of the disassembly of the 3-D networks of the self-assembled zwitterionic trivalent 1,3,5-trisphenylbenzene core due to the addition of the zwitterionic [G3]-dendrons and the formation of the templated supramolecular dendrimer (core-shell architecture)

Force field calculations (Macromodel, OPTS 2005, water solvation model; calculations done with the help of Dipl. Ing. Wilhelm Sicking) helped to predict the size and shape of a templated supramolecular dendrimer. These calculations revealed that the core-shell architectures can be expected to be not perfectly spherical with a diameter of approx. 3.3-4.4 nm. The dendrons do not surround the 1,3,5-trisphenylbezene core evenly, but rather gather on one side. The calculated structure is illustrated in Figure 104.

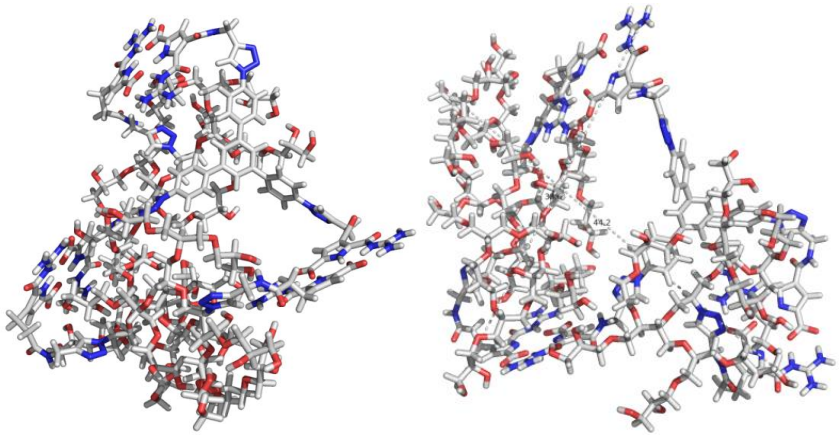

Figure 104: Molecular modelling (conformational search) of the structure of a supramolecular dendrimer (Macromodel, OPTS 2005, water solvation model, 1000 cycles), seen from two different angles, Size 3.3 nm x 4.4 nm; calculations were done with the help of Dipl. Ing. Wilhelm Sicking

So the hope was that the addition of a minimum of three equivalents of the zwitterionic dendron should lead to a destruction of the core networks and to the formation of distinct 1 : 3 aggregates. This however is not that easy for several reasons. The binding constant of the zwitterionic guanidiniocarbonyl pyrrole dimer is very strong even in water (K_{ass} = 170 M^{-1}), so although it is a dynamic system the networks are reasonably stable. The zwitterionic dendrons form dimers, which are even more stable than the usual binding motif because the dendrons fold themselves around the zwitterions and shield them from the solvent creating a less polar micro-environment.[128] A similar effect for the 3-D network of the 1,3,5-trisphenylbezene core is quite plausible, which makes the breaking up of these networks and thus the core-shell architecture formation even harder.

4.3.1 Methods in Solution

In a first attempt of forming the core-shell architectures zwitterionic [G2]-dendrons **131** were added to a 0.42 mM solution of the zwitterionic core molecule **74** in a 5 % DMSO in water mixture. DLS measurements of the tritopic zwitterionic core after 155 minutes of ultrasonification showed sizes of around 5-6 nm. The addition of 12 equivalents zwitterionic [G2]-dendron revealed an increase of the size to 8-10 nm. Both measurements are depicted in Figure 105.

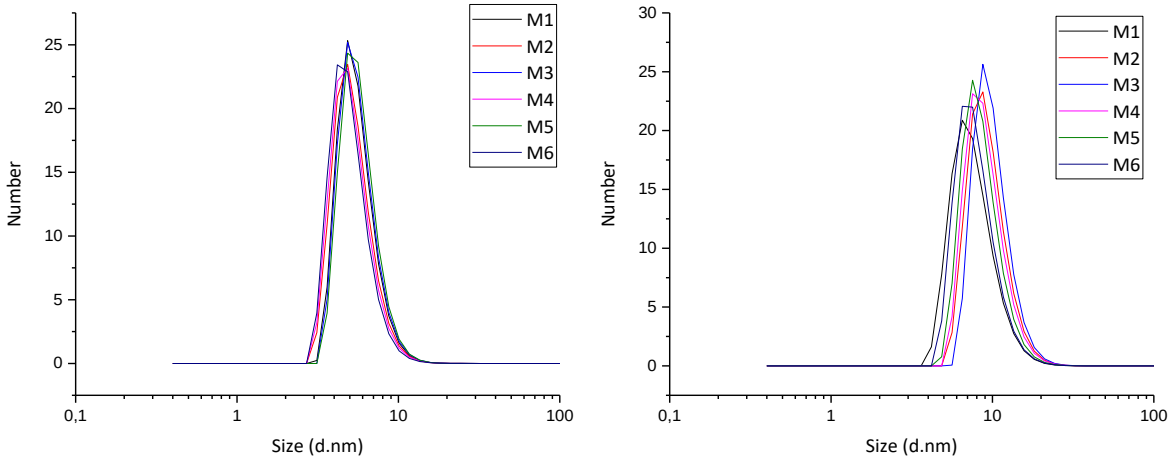

Figure 105: Left: DLS measurements (size distribution by number) of a 0.42 mM solution of the tritopic zwitterionic core molecule 74 in water/5 % DMSO after ultrasonification for 155 minutes; measured sizes of 5-6 nm; Right: DLS measurements (size distribution by number) of a 0.42 mM solution of the tritopic zwitterionic core molecule 74 in water/5 % DMSO with 12 equivalents of zwitterionic [G2]-dendron; measured sizes 8-10 nm

The increase of the size after the addition of zwitterionic [G2]-dendron **131** means that the dendrons surround the core networks instead of breaking these up as illustrated in Figure 106, while the spare dendrons should be present as [G2]-dimers.

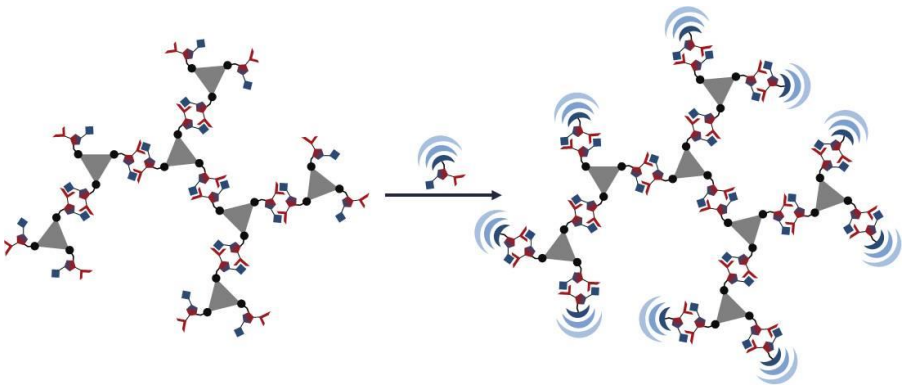

Figure 106: Simplified illustration of the addition of an insufficient amount of [G3]-zwitterions to the networks formed by the tritopic zwitterionic 1,3,5-trisphenylbenzene core molecules

One option to overcome this problem is to simply increase the amount of dendron. However, an even better suitable approach is to additionally mix the core and dendron as anion and cation respectively and subsequently readjust the pH back to the required value of 6. This approach was pursued with different equivalents of [G3]-dendron **46** and the results were measured by DLS. The DLS measurements after the addition of 3 equivalents of [G3]-dendron dissolved in 0.1 M aqueous HCl to an aqueous solution of the tritopic core in 0.1 M NaOH are depicted in Figure 107.

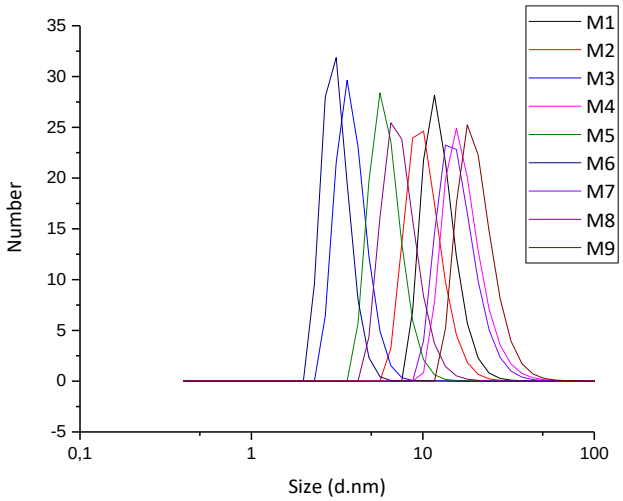

Figure 107: DLS measurements (size distribution by number) of an aqueous solution of the tritopic zwitterionic core molecule 74 with 3 equivalents of zwitterionic [G3]-dendron (sample prepared from the respective aqueous NaOH and HCl stock solutions); measured sizes between 3-20 nm

The results of several DLS measurements gave several different sizes between 3-20 nm. Thus, these results are comparable with the DLS measurements of the core **74** without [G3]-dendron **46** in aqueous solution (Figure 101, 6-18 nm). Only the small sizes between 3-6 nm differ from the previous results. That means that the sample probably consists of all possible aggregates including higher network-like structures formed by the core **74**, network-like structures surrounded by [G3]-dendrons, [G3]-dendron dimers and potentially also some 1 : 3 aggregates. The consequence was to increase the amount of zwitterionic [G3]-dendron up to 10 equivalents. These DLS results are depicted in Figure 108.

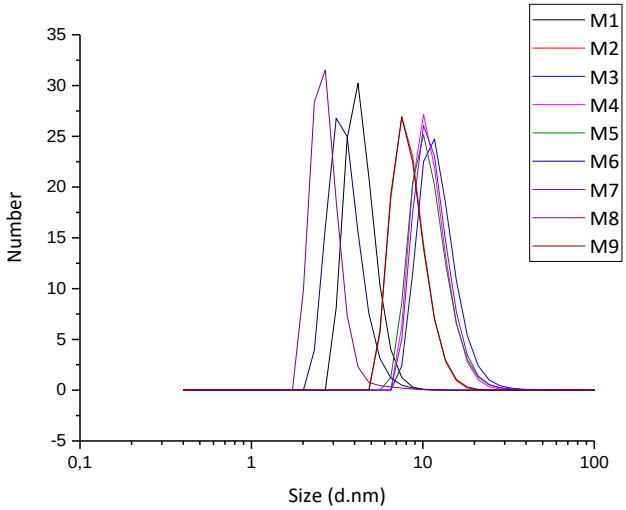

Figure 108: DLS measurements (size distribution by number) of an aqueous solution of the tritopic zwitterionic core molecule 74 with 10 equivalents of zwitterionic [G3]-dendron (sample prepared from the respective aqueous NaOH and HCl stock solutions); measured sizes between 3-12 nm

The DLS measurement results of the sample with 10 equivalents zwitterionic [G3]-dendron **46** and the core **74** reveal a narrower size distribution of the aggregates between 3-12 nm, meaning that the addition of a larger amount of dendron led to a higher degree of network disruption and therefore a bigger fraction of smaller aggregates probably including the 1 : 3 aggregate. However, it did not show the hoped for result thus the amount of [G3]-dendron was further increased up to 45 equivalents. These DLS measurement results are shown in Figure 109.

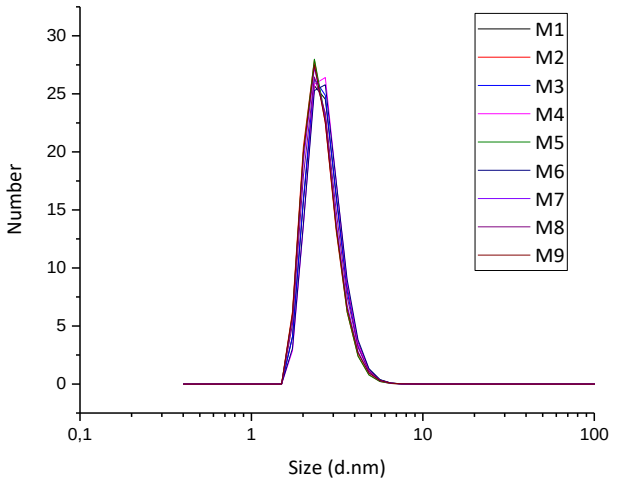

Figure 109: DLS measurements (size distribution by number) of an aqueous solution of the tritopic zwitterionic core molecule 74 with 45 equivalents of zwitterionic [G3]-dendron (sample prepared from the respective aqueous NaOH and HCl stock solutions); measured sizes around 3 nm

After the addition of 45 equivalents of zwitterionic [G3]-dendron **46** DLS measurements indicate a consisting size of aggregates of around 3 nm, which can be deceptive, since we have two different kinds of aggregates in this sample. These are the [G3]-dendron dimers and probably the 1 : 3 aggregate. However, the peak in the DLS measurements is quite broad, including a range from 1.5-5 nm. Only the maximum of the peak is at a hydrodynamic radius of 3 nm. The sample includes 45 mM zwitterionic [G3]-dendron **46** and 1 mM tritopic zwitterionic core molecule **74**, meaning that only 1 mM of the templated dendrimer can exist, while the [G3]-dendron dimers can have a concentration of 21 mM. Thus approximately only 5 % of the assemblies within the sample are the supramolecular dendrimer and correspond to the measured DLS values higher than 3 nm, probably around 4.5 nm, while the majority of the nano-assemblies within the sample are the [G3]-dendron dimers, corresponding to 3 nm (lit DLS 3.4 nm[128]). The size difference between these two aggregates is so small, that it is not possible to distinguish between them with DLS and thus resulting only in one broad peak. However, these measurement results allow to conclude, that using this sample preparation and a high excess of dendron there are no longer any larger aggregates formed by the tritopic zwitterionic core, instead only the distinct 1 : 3 aggregates are formed by the core and the [G3]-dendron.

To verify the measured hydrodynamic radii with another method in solution, diffusion-ordered spectroscopy, short called DOSY-NMR[130], measurements were done. With DOSY-NMR it is possible to determine the size of a molecule by measuring the diffusion coefficient. Similar to DLS, the principle of DOSY NMR is based on the Brownian motion or self-diffusion, which is the translational random motion of particles. The use of pulsed magnetic field gradients allows the measurement of spatially resolved NMR and hence allows the determination of the diffusion coefficient. The self-diffusion can be described by the diffusion coefficient and depends on several factors such as effective weight, size and shape of the molecule at given conditions like viscosity and temperature. The *Von Smoluchowski* equation (equation 4) describes the correlation of diffusion coefficient and molecular size, whereat the molecular size is implied in the hydrodynamic friction coefficient *f*.

$$D = \frac{kT}{f} = \frac{RT}{Nf} \tag{4}$$

Equation 4: Von Smoluchowski equation for correlation of diffusion coefficient and molecular size; D = diffusion coefficient [$m^2 \cdot s^{-1}$], k = Boltzmann constant [$J \cdot K^{-1}$], T = temperature [K], N = Avogadro's constant[mol^{-1}], R = gas constant [$J \cdot mol^{-1} \cdot K^{-1}$], f = hydrodynamic friction coefficient

The *Einstein* equation (equation 5) describes the hydrodynamic friction coefficient *f*, which correlates to the hydrodynamic radius of a spherical object in a medium of defined viscosity η.

$$f = 6\pi\eta r \tag{5}$$

Equation 5: Einstein equation for spherical objects in a homogenous medium of defined viscosity for *f*, η = viscosity [Ns·m^{-2}].

Combining both, the *Von Smoluchowski* and the *Einstein* equation yields the *Stokes-Einstein* equation (equation 1) which describes the diffusion coefficient for spherical objects in a constant medium of distinct viscosity.

$$D = \frac{kT}{6\pi\eta r} \tag{1}$$

Equation 1: Stokes-Einstein equation for spherical objects in a constant medium of distinct viscosity

With the *Stokes-Einstein* equation the hydrodynamic radius of a spherical object can be calculated after the determination of the diffusion coefficient by DOSY NMR.

The COSY NMR experiment was performed in a water : D_2O (9 : 1) mixture with a concentration of 1 mM core **74** and 30 equivalents of zwitterionic [G3]-dendron **46**. The spectrum is depicted in Figure 110.

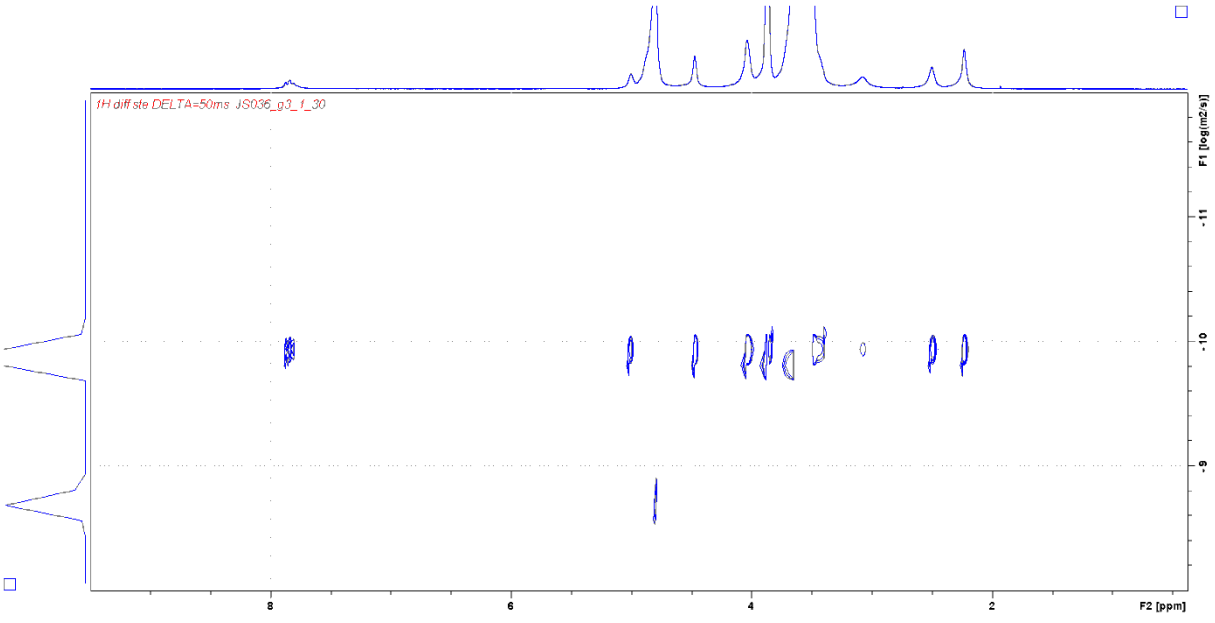

Figure 110: DOSY NMR spectrum of 1 mM zwitterionic core 74 with 30 equivalents zwitterionic [G3]-dendron 46 in a water : D2O mixture (9 : 1)

Two diffusion coefficients were determined by using two peaks in the spectrum, which belong distinctively to either the core (7.84 ppm; aromatic CH) or the dendron (3.57 ppm; polyglycerol CH_2/CH).

Table 2: Determined diffusion coefficients

Chemical shift	Molecule	Diffusion coefficient [m^2/s]	Hydrodynamic radius [nm]
3.57 ppm	Dendron (polyglycerol CH_2/CH)	1.05E-10	2.33
7.84 ppm	Core (aromatic CH)	1.06E-10	2.31

However, the values of these diffusion coefficients are very close together, although there were two different aggregates present in the sample. This is due to a high exchange rate of single molecules between dimer and the core-shell architecture and their small size difference. The determined diameter of the aggregates was 4.62 nm and 4.66 nm respectively, and therefore within the size range that would have been assumed by previous calculations and DLS measurements.

4.3.2 Microscopy

The change of the aggregate upon dendron addition was also monitored by atomic force microscopy. This allows, in addition to the already by DLS and DOSY NMR determined particle sizes, also the determination of a visible picture of the type of aggregation. However, the AFM samples are prepared from a DMSO solution for two reasons. First it was not possible to detect any networks-like structures formed by the tritopic zwitterionic core molecule **74** for a sample prepared from an aqueous solution even with a sample containing solely core **74** (see 4.2.1, Figure 94). So the measurement in pure water would not allow a comparison of aggregates formed by the core and aggregates formed by core and dendron. Second, the sample preparation in pure water includes the use of NaOH and aqueous HCl, thus sodium chloride was present on the surface and overshadowed the structures we actually wanted to see.

Again, for an early attempt to detect a significant change of the aggregation after the addition of zwitterionic dendron, the smaller [G2]-dendrons **131** were used. A sample of the core **74** (prepared with a 0.08 mM DMSO solution) and 16 equivalents of [G2]-dendron **131** was analyzed with tapping mode AFM. The AFM images still clearly showed the network formation of the core **74**. Figure 111 shows this AFM image, while Figure 111 b) depicts a close up of the area within the white square in a), allowing a more detailed view on the structures on the mica surface.

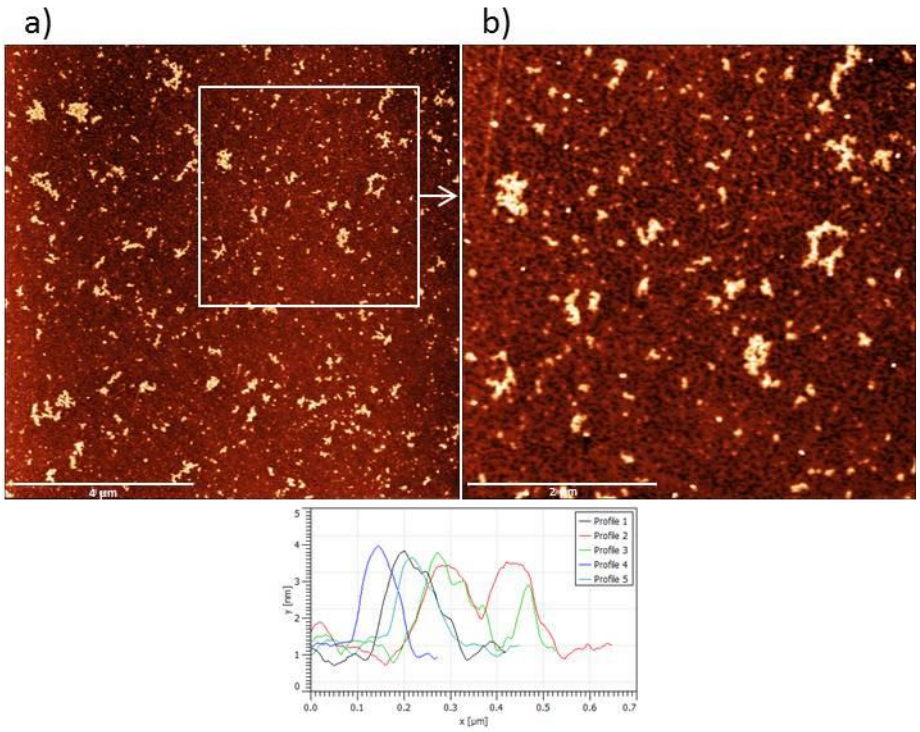

Figure 111: a) AFM image of the tritopic zwitterionic core molecule 74 (0.08 mM in DMSO) with 16 equivalent zwitterionic [G2]-dendron 131, showing network like structures with heights of around 3 nm; b) close up of the in a) framed area

However, the visible aggregates are smaller and cover a smaller area on the surface as the aggregates, which were observed for only core molecule **74** in this concentration range (around 0.1 mM). This allows the conclusion that the networks formed by the core **74** were already disrupted by the addition of the [G2]-dendron **131** to a certain extent and thus smaller. The next step was to use the better water-soluble and bigger [G3]-dendron **46** again and a stepwise increase of the [G3]-dendron equivalents from 3, 10 to 30 equivalents. The resulting AFM images are depicted in Figure 112. The samples were prepared in DMSO solution with a concentration of the tritopic zwitterionic core molecule **74** of 0.001 mM.

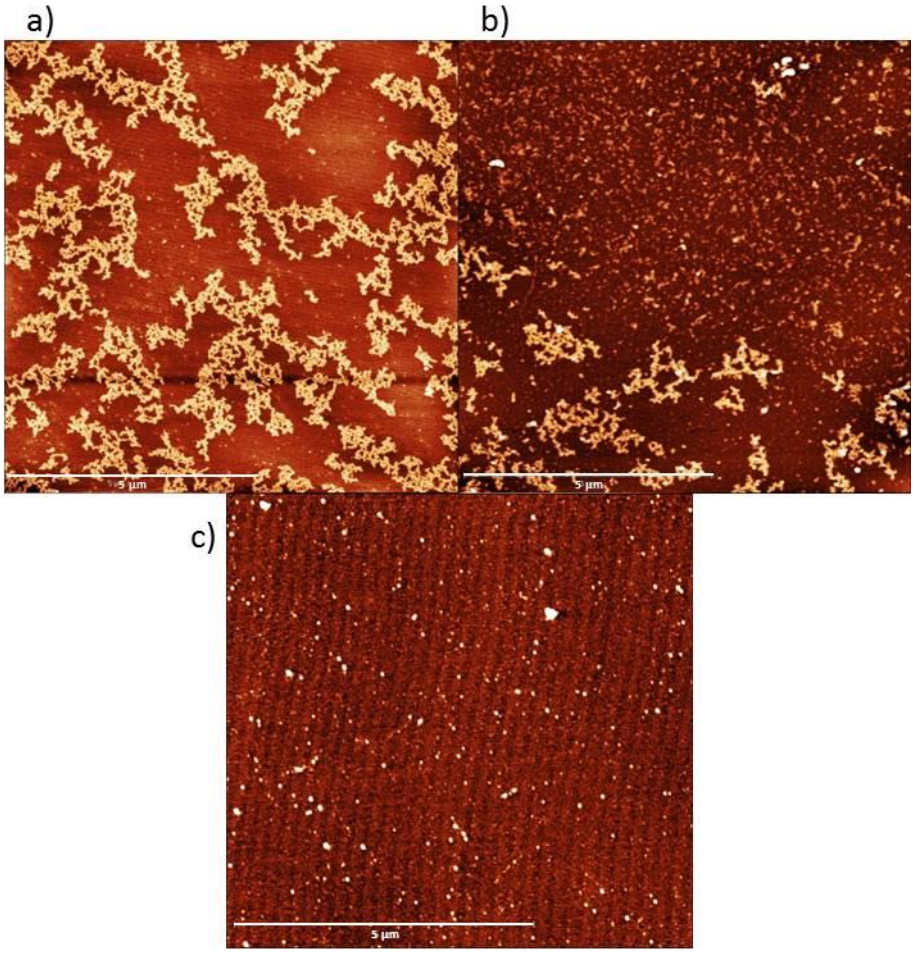

Figure 112: AFM images of the tritopic zwitterionic core molecule 74 (0.001 mM in DMSO) with increasing equivalents of zwitterionic [G3]-dendron 46; a): 3 equivalents [G3]-dendron, heights around 3 nm; b): 10 equivalents [G3]-dendron, heights around 3 nm; c) 30 equivalents [G3]-dendron, heights around 1.5-10 nm

The addition of only 3 equivalents zwitterionic [G3]-dendron **46** did not significantly influence the aggregation behavior of the core molecule, since distinct network-like structures with a height of around 3 nm could be observed in Figure 112 a). These structures are comparable with those observed for the 0.001 mM sample solely containing core **74**. A mixture of the core molecule with 10 equivalents of [G3]-dendron is shown in Figure 112 b). Here, some core networks are still present too, but they are not as dominant as in the sample with only 3 equivalents zwitterionic [G3]-dendron. So an increasing amount of [G3]-dendron lead to decreasing number of visible network-like structures. Finally with an amount of 30 equivalents of the zwitterionic [G3]-dendron **131** no networks were formed by the core molecule **74** shown by the AFM image in Figure 112 c). The mica surface is covered with dots of different sizes with heights between 1.5 and 10 nm.

These AFM measurement illustrated that the network formation by the tritopic zwitterionic core molecule **74** decreased with increasing [G3]-dendron equivalents and could not be observed for 30 equivalent of dendron. Although the sample preparation took place in DMSO and core and dendron

were mixed as zwitterions, the disruption of higher network could be achieved. AFM measurement using a ten times higher concentration of the core and dendron, but in the same 1 : 30 ratio, showed the same result. No higher network-like structures were visible on the mica surface in the AFM image (Figure 113), only small dot-like particles.

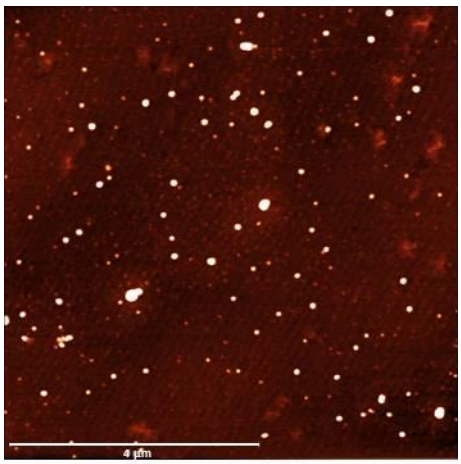

Figure 113: AFM images of the tritopic zwitterionic core molecule 74 (0.01 mM in DMSO) with 30 equivalents [G3]-dendron, heights between 1-14 nm

Another imaging method used was TEM. This however did not seem to be the most appropriate method for given molecules. Despite staining the samples with uranyl acetate the contrast was rather poor, so the pictures are not ideal. For the sake of comparison the measurement of the sample without dendron and the TEM measurement of core with dendron are depicted in Figure 114. Both samples were prepared from a DMSO solution, one with 0.001 mM core (Figure 114 a), left) and the other with 1 µM core and 30 equivalents 3rd generation dendron (Figure 114 b), right).

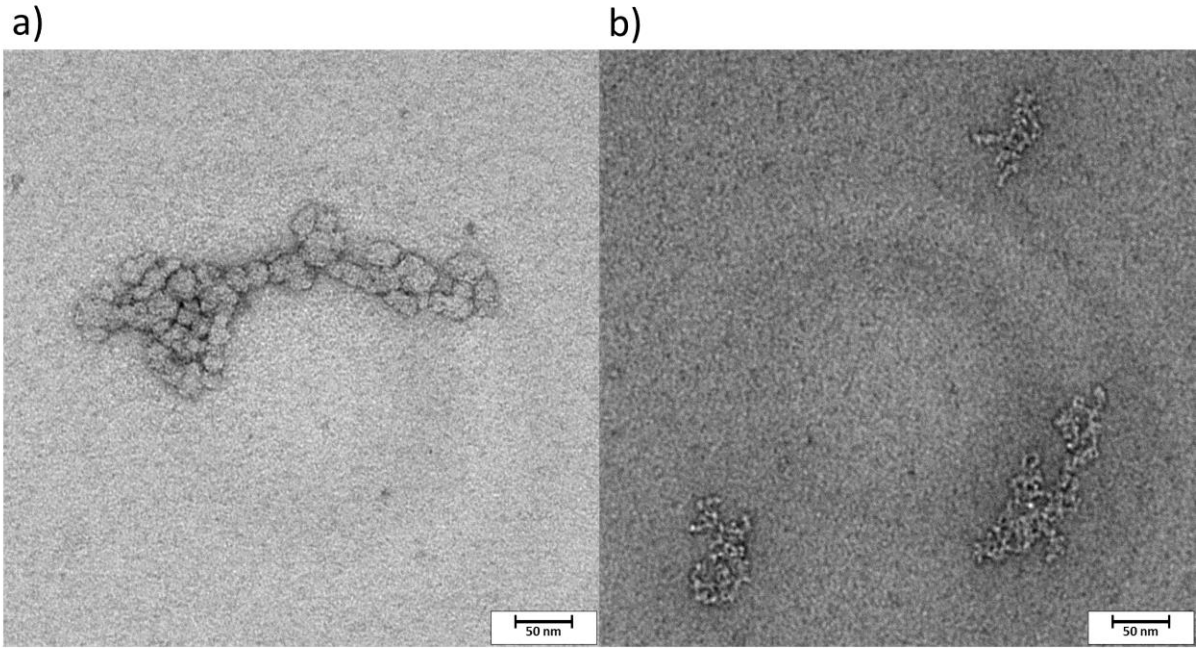

Figure 114: Comparison of TEM picture of the aggregates formed by the tritopic zwitterionic core (left a), 0.001 mM in DMSO) and the TEM picture of the mixture of the trivalent zwitterionic core and 30 equivalents [G3]-dendron (right b), 0.001 mM core and 0.03 mM [G3]-dendron in DMSO)

On picture Figure 114a) one can see the assembly formed just by the tritopic zwitterionic core molecule **74**. This aggregate shows a length of around 350 nm and width of at least 20-30 nm. As discussed earlier the size of the aggregate found via TEM measurement are within the same dimension found on AFM at the same concentration. After the addition of 30 equivalents [G3]-dendron **131**, the aggregates on the TEM picture (Figure 114b) are significantly smaller with sizes around 50-70 nm. These TEM pictures do not show the difference between the core molecule and the mixture with core and G3 dendron as clearly as the previous DLS and AFM measurements, but they follow the overall trend nonetheless.

4.3.3 Summary

The formation of a templated supramolecular dendrimer was studied by the addition of guanidiniocarbonylpyrrole carboxylate zwitterion functionalized [G2] and [G3]-dendron to the tritopic guanidiniocarbonylpyrrole carboxylate zwitterion functionalized template in DMSO and aqueous solution. DLS measurement showed that after the addition of 45 equivalents [G3]-dendron **46** to the core **74** only small aggregates in the rage of 1.5-5 nm were formed. These sizes are in good agreement to the size of the [G3]-dendron dimers, with 3 nm, and to the 1 : 3 aggregate of the templated dendrimer, with s size around 4.5 nm. Calculations of the structure of the supramolecular

templated dendrimer indicated a size of 3.3-4.4 nm, which fits well with the measured sizes in DLS. Also DOSY-NMR measurement of the mixture of the tritopic zwitterionic core molecule with 30 equivalents of zwitterionic [G3]-dendron revealed a size of 4.6 nm for the formed 1 : 3 aggregates.

Table 3: Measured or calculated sizes for the templated supramolecular dendrimer

Method	**Core-dendron ratio [eq]**	**Size in [nm]**
DLS	1 - 45	3-5
DOSY-NMR	1 - 30	4.6
Force field calculation	1 - 3	3.3-4.4

AFM measurements visualized the decreasing network structure of the core with increasing [G3]-dendron concentration. At a core-dendron ratio of 1 : 30 no network formation could be observed. This confirms the results of DLS and DOSY-NMR measurements in solution.

4.4 Solubilization studies

In this chapter the potential application of these pH switchable core-shell architectures will be discussed. The capability to solubilize poorly or non-water-soluble substances by the supramolecular dendrimer was studied to verify if these architectures could possibly be a tool to transport active agents such as cancer drugs, which were not well accessible due to solubility issues, into the body. For this project it is crucial that the formed core-shell-architectures are not only able to solubilize non-water-soluble molecules in aqueous solution, but especially that they can be triggered to release its load upon an outer stimulus, in this case the change of the pH value should trigger the release.

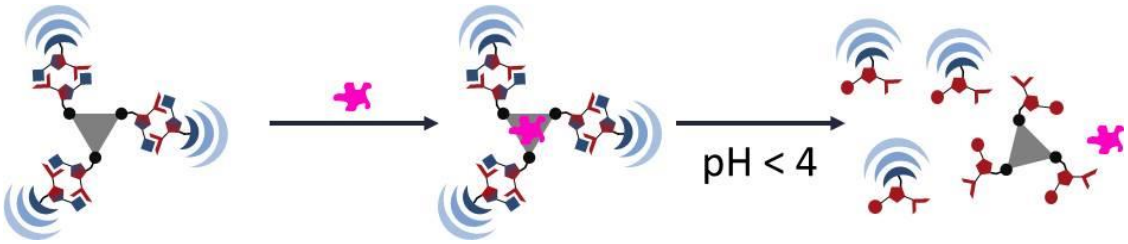

Figure 115: Simplified illustration of the uptake of a non-water soluble molecule (illustrated by the pink dot) by the core-shell architecture and the release of this molecule upon a pH change to acidic conditions resulting in the protonation of the guanidiniocarbonylpyrrole binding motif and hence the disaggregation of the core-shell architectures

This concept was first tested with Nile Red, a non-water soluble dye as a model substance and later with a potential cancer drug (University of Cologne, Aram Prokop)[131]. As the suitable dendron the 3rd generation dendron was chosen, simply because of it is bigger than the 2nd generation dendron and hence better water soluble.

For logical reasons the principal sample preparation and processing will be explained on the example of the Nile red first, before coming to the actual results of the solubilization studies.

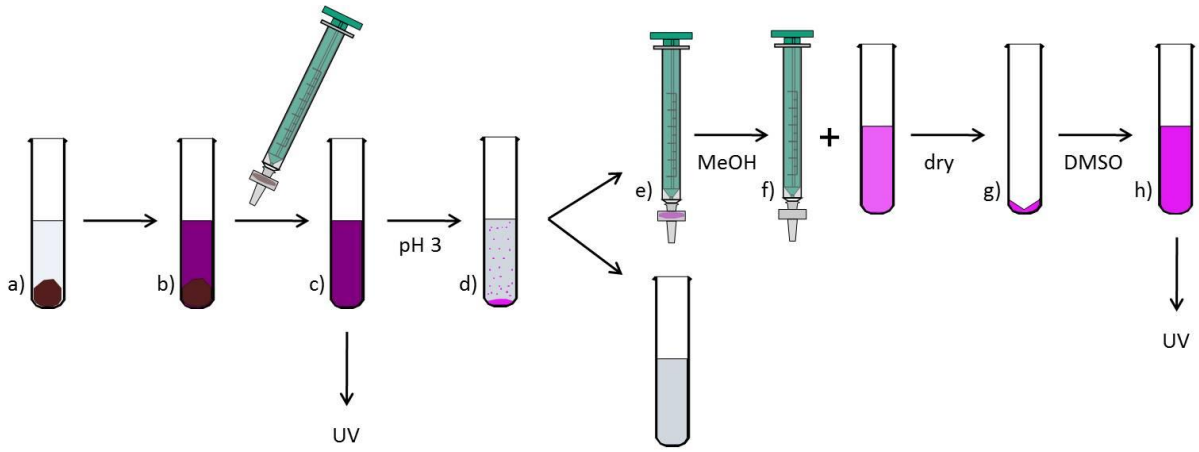

Figure 116: Scheme explaining the overall sample preparation for the solubilization experiments (explained with Nile red as Model substance). (a) Nile red was dispensed in the respective aqueous sample, (b) treated with ultrasound for approx. 5 seconds and kept at room temperature with occasionally shaking. (c) After three days the excess Nile red was filtered off using a syringe filter. The Nile red concentration of the respective sample was determined my measuring UV spectroscopy. (d) After the addition of aqueous HCl Nile red should precipitate, due to the disaggregation of the supramolecular dendrimer in low pH values. (e) The precipitate could be filtered off using a syringe filter, (f) which was subsequently washed with methanol. (g) The methanol was evaporated and (h) the remaining Nile Red was dissolved in 500µL DMSO to perform UV measurement. This way the concentration of the sample could be determined by comparing the sample with a calibration based on known concentrations. The resulting amount of substance allowed one to calculate the NR concentration of the original sample and hence the ratio of NR and core 74.

The scheme in Figure 116 explains the overall sample preparation. After the preparation of the aqueous solution of the solubilization agent solid Nile red was added in a vast excess and the sample was treated with ultra sound for 5 seconds to allow a fine distribution of the solid dye (Figure 116 a). This sample was kept for three days and was shaken occasionally to evenly redistribute the sediment dye through the sample (Figure 116 b). After this the excess Nile red was filtered off by using a PTFE syringe filter leaving a clear solution of the solubilization agent and the solubilized Nile Red in water (Figure 116 c). To verify the assumption, that the solubilized molecule will be released upon a significant pH change, hydrochloric acid was added to the sample. A possible precipitate could then be filtered off again by using a syringe filter (Figure 116 d). This filtration should leave a clear and colorless filtrate (Figure 116 e). The dye should be re-dissolved by washing the syringe filter with an appropriate solvent. The used solvent should be mixable with water and the substance in question (the dye) should be well soluble in it (Figure 116 f). After re-dissolving the dye, the solvent will be removed again (Figure 116 g), to be able to re-dissolve the dye in a specific amount of DMSO (Figure 116 h). UV-Vis spectroscopy provides a suitable method to determine the concentration of Nile Red. During the sample processing UV-Vis measurements make sense for the aqueous solution of the dye and the DMSO solution. Both measurements can then be compared to calibration measurements of

the dye with known concentrations in DMSO respectively. This allows the calculation of the dye concentration in question.

4.4.1 Nile Red

Nile Red is a solvatochromic dye and is suitable for the solubilization studies, because it is well visible due to its strong color, the solvatochromic properties and its poor water solubility[132]. The chemical structure of Nile Red is depicted in Figure 117.

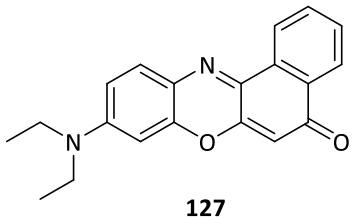

127

Figure 117: Chemical structure of the solvatochromic dye Nile Red

Moreover this dye was already used in solubilization studies of literature known core-shell architectures[112,118], which allows a certain comparison of the systems.

In a first attempt to study the solubilization of Nile Red by the core-shell architectures the [G2]-dendrons were used. A sample of 0.1 mM core and 3 mM [G2]-dendron was mixed with solid Nile Red. After 3 days the excess of Nile Red was filtered using a syringe filter. The sample indeed showed a blueish color, which is shown in Figure 119 (left picture). This coloring indicates the solubilization of Nile Red by the templated supramolecular dendrimer, since a pure water sample would not show any color due to the poor water-solubility of the dye. Thus this first experiment showed that the solubilization of a non-water-soluble substance is possible using this supramolecular templated dendrimer.

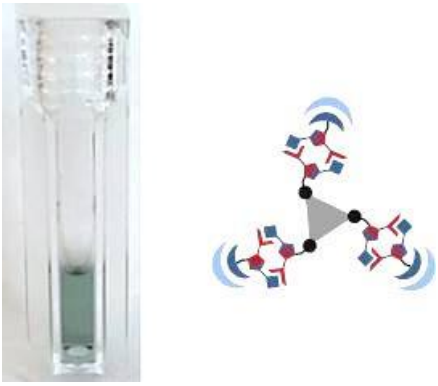

Figure 118: First attempt of the solubilization of Nile Red using the trivalent zwitterionic 1,3,5-trisphenylbenzene core and [G2]-zwitterions in a 1 : 30 ratio; left: picture of the sample showing a blueish color; right: simplified illustration of the second generation templated supramolecular dendrimer

After the first successful attempt to solubilize Nile Red, its release from the supramolecular templated dendrimer was tested. Aqueous HCl was added to change the pH value of the sample to acidic conditions. This pH change indeed induced the release of the solubilized dye, which resulted in its precipitation. The precipitate was filtered off, dried and subsequently resolved in DMSO. The DMSO solution showed the characteristic pink color of Nile red in DMSO; however the pink color is rather weak, indicating a low Nile red concentration.

Figure 119: First attempt of the solubilization of Nile Red using the trivalent zwitterionic 1,3,5-trisphenylbenzene core and [G2]-zwitterions in a 1 : 30 ratio; left picture shows the Nile Red in aqueous solution; right picture shows the pH induced released amount of NR resolved in DMSO

The Nile red solution in DMSO was used to measure UV-Vis spectroscopy. The UV-Vis spectrum of the Nile Red DMSO sample is depicted in Figure 120.

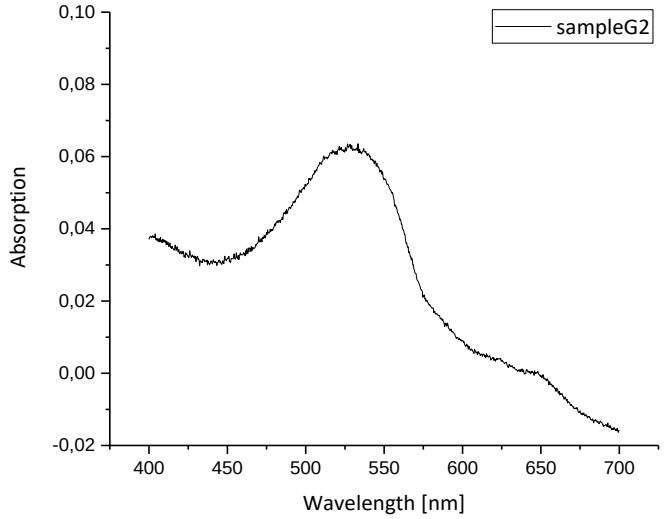

Figure 120: UV-Vis spectrum of the Nile Red sample resolved in DMSO

By measuring UV-Vis spectroscopy of the Nile Red sample it is possible to determine the Nile Red concentration by comparing the sample`s absorption maximum with calibration measurements of samples with known concentrations. Making calibration measurements with several Nile Red samples of known concentration in DMSO can help to determine the absolute concentration of the samples. After plotting a linear fit of the maxima of these measurements, the absorption maxima of the samples in question can be used to calculate the wanted concentration.

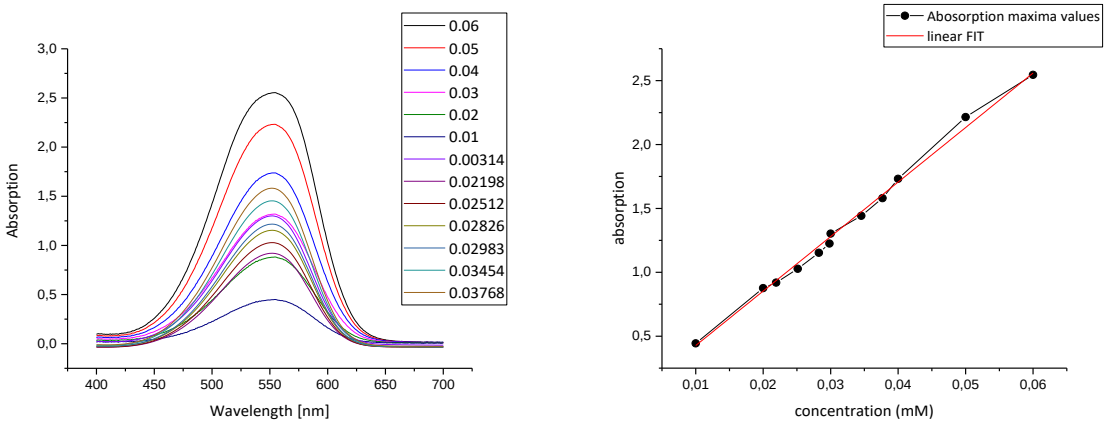

Figure 121: Calibration UV-Vis measurements of Nile Red samples of known concentration (left); Plot of the maxima against respective concentration (grey) and linear fit (red) (right)

The calibration measurements were done in DMSO in a concentration range between 3.14 µM and 60 µM. The absorption maxima were then plotted against their respective concentration. This allowed the calculation of the concentration of an unknown sample by inserting each absorption maxima into the linear equation of the linear data fit.

The calculated Nile Red concentration for the core and [G2]-dendron sample is 0.002 mM, which is only a fiftieth of the core concentration and thus a rather low Nile Red concentration.

However, this first experiment showed that the concept was working in principle, but since the concentration of solubilized Nile Red was rather low, further experiments were done with the bigger [G3]-dendron, hoping that the solubilization capacity was higher.

For this, eight aqueous solutions containing either the tritopic zwitterionic core, zwitterionic [G3]-dendron or both in different equivalents were prepared. Three of these samples contained the core-shell architecture with a core concentration of 1 mM. The equivalents of added dendron were 3 (C1), 10 (B1) and 30 (A1) respectively. The comparison of the results of those samples should resolve the question to what extent the sizes of the particles influence the solubilization properties. Another three samples only contained the dendron in concentrations of 3 mM (C2), 10 mM (B2) and 30 mM (A2), same concentrations as in samples C1, B1 and A1, testing the solubilization capability of the dendrons without the aromatic core. One sample containing only the anionic core (ABC3) should clarify if the core alone is able to solubilize any Nile red on its own. Pure water served as a blank sample in which none or just very little Nile red should be dissolved. A vast excess of solid Nile Red was dispensed in the solutions and the samples were treated with ultrasound for about 5 seconds to obtain a fine distribution of the Nile Red in the resulting suspension. After 3 days at ambient conditions the excess Nile red was filtered off, using a 45 µm PTFE syringe filter. The picture in Figure 122 shows the color of the different samples.

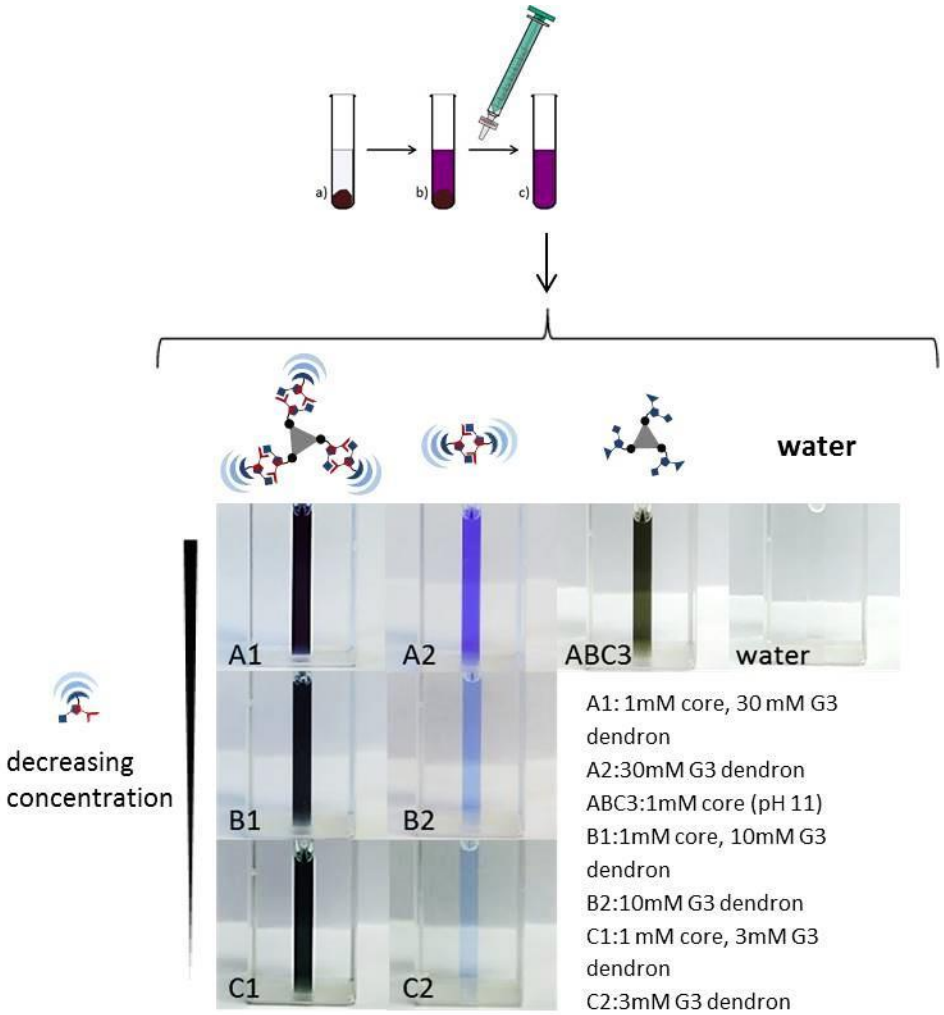

Figure 122: Samples prepared to study the solubilization properties of the templated supramolecular dendrimer. The samples contained the tritopic zwitterionic core with different equivalents of zwitterionic [G3]-dendron (A1, B1, C1). For comparison reasons the samples contained only zwitterionic [G3]-dendron in respective concentrations, one sample only the anionic tritopic core and one blind sample contained pure water

All samples, except for the blank sample containing only pure water, did solubilize a certain amount of Nile Red. Since Nile Red is a solvatochromic dye it changes its color in solvents with different polarity. This solvatochromism of Nile red gives a hint on how polar the environment of the Nile red molecules is and thus helps to predict where the Nile red is located within the solubilization agent. In a less polar environment a bathochromic shift can be observed, while a hypsochromic shift occurs in a more polar environment. For example Nile red exhibits a yellow color in nonpolar cyclohexane and a violet color in more polar methanol. Figure 123 gives a closer look at the samples containing only the dendron and their respective color.

Figure 123: Samples containing only the zwitterionic [G3]-dendrons (A 2 30 mM; B 2 10 mM; C 2 3 mM)

The samples, which only contain [G3]-dendron dimers (A2, B2 and C2) show clearly a blue color, meaning that Nile red is located within a highly polar microenvironment, presumably close or within the polyglycerol dendrons.

Figure 124 gives a closer look at the samples containing the core and their respective color.

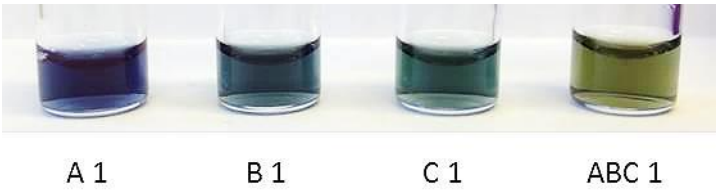

Figure 124: Samples containing the core molecule (A1: 1 mM zwitterionic core with 30 equivalents [G3]-dendron; B1: 1 mM zwitterionic core with 10 equivalents [G3]-dendron; C1: 1 mM zwitterionic core with 3 equivalents [G3]-dendron; ABC3: 1 mM anionic core in basic solution)

The samples with the core and dendron molecule also show blueish colors, however the color is darker and slightly greenish. The green tint indicated a bathochromic shift and gets stronger with decreasing [G3]-dendron concentration. Sample ABC3, which only contains the anionic core molecule, shows clearly a dark green color. This slight bathochromic shift probably results from a slightly less polar microenvironment due to the aromatic system of the core molecule. Thus, Nile red is located close to the core molecule.

The color of these samples can not only give information about the approximate location of Nile red within the dendrimers, but also the relative amount of solubilized Nile red can be estimated by the color intensity. The three samples containing core and [G3]-dendron (A1, B1, C1) obviously exhibit the darkest color. Whereas the A1 sample with 30 equivalents [G3]-dendron is the darkest of these three and C1 with only 3 equivalents is the lightest. Consequently the amount of solubilized NR is dependent on the ratio of core and dendron hence on the size of the aggregates. Meaning the 1 : 3 core-shell architecture seems to exhibit the best solubilization properties compared to higher network like structures surrounded with dendrons. Sample A2, B2 and C2 only contain [G3]-dendron

with decreasing concentration (30 mM, 10 mM and 3 mM). These samples show a different and lighter shade of blue. The color intensity decreases with decreasing [G3]-dendron concentration. The 1 mM sample containing only the core is the only sample with a basic pH value instead of 6. That is due to the poor solubility of the zwitterionic core in water. It shows a greenish-grey color, meaning that also in this sample a certain amount of Nile Red was solubilized. Overall, sample A1 has the highest color intensity of all samples and thus the highest Nile red concentration.

To confirm these visual impressions those colors give with some quantitative data, UV-Vis measurement were done. Figure 125 shows the UV-Vis measurement of the discussed eight samples.

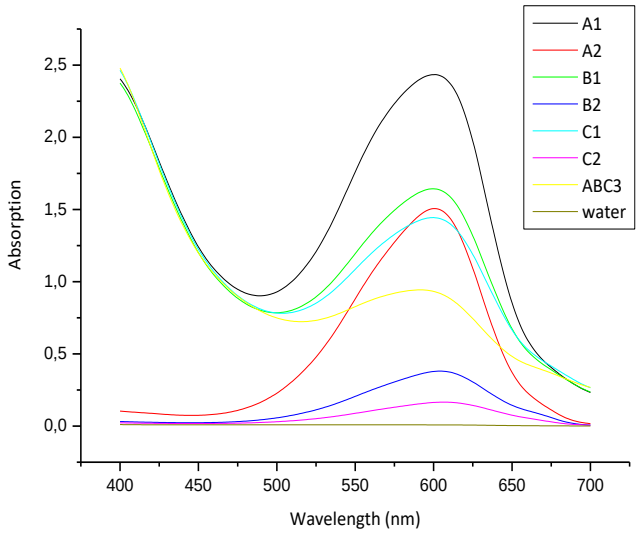

Figure 125: UV-Vis measurements of the samples of the NR solubilization experiments

Indeed the trend assumed by the colors could be confirmed by the measurements. Sample A1 shows the strongest absorption, followed by B1. The absorption values of A2 and C1 are very close to each other though A2 is minimally higher. The next absorption is from sample ABC3 followed by B2 and C2. The maximum of the water data curve is not even visible. These measurements enable to tell which sample holds the highest and the lowest amount of NR, but it is still not possible to make a proposition about the absolute NR concentration.

The absolute Nile red concentrations were calculated the same way the Nile red concentration of the [G2]-dendron sample was determined. Using calibration measurements of several samples of known concentrations (range between 3.14 µM and 60 µM) and plotting their absorption maxima against their respective concentration (see Figure 121). The concentration of the samples can be calculated by inserting each absorption maxima into the linear equation of the linear data fit (see Figure 121).

The calculated concentration values for all eight samples are listed in table 2. The highest Nile Red concentration measured was 57 µM, which was found for sample A1, consisting of 1mM core and 30 mM [G3]-dendron. This is the sample with the highest equivalents [G3]-dendron in core-dendron ratio of 1 : 30 and thus the one sample with discrete core-shell architectures. The sample A2, without 1 mM core but only 30 mM [G3]-dendron, shows a significant lower Nile Red concentration compared to A1 by a factor of 1.6. The other two samples with 1 mM core and either with 10 mM or 3 mM [G3]-dendron respectively, have almost the same Nile Red concentrations of 38 µM and 34 µM respectively, while both samples without the core showcase very low Nile Red concentrations. Even the sample of only core in basic solution exhibits a significant higher Nile Red concentration (22 µM).

Table 4: Nile Red concentrations

A1	0.057 mM
A2	0.035 mM
B1	0.038 mM
B2	0.009 mM
C1	0.034 mM
C2	0.004 mM
ABC3	0.022 mM
Water	0.00078 mM

Looking at these values it is striking that the sum of Nile red concentrations of the samples A2 (30 mM [G3]-dendron; c = 0.035 mM) and ABC1 (1 mM anionic core; c = 0.022 mM) results in the same concentration of sample A1 (1 mM core and 30 mM [G3]-dendron; c = 0.057). Two reason for this are thinkable. For one, the total concentration of Nile red in sample A1 could indeed result from the additive concentration of both the dendron and the core molecule. But if this would be the case, the same effect should have been observed for sample B1 and C1. This is however not the case. Moreover in sample A1 less [G3]-dendron dimers (13.5 mM dimers) are available for the solubilization of Nile red than in sample A2 (15 mM dimers), since 3 mM of the zwitterionic [G3]-dendron formed aggregates with the core. So if the dendron and the core should have the an equal effect on the solubilization in the mixture as in the individual samples, the total concentration of Nile red in A1 should be lower than the sum of the Nile red concentrations of sample A2 and ABC1. The same should be in effect for samples B1 and C1. However, the determined Nile red concentrations of samples B1 and C1 are higher than the sum of the concentrations of B2 and ABC1 and C2 and ABC1 respectively. So the fact that the Nile red concentration of sample A1 matches with the sum of samples A2 and ABC1 could be purely coincidental, which would be the second thinkable option.

These Nile red concentration values indicate that the core seems to be crucial for the solubilization of a reasonable amount of Nile red. Furthermore, it is obvious that the aggregate size plays an important role, since the NR concentration increases significantly for the sample containing the core-shell architectures while the Nile Red concentration of the samples with higher aggregates (3 and 10 eq [G3]-dendron) is rather constant.

The solubilization properties of the [G3]-dimers is roughly in the same range as the solubilization properties of [G1]-dendrimer with bipyridine core developed by Haag *et al.*[118], which have a similar molecular architecture with two dendrons each.

The solubilization capabilities of the templated supramolecular dendrimer can be compared to these of the covalently "clicked" core-shell architectures by Haag *et al.*[112]. A suitable way to directly compare solubilization capabilities is to compare the ratio of the amount of Nile Red in solution (in mmol) with the amount of core molecule or dendrimer (in mol) respectively. The bar graph in Figure 126 directly compares the ratios of the covalently bound [G1]-, [G2]- and [G3]-dendrimers, which are marked with a star, with the ratios of the templated supramolecular [G2] and [G3] dendrimers (core : dendrimer 1:30). The templated supramolecular [G2]-dendrimer has a ratio of 20, which is within the same solubilization capacity range as the covalently bound [G1]-dendrimer with a Nile red : dendrimer ratio of 18. The templated supramolecular [G3]-dendrimer exhibits the best Nile Red solubilization capacity with a ratio of 57, solubilizing even more Nile Red than the covalently bound [G3]-core-shell dendrimer by Haag *et al.*[112] with a Nile red : dendrimer ratio of only 45. The reason for this behavior could be the extended aromatic core due to the zwitterionic pyrrole dimers.

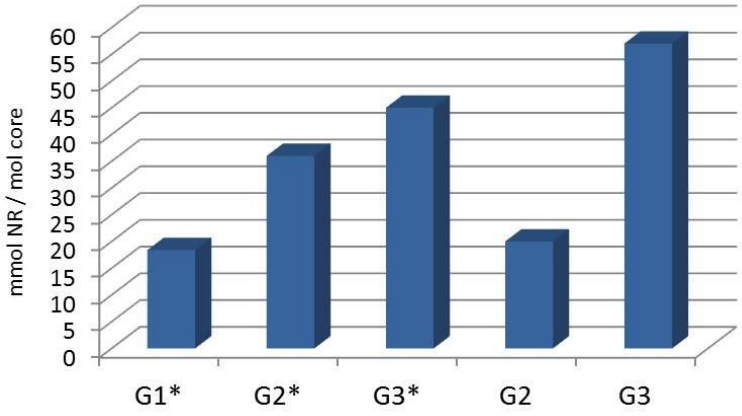

Figure 126: Comparison of the solubilization capabilities of the [G1]-, [G2]- and [G3]-dendrimers with the trisphenylbenzene core by Haag *et al.* [112] (marked with *; 18, 36 and 45) and the templated supramolecular [G2] and [G3]-dendrimers (20 and 57)

While the solubilization of a reasonable amount of Nile red is a crucial factor for the success of this project, the release triggered by a pH change makes it unique. The first solubilization studies with the [G2]-dendron successfully showed that the release of Nile red upon the addition of aqueous HCl was possible. The payload release from the templated supramolecular [G3]-dendrimer will be discussed in more detail. Figure 127 displays the addition HCl to sample A1 (1 mM core and 30 mM [G3]-dendron) and A2 (30 mM [G3]-dendron) to a pH value of around 3.

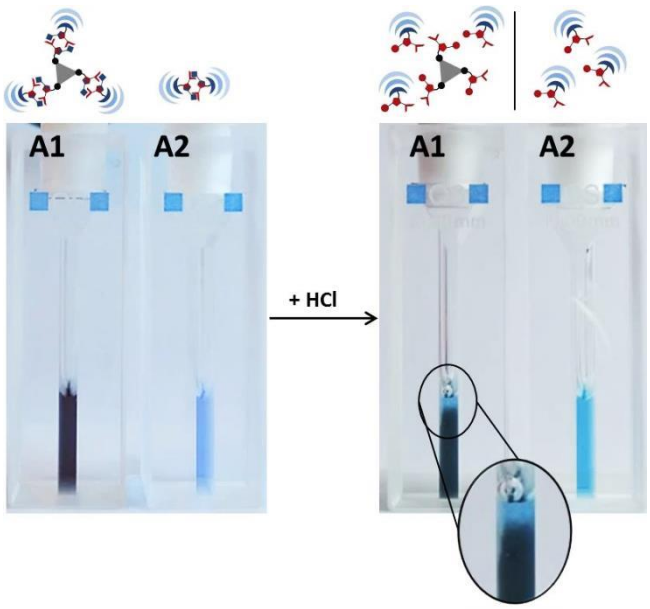

Figure 127: Addition of aqueous HCl to samples A1 (1 mM core and 30 mM [G3]-dendron) and A2 (30 mM [G3]-dendron); before both solutions were clear, after the addition of HCl (pH 3) only sample A1 showed precipitation

Before the addition of the acid both samples were clear solutions. A precipitation occurred in sample A1 at an acidic pH range of around 3, while sample A2 slightly changed color but stayed clear. This means, that the payload release upon pH change is only possible for the templated supramolecular dendrimer, but not for the [G3]-dendron dimers. A reason for this behavior could be a co-precipitation of the Nile Red with the cationic core molecule. This assumption is backed by the blueish color of the samples, which indicates a rather polar environment of the Nile Red. Thus the Nile red molecules are located close to the dendrons and are still solubilized by the protonated pyrrole-dendrons. A co-precipitation of the NR with the core molecule can explain why the NR precipitates after the addition of acid to sample A1.

To verify the quantity of the released amount of Nile Red, the precipitate of sample A1 was filtered using a PTFE syringe filter as shown in the third picture in Figure 128. The resulting filtrate was colorless and clear, so all the Nile red was caught by the filter membrane. The membrane was

washed with methanol to dissolve the Nile red again. Subsequently the methanol was evaporated, to resolve the Nile Red in 300 µL DMSO afterwards.

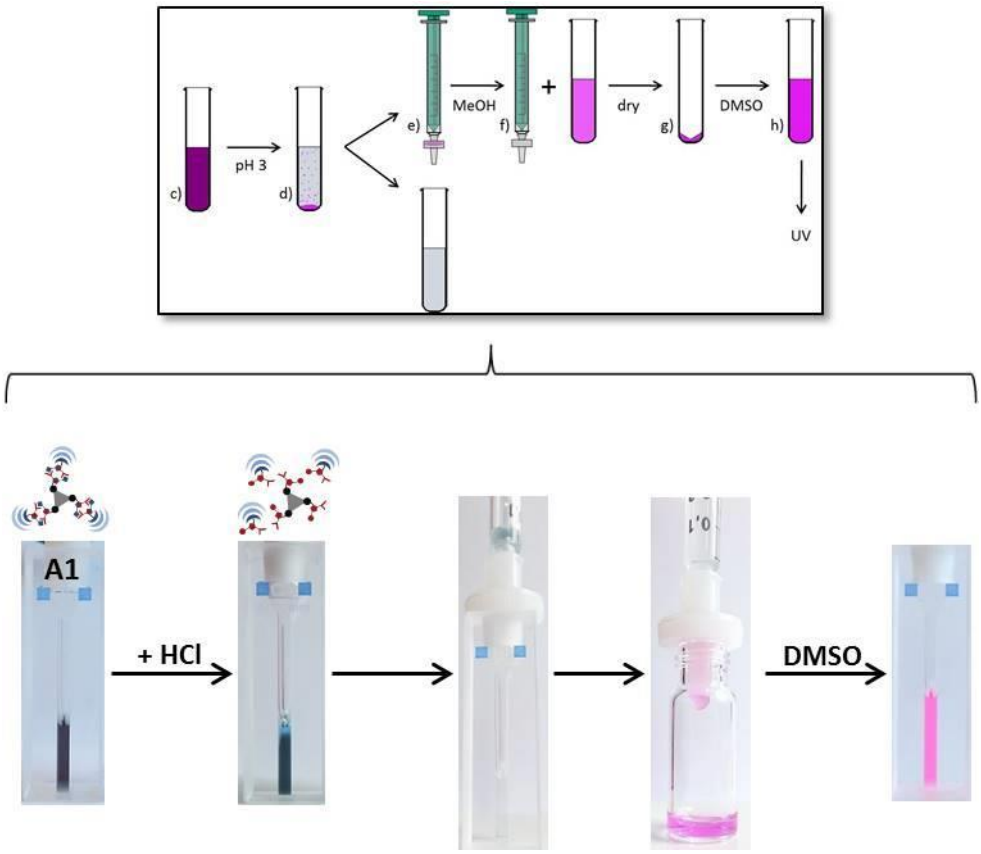

Figure 128: After the addition of HCl to sample A1 and the subsequent precipitation of Nile red, the precipitate was filtered off using a PTFE syringe filter. The filter was washed with MeOH and the resulting solution was dried, followed by resolving of the Nile Red in DMSO to measure UV-Vis

UV measurements of the precipitate in DMSO and its comparison to the calibration allowed calculating the NR concentration. In this case it is also important to consider, that only a fraction of 200 µL of the original sample were mixed with acid. So only a fraction of the Nile Red precipitated and was subsequently resolved in 300 µL DMSO. Meaning the concentration of the DMSO sample is not one to one transferable to the overall Nile Red concentration in the original sample, but has to be calculated. The concentration of NR was 0.057 mM in the original sample. After recalculating the concentration from the DMSO sample back to the original sample, we get the same value. So 100 % of the NR could be released upon the pH change.

It was also studied if the release of Nile Red upon a basic pH change works as well as acidic pH values. Unfortunately, after the addition of aqueous NaOH no precipitation was observed. One reason for this behavior could be the fact that the anionic core molecule is water soluble and hence

stabilizes Nile red in solution. That also confirms that the precipitation of Nile red in acidic conditions is probably due to a co-precipitation with the cationic core molecule.

4.4.1.1 Summary

The solubilization studies with Nile red showed that a reasonable amount of Nile red could be solubilized by the templated supramolecular (core-shell) dendrimer. Moreover, the solubilization of Nile red in three samples with a concentration of 1 mM core, but decreasing [G3]-dendron equivalents (30, 10 and 3 equivalents) showed that the sample with 30 equivalents of [G3]-dendron solubilized the significantly highest Nile Red concentration. Since the 1 : 30 ratio of core and [G3]-dendron is also the ratio in which studies (DOSY-NMR, DLS, AFM, force field calculation) showed no higher aggregates, but only small assemblies, a clear dependency of the solubilization capabilities by the structure or size of the assemblies was found.

Compared to the covalently bound analogous dendrimers, the supramolecular [G2]-dendrimer showed lower solubilization capabilities, but the templated supramolecular [G3]-dendrimer solubilized a significantly higher amount Nile red than the covalently bound [G3]-dendrimer with the trisphenylbenzene core.

The controlled release of Nile Red upon changing the pH to more acidic values was successfully tested by adding aqueous HCl to sample A1. Via filtration and resolving of the precipitated Nile red, it was able to determine the amount of released Nile red, which indeed is 100 %.

4.4.2 8-Nitrotryptanthrin-3-carboxylic acid

Nile Red is a good and valuable model for making a proof of principle. Even more interesting is the question, if the principle is applicable to other non-water soluble substances in particular a potential cancer drug. The reason why potential cancer drugs are particularly interesting for pH switchable carrier systems are the characteristics of cancer cells. Cancer cells differ from regular cells, in terms of their state of the cell membrane and also their pH value inside the cell media. Thus cancer cells are likely to let bigger particles into the cell interior (enhanced permeation and retention effect[7]) and due to the more acidic pH value could trigger the pH switch to open the core-shell architectures and release their load. 8-Nitrotryptanthrin-3-carboxylic acid was used as a second test-substance for the ability of the core-shell architectures to solubilize a poor water-soluble substance. 8-

Nitrotryptanthrin-3-carboxylic acid was developed by *Prokop et al.*[131] and is a highly toxic but poorly water-soluble potential cancer drug.

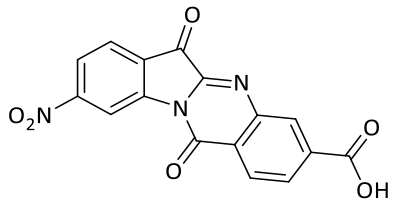

128

Figure 129: Chemical structure of 8-nitrotryptanthrin-3-carboxylic acid

The preparation of the samples for the solubilization studies was equal to the Nile red samples, except this time only three samples were made. The samples are depicted in Figure 130. The first one is the mixture of 1 mM core with 30 equivalents of [G3]-dendron (Figure 130, left), the second contains only 30 mM G3 dendron (Figure 130, middle) and the third is a blind sample with pure water (Figure 130, right). The reason for this choice was that each of these concentrations featured the highest Nile red concentrations in the previous solubilization experiments for the given mixtures. 8-Nitrotryptanthrin-3-carboxylic acid is a yellow solid substance, thus yellow colored solutions were expected, if the solubilization of 8-nitrotryptanthrin-3-carboxylic acid in the given samples is successful.

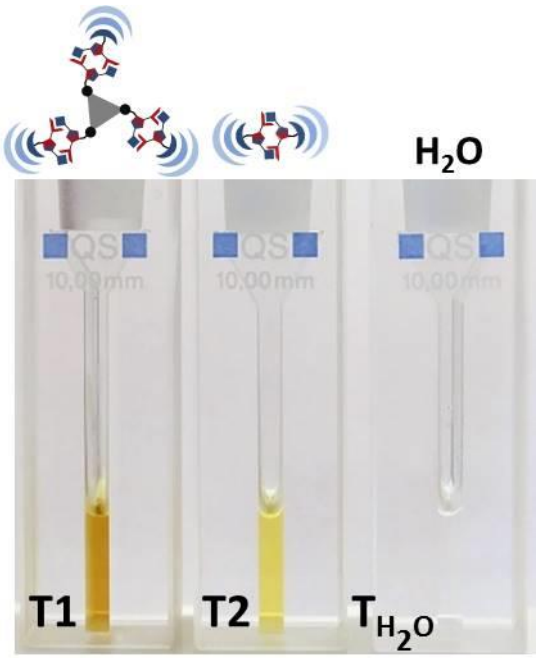

Figure 130: Solubilization of 8-nitrotryptanthrin-3-carboxylic acid; the left sample represents the mixture of 1 mM zwitterionic 1,3,5-trisphenylbenzene core with 30 mM [G3]-zwitterion; the sample in the middle contains 30 mM [G3]-zwitterion; the right sample is the control sample with pure water

It was obvious that the blind sample (TH_2O; right) does not contain any or only a very small amount 8-nitrotryptanthrin-3-carboxylic acid, since was is clear and colorless. Both samples containing either core and dendron or only dendron exhibit a yellow respectively yellow/brownish color. Sample T1 (1 mM core and 30 mM [G3]-dendron) exhibits the darkest almost brownish color, while T2 (30 mM [G3]-dendron) shows a bright yellow color. Only based on the visible colors on this picture, we could assume that T1 has a higher 8-nitrotryptanthrin-3-carboxylic acid concentration than T2. But we have to take into account, that the zwitterionic 1,3,5-trisphenylbenzene core with a 1 mM concentration already colors a solution lightly yellow/brownish, but definitely in a significant lighter color. The [G3]-zwitterion sample is colorless before the addition of 8-nitrotryptanthrin-3-carboxylic acid. That makes the evaluation of this sample in case of the 8-nitrotryptanthrin-3-carboxylic acid more difficult and it is only possible to conclude, that the solubilization was successful for both T1 an T2.

The samples were measured with UV-Vis spectroscopy, in hopes to be able to determine the 8-nitrotryptanthrin-3-carboxylic acid concentration similar as done before with the Nile red samples. First calibration measurements with known 8-nitrotryptanthrin-3-carboxylic acid concentration were done. These measurements are shown in Figure 131. By viewing at these UV curves, it is noticeable that the shape of the curves changes concentration dependently. Lower concentrations up to 0.48 mM show a maximum at 400 nm whereas samples above 0.689 mM only show a sharp bend at

around 430 - 440 nm. So two different types of UV curves exist for 8-nitrotryptanthrin-3-carboxylic acid depending on whether the concentration is lower or higher than around 0.5 mM.

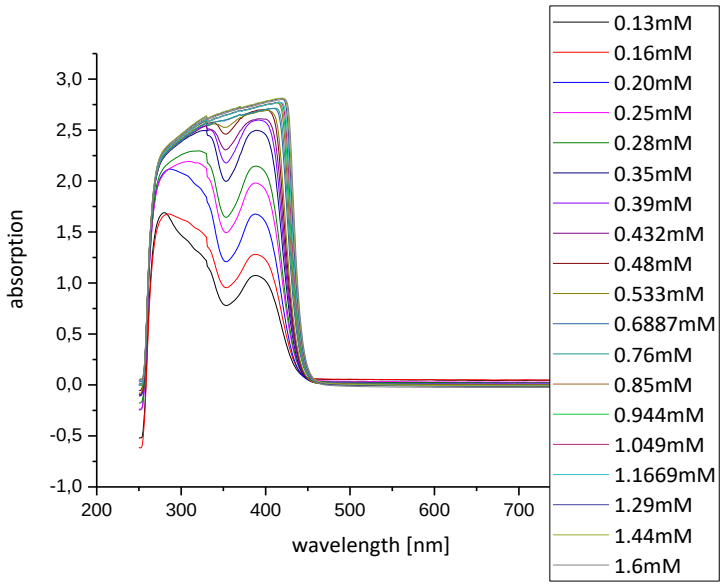

Figure 131: UV-Vis calibration measurements of 8-Nitrotryptanthrin-3-carboxylic acid samples of known concentration; shape of the UV-curves changes significantly at a concentration of around 0.5 mM

This concentration dependent change in the UV-Vis curves could be caused by a self-aggregation of 8-nitrotryptanthrin-3-carboxylic acid, presumably induced by π-π stacking. This self-aggregation behavior might even contribute to the poor water solubility of 8-nitrotryptanthrin-3-carboxylic acid.

The fact that concentration dependently two types of UV-Vis curves occur makes the determination of the 8-nitrotryptanthrin-3-carboxylic acid concentrations of the three samples more challenging and probably more inaccurate than with the Nile red samples. The UV measurements of the samples T1, T2 and TH_2O are illustrated in Figure 132 and show clearly, that the 8-nitrotryptanthrin-3-carboxylic acid concentration of T(H_2O) is negligibly small compared to T1 and T2. However, it seems that the 8-nitrotryptanthrin-3-carboxylic acid concentration of T2 is higher than T1, because it exhibits a higher absorption maximum. This would be a surprising result, since T2 is the sample containing no zwitterionic 1,3,5-trisphenylbenzene core, which proofed to be crucial for a good solubilization result with Nile red. However, a closer look at the UV curves of T1 and T2 revealed, that the shapes of both curves differ. T2 has a maximum at 400 nm and thus corresponds to the shape of the samples below 0.6 mM. T1 on the other hand resembles the UV curves of the samples with higher concentrations, even though the maximum absorption lies beneath T2. The shape of the UV curve of sample T1 corresponding to the UV-Vis curve type above 0.6 mM does not necessarily contradict with the fact that the concentration dependent change of the UV curve results from self-aggregation of 8-nitrotryptanthrin-3-carboxylic acid. The solubilization of 8-nitrotryptanthrin-3-

carboxylic acid by the templated supramolecular dendrimer is likely based on an aggregation of the 8-nitrotryptanthrin-3-carboxylic acid and the 1,3,5-trisphenylbenzene core. That could have led to the observed UV-Vis spectrum of sample T1.

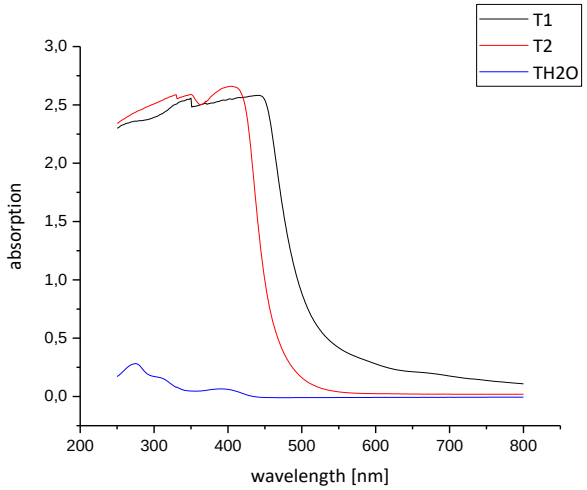

Figure 132: UV-Vis measurements of sample T1 (black), T2 (red) and TH_2O (blue)

However, two factors differentiate the calibration samples from sample T1, these are solvent and the solubilization by the zwitterionic 1,3,5-trisphenylbenzene and the [G3]-zwitterions. To be able to determine the 8-nitrotryptanthrin-3-carboxylic acid concentration it makes sense to release the 8-nitrotryptanthrin-3-carboxylic acid from the core-shell architecture and subsequently resolve the released amount in DMSO and then determine the concentration of the resulting DMSO solution. The release was realized by inducing a pH change to acidic conditions.

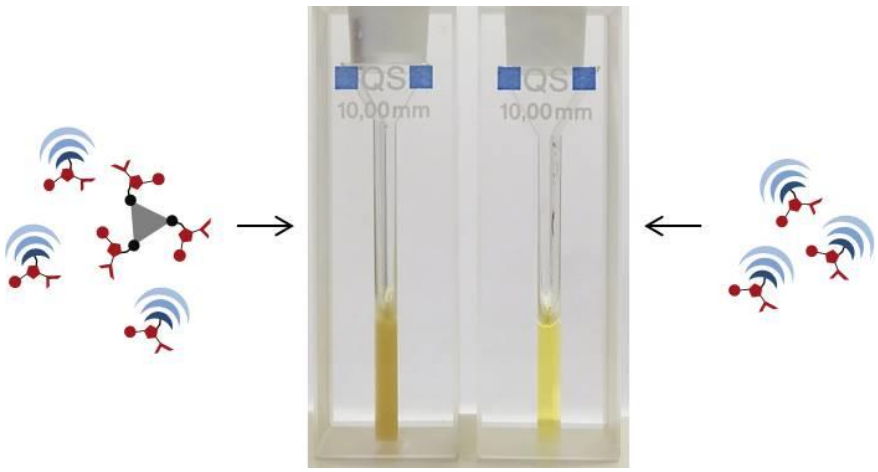

Figure 133: Samples T1 and T2 after the addition of aqueous HCl; only sample T1 containing the core and dendron shows precipitation of 8-Nitrotryptanthrin-3-carboxylic acid, while T2 only containing dendron stays a clear solution

Figure 133 shows both samples T1 and T2 after the addition of 30 µL 1 M HCl. The sample T2 containing only [G3]-zwitterion is still clear and shows no signs of any precipitation, while the sample T1 containing both core and dendron is opaque. So the same behavior can be observed with 8-nitrotryptanthrin-3-carboxylic acid as with Nile red. The pyrrole functionalized 1,3,5-trisphenylbenzene core molecule is essential for the release of the solubilized substance, probably due to co-precipitation. To verify the precipitation of the 8-nitrotryptanthrin-3-carboxylic acid, the precipitate was filtered off.

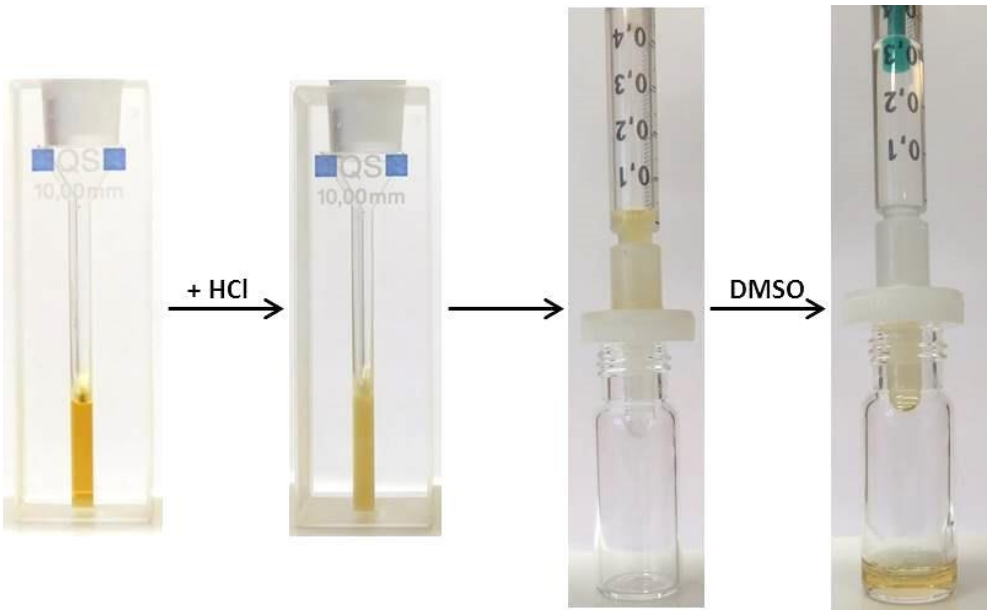

Figure 134: Addition of HCl to sample T1, filtration of the precipitate and subsequent resolving in DMSO

Figure 134 shows sample T1 before and after the addition of HCl. The resulting precipitate was filtered off with a PTFE syringe filter and the resulting filtrate showed no color. The resulting solid was washed from the filter with DMSO. This solution was then freeze dried and the residue was resolved in 300 µL DMSO, which is the same amount as water before.

The resulting UV measurement is shown in Figure 135 and is labeled as T1DMSO. The curve measured in DMSO is now comparable to the calibration measurements above 0.6 mM, in Figure 131 represented by the 1.6 mM concentration. That means that the solubilization of the 8-nitrotryptanthrin-3-carboxylic acid by the core-shell architecture resulted in a bathochromic and hyprochromic shift, which was reversed by releasing and resolving it in DMSO.

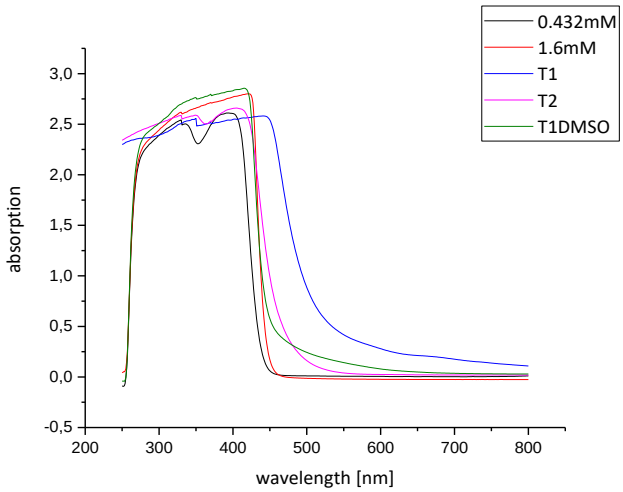

Figure 135: UV-Vis measurement of T1, T2, and T1DMSO and two samples with known concentration which were closest to T1DMSO and T2 respectively

To be able to calculate the respective concentrations of sample T1, T2 and T(H_2O), the absorption values of the calibrations were plotted against the concentrations. This did not result in one linear function, but in two linear functions corresponding to the concentration range below 0.4 mM and above 0.5 mM. Both values were plotted against the absorption values separately and subsequently a linear fit was added.

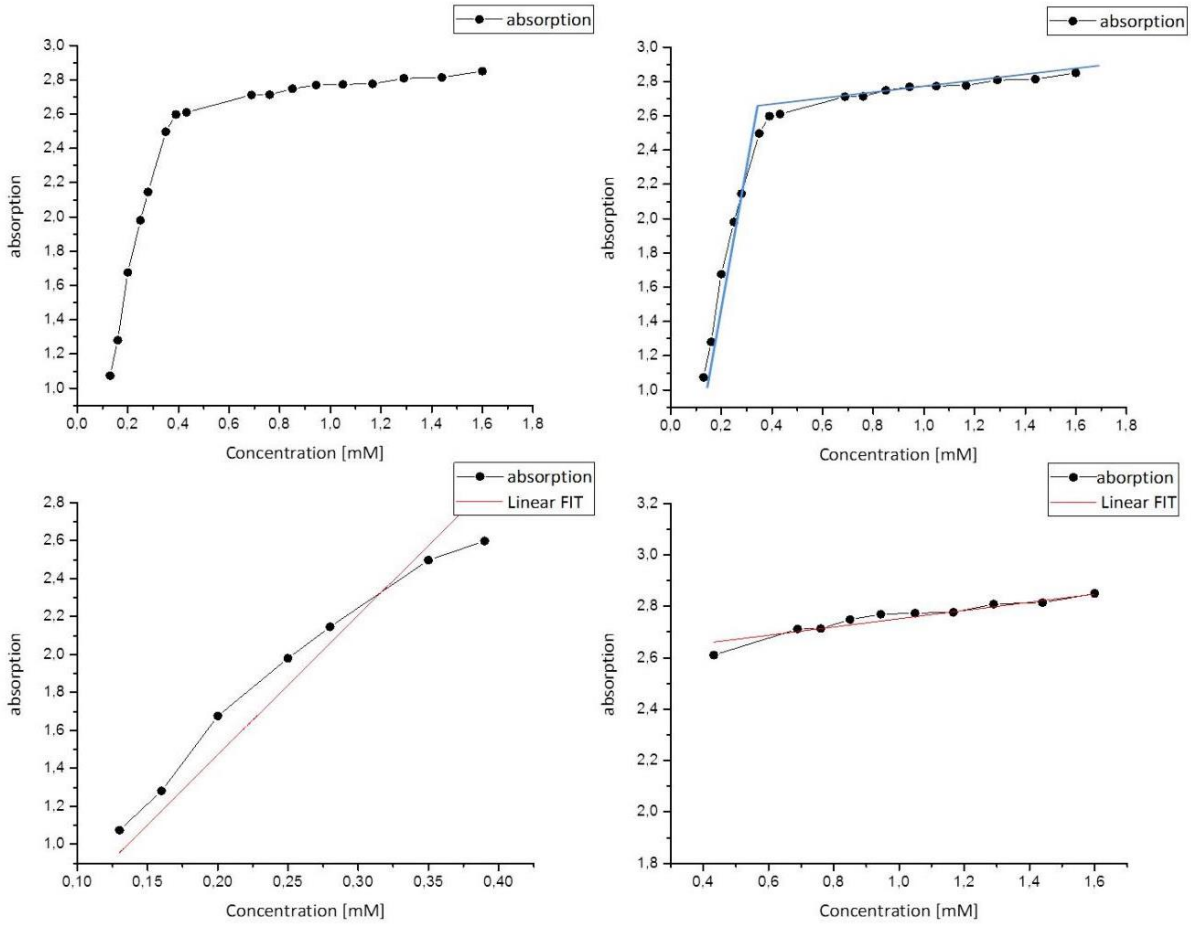

Figure 136: Top left: absorption maxima plotted against concentration; top right: illustration of two possible linear fits; bottom left: Linear fit of the absorption maxima of lower concentrations (A); bottom right: linear fit of the absorption maxima of higher concentrations (B)

So unfortunately, the calculation of the 8-nitrotryptanthrin-3-carboxylic acid concentrations of the different samples was not straight forward. The respective absorption maxima were used to calculate the sample concentrations using the suitable linear fit A or B for the respective absorption maximum. Thus, the concentration of T(H_2O) was estimated with the help of linear fit A, because the absorption maximum of this sample is very low. The concentration of T1 was estimated using the absorption maximum of the DMSO sample and was calculated with linear fit B, since the absorption maximum of this sample was a rather high value and thus in the area of fit B. The absorption maximum of sample T2 (around 2.6) lies in the range of the intersection of the two linear fits, thus two concentrations were estimated using both linear fits A and B. The concentrations of the samples are listed in table below.

Table 5: 8-Nitrotryptanthrin-3-carboxylic acid concentrations

Sample	Concentrations calculated from linear fit A	Concentrations calculated from linear fit B
T1DMSO	-	1.66 mM
T2	0.362 mM	0.425 mM
TH_2O	0.0088 mM	-

The 8-nitrotryptanthrin-3-carboxylic acid concentration of the control sample (TH_2O) was calculated to be around 8.8 µM. The 8-nitrotryptanthrin-3-carboxylic acid concentration of the [G3]-dendron sample (T2) was calculated using both linear fits, resulting in two different calculated concentrations. These values are with 0.362 mM and 0.425 mM not exactly identical, but are within the same magnitude. The calculated with a value of 1.66 mM the calculated 8-nitrotryptanthrin-3-carboxylic acid concentration of the sample containing the templated dendrimer was rather high.

The calculated or rather estimated concentrations are only approximate values, but they are helpful to get an idea of how well the solubilization of 8-nitrotryptanthrin-3-carboxylic acid works. For the core shell architectures it is safe to say that the system solubilizes a minimum of 1 8-nitrotryptanthrin-3-carboxylic acid per one core molecule, likely up to 1.5 8-nitrotryptanthrin-3-carboxylic acid molecules per core.

To test the effect the three different 8-nitrotryptanthrin-3-carboxylic acid samples have on cells, we tested them on Hela cells in buffer solution. Since the 8-nitrotryptanthrin-3-carboxylic acid concentrations of T1, T2 and TH_2O could only be estimated with the help of UV-Vis spectroscopy, the concentrations used in the cell test are rather guide values than fixed concentration. Anyhow, these tests can give us an insight of the degree to which 8-nitrotryptanthrin-3-carboxylic acid is shielded by the core-shell architecture in cells. 8-Nitrotryptanthrin-3-carboxylic acid is cell toxic since it is a potential cancer drug. 5 µL of each sample were added to 95 µL buffer. Moreover, an additional measurement was conducted with only 1 µL of sample T1. Assuming that the 8-nitrotryptanthrin-3-carboxylic acid concentration of sample T1 is at least 1.6 mM, the concentration of sample T2 at least 0.35 mM the respective 8-nitrotryptanthrin-3-carboxylic acid concentrations in the cell medium are 80 µM (T1), 16 µM (T1_1 µL) and 17.5 µM (T2) respectively. The best efficiency of 8-nitrotryptanthrin-3-carboxylic acid to kill cancer cell starts at concentration of 10 µM. So the exposure of Hela cells to solutions with 8-nitrotryptanthrin-3-carboxylic acid concentrations of approximately 80 µM (T1), 16 µM (T1_1 µL) and 17.5 µM (T2) should kill all cells. The Hela cells were incubated at 37 °C for 24 hours after the addition of each sample and subsequently checked for their viability by means of alamarBlue assays. The values were compared to PEI and a control, which was

normalized as the 100 % mark. The results show that around 85 % of the cells survived the addition of 5 µL of sample T(H_2O) to 100 µl of the cell medium, which resulted in an almost insignificant low 8-nitrotryptanthrin-3-carboxylic acid concentration of approx. 0.45 µM. This means that even such a low 8-nitrotryptanthrin-3-carboxylic acid concentration led to lower cell viability rate compared to the control. In sample T2 with an approximate 8-nitrotryptanthrin-3-carboxylic acid concentration of 17.5 µM even more than 100 % of the tested cells were viable compared to the control, with around 105 %. The result of the addition of the sample T1 and T1_1 µL showed an even higher cell viability of 130 % and 126 % respectively.

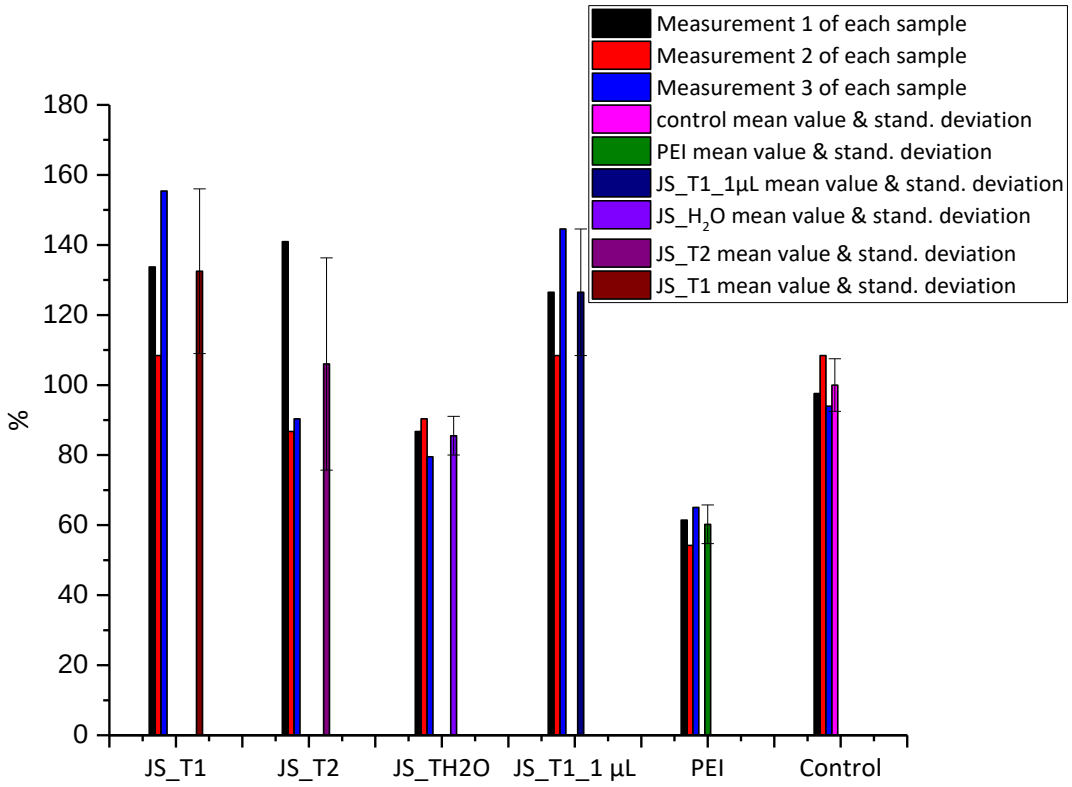

Figure 137: Bar graph of the cell viability determined with an alamarBlue essay of cell lines treated with 5 µL T1, T2 and TH_2O, with 1 µL T1 and with PEI as a standard

However, the results for samples T1, T1_1 µL and T2 show a rather high standard deviation and thus hold a high error range. The values of the three individual measurement of sample T2 range from 86 % to 140 %. Also the values of the three individual measurement of sample T1 and T1_1 µL range from 108 % to 155 and 108 % to 144 % respectively. That means that the significance of these results is somehow doubtful.

The viability of the cells was tested by an alamarBlue assay. In this assay, resazurin is added to the cell lines and only viable cells can reduce resazurin to resorufin, which is highly fluorescent. So the measured fluorescence emission intensity at a wavelength of 580-610 nm is an indicator for the

viability of the cells. To be sure that the core does not enhance the fluorescence signal of the assay, fluorescence was measured with the core at alamarBlue assay conditions.

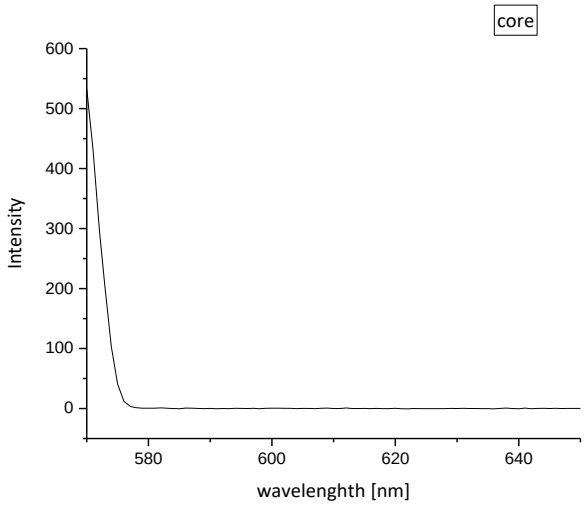

Figure 138: Fluorescence measurement of the tritopic zwitterionic core molecule 74, excitation wavelength is 570 nm (alamarBlue essay conditions)

The fluorescence measurement of the tritopic zwitterionic core molecule **74** using a fluorescence excitation wavelength of 570 nm showed no peak in the relevant area between 580 and 610 nm. Thus, at least the core alone has no influence on the results found with the alamarBlue cell viability esseys, whereas an influence of assemblies formed by the core and the dendron, the 8-nitrotryptanthrin-3-carboxylic acid or any other present molecules cannot be ruled out completely. This possibility portraits only one variable concerning the cell viability tests. Another important question is, if the core-shell architectures are able to migrate into cancer cells and are able to release their payload. During these tests it was not possible to test the release of the 8-nitrotryptanthrin-3-carboxylic acid, because of the fact that they were carried out in a pH 7.4 buffer system and hence no pH change was induced. Thus it is also not clear if the core-shell architectures penetrated into the cell.

Although the cell toxicity test gave more open questions than answers one can at least conclude from the results, that the templated core-shell dendrimers shield the 8-nitrotryptanthrin-3-carboxylic acid as much as it does not show any toxicity anymore. It was even not only non-toxic but one can possibly assume that the core-shell architectures might have a protective characteristic concerning the cell viability. This however could not be further proofed. The effect of the [G3]-dendron dimers was however even more unclear, since the determined cell viability ranged between 86 % (slightly toxic) to 106 %. Further experiments should concentrate on clarifying the mechanisms the core and

the dendrons affect the cell viability and if the core-shell architectures with or without their payload are able to migrate into the cells at all.

4.4.3 Summary

The solubilization of the 8-nitrotryptanthrin-3-carboxylic acid by the templated supramolecular dendrimer was successfully studied. Although the determination of the concentration of 8-nitrotryptanthrin-3-carboxylic acid was not straight forward, it was possible to estimate a reasonable concentration. The release of the 8-nitrotryptanthrin-3-carboxylic acid upon acidifying the solution showed good results with a release of 100 %. Furthermore, HeLa cell lines were incubated with samples of solubilized 8-nitrotryptanthrin-3-carboxylic acid and checked for their viability using alamarBlue assay. These results indicate that the supramolecular dendrimers shield the 8-nitrotryptanthrin-3-carboxylic acid, the substance did not show any toxicity anymore. On the contrary, the addition of the templated supramolecular dendrimers seems to have a potentially stabilizing effect on the HeLa cell lines.

5 SUMMARY AND OUTLOOK

The goal of this work was to develop a templated supramolecular dendrimer, which is stable in aqueous solution and hence could be investigated regarding its ability to be used as nano carrier in biomedical applications. To achieve this goal two building blocks, the template and dendron, were synthesized. Both were functionalized with the 5-(guanidiniocarbonyl)-1*H*-pyrrole-2-carboxylate zwitterion, which forms highly stable self-complementary dimers even in aqueous solution, as the supramolecular pH switchable binding motif.

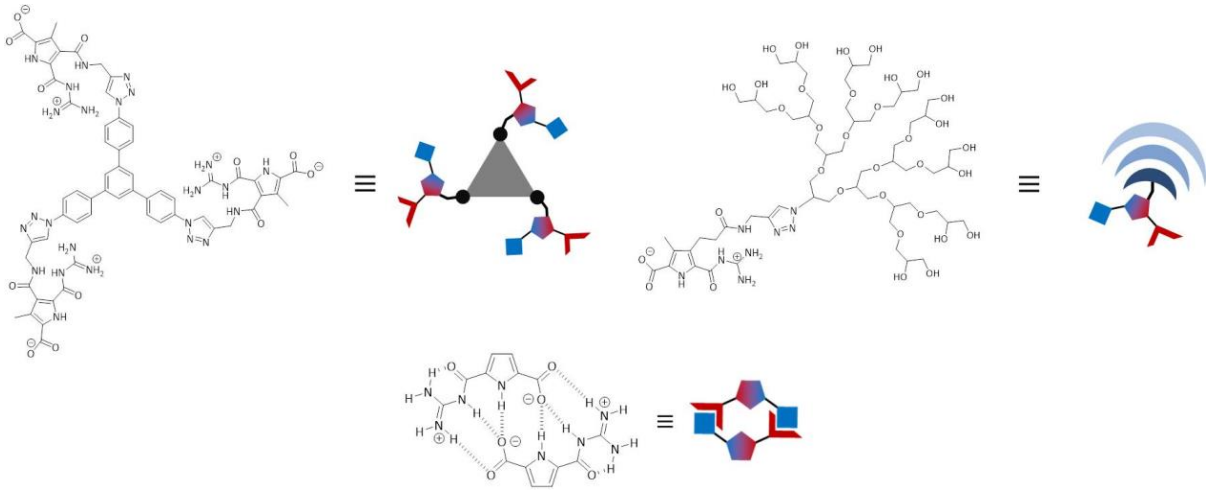

Figure 139: Chemical structures and the respective simplified illustrations of the trivalent zwitterionic core molecule (top, left), the zwitterionic [G3]-dendron (top, right) and the supramolecular binding motif, the 5-(guanidiniocarbonyl)-1*H*-pyrrole-2-carboxylate zwitterion dimer (bottom)

The dendron was synthesized mostly according to literature protocols[24,112] with moderate to good yields. For the template a reasonable sized aromatic scaffold, the 1,3,5-trisphenylbenzene, was chosen as the core entity, due to the fact that it already showed good results in solubilization studies of Nile red, done with covalently bound core-shell architectures.[118] The connection between the core and the pyrrole building blocks was realized with a short linker to avoid intramolecular interactions and thus the formation of intramolecular loops of the zwitterions. Initially the aggregation of the tritopic zwitterionic core was investigated on surface as well as in solution. Later the zwitterionic dendrons were added to the core molecule **74** and the resulting changes of the aggregation, that is the formation of the templated dendrimers, were observed again on surface and in solution. Finally the solubilization capacity of the templated dendrimers was studied with two different poorly water-

soluble molecules. Figure 140 shows a schematic overview of all found aggregation states of the tritopic zwitterionic core alone and after the addition of [G3]-dendron, as well as the solubilization and release of a guest molecule, which is here represented as a pink spot.

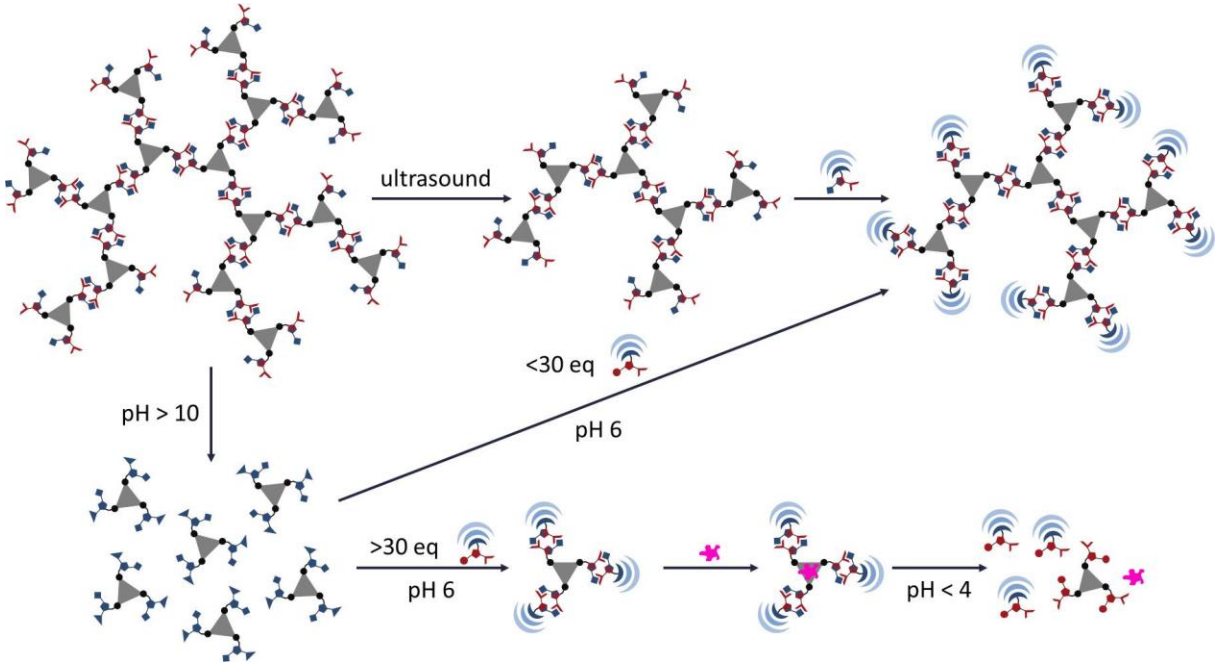

Figure 140: Schematic overview showing all aggregation states of the tritopic zwitterionic core alone and after the addition of [G3]-dendron. Moreover the schematic illustration of the solubilization and release of a poor water-soluble guest molecule (represented in pink) is depicted.

Due to the architecture of the tritopic zwitterionic core, the formation of three-dimensional network-like structures was expected. Indeed, these structures could be observed and were strikingly visualized by using tapping mode AFM. Three AFM pictures with concentrations of the core **74** of 1 mM (a), 0.01 mM (b) and 0.001 mM (c) are exemplary depicted in Figure 141. In the AFM image of the 1 mM sample (Figure 141 a), one can see a fully covered mica surface where a distinct 3-D network is noticeable on top of all. The height of these network structures is between 10 to 40 nm, indicating numberous layers of molecules are piling up. The dilution of the tritopic zwitterionic core **74** solution in DMSO to 0.01 mM (Figure 141 b) still results in the formation of networks on the mica surface. The height of these networks is 3-4 nm. In this case however the network structure is more distinct and defined and the surrounding areas show the uncovered mica surface, recognizable by the visible, slightly darker crosslines in the picture. This picture depicts very nicely and detailed the networked formed by the zwitterionic 1,3,5-trisphenylbezene core **74**. A concentration of only 1 µM 63 in DMSO (Figure 141 c) still showed network like structures with a height of 2-3 nm. Here, these structures are smaller in it-self, but these small aggregates cover nearly the whole surface. The fact that even in this highly diluted samples network-like structures were formed, confirmed that

intramolecular interactions could be avoided by the rigid molecular setup of the trivalent zwitterionic core molecule **74**.

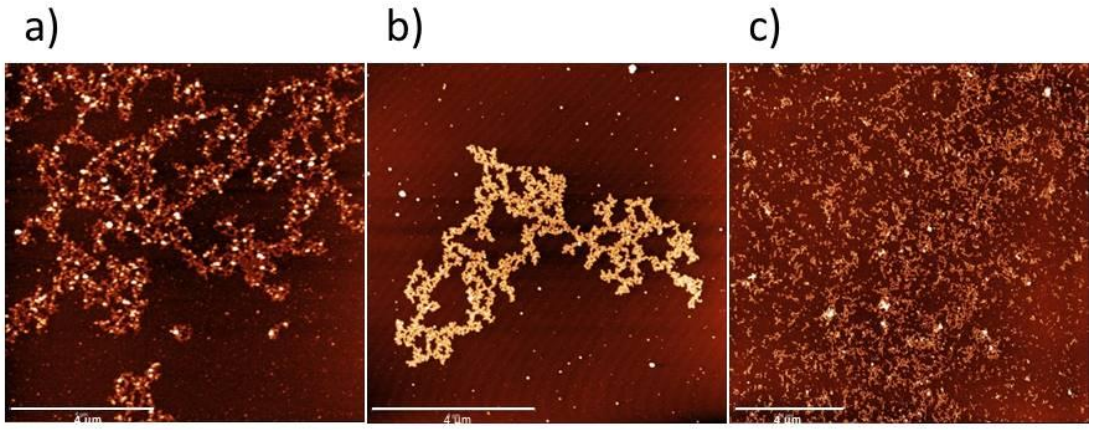

Figure 141: AFM images of the tritopic zwitterionic core molecule 74; pictures were prepared by dropping a DMSO solution of the respective concentration on a mica surface with subsequent spin-coating (60rps, 10 min) and analyzed by AFM tapping mode a) 1 mM sample; height up to 40 nm; b) 0.01 mM sample, height around 3 nm; c) 0.001 mM sample, height up to 2-3 nm (scale bar 4 µm)

These aggregates were also investigated in solution using DLS. The measurements showed that after 155 consecutive minutes of ultrasound treatment the smallest particle size of only around 5 nm could be found in DMSO solution (0.42 mM). After 10 months of aging the particle size increased up to 20 nm. To be able to compare the DLS results of the network-like aggregates with the aggregates formed by [G3]-dendrons and the core, measurements were also done in water. To be able to perform these measurements in pure water, the core was dissolved in 0.1 M aqueous NaOH solution and subsequently the pH-value was set back to a value around 6. The resulting aggregates were stable in water to perform the DLS measurements and showed sizes between round 6 to 20 nm.

The addition of at least 3 equivalents zwitterionic [G3]-dendron to the trivalent zwitterionic core should result in the formation of templated dendrimers with a core-shell architecture. However, as indicated schematically in Figure 140, the addition of less than 30 equivalents [G3]-dendron resulted in higher aggregates of the core surrounded with the dendrons. Only after the addition of a vast excess of the [G3]-dendron the templated supramolecular dendrimers were formed. AFM measurements visualized the decreasing network formation of the core with increasing [G3]-dendron concentration (Figure 142). As shown in Figure 142 c), at a core-dendron ratio of 1 : 30 no network formation could be observed.

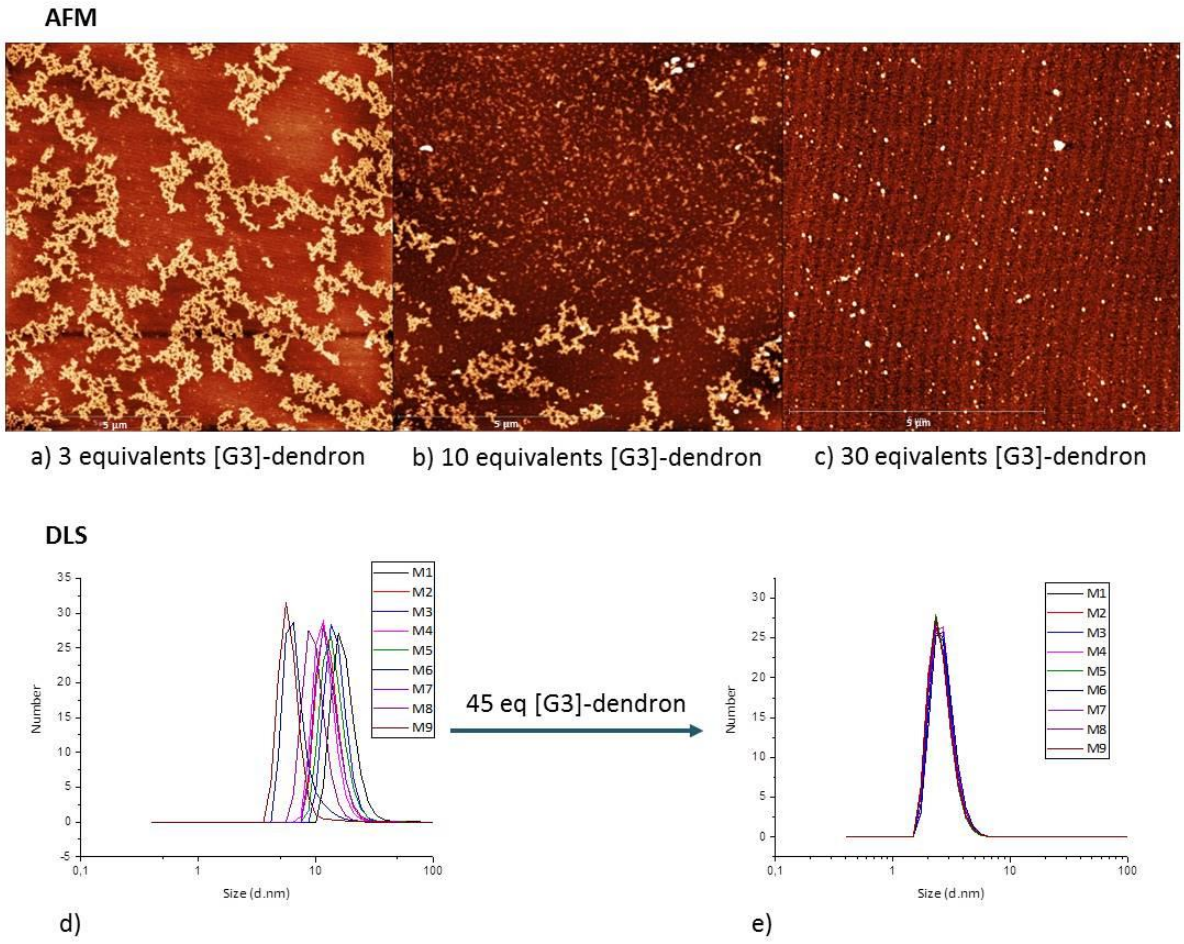

Figure 142: Top: AFM images of the tritopic zwitterionic core molecule 74 (0.001 mM in DMSO) with increasing equivalents of zwitterionic [G3]-dendron; a): 3 equivalents [G3]-dendron, heights around 3 nm; b): 10 equivalents [G3]-dendron, heights around 3 nm; c) 30 equivalents [G3]-dendron, heights around 1.5-10 nm; Bottom: d) DLS measurement (size distribution by number) of a 0.1 mM sample of the tritopic zwitterionic core molecule 74 in water (prepared from 0.1 M NaOH stock solution); measured hydrodynamic radii between 6-18 nm; e) DLS measurements (size distribution by number) of an aqueous solution of the tritopic zwitterionic core molecule 74 with 45 equivalents of zwitterionic [G3]-dendron (sample prepared from the respective aqueous NaOH and HCl stock solutions); measured sizes around 3-4 nm

DLS measurement showed that after the addition of 45 equivalents [G3]-dendron to the core **74** only small aggregates in the rage of 1.5-5 nm were formed. These sizes are in good agreement to the size of the [G3]-dendron dimers, with 3 nm, and to the 1 : 3 aggregate of the templated dendrimer, with around 4.5 nm. Force field calculations of the structure of the supramolecular templated dendrimer indicated a size of 3.3-4.4 nm, which fits well with the measured sizes in DLS. Also DOSY-NMR measurement of the mixture of the tritopic zwitterionic core molecule with 30 equivalents of zwitterionic [G3]-dendron revealed a size of 4.6 nm for the formed 1 : 3 aggregates.

Table 6: Measured or calculated sizes for the templated supramolecular dendrimer

Method	Core-dendron ratio [eq]	Size in [nm]
DLS	1 - 45	3-5
DOSY-NMR	1 - 30	4.6
Force field calculation	1 - 3	3.3-4.4

An idea to avoid the need for the addition of a vast excess of dendron would be, instead of using a self-complementary binding motif the use of an orthogonal AB binding motif. However, it is a big challenge to find a suitable binding motif, which will be stable in aqueous solution but still sensitive to outer stimuli. Since the carboxylate-guanidinium pair is so well suitable, it could be one option to functionalize two pyrrole backbones with either two carboxylate groups or two guanidinium moieties respectively (Figure 143).

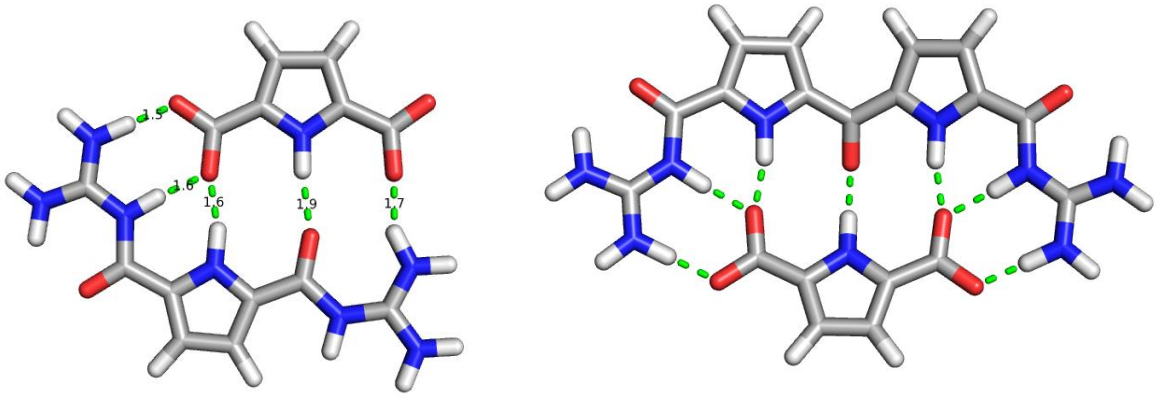

Figure 143: Force field calculations of two possible orthogonal binding motifs

Since the dimer geometry of the classical di-carboxylate/ di-guanidinium pair is not ideal, because it forms only 5 hydrogen bonds, which is one less than the 5-(guanidiniocarbonyl)-1*H*-pyrrole-2-carboxylate zwitterion, it can make sense to expand the pyrrole backbone of the di- guanidinium cation. This provides seven hydrogen bonds, which can add to the overall binding stability of this pair.

The poor water-soluble dye Nile red was chosen as a model substance for solubilization studies. Nile red was already used in literature for similar solubilization studies done with a covalently bound dendritic core-shell architecture[112] allowing a comparison between literature results and the results of this thesis.

The solubilization studies with Nile red showed that a reasonable amount of Nile red could be solubilized by the templated supramolecular (core-shell) dendrimer. Moreover, the solubilization of

Nile red in three samples with 1 mM core concentration, but decreasing [G3]-dendron equivalents (30, 10 and 3 equivalents) showed that the sample with 30 equivalents of [G3]-dendron solubilized the significant highest Nile red concentration. Since the 1 : 30 ratio of core and [G3]-dendron is also the ratio in which studies (DOSY-NMR, DLS, AFM) showed no higher aggregates, but only small assemblies which sizes are in good agreement to the size of the calculated structure of the templated dendrimer, a clear dependency of the solubilization capabilities by the structure/size of the assemblies was found.

Compared to the covalently bound analogous dendrimers, the supramolecular [G2]-dendrimer showed lower solubilization capabilities, but the templated supramolecular [G3]-dendrimer solubilized a significantly higher amount of Nile red than the covalently bound [G3]-dendrimer with trisphenylbenzene core.[112] To further increase the solubilized amount of Nile red or any other encapsulated molecule by the templated supramolecular dendrimer, the dendron size could be further enlarged to four or even five generations.

The controlled release of Nile red upon changing the pH to more acidic values was successfully tested by adding aqueous HCl to sample A1, as shown in Figure 144. However, the release of Nile red from sample A2 containing only [G3]-dendron was not successful. This allows the conclusion that the release of the payload might be caused by a co-precipitation with the cationic core molecule.

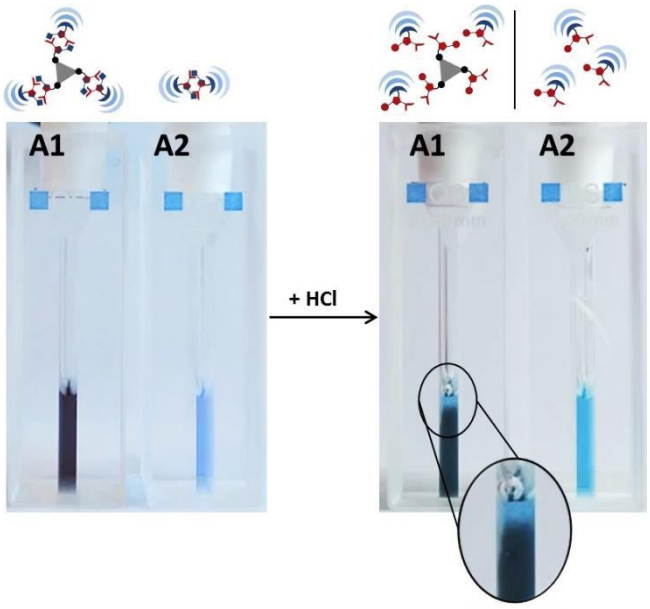

Figure 144: Addition of aqueous HCl to samples A1 (1 mM core and 30 mM [G3]-dendron) and A2 (30 mM [G3]-dendron); before the both solutions were clear, after the addition of HCl (pH 3) only sample A1 showed precipitation

Via filtration and resolving of the precipitated Nile red, it was able to determine the amount of released Nile red, which indeed is 100 %.

The second substance used for solubilization studies was the 8-nitrotryptanthrin-3-carboxylic acid, a poorly water-soluble potential cancer drug.[131] The solubilization of the 8-nitrotryptanthrin-3-carboxylic acid by the templated supramolecular dendrimer was successfully studied (Figure 145). Although the determination of the 8-nitrotryptanthrin-3-carboxylic acid was not straight forward, it was possible to estimate a reasonable concentration. The release of the 8-nitrotryptanthrin-3-carboxylic acid upon acidifying the solution showed good results with a release of 100 %.

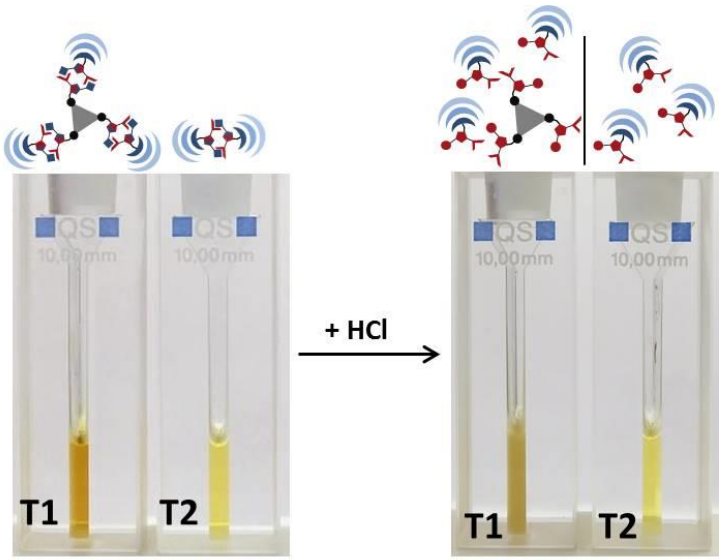

Figure 145: Left: Solubilization of 8-nitrotryptanthrin-3-carboxylic acid; The left sample (T1) represents the mixture of 1 mM zwitterionic 1,3,5-trisphenylbenzene core with 30 mM [G3]-zwitterion; the right sample (T2) contains 30 mM [G3]-zwitterion; Right: T1 and T2 after the addition of aqueous HCl; Only sample T1 containing the core and dendron shows precipitation of 8-nitrotryptanthrin-3-carboxylic acid, while T2 only containing dendron stays a clear solution

Furthermore, HeLa cell lines were incubated with samples of solubilized the 8-nitrotryptanthrin-3-carboxylic acid and checked for their viability using alamarBlue assay. These results indicate that the supramolecular dendrimers shield the 8-nitrotryptanthrin-3-carboxylic acid, as the substance did not show any toxicity anymore. On the contrary, the addition of the templated supramolecular dendrimers seems to have a potentially stabilizing effect on the HeLa cell lines. This toxicity test however, leaves many open questions. A first step to find more answers would be a repetition of the toxicity test with and without 8-nitrotryptanthrin-3-carboxylic acid to verify if the obtained result is reproducible and the observed potential stabilizing effect on the cells is indeed correct. Moreover it is important to know, if the templated dendrimer is able to migrate into the cell. Using a poorly water-soluble fluorophore as guest molecule within the dendrimer and using confocal microscopy as an analytic method could help to answer the question. Also the question if the 8-nitrotryptanthrin-3-carboxylic acid can be released from the supramolecular dendrimer within the cell could not be answered during this work, since the toxicity test was done in a pH 7.4 buffer solution. In addition

and depending on the results of these studies, *in vivo* studies could help to clarify if the templated dendrimer is indeed applicable as a nano-carrier for cancer drugs.

Aside from these open questions concerning the definitive applicability of the system, in the course of this thesis it was possible to develop a pH switchable templated dendrimer which proved to solubilize reasonable amounts of two different poorly water-soluble test molecules, which were Nile red and 8-nitrotryptanthrin-3-carboxylic acid. More importantly it was also possible to release the guest molecules quantitatively upon an external stimulus, in this case a change of the pH toward acidic values. This proof of principle demonstrates the potential of a supramolecular templated dendrimer, based on the guanidiniocarbonylpyrrole carboxylate zwitterion as the binding motif, for encapsulation and potentially even the transport of poorly water-soluble drugs.

6 ZUSAMMENFASSUNG UND AUSBLICK

Ziel dieser Arbeit war die Entwicklung eines selbstassemblierenden, supramolekularen Dendrimers, mit einer Kern-Schale-Architektur. Dabei sollte das hierfür verwendete supramolekulare Bindungsmotiv in wässrigen Medien stabil sein, um das gebildete Dendrimer bezüglich seiner Eigenschaften als Nanocarrier für biomedizinische Anwendungen zu untersuchen. Als Modellgastmoleküle sollten die nahezu wasserunlöslichen Verbindungen Nilrot und 8-Nitrotryptanthrin-3-carbonsäure dienen. Um diese Ziele zu erreichen wurden zwei molekulare Bausteine, der Kern und das Dendron, synthetisiert. Beide wurden mit dem 5-(Guanidiniocarbonyl)-1*H*-pyrrol-2-carboxylatzwitterion funktionalisiert, welches im wässrigen Medium selbstkomplementäre Dimere bildet und dient somit als supramolekulares, pH-schaltbares Bindungsmotiv.

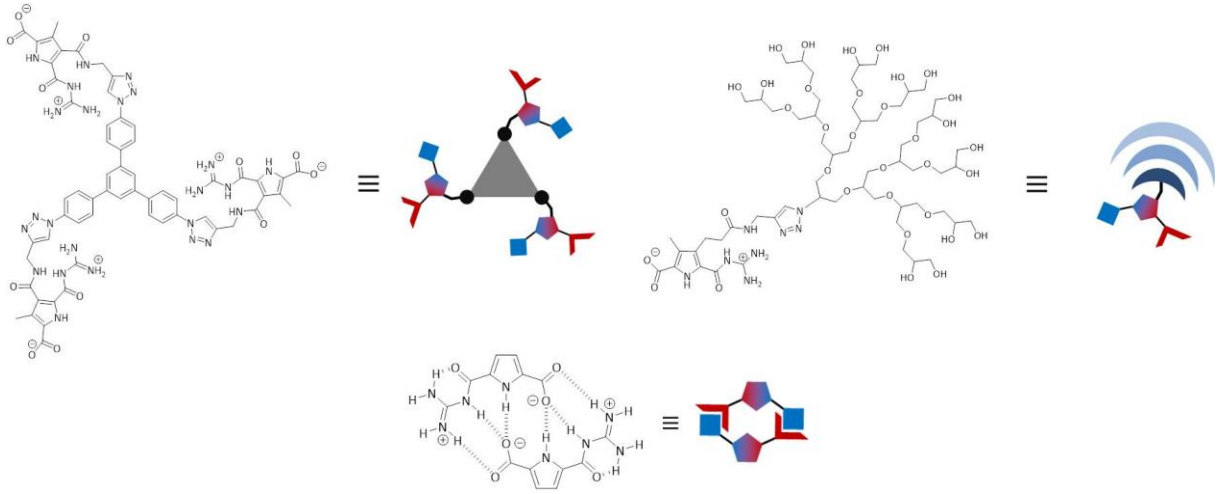

Abbildung 139: Molekülstrukturen und die jeweiligen vereinfachten Illustrationen des zwitterionischen 1,3,5-Triphenylbenzol Kernbausteins mit drei Bindungsstellen (oben links), des zwitterionischen [G3]-Dendrons (oben rechts) und des supramolekularen Bindungsmotivs, das 5-(Guandidiniocarbonyl)-1*H*-pyrrol-2-carboxylatzwitterion Dimer (unten)

Die Synthese des Dendrons erfolgte größtenteils nach den Vorgaben zweier Literaturvorschriften[24,112] und lieferte mittelmäßige bis gute Ausbeuten. Für den Kern wurde 1,3,5-Triphenylbenzol, ein aromatischer Baustein mittlerer Größe ausgewählt. Dieser Kernbaustein wurde bereits in kovalent-gebundenen Kern-Schale-Systemen verwendet und zeigte in vorausgehenden Studien gute Eigenschaften Nilrot im wässrigen Medium zu solubilisieren.[112] Der aromatische Kern und die Pyrrolbindunsmotive wurden über einen möglichst kurzen Linker verbunden, um intramolekulare

Wechselwirkungen der Zwitterionen, wie zum Beispiel die Ausbildung intramolekularer Ringe, zu verhindern. Zunächst wurde das Aggregationsverhalten des zwitterionischen Kernbausteins mit drei Bindungsstellen auf Oberflächen und in Lösung untersucht. Anschließend wurden die zwitterionischen Dendronen hinzugegeben und die daraus resultierende Veränderung des Aggregationsverhaltens des zwitterionischen Kernbausteins bis hin zur Bildung der supramolekularen Kern-Schale-Architekturen betrachtet. Schließlich wurden die Lösungseigenschaften des supramolekularen Dendrimers mit zwei nicht, beziehungsweise schlecht, wasserlöslichen Molekülen, Nilrot und 8-Nitrotryptanthrin-3-carbonsäure, untersucht. Abbildung 140 gibt einen Überblick über die Aggregationsarten, die für den zwitterionischen Kernbaustein alleine und nach der Zugabe der zwitterionischen Dendronen gefunden wurden. Außerdem sind die Solubilisierung und die kontrollierte Freisetzung eines Gastmoleküls (pink hervorgehoben) das selbst-assemblierte Dendrimer schematisch dargestellt.

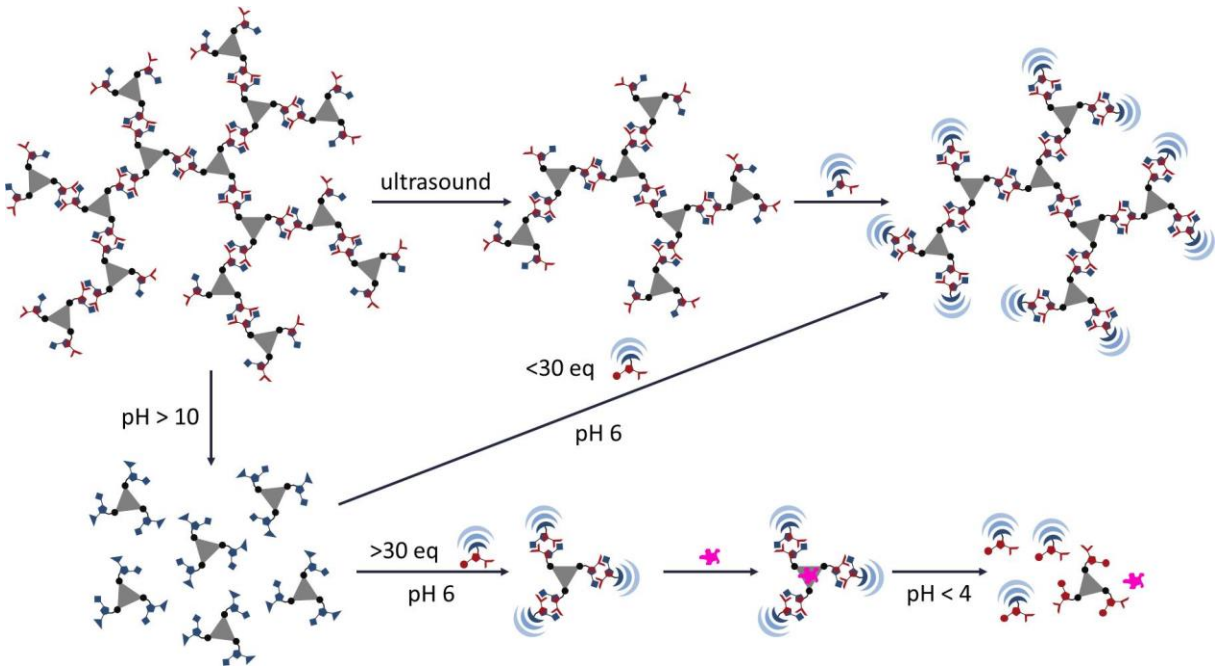

Abbildung 140: Schematischer Überblick über die gefundenen Aggregationsarten des zwitterionischen Kernbausteins alleine und nach Zugabe der zwitterionischen Dendronen. Die Solubilisierung sowie kontrollierte Freisetzung eines Gastmoleküls (pinkfarben hervorgehoben) ist ebenfalls vereinfacht dargestellt.

Aufgrund der Molekülstruktur des zwitterionischen Kernbausteins **74** mit drei Bindungsstellen erwartet man die Bildung von dreidimensionalen, netzwerkähnlichen Aggregaten. Tatsächlich konnten Strukturen dieser Art mit Hilfe der Kraftfeldmikroskopie nachgewiesen und eindrucksvoll bildlich wiedergegeben werden. In Abbildung 141 veranschaulichen drei exemplarische AFM Bilder das Aggregationsverhalten des zwitterionischen Kernbausteins **74** mit Konzentrationen von 1 mM (a), 0,001 mM (b) und 0,0001 mM (c) DMSO-Lösungen. Das AFM Bild der 1mM Probe (Abbildung 141a)

zeigt eine vollständig, mit einem eindeutig dreidimensionalen Netzwerk bedeckte Micaoberfläche. Die gemessenen Höhen dieser Netzwerkstrukturen betrugen zwischen 10 und 40 nm, was dafür spricht, dass zahlreiche Molekülschichten übereinander gestapelt vorlagen. Nach der Verdünnung der 1 mM DMSO-Lösung des Kernbausteins **74** auf eine Konzentration von 0,001 mM (Abbildung 141b), zeigten die AFM Messungen noch immer dreidimensionale Netzwerke auf der Micaoberfläche, wobei die Höhe dieser Aggregate allerdings nur 3-4 nm betrug. Die Strukturen dieser Netzwerke sind zudem augenscheinlich sowohl deutlicher als auch definierter. Die umliegende Oberfläche ist frei von Aggregaten, da die typische freie Micaoberfläche, zu erkennen an den sich abwechselnden breiten, hellen und schmalen, dunklen Linien, in diesem Bild ebenfalls gut sichtbar ist. Dieses Bild zeigt die dreidimensionalen Netzwerkstrukturen, die der zwitterionische 1,3,5-Trisphenylbenzol Kernbaustein formt, besonders detailliert und eindrucksvoll. Eine Probe mit einer Konzentration von nur 100 nM **74** in DMSO wurde ebenfalls mittels AFM vermessen. In Abbildung 141c lassen sich auch noch netzwerkähnliche Strukturen finden, wobei diese Strukturen kleiner sind, jedoch die ganze Oberfläche bedecken, und Höhen zwischen 2-3 nm aufwiesen. Die Tatsache, dass sogar bei sehr starker Verdünnung Netzwerkaggregate gefunden werden konnten, bestätigt, dass intramolekulare Wechselwirkungen durch die richtige Wahl des Linkers zwischen Pyrrol- und Kerneinheit und die dadurch resultierende Rigidität des Moleküls **74** verhindert werden konnten.

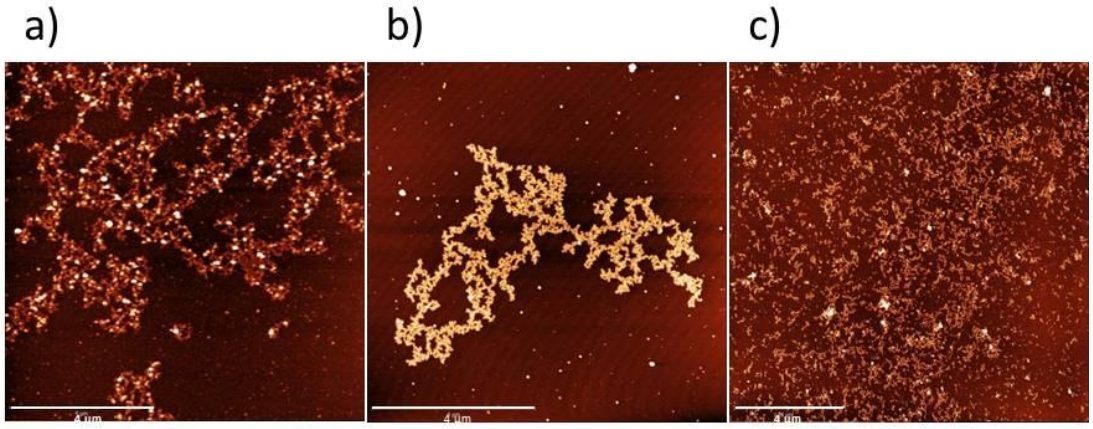

Abbildung 141: AFM Bilder des trivalenten zwitterionischen Kernbausteins 74; die Bilder wurden durch das Auftropfen der jeweiligen DMSO Lösung mit der entsprechenden Konzentration des Moleküls 74 auf eine Micaoberfläche und anschließendem "Spin-Coatings" (60 rps, 10 min) präpariert und im AFM "Tapping-Modus" aufgenommen. A) 1 mM Probe, Höhe bis zu 40 nm; b) 0,001 mM Probe, Höhe bis zu 3 nm; c) 0,0001 mM Probe, Höhe bis zu 2-3 nm (Maßstabsbalken je 4 µm)

Das Aggregationsverhalten des Kernbausteins wurde ebenfalls in Lösung untersucht. Als geeignete Analysemethode wurde die dynamische Lichtstreuung (DLS) gewählt. Nach einer Ultraschallbehandlung der zu untersuchenden DMSO-Lösung (0,42 mM) für 155 Minuten, wurden die

kleinsten Partikelgrößen von nur 5 nm gemessen. Dieselbe Probe wurde nach 10 Monaten erneut gemessen, wobei festgestellt wurde, dass die Partikelgrößen auf bis zu 20 nm angestiegen waren. Um die DLS Ergebnisse der von dem Kernbaustein **74** gebildeten Aggregate und den Aggregaten, die durch die Kombination der zwitterionischen Dendronen und des Kernbausteins **74** gebildet wurden, zu vergleichen zu können, wurden auch DLS-Messungen in Wasser durchgeführt. Dafür musste der Kernbaustein **74** zunächst in 0,1 M wässriger NaOH-Lösung gelöst werden und anschließend der pH-Wert wieder auf 6 eingestellt werden. Die resultierenden Aggregate waren stabil genug in Wasser, um DLS Messungen durchzuführen und zeigten Größen zwischen 6 und 20 nm.

Durch Zugabe von mindestens 3 Äquivalenten des zwitterionischen [G3]-Dendrons zu dem Kernbaustein **74** sollten sich die selbstassemblierten Dendrimere mit Kern-Schale-Architektur bilden. Jedoch, wie in Abbildung 140 bereits angedeutet, führte die Zugabe von weniger als 30 Äquivalenten des Dendrones immer noch zu höheren Aggregaten des Kernbausteines (siehe hierzu Abbildung 142a und 142b), welche von außen mit Dendronen umgebenen waren, und noch nicht zu der Bildung der Dendrimere. Erst nach der Zugabe eines starken Überschusses an Dendronen wurde das gewünschte selbst-assemblierte Dendrimer mit Kern-Schale-Architektur gebildet. In den AFM Bildern des Kernbausteins **74** mit zunehmender Konzentration des [G3]-Dendrons (Abbildung 142) wird das Abnehmen der Netzwerkbildung verdeutlicht. In Abbildung 142c sind keine netzwerkartigen Aggregate bei einem 1 : 30-Mischungsverhältnis von Kernbaustein und Dendron mehr zu beobachten.

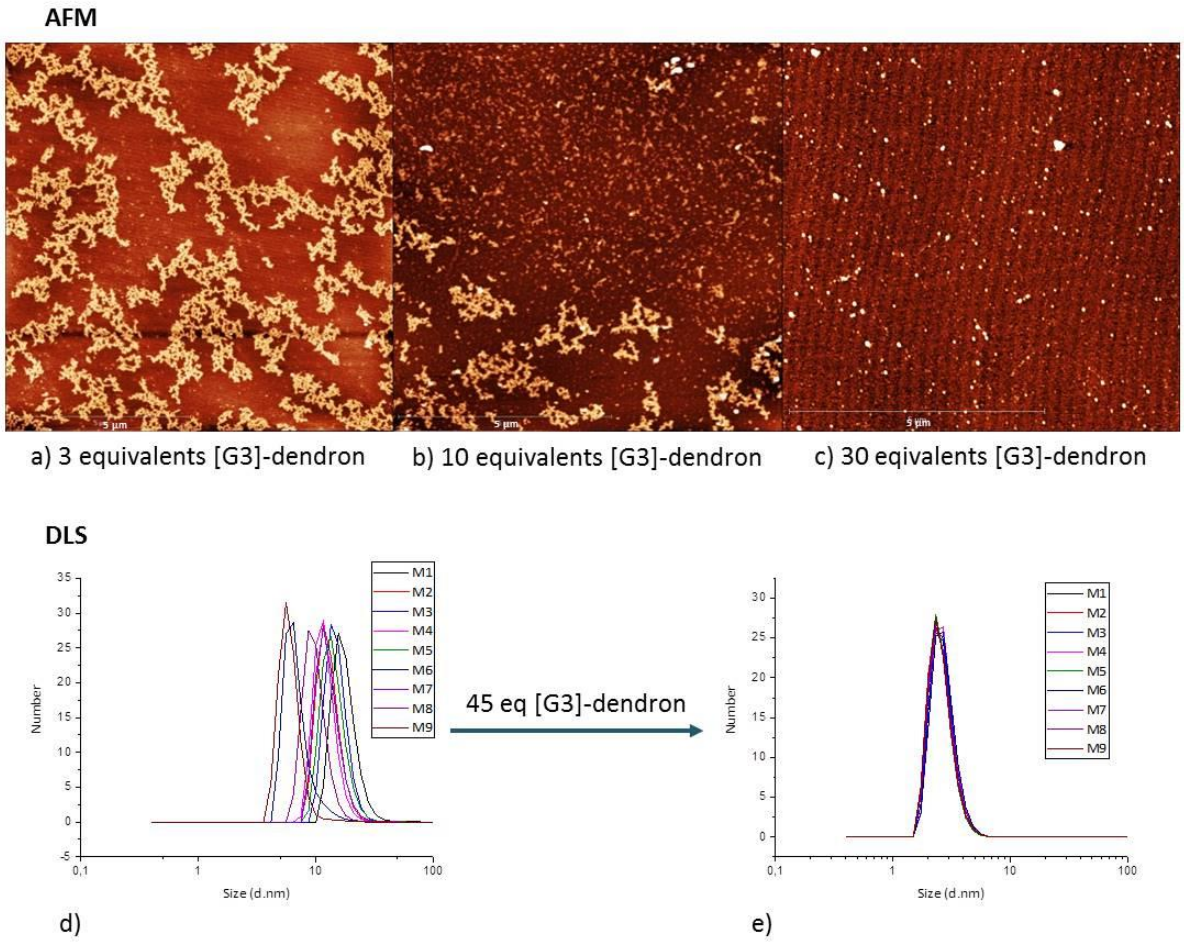

Abbildung 142: AFM Bilder des zwitterionischen Kernbausteins 74 mit drei Bindungsstellen (0,001 mM in DMSO) mit steigenden Äquivalenten an zwitterionischen [G3]-Dendron; a) 3 Äquivalente [G3]-Dendron, Höhe ca. 3 nm; b) 10 Äquivalente [G3]-Dendron, Höhe ca. 3 nm; c) 30 Äquivalente [G3]-Dendron, Höhe ca. 1,5-10 nm; Skalierungsbalken je 5 µm. Unten: d) DLS Messung (Größenverteilung nach Anzahl) einer wässrigen Lösung des zwitterionischen Kernbausteins 74 (0,1 mM Probe, hergestellt aus einer 0,1 M NaOH Stammlösung), gemessener hydrodynamischer Radius zwischen 6-18 nm; e) DLS Messung (Größenverteilung nach Anzahl) einer wässrigen Lösung des zwitterionischen Kernbausteins 74 (0,1 mM Probe) und 45 Äquivalenten des zwitterionischen [G3]-Dendrons (hergestellt aus den jeweiligen wässrigen NaOH und HCl Stammlösungen), gemessener hydrodynamischer Radius zwischen 3-4 nm

Die DLS Messungen zeigen, dass nach der Zugabe von 45 Äquivalenten [G3]-Dendrons zum Kernbaustein nur sehr kleine Aggregate mit einer Größe von 1,5-5 nm gebildet wurden. Dieser Größenbereich ist in guter Übereinstimmung mit den Größen der [G3]-Dendron Dimere, welche eine Größe von etwa 3 nm haben, und dem 1 : 3-Aggregat des Dendrimers, welches eine Größe von etwa 4,5 nm aufweist. Kraftfeldrechnungen des Dendrimers wiesen auf eine Größe von 3,3-4,4 nm hin, was gut mit den mit DLS bestimmten Größen übereinstimmt. Zudem wurde auch DOSY-NMR-Messungen von dem trivalenten zwitterionischen Kern mit 30 Äquivalenten zwitterionischen [G3]-Dendrons durchgeführt. Diese Messung bestätigte die bisher bestimmten Größen des selbst-assemblierten Kern-Schale- Dendrimers, da eine Größe von 4,6 nm bestimmt werden konnte.

Tabelle 6: Gemessene und berechnete Größen des supramolekularen Dendrimers

Methode	**Kern-Dendron Mischverhältnis [Äqiv.]**	**Größe in [nm]**
DLS	1 - 45	3-5
DOSY-NMR	1 - 30	4,6
Kraftfeldrechnung	1 - 30	3,3-4,4

Um einen großen Überschuss an Dendron zu vermeiden, wäre der Einsatz eines orthogonalen AB Bindungsmotivs anstelle des selbstkomplementären Bindungsmotivs vorstellbar. Jedoch ist es eine große Herausforderung ein geeignetes Bindungsmotiv zu finden, das im wässrigen Medium stabil ist, aber trotzdem sensitiv auf äußere Stimuli reagiert. Da das Carboxylat-Guanidinium Paar sehr gut funktioniert, könnte eine Möglichkeit sein, zwei Pyrrolbausteine mit je zwei Carboxylat- und Guanidiniogruppen zu funktionalisieren (siehe Abbildung 143 links).

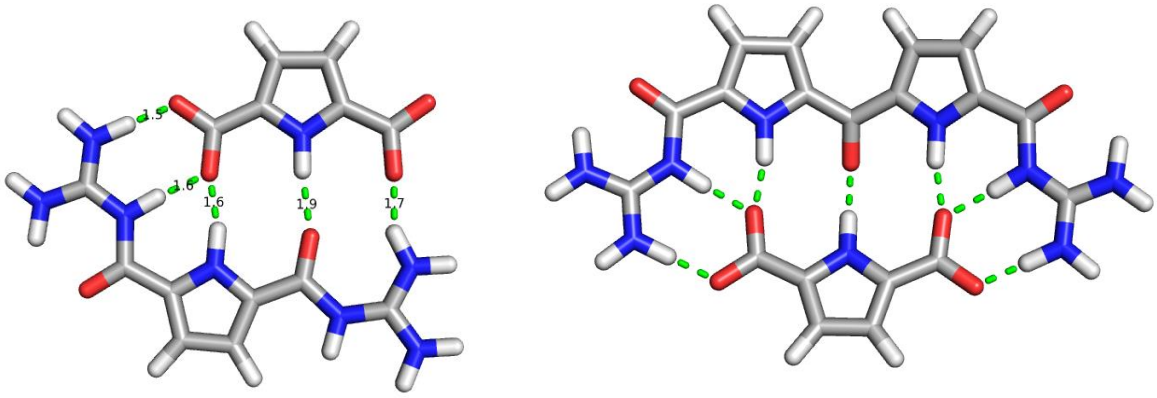

Abbildung 143: Kraftfeldberechnungen zweier möglicher orthogonaler Bindungsmotive

Da die Geometrie des Dicarboxylat/Diguanidinium Paares mit jeweils einem Pyrrolring nicht optimal ist, da es mit fünf Wasserstoffbrückenbindungen eine weniger aufweist als das 5-(Guanidiniocarbonyl)-1*H*-pyrrol-2-carboxylatzwitterion, kann es Sinn machen das Diguanidinium durch einen weiteren Pyrrolring zu erweitern, wie in Abbildung 143 rechts dargestellt. Diese Erweiterung führt auch dazu, dass die Ausbildung von insgesamt sieben Wasserstoff-brückenbindungen möglich ist, wodurch der Komplex an Stabilität dazugewinnen könnte.

Des Weiteren sollte nun das supramolekulare Dendrimer zum einen auf sein Vermögen hin getestet werden nahezu wasserunlösliche Verbindungen in Lösung zu bringen und zum anderen diese Gastmoleküle gezielt wieder freizusetzen.

Der schlecht wasserlösliche Farbstoff Nilrot wurde als Modellsubstanz für die Löslichkeitsstudien ausgewählt. Dieser Farbstoff wurde bereits zum Studium der Lösungseigenschaften kovalent-gebundener, dendritischer Kern-Schale-Systeme[112] genutzt, was eine Vergleichbarkeit der literaturbekannten Ergebnisse mit den Ergebnissen dieser Arbeit erlaubt.

Die Löslichkeitsstudien zeigten, dass das selbst-assemblierte Kern-Schale Dendrimer in der Lage war Nilrot zu solubilisieren. Zudem konnte nachgewiesen werden, dass die Löslichkeit von Nilrot von der Konzentration des zwitterionischen Dendrons abhängig ist. Es wurden drei Proben mit einer 1 mM Konzentration des Kernbausteins **74** mit abnehmenden Äquivalenten Dendron (30, 10, und 3 Äquivalente) vermessen, wobei die Probe mit einem 1 : 30 Kern-Dendron Verhältnisses eine signifikant höhere Nilrot Konzentration aufwies als die Probe mit einem geringeren Dendronanteil. Da in vorangegangenen Größenuntersuchungen der jeweils vorliegenden Aggregate ermittelt wurde, dass bei einem 1 : 30 Kern-Dendron Verhältnis keine höheren Aggregate vorliegen und nur kleine Aggregate, die mit der berechneten Größe des supramolekularen Dendrimers in Einklang stehen, gefunden wurden, konnte eine klare Abhängigkeit der Lösungseigenschaften von der Struktur bzw. der Größe der Aggregate festgestellt werden.

Verglichen mit den literaturbekannten analogen kovalent-gebundenen Kern-Schale Dendrimeren zeigte das supramolekulare [G2]-Dendrimer geringere Lösungseigenschaften, das supramolekulare [G3]-Dendrimer löste jedoch eine signifikant höhere Nilrotmenge als das kovalent-gebundene [G3]-Dendrimer.[112]

Die erfolgreiche kontrollierte Freisetzung des Farbstoffes konnte durch eine pH-Wertveränderung in Richtung niedrigeren pH-Werten, ausgelöst werden. Dafür wurde wässrige Salzsäure zu Probe A1 (1 mM Kern und 30 mM[G3]-Dendron) gegeben, was in Abbildung 144 dargestellt ist, wodurch sich ein Niederschlag bildete, was auf die Freisetzung des wasserunlöslichen Gastmoleküls hindeutet. Die Probe A2 (30 mM[G3]-Dendron), die ausschließlich das zwitterionische [G3]-Dendron enthielt, zeigte jedoch keinen Niederschlag nach der Zugabe von HCl, sodass die kontrollierte Freisetzung des Gastmoleküls in diesem Fall nicht möglich war. Diese Tatsache erlaubt die Annahme, dass die Freisetzung und das Ausfällen von Nilrot durch eine Co-Ausfällung mit dem kationischen Kernbaustein ausgelöst wurden.

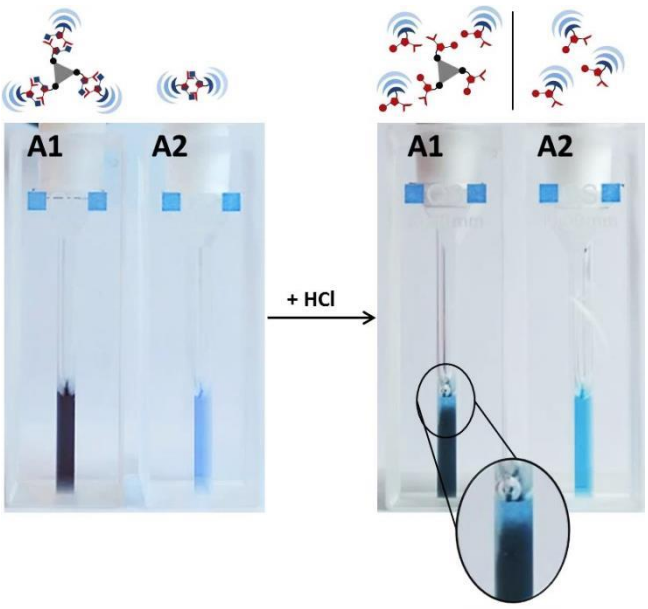

Abbildung 144: Zugabe wässriger HCl zu den Proben A1 (1 mM Kern und 30 mM[G3]-Dendron) und A2 (30 mM[G3]-Dendron); vor der Zugabe sind beide Proben klare Lösungen, nach der Zugabe von HCL (pH3) zeigt ausschließlich Probe A1 eine Trübung

Durch Abfiltrieren und erneutes Aufnehmens des Nilrot Niederschlags in DMSO konnte die Nilrotmenge bestimmt und mit der vorherig bestimmten Nilrot Probenkonzentration verglichen werden. Dabei wurde festgestellt, dass tatsächlich 100 % der ursprünglich gelösten Nilrotmenge durch die pH-Wertveränderung ausgefallen und so wieder freigesetzt worden sind.

Die Solubilisierungseigenschaften des supramolekularen Kern-Schale-Dendrimers wurden mit einer weiteren Substanz, der 8-Nitrotryptanthrin-3-carbonsäure, untersucht. Diese Substanz ist ein schlecht wasserlösliches, potenzielles Krebsmedikament.[131] Die 8-Nitrotryptanthrin-3-carbonsäure konnte ebenfalls erfolgreich mit Hilfe des supramolekularen Dendrimers in Lösung gebracht werden (Abbildung 145) Obwohl die Konzentrationsbestimmung der 8-Nitrotryptanthrin-3-carbonsäure nicht ganz einfach war, war es doch möglich die Konzentration auf einen vernünftigen Wert abzuschätzen. Die Freisetzung der 8-Nitrotryptanthrin-3-carbonsäure durch Säurezugabe konnte erfolgreich durchgeführt werden und zeigte ebenfalls eine Freisetzungsrate von 100 %.

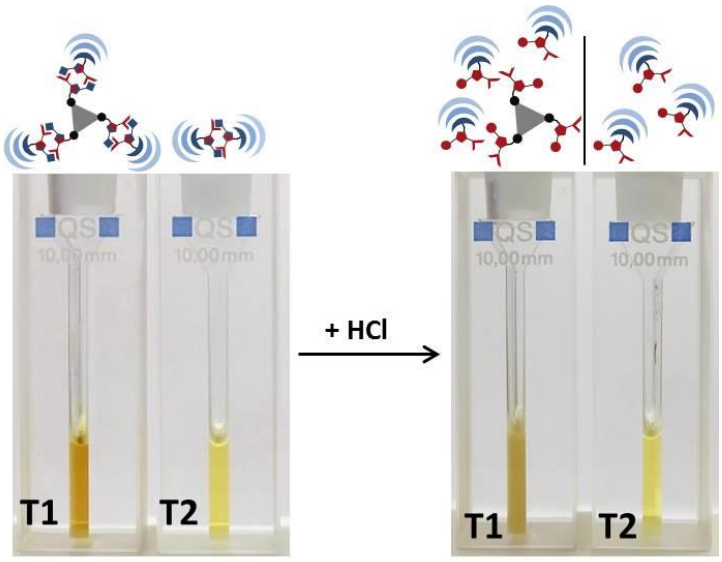

Abbildung 145: Löslichkeitsverhalten von 8-Nitrotryptanthrin-3-carbonsäure; Linke Seite: die linke Probe T1 entspricht einer Mischung aus 1 mM zwitterionischem Kernbaustein 74 und 30 mM zwitterionischen [G3]-Dendron; die rechte Probe T2 beinhaltet nur 30 mM zwitterionische [G3]-Dendron. Rechte Seite: T1 und T2 nach der Zugabe von wässriger HCl Lösung; nur T1 zeigt eine Trübung durch den Niederschlag der 8-Nitrotryptanthrin-3-carbonsäure, wobei Probe T2, die keinen Kernbaustein enthält, weiterhin als klare Lösung zu erkennen war.

Als weiteres Experiment wurden HeLa Zellen mit Lösungen von solubilisierten 8-Nitrotryptanthrin-3-carbonsäure inkubiert und anschließend mit Hilfe eines alamarBlue Assays auf ihre Vitalität geprüft. Die Ergebnisse deuten darauf hin, dass das supramolekulare Dendrimer die 8-Nitrotryptanthrin-3-carbonsäure abschirmt, da diese keine Toxizität mehr aufzeigte. Im Gegenteil, die Zugabe des supramolekularen Dendrimer schien einen stabilisierenden Effekt auf die Zellen zu haben, da diese eine größere Vitalität als die Referenzzellen aufwiesen. Der durchgeführte Toxizitätstest wirft jedoch mehr offene Fragen als Antworten auf. Ein erster Schritt einige dieser Fragen zu beantworten ist die Wiederholung dieses Toxizitätstest mit und ohne 8-Nitrotryptanthrin-3-carbonsäure, um die Reproduzierbarkeit zu überprüfen und zu verifizieren, ob der Stabilitätseffekt tatsächlich auftritt. Zudem wäre es wichtig zu wissen, ob das supramolekulare Dendrimer in der Lage ist in die Zelle zu gelangen. Testen könnte man dies, indem man ein schlecht wasserlösliches Fluorophor mit Hilfe des supramolekularen Dendrimers solubilisiert, mit dieser Lösung Zellen inkubiert und anschließend mit Konfokal Mikroskopie untersucht. Auch die Frage, ob die Freisetzung des Gastmoleküls innerhalb der Zelle funktioniert, konnte im Zuge dieser Arbeit nicht geklärt werden, da der durchgeführte Toxizitätstest in einem Puffer mit einem pH-Wert von 7,4 durchgeführt wurde. Zusätzlich und in Abhängigkeit der Ergebnisse der anderen vorgeschlagenen Experimente, könnten *in vivo* Tests helfen zu klären, ob das supramolekulare Kern-Schale Dendrimer als Nanotransporter für Krebsmedikamente praktisch anwendbar wäre.

Abgesehen von diesen offenen Fragen der praktischen Anwendbarkeit dieses Systems, war im Rahmen dieser Arbeit die Entwicklung und Synthese eines pH-schaltbaren Dendrimers möglich, zwei verschiedene, schlecht wasserlöslicher Substanzen solubilisieren konnte. Überdies war es möglich die Gastmoleküle durch einen äußeren Stimulus, in diesem Fall eine pH-Wert Veränderung, wieder kontrolliert freizusetzen. Dieser „proof of principle“ demonstriert das Potential supramolekularer Kern-Schale Dendrimere, basierend auf dem Guanidiniocarbonylpyrrolcarboxylatzwitterion als Bindungsmotiv, für die Solubilisierung und möglicherweise sogar für den Transport nicht oder schlecht wasserlöslicher Medikamente.

7 EXPERIMENTAL PART

7.1 General experimental and analytical methods

Solvents and Chemicals

All solvents were dried according to literature protocols. Diethyl ether and tetrahydrofurane were distilled from sodium with benzophenone as indicator. DMF was distilled from calcium hydride. Water for chromatographic and spectroscopic measurements was purified with a *TKA MicroPure* ultrapure water system. All other commercial reagents were purchased and used as received unless otherwise specified.

Inert Gas

Reactions with inert gas were carried out under technical argon from *Air Liquide* (99.996 % purity), which was dried with orange gel and phosphor pentoxide.

Lyophilization

For lyophilization a *Christ* Alpha 1-4 LD plus freeze dryer was used.

Melting Point (mp)

Melting points were determined using the melting point instrument B-540 by *Büchi*, whereas the measurements were done in open melting point tubes.

Measurement of pH values

The determination of pH values was done with the pH-meter 766 by *Knick* in combination with the sensor minitrode by *Hamilton*. For calibration of the pH-meter, commercially available buffer solutions (pH 4.00 and 7.00) were used.

Thin Layer Chromatography (TLC) and Column Chromatography (CC)

Thin layer chromatography as reaction control was performed with *Macherey-Nagel* POLYGRAM SIL/UV254 TLC pre-coated silica gel plates. The TLC elution mixtures are reported in volume percent (v : v).

Column chromatography was performed with silica gel MN Kieselgel 60M, 0.04–0.063 mm, 230–400 mesh from *Macherey Nagel* in glass columns of various diameter and length. The CC elution mixtures are also reported in volume percent (v : v).

High Performance Liquid Chromatography (HPLC), Reversed-Phase, Analytical

Dionex HPLC system: P680 pump, ASI-100 automated sample injector, UVD340U UV detector, UltiMate 3000 Column Compartment Software: Dionex Chromeleon 6.80

Column: YMC-Pack ODS-A, 150 mm length, 3.0 mm diameter, 5 µm,

Nuclear Magnetic Resonance Spectrometry (NMR)

- *Bruker* DMX 300 (^{1}H: 300 MHz; ^{13}C: 75 MHz)
- *Bruker* DRX 500 (^{1}H: 500 MHz; ^{13}C: 125 MHz)

All measurements were performed at room temperature, using varying solvents. The chemical shifts were measured against the solvent signal and are reported in ppm from TMS (δ scale). The coupling constants are given in Hertz. The following abbreviations for the description of the fine structure were used: s = singlet, bs = broad singlet, d = doublet, t = triplet, q = quartet, m = multiplet.

Mass Spectrometry (MS)

Bruker amaZon SL (ESI)

*Bruke*r autoFlex Speed (MALDI)

The ESI samples were measured at a concentration of 10^{-6} M and introduced into the ionization chamber via liquid injection. For MALDI, the samples were mixed with the 2,5-DHBA-matrix solution in a ratio of 1:3 (sample/matrix) and added drop wise (0.5µL) onto the target plate.

Fourier Transformation Infrared Spectroscopy (FT-IR)

Jasco FT-IR 430 spectrophotometer

The compounds were measured in pure form with the *JASCO* ATR-500M unit. The maxima are classified in three intensities: s (strong), m (middle), w (weak), which are reported in cm^{-1}.

UV-Spectroscopy (UV/vis)

Jasco V-660 UV-spectrometer

All UV/vis-spectra were measured at 25 °C in 114-QS quartz cuvettes (10 mm or 2 mm) from *Hellma*.

Atomic Force Microscopy (AFM)

Veeco Innova Scanning Probe Microscope
Veeco NanoDrive Controller
HALCYONICS Micro 40 active vibration isolation unit
AC 160TS *OLYMPUS* cantilever

Software: Gwyddion-2.41

All AFM measurements were done on mica surface and were prepared by spin coating. First, the freshly cleaved mica surface was placed on the spin coater, which was set to 60 rps. An amount of 6 µL of the respective sample solution was dropped on the rotating mica surface, which was then spin coated for another 10 minutes at 60 rps. All AFM measurements were performed in tapping mode.

Molecular Modelling (MM)

Software: Schrödinger Maestro, MacroModel V. 9.6

The structure calculations with MacroModel were performed based on the force field OPLS 2005 and water as solvent.

Dynamic Light Scattering (DLS)

DLS measurements were performed using the Zetasizer „Nano ZS“ by *Malvern* at 25 °C in disposable polystyrene (10 mm, 400 µL) cuvettes. All used solvents were filtered via PTFA (45 µm) syringe filter before the preparation of the respective samples.

Fluorescence Spectroscopy

Fluorescence measurements were performed with a Cary-Eclipse spectrometer by *Varian* at 25 °C in quartz cuvette (10 mm) from *Hellma*.

Ultrasound

Ultrasound treatment was performed using the Sonorex Super RK 510H by *Bandelin.*

7.2 General sample preparation for solubilization studies

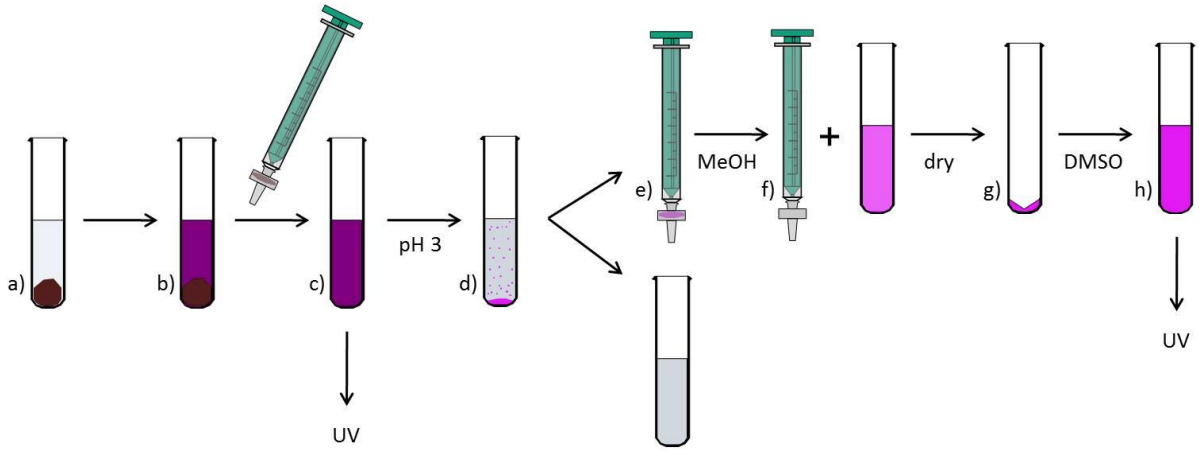

Figure 146: Schematic illustration of the sample preparation during the solubilization studies of Nile red and 8-nitrotryptanthrin-3-carboxylic acid.

The scheme in Figure 146 explains the general sample preparation for the solubility studies. After the preparation of the respective aqueous solution of the solubilization agent solid Nile red or 8-nitrotryptanthrin-3-carboxylic acid was added in a vast excess and the sample was treated with ultra sound for 5 seconds to allow a fine distribution of the solid dye. This suspension was kept for three days and was shaken occasionally to evenly redistribute the sediment dye through the sample. After this the excess Nile red or 8-nitrotryptanthrin-3-carboxylic acid was filtered off by using a PTFE syringe filter leaving a clear solution of the solubilization agent and the solubilized Nile Red or 8-nitrotryptanthrin-3-carboxylic acid in water. To verify the assumption, that the solubilized molecule will be released upon a significant pH change, hydrochloric acid was added to the sample. A possible precipitate could then be filtered off again by using a syringe filter. This filtration left a clear colorless filtrate. The dye or 8-nitrotryptanthrin-3-carboxylic acid was be re-dissolved by washing the syringe filter with an appropriate solvent. The used solvent should be mixable with water and the substance in question (the dye or 8-nitrotryptanthrin-3-carboxylic acid) should be well soluble in it (methanol for Nile red and DMSO for 8-nitrotryptanthrin-3-carboxylic acid). After re-dissolving the dye or 8-nitrotryptanthrin-3-carboxylic acid, the solvent was removed again, to be able to re-dissolve the dye in a specific amount of DMSO. UV-Vis spectroscopy provided a suitable method to determine the concentration of Nile red or 8-nitrotryptanthrin-3-carboxylic acid respectively. During the sample processing UV-Vis measurements were done with the aqueous solution of the dye or 8-nitrotryptanthrin-3-carboxylic acid and the respective DMSO solution. Both measurements can then be compared to calibration measurements of the respective compound with known concentrations in DMSO respectively. This allowed the calculation of the dye concentration in question.

7.3 Synthesis

7.3.1 Zwitterionic Dendron

The synthesis of the polyglycerol dendrons was performed according to a synthesis protocol from the *Haag* group[112] and the syntheses of the zwitterionic [G2]- and [G3]-dendrons were performed according to literature protocol by *Merschky*[24,128]. The synthesis of the pyrrole precursor ("triester") **91** is a standard synthesis in the *Schmuck* group and its synthesis and the alkyne functionalization was performed according to literature.[22,128] For additional data concerning the characterization of the respective molecules, which are not given in this experimental part, the cited literatures can be consulted.

Synthesis of [G1]-OH

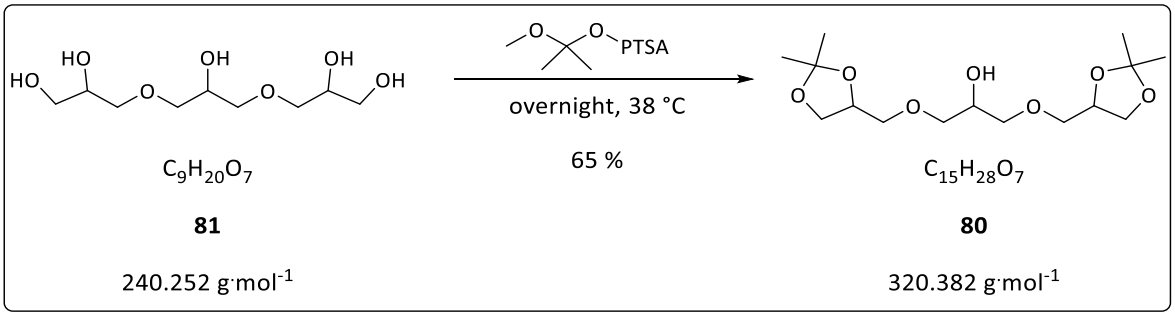

Triglycerol (150.0 g, 625.0 mmol, 1.0 eq) was slowly heated with a heat gun to get it into liquid state and 2,2-dimethoxypropane (258.4 g, 304.0 mL, 2.5 mol, 4.0 eq) was added. Subsequently PTSA (7.6 g, 62.5 mmol, 0.1 eq) was added slowly and the reaction mixture was stirred overnight at 38 °C. The resulting mixture was neutralized with triethylamine (6.3 g, 8.7 mL, 62.5 mmol, 0.1 eq) and was stirred for 0.5 hours at room temperature. The solvent was removed under reduced pressure and the crude product was purified *via* fractional distillation (0.2 mbar, 140 °C). The product **80** (131.0 g, 408.9 mmol) was obtained as slightly yellow oil with a yield of 65 %.

^{1}H-NMR (300 MHz, $CDCl_3$) δ = 1.16 (s, 6 H, methyl-C*H*$_3$), 1.22 (s, 6 H, methyl-C*H*$_3$), 1.97 (s, 1 H, O*H*), 3.31 – 3.42 (m, 8 H, C*H*$_2$), 3.51 – 3.56 (m, 2 H, C*H*), 3.75 (m, 1 H, C*H*), 3.83 – 3.88 (m, 2 H, C*H*$_2$), 4.04 – 4.10 (m, 2 H, C*H*$_2$) ppm.

^{13}C-NMR (75.5 MHz, $CDCl_3$) δ = 25.09 (2 C, *C*H_3), 26.44 (2 C, *C*H_3), 66.24 (2 C, *C*H_2), 69.03 (2 C, *C*H), 72.14 (2 C, *C*H_2), 72.58 (2 C, *C*H_2), 74.39 (1 C, *C*H), 109.07 (2 C, C_q) ppm.

MS (ESI) m/z = 343.14 $[M + Na]^+$, calculated ($C_{15}H_{28}NaO_7$) 343.17 $g \cdot mol^{-1}$

Synthesis of [G2]-ene

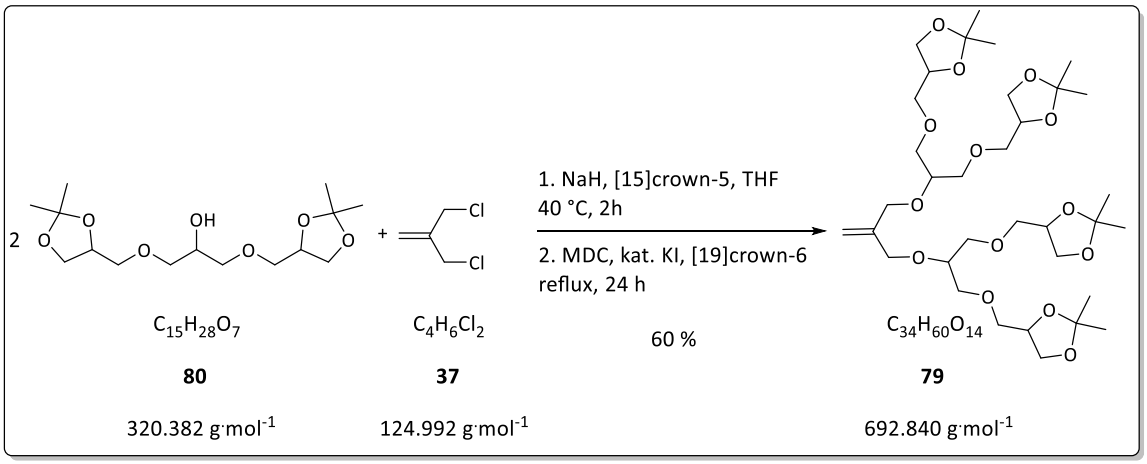

The [G1]-OH dendron **80** (46.5 g, 145.2 mmol, 2.1 eq) was dissolved in absolute THF (325 mL) under argon atmosphere. Sodium hydride (60 % NaH in mineral oil; 14.1 g, 363.0 mmol, 5.25 eq) and 15-crown-5 ether (catalytic amount) were added and the mixture was heated to 40 °C for 3 hours. Subsequently 18-crown-6 ether, potassium iodide (both in catalytic amounts) and MDC (8.6 g, 69.1 mmol, 1.0 eq) were added. After the reaction mixture was refluxed for 24 hours and cooled down to room temperature, water (50 mL) was added dropwise. The mixture was extracted with DCM (5 x 100 mL; addition of 50 mL brine for better phase separation) and the combined organic phases were dried with sodium sulfate. The solvent was evaporated under reduced pressure. The resulting yellow oil was purified *via* fractionated distillation (0.1 mbar, 168-185 °C). Since the distillation residue still contained a large amount of [G2]-ene, it was further purified *via* liquid chromatography (MPLC, SiO_2, 50 x 500 mm glass column, flow 60 mL·minute^{-1}, 4 g per chromatography sequence, 60 minutes per sequence, retention 17 to 31 minutes, 2-propanol : *n*-hexane 2.5 : 7.5). The [G2]-ene dendron **79** (28.7 g, 41.4 mmol) was obtained as a colorless oil with a yield of 60 %.

^{1}H-NMR (300 MHz, $CDCl_3$) δ = 1.23 (s, 12 H, methyl-C*H*$_3$), 1.29 (s, 12 H, methyl-C*H*$_3$), 3.37 – 3.52 (m, 18 H, C*H* /C*H*$_2$), 3.57 – 3.64 (m, 7 H, C*H* /C*H*$_2$), 3.85 (m, 1 H, C*H*), 3.91 – 3.96 (m, 4 H, C*H*$_2$), 4.08 – 4.16 (m, 4 H, C*H* /C*H*$_2$), 5.06 (m, 2 H, C*H*$_2$) ppm.

^{13}C-NMR (75.5 MHz, $CDCl_3$) δ = 25.25 (4 C, *C*H$_3$), 26.60 (4 C, *C*H$_3$), 66.39 (2 C, *C*H$_2$), 66.56 (4 C, *C*H$_2$), 69.21 (1 C, *C*$_q$), 72.32 (4 C, *C*H$_2$), 72.68 (4 C, *C*H$_2$), 74.48 (4 C, *C*H), 74.55 (2 C, *C*H), 78.48 (1 C, *C*H$_2$), 109.33 (4 C, *C*$_q$) ppm.

MS (ESI) m/z = 715.38 $[M + Na]^+$, calculated ($C_{34}H_{60}NaO_{14}$) 715.39 g·mol^{-1}

Synthesis of [G2]-OH

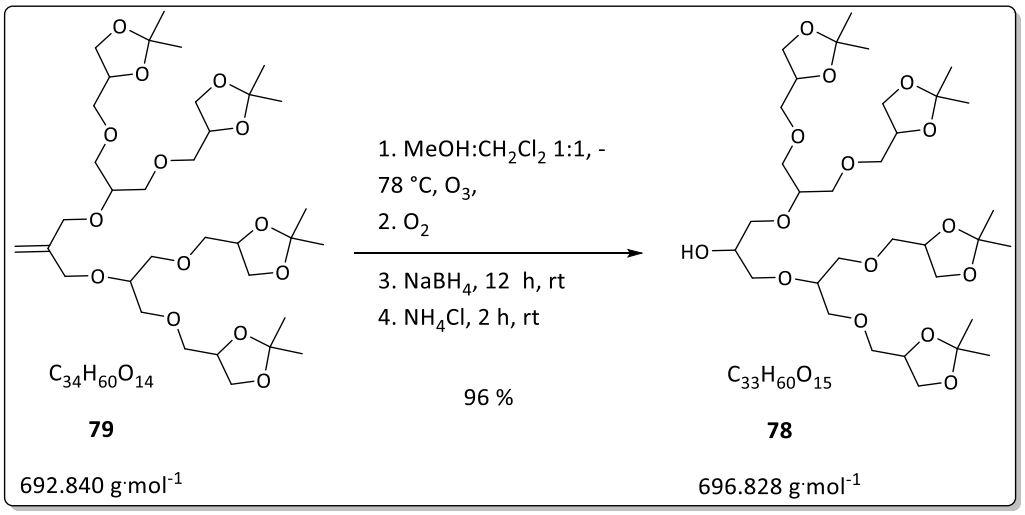

The [G2]-ene dendron **79** (15.0 g, 21.7 mmol, 1.0 eq) was dissolved in a mixture of dichloromethane and methanol (167 mL, 1 : 1 ratio) and the solution was cooled to -78 °C using a acetone/dry ice cooling bath. Subsequently ozone was bubbled thru the solution until it turned blue. With a stream of oxygen, excess ozone was then removed. Afterwards sodium borohydride (8.2 g, 217.0 mmol, 10.0 eq) was added, the cooling bath was removed and the solution was stirred for 12 hours, while the reaction mixture was allowed to reach room temperature. The reaction was quenched by adding saturated aqueous solution of ammonium chloride (200 mL) and the mixture was then stirred for 2 hours at room temperature. The organic phase was separated, while the aqueous phase was extracted with DCM (3 x 100 mL). The combined organic phases were washed with water (100 mL), dried with sodium sulfate, filtrated and eventually DCM was removed under reduced pressure. The [G2]-OH dendron **78** (14.5 g, 4.8 mmol) required no further purification and was obtained as a colorless viscous oil with a yield of 96 %.

^{1}H-NMR (300 MHz, $CDCl_3$) δ = 1.23 (s, 12 H, methyl-C*H*$_3$), 1.29 (s, 12 H, methyl-C*H*$_3$), 3.37 – 3.49 (m, 18 H, C*H* /C*H*$_2$), 3.57 – 3.64 (m, 8 H, C*H* /C*H*$_2$), 3.90 – 3.95 (m, 4 H, C*H*$_2$), 4.03 (m, 1 H, C*H*), 4.09 – 4.18 (m, 4 H, C*H*$_2$), 4.42 (bs, 1 H, O*H*) ppm.

^{13}C-NMR (75.5 MHz, $CDCl_3$) δ = 25.23 (4 C, *C*H$_3$), 26.61 (4 C, *C*H$_3$), 66.53 (4 C, *C*H$_2$), 69.26 (1 C, *C*H), 70.60 (1 C, *C*H$_2$), 71.46 (4 C, *C*H$_2$), 72.32 (4 C, *C*H$_2$), 72.70 (1 C, *C*H$_2$), 74.47 (4 C, *C*H), 78.50 (2 C, *C*H), 109.26 (4 C, *C*$_q$) ppm.

MS (ESI) m/z = 719.38 $[M + Na]^+$, calculated ($C_{33}H_{16}NaO_{15}$) 719.39 g·mol^{-1}

Synthesis of [G2]-Pyrrole (JS065)

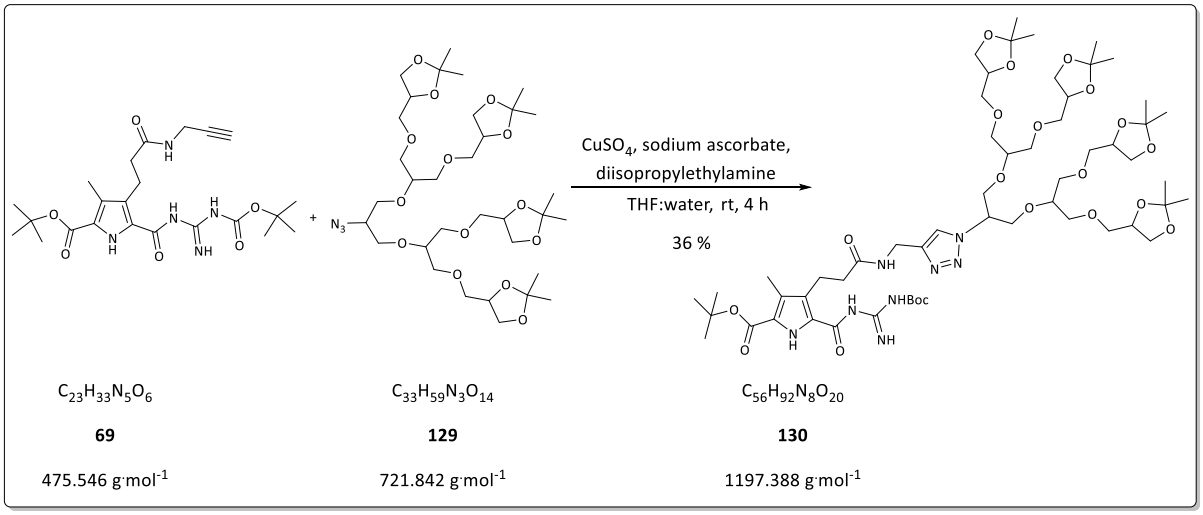

Pyrrole building block **69** (200.0 mg, 420.0 µmol, 1.0 eq), [G2]-N_3 dendron **129** (365.0 mg, 506.0 µmol, 1.2 eq) and diisopropylethylamine (22.0 µL, 16.3 mg, 126.0 µmol, 0.3 eq) were dissolved in THF (6 mL) and fresh aqueous solutions of sodium ascorbate (0.5 mL, 25.0 mg, 126.0 µmol, 0.3 eq) and copper sulfate pentahydrate (0.5 mL, 15.7 mg, 63.0 µmol, 0.15 eq) were added. Subsequently the THF : water ratio was adjusted to 1 : 1 by addition of water. The reaction mixture was stirred at room temperature and monitored by TLC. After 48 hours no further process of the reaction was observed, thus freshly prepared aqueous solutions of sodium ascorbate (0.5 mL, 25.0 mg, 126.0 µmol, 0.3 eq) and copper sulfate pentahydrate (0.5 mL, 15.7 mg, 63.0 µmol, 0.15 eq) were added a second time, and again the THF : water ratio was set to 1 : 1. After another 48 hours a third addition of both sodium ascorbate and copper sulfate pentahydrate (same amounts as before) was done. TLC indicated full consumption of the starting material after further 24 hours. The reaction mixture was diluted with water (10 mL) and extracted with DCM (3 x 10 mL). The combined organic fractions were washed with saturated EDTA solution (5 x 15 mL) to remove the copper ions, until the slightly bluish color of the DCM solution disappeared. Subsequently the organic fractions were dried with sodium sulfate and the solvent was then evaporated under reduced pressure. The crude product was purified *via* liquid chromatography (MPLC, SiO2, 15 g cartridge, flow 25 mL·min^{-1}, isopropanol : *n*-hexane 30 : 70 to 100 % isopropanol in 40 minutes, retention time 25-35 minutes). The [G2]-pyrrole dendron **130** (180.0 mg, 151.0 µmol) was obtained as a colorless viscous oil with a yield of 36 %.

^{1}H-NMR (500 MHz, $CDCl_3$) δ = 1.32 (s, 12 H, acetal-CH_3), 1.37 (s, 12 H, acetal-CH_3), 1.51 (s, 9 H, CH_3), 1.55 (s, 9 H, CH_3), 2.23 (s, 3 H, methyl-CH_3), 2.43 – 2.48 (t, ^{3}J = 7.31 Hz, 2 H, CH_2), 3.08 – 3.13 (t, ^{3}J = 7.74 Hz, 2 H, CH_2), 3.41 – 3.68 (m, 22 H, CH/CH_2), 3.85 – 3.91 (m, 2 H, CH), 3.97 – 4.04 (m, 6 H, CH_2), 4.14 – 4.24 (m, 4 H, CH_2), 4.47 – 4.48 (d, ^{3}J = 5.30, 2 H, CH_2), 4.80 – 4.85 (m, 1 H, CH), 7.14 (bs, 1 H, CH), 7.58 – 7.65 (m, 1 H, NH), 7.70, 8.50, 9.16, 9.61 (bs, 1 H, NH) ppm.

^{13}C-NMR (125 MHz, $CDCl_3$) δ = 10.03 (1 C, CH$_3$), 21.68 (1 C, CH$_2$), 25.49 (4 C, CH$_3$), 26.88 (4 C, CH$_3$), 28.07 (3 C, CH$_3$), 28.55 (3 C, CH$_3$), 35.03 (2 C, CH$_2$), 37.24 (2 C, CH$_2$), 61.05 (1 C, CH), 66.69 (4 C, CH$_2$), 69.45 (1 C, CH$_2$), 70.41 (1 C, CH$_2$), 71.64 (4 C, CH$_2$), 72.61 (2 C, CH$_2$), 74.72 (4 C, CH), 77.36 (1 C, CH), 78.53 (1 C, CH), 78.84 (1 C, CH), 80.37 (1 C, C_q), 82.59 (1 C, C_q), 109.56 (4 C, C_q), 121.69 (1 C, C_q), 122.54 (1 C, CH), 125.96 (1 C, C_q), 128.34, 144.36 (1 C, C_q), 153.91, 157.83, 160.53, 171.29, 173.62 (1 C, CN/CO) ppm.

Synthesis of [G2]-Pyrrole cation (JS066)

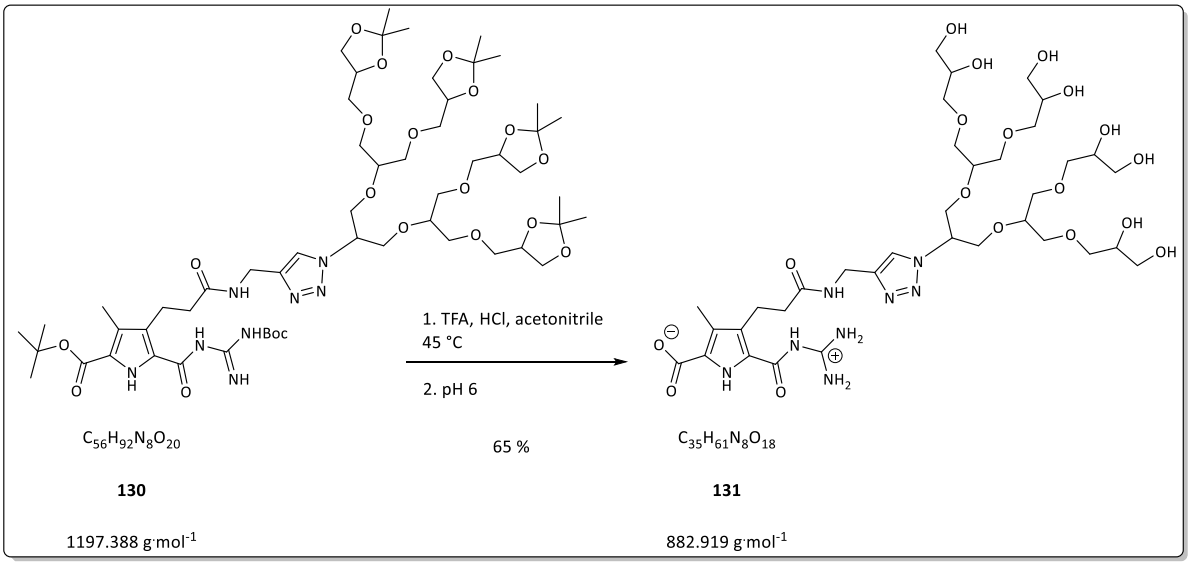

The protected [G2]-pyrrole dendron **130** (170.0 mg, 142.0 µmol, 1.0 eq) was dissolved in acetonitrile (2 mL). TFA (1.6 g, 1.1 mL, 14.2 mmol, 100.0 eq) and aqueous HCl (5 %, 1.0 mL) were added and the reaction mixture was stirred at 40 °C for 24 hours. The solvent was evaporated under reduced pressure; the residue was re-dissolved in aqueous HCl (5 %) and freeze dried (2 times). To obtain the zwitterionic form of the molecule, the residue was re-dissolved in water and the pH value was set to 5.9 using 0.1 M aqueous sodium hydroxide solution and 0.1 M hydrochloric acid. Subsequently the solution was freeze dried again and he zwitterionic product was purified *via* liquid chromatography (MPLC, RP18, 50 g, flow 25 mL·min^{-1}, gradient methanol 40 – 70 % in 8 minutes, 70 % for 10 minutes retention time 10-12 minutes). The zwitterionic [G2]-dendron **131** (74.0 mg, 84.0 µmol) was obtained as a white solid substance with a yield of 59 %.

^{1}H-NMR (300 MHz, DMSO-d_6) δ = 2.23 (s, 3 H, methyl-C*H*$_3$), 2.25 – 2.31 (m, 2 H, C*H*$_2$), 2.95 – 2.99 (t, ^3J = 7.64 Hz, 2 H, C*H*$_2$), 3.26 – 3.58 (m, 31 H, C*H*/C*H*$_2$/O*H*), 3.78 – 3.82 (m, 2 H, C*H*), 3.91 – 3.94 (m, 2 H, C*H*), 4.27 – 4.29 (m, 2 H, C*H*$_2$), 4.48 – 4.51 (m, 4 H, C*H*$_2$), 4.55 – 4.58 (m, 1 H, C*H*), 4.62 – 4.65 (m, 3 H, C*H*$_2$), 4.81 – 4.92 (m, 1 H, C*H*), 7.90 (bs, 1 H, C*H*), 7.93 (bs, 2 H, N*H*), 8.20 – 8.23 (t, ^3J = 5.25 Hz, 1 H, N*H*), 10.11 (bs, 2 H, N*H*), 12.63, 14.61 (bs, 1 H, N*H*) ppm.

MS (MALDI) m/z = 881.97 [M], calculated ($C_{35}H_{61}N_8O_{18}$) 881.41 g·mol^{-1}

Synthesis of [G3]-ene

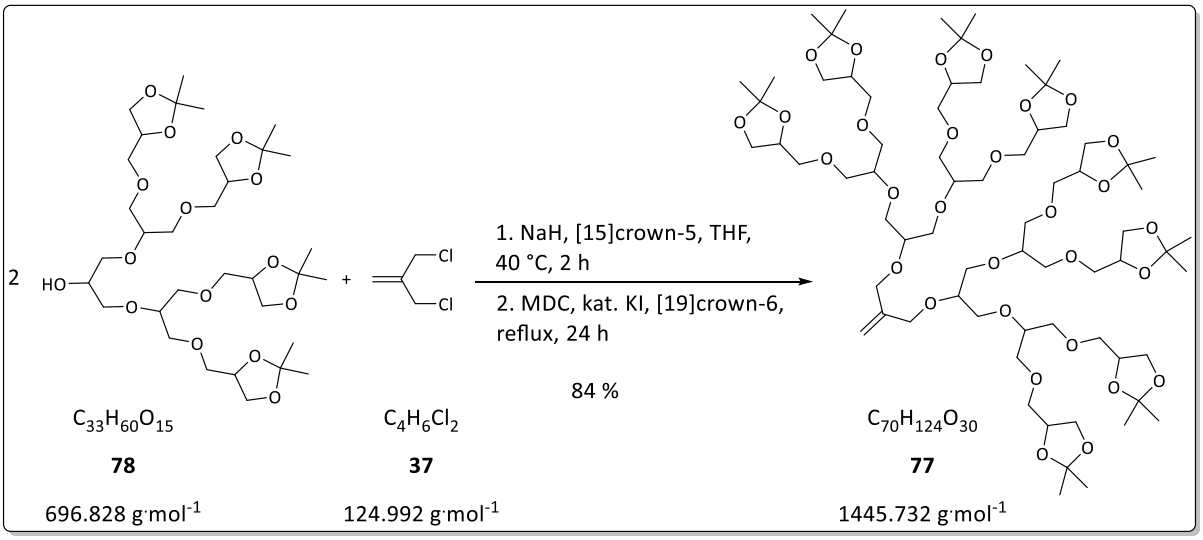

The [G2]-OH dendron **78** (14.4 g, 20.6 mmol, 2.1 eq) was dissolved in absolute THF (115 mL) under argon atmosphere. Sodium hydride (60 % NaH in mineral oil; 4.1 g, 103.0 mmol, 10.45 eq) and 15-crown-5 ether (catalytic amount) were added and the mixture was heated to 40 °C for 3 hours. Subsequently 18-crown-6 ether, potassium iodide (both in catalytic amounts) and MDC **37** (1.2 g, 981.0 µmol, 1.0 eq) were added. After the reaction mixture was refluxed for 24 hours and cooled down to room temperature, water (100 mL) was added dropwise. The mixture was extracted with DCM (7 x 70 mL) and the combined organic fractions were dried with sodium sulfate. The solvent was evaporated under reduced pressure. The resulting yellow oil was purified *via* liquid chromatography (MPLC, SiO_2, 50 x 500 mm glass column, flow 60 mL·min^{-1}, 4 g per chromatography sequence, 50 minutes per sequence, retention 17 to 26 minutes, 2-propanol : *n*-hexane 5 : 5). The [G2]-ene dendron **77** (11.9 g, 8.2 mmol) was obtained as a slightly yellow oil with a yield of 84 %.

^{1}H-NMR (300 MHz, $CDCl_3$) δ = 1.20 (s, 24 H, acetal-CH_3), 1.26 (s, 24 H, acetal-CH_3), 3.31 – 3.49 (m, 46 H, CH/CH_2), 3.55 – 3.60 (m, 10 H, CH/CH_2), 3.70 (m, 2 H, CH), 3.87 – 3.92 (m, 8 H, CH/CH_2), 4.05 – 4.12 (m, 8 H, CH_2), 5.03 (s, 2 H, CH_2) ppm.

^{13}C-NMR (75.5 MHz, $CDCl_3$) δ = 25.19 (8 C, CH_3), 26.55 (8 C, CH_3), 66.51 (8 C, CH_2), 70.45 (2 C, CH_2), 71.25 (8 C, CH_2), 72.22 (8 C, CH_2), 72.74 (4 C, CH_2), 74.39 (8 C, CH), 74.54 (2 C, CH), 78.23 (2 C, CH), 78.41 (2 C, CH), 109.11 (8 C, C_q), 113.6 (1 C, CH), 143.05 (1 C, C_q) ppm.

MS (ESI) m/z = 745.39 $[M + Na]^{2+}$, calculated ($C_{70}H_{124}Na_2O_{30}$) 1490.80 g·mol^{-1}

Synthesis of [G3]-OH

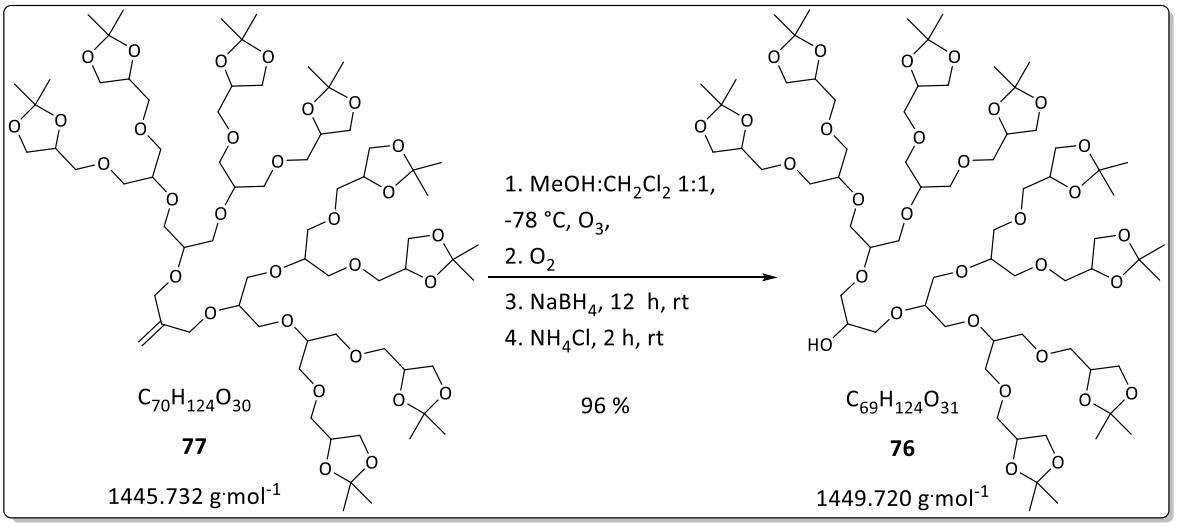

The [G3]-ene dendron **77** (7.2 g, 497.0 µmol, 1.0 eq) was dissolved in a mixture of dichloromethane and methanol (38.2 mL, c = 0.13 mol·L^{-1}, 1 : 1 ratio) and the solution was cooled to -78 °C using a acetone/dry ice cooling bath. Subsequently ozone was bubbled thru the solution until it turned blue. With a stream of oxygen excess ozone was then removed. Afterwards sodium borohydride (1.9 g, 49.7 mmol, 10.0 eq) was added, the cooling bath was removed and the solution was stirred for 12 hours, while the reaction mixture was allowed to reach room temperature. The reaction was quenched by adding saturated ammonium chloride solution (100 mL) and was then stirred for 2 hours at room temperature. The organic phase was separated, while the aqueous phase was extracted with DCM (3 x 100 mL). The combined organic phases were washed with water (100 mL), dried with sodium sulfate, filtrated and eventually DCM was evaporated under reduced pressure. The [G3]-OH dendron **76** (6.9 g, 476.0 µmol) required no further purification and was obtained as a colorless viscous oil with a yield of 96 %.

^{1}H-NMR (300 MHz, $CDCl_3$) δ = 1.24 (s, 24 H, acetal-CH_3), 1.30 (s, 24 H, acetal-CH_3), 3.34 – 3.51 (m, 46 H, CH/CH_2), 3.60 – 3.64 (m, 10 H, CH/CH_2), 3.75 (m, 2 H, CH), 3.91 – 3.96 (m, 8 H, CH/CH_2), 4.12 – 4.15 (m, 8 H, CH_2), 5.22 (s, 1 H, OH) ppm.

^{13}C-NMR (75.5 MHz, $CDCl_3$) δ = 25.30 (8 C, CH_3), 26.66 (8 C, CH_3), 66.21 (8 C, CH_2), 70.28 (1 C, CH), 70.61 (2 C, CH_2), 71.38 (12 C, CH_2), 72.35 (8 C, CH_2), 74.51 (8 C, CH), 74.64 (2 C, CH), 78.35 (2 C, CH), 78.46 (2 C, CH), 109.20 (8 C, C_q)ppm.

MS (ESI) m/z = 1471.82 $[M + Na]^+$, calculated ($C_{69}H_{124}NaO_{31}$) 1471.81 g·mol^{-1}

Synthesis of [G3]-N_3

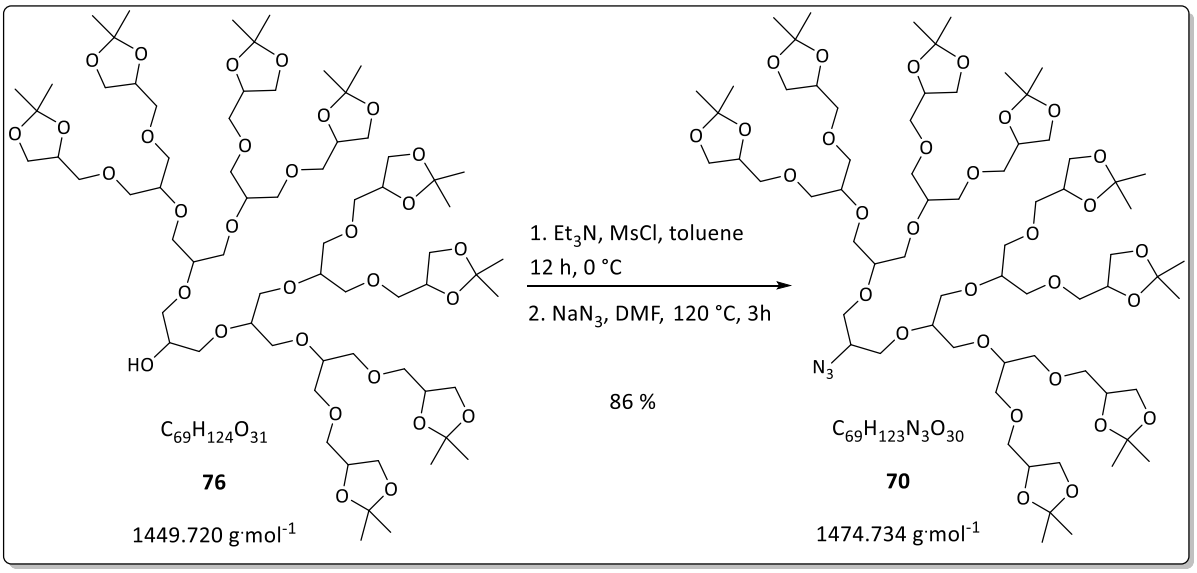

The [G3]-OH dendron **76** (6.8 g, 389.0 µmol, 1.0 eq) was dissolved with triethylamine (788.4 mg, 1.1 mL, 777.0 µmol, 2.0 eq) in toluene (100 mL). The solution was cooled to 0 °C using an ice bath. Methanesulfonyl chloride (888.0 mg, 0.6 mL, 777.0 µmol, 2.0 eq) was added and the mixture was stirred for 12 hours at 0 °C. The resulting white precipitate was filtered off and the toluene was subsequently evaporated from the filtrate under reduced pressure. The [G3]-OMs was obtained as yellow oil. Without any further purification the [G3]-OMs was dissolved under argon atmosphere in dry DMF (60 mL). Sodium azide (1.3 g, 19.4 mmol, 5.0 eq) was added and the reaction mixture was heated to 120 °C for 3 hours. Subsequently excess NaN_3 was filtered off and DMF was removed under reduced pressure. The crude product was purified *via* liquid chromatography (MPLC, SiO_2, flow 25 mL·min^{-1}, gradient 2-propanol : *n*-hexane 30 : 70 to 50 : 50 in 10 min, 50 : 50 for 10 min, 50 : 50 to 70 : 30 in 10 min, retention time 16-25 minutes). [G3]-N_3 dendron **70** (4.9 g, 332.0 µmol) was obtained as a yellow highly viscous oil with a yield of 86 %.

^{1}H-NMR (300 MHz, $CDCl_3$) δ = 1.22 (s, 24 H, acetal-C*H*$_3$), 1.28 (s, 24 H, acetal-C*H*$_3$), 3.34 – 3.53 (m, 46 H, C*H*/C*H*$_2$), 3.56 – 3.61 (m, 10 H, C*H*/C*H*$_2$), 3.71 (m, 2 H, C*H*), 3.88 – 3.93 (m, 8 H, C*H*/C*H*$_2$), 4.09 – 4.13 (m, 8 H, C*H*$_2$) ppm.

^{13}C-NMR (75.5 MHz, $CDCl_3$) δ = 25.25 (8 C, *C*H$_3$), 26.61 (8 C, *C*H$_3$), 66.56 (8 C, *C*H$_2$), 70.18 (2 C, *C*H$_2$), 71.14 (4 C, *C*H$_2$), 71.31 (8 C, *C*H$_2$), 72.32 (8 C, *C*H$_2$), 74.543 (8 C, *C*H), 74.60 (2 C, *C*H), 78.30 (2 C, *C*H), 78.46 (2 C, *C*H), 78.98 (1 C, *C*H), 109.20 (8 C, *C*$_q$)ppm.

MS (ESI) m/z = 1496.80 $[M + Na]^+$, calculated ($C_{69}H_{123}N_3NaO_{30}$) 1496.8 g·mol^{-1}

Synthesis of [G3]-Pyrrole 75 – Click Reaction

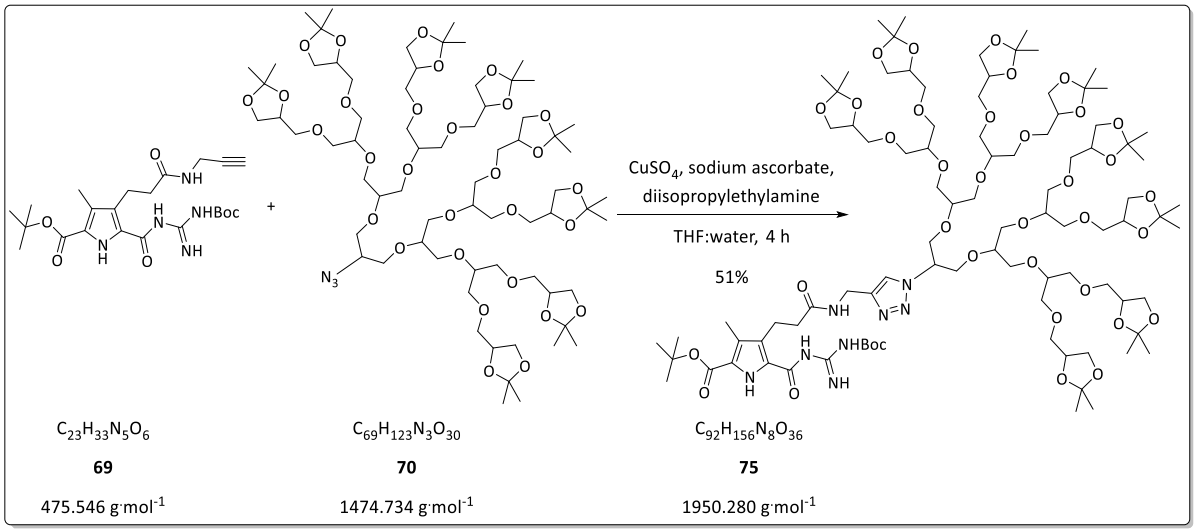

Pyrrole building block **69** (210.0 mg; 44.0 µmol; 1.0 eq) and [G3]-N_3 (714.0 mg; 48.0 µmol; 1.1 eq) were dissolved in THF (8 mL) under argon atmosphere. Subsequently DIPEA (17.0 mg; 23.0 µL; 132.0 µmol; 0.3 eq) was added to this mixture. Copper(II) sulfate pentahydrate (16.5 mg; 66.0 µmol; 0.15 eq) and sodium ascorbate (26.2 mg; 132.0 µmol; 0.3 eq) were each solved in 1 mL millipore water and these solutions were then added to the THF solution. To obtain a THF : water ratio of 1 : 1 another 6 mL of millipore water were added. Due to the *in situ* reduction of Cu(II) to Cu(I), the reaction mixture showed a green color. After stirring the reaction mixture for 4 hours at room temperature and under argon atmosphere, TLC (*n*-hexane : isopropanol – 8 : 2) indicated a completed reaction. The mixture was diluted with water and extracted with DCM (3 x 6 mL). The organic phases were collected and washed with a saturated sodium-EDTA solution (4 x 10 mL) to remove the copper salts until the slightly bluish color of the DCM solution disappeared. Subsequently the organic phase was dried with $MgSO_4$, the drying agent was removed by filtration and the solvent was evaporated under reduced pressure. The crude product (830.0 mg) was colorless highly viscous oil. The purification was done *via* liquid chromatography (MPLC, SiO_2, 80g column, flow 30 mL·min^{-1}, step gradient *n*-hexane : isopropanol – 70 : 30 to 50 : 50 in 12 min – 50 : 50 for 10 min - 50 : 50 to 100 % isopropanol in 12 min). The [G3]-pyrrole dendron **75** (440.0 mg; 226.0 µmol) was obtained as a colorless viscous oil with a yield of 51 %

R_f-Value (*n*-hexane : isopropanol – 8 : 2) = 0.07

^{1}H-NMR (500 MHz, $CDCl_3$) δ = 1.30 (s, 24 H, acetal-CH_3), 1.35 (s, 24 H, acetal-CH_3), 1.49 (s, 9 H, CH_3), 1.53 (s, 9 H, CH_3), 2.21 (s, 3 H, methyl-CH_3), 2.42 – 2.45 (t, ^{3}J = 8.09 Hz, 2 H, CH_2), 3.08 – 3.10 (t, ^{3}J = 8.09 Hz, 2 H, CH_2), 3.39 – 3.52 (m, 40 H, CH/CH_2), 3.55 – 3.58 (m, 4 H, CH), 3.61 – 3.69 (m, 10 H, CH/CH_2), 3.93 – 4.01 (m, 12 H, CH_2), 4.14 – 4.21 (m, 8 H, CH_2), 4.45 – 4.46 (d, ^{3}J = 4.60 Hz, 2 H, CH_2), 4.77 – 4.79 (m, 1 H, CH), 7.14 (bs, 1 H, CH), 7.71 – 7.74 (m, 1 H, NH), 8.38, 9.06, 9.47, 10.08 (bs, 1 H, NH) ppm.

^{13}C-NMR (125 MHz, $CDCl_3$) δ = 10.13 (1 C, CH$_3$), 21.72 (1 C, CH$_2$), 25.44 (8 C, CH$_3$), 26.84 (8 C, CH$_3$), 28.07 (3 C, CH$_3$), 28.47 (3 C, CH$_3$), 35.01 (2 C, CH$_2$), 37.55 (2 C, CH$_2$), 61.32 (1 C, CH), 66.73 (8 C, CH$_2$), 69.41 (2 C, CH$_2$), 70.24 (1 C, CH$_2$), 70.40 (1 C, CH$_2$), 71.25 (2 C, CH$_2$), 71.49 (4 C, CH$_2$), 71.63 (2 C, CH$_2$), 72.53 (8 C, CH$_2$), 74.64 (8 C, CH), 74.78 (2 C, CH), 78.39 (2 C, CH), 78.64 (2 C, CH), 81.24 (1 C, C_q), 83.23 (1 C, C_q), 109.41 (8 C, C_q), 121.60 (1 C, C_q), 122.64 (1 C, CH), 126.16 (1 C, C_q), 128.48 (2 C, C_q), 143.86 (1 C, C_q), 153.28, 158.43, 160.55, 171.58, 173.54 (1 C, CN/CO) ppm.

MS (ESI) m/z = 1972.04 $[M + Na]^+$, calculated ($C_{92}H_{156}N_8NaO_{36}$) 1972.04 $g \cdot mol^{-1}$

Synthesis of [G3]-Zwitterion

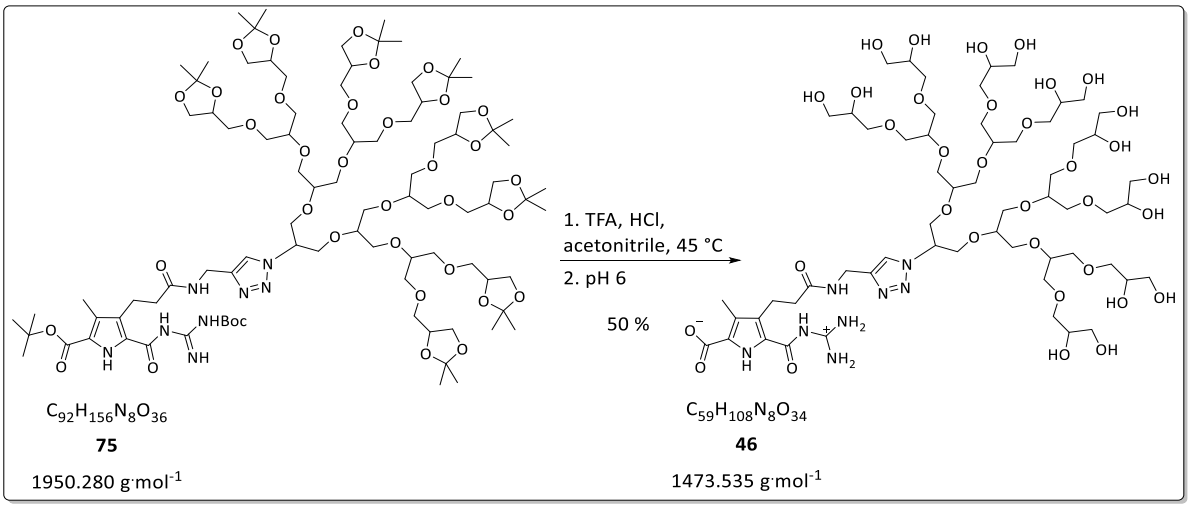

The protected [G3]-pyrrole **75** (658.0 mg; 337.0 µmol; 1.0 eq) was solved in 5.2 mL acetonitrile. TFA (5.2 ml) and aqueous HCl (5 %; 2.0 ml) were added and the mixture was stirred at 45 °C until HPLC control indicated the end of the reaction. In the early stage of the deprotection HPLC control was not practical, since the starting material and the intermediate products, with too many acetal groups still un-cleaved is not soluble in the required solvent mixture for HPLC (MeOH : H_2O – 80 : 20). So the solubility of the taken sample is a first indication for the progress of the deprotection reaction. After the completion of the reaction the crude product (850.0 mg due to many salts) was concentrated in vacuum. The purification was done *via* reversed phase liquid chromatography (MPLC, RP18; 120 g column; MeOH : H_2O with 0.05 % TFA, 20 : 80 to 50 : 50 in 50 minutes; 30 $mL \cdot min^{-1}$, retention time 35 min). The resulting product (360.0 mg) was resolved in hydrochloric acid (5 %) and freeze dried. The pH value was set to 5.9 by the addition of sodium hydroxide (0.1 M). To remove the salts the zwitterionic product was purified *via* reversed phase liquid chromatography (MPLC, RP18; 17 g column; MeOH : H_2O -30 : 70 to 60 : 40 in 15 min; 30 $mL \cdot min^{-1}$, retention time 12 min). The zwitterionic [G3]-dendron **46** (195.0 mg, 132.0 µmol) was obtained as a highly viscous oil with a yield of 40 % and a purity (determined via HPLC) of 95 %.

Sample Name:	G3 Zwio		Quant. Method:	HPLC_1\Jule\G3 Zw.SEQ			
Vial Number:	RA13		Value A	20.00122 %	MeOH	Injection Volume:	20.0
Recording Time:	17/6/2014 7:42		Value B	79.99878 %	H2O	Channel:	UV_VIS_1
Run Time (min):	25.00		Value C	0 %	H2O + TFA	Wavelength:	220
Flow (ml/min):	0.430		Value D	0 %	MeOH + TFA	Bandwidth:	1

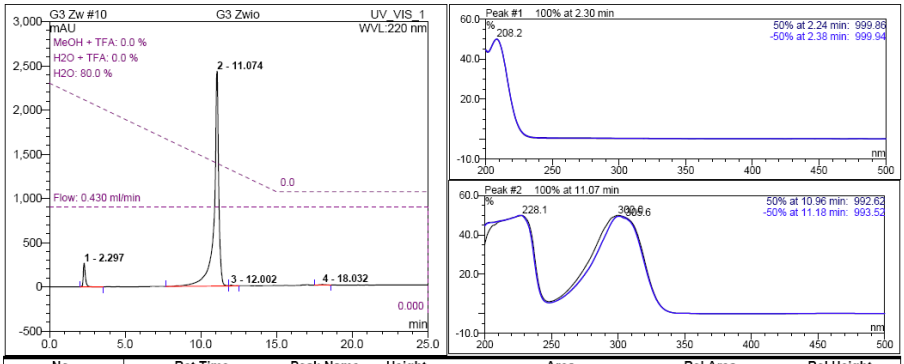

No.	Ret.Time min	Peak Name	Height mAU	Area mAU*min	Rel.Area %	Rel.Height %
1	2.30	n.a.	268.860	44.040	4.81	9.91
2	11.07	n.a.	2427.875	867.644	94.68	89.51
3	12.00	n.a.	7.621	1.694	0.18	0.28
4	18.03	n.a.	8.034	3.030	0.33	0.30
Total:			*2712.3892*	*916.41*	*100.00*	*100.00*

^{1}H-NMR (300 MHz, DMSO-d_6) δ = 2.23 (s, 3 H, methyl-CH_3), 2.25 – 2.31 (m, 2 H, CH_2), 2.94 – 2.99 (t, ^{3}J = 7.61 Hz, 2 H, CH_2), 3.26 – 3.58 (m, 70 H, CH/CH_2/OH), 3.91 – 3.93 (m, 4 H, CH), 4.28 – 4.30 (m, 2 H, CH), 4.40 – 4.47 (m, 8 H, CH_2), 4.51 – 4.52 (d, ^{3}J = 4.77 Hz, 2 H, CH_2), 4.57 – 4.59 (d, ^{3}J = 5.20 Hz, 6 H, CH_2), 4.81 – 4.85 (t, ^{3}J = 5.90 Hz, 1 H, CH), 7.92 (bs, 1 H, CH), 7.94 (bs, 2 H, NH), 8.17 – 8.21 (t, ^{3}J = 5.15 Hz, 1 H, NH), 10.12 (bs, 2 H, NH), 12.63, 14.61 (bs, 1 H, NH) ppm.

^{13}C-NMR (75.5 MHz, DMSO-d_6) δ = 9.22 (1 C, CH_3), 20.86 (1 C, CH_2), 37.50 (4 C, CH_2), 60.72 (1 C, CH), 63.06 (8 C, CH_2), 68.78, 69.41 (2 C, CH_2), 70.45 (10 C, CH), 70.63, 70.70 (4 C, CH_2), 72.82 (8 C, CH_2), 77.81 (4 C, CH), 118.61 (1 C, C_q), 122.41 (1 C, CH), 122.87, 129.24, 134.30, 144.20 (1 C, C_q), 156.49, 160.90, 166.51, 171.65 (1 C, CN/CO) ppm.

MS (MALDI) m/z = 1474.58 $[M+H]^+$, calculated for ($C_{59}H_{109}N_8O_{34}$) 1474.53 g·mol^{-1}

Synthesis of the triester precursor – step 1 (85)

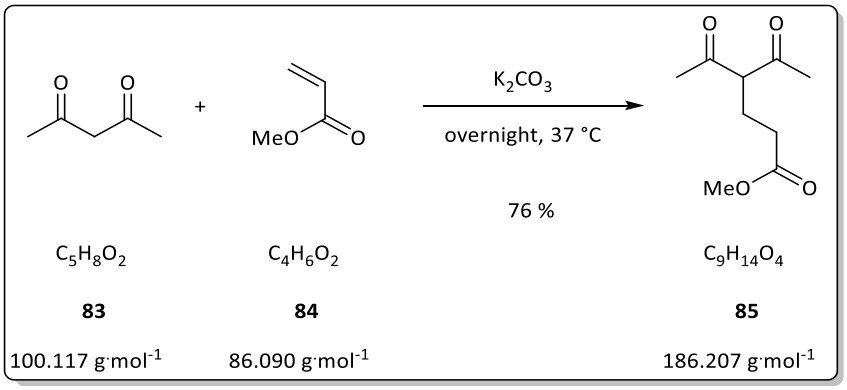

Methyl acrylate **84** (30.2 g, 31.6 mL, 351.0 mmol, 1.0 eq) and acetylacetone **83** (112.0 g, 115.0 mL, 1.1 mol, 3.2 eq) were mixed, potassium carbonate (48.3 g, 350.0 mmol, 1.0 eq) was added and this mixture was stirred at 37 °C overnight. Next morning, the precipitate was filtered off and washed with chloroform (3 x 100 mL). The chloroform was evaporated under reduced pressure from the filtrate and the slightly oily residue was purified *via* fractionated distillation under reduced pressure (0.1 mbar, 100 °C). The product **85** (49.6 g, 266.0 mmol) was obtained as yellow oil with a yield of 76 %.

^{1}H-NMR (300 MHz, $CDCl_3$) δ = 1.96 – 2.03 (m, 6 H, C*H*$_3$), 2.07 (s, 6 H, C*H*$_3$), 2.14 – 2.20 (m, 2 H, C*H*$_2$), 2.25 – 2.31 (m, 1 H, C*H*), 2.44 – 2.49 (m, 1 H, C*H*), 3.53 (s, 3 H, C*H*$_3$), 3.55 (s, 1 H, CH), 3.60 – 3.65 (t, ^3J = 5.61 Hz, 1H, C*H*) ppm.

Synthesis of the triester precursor – step 2 (87) – pyrrole synthesis

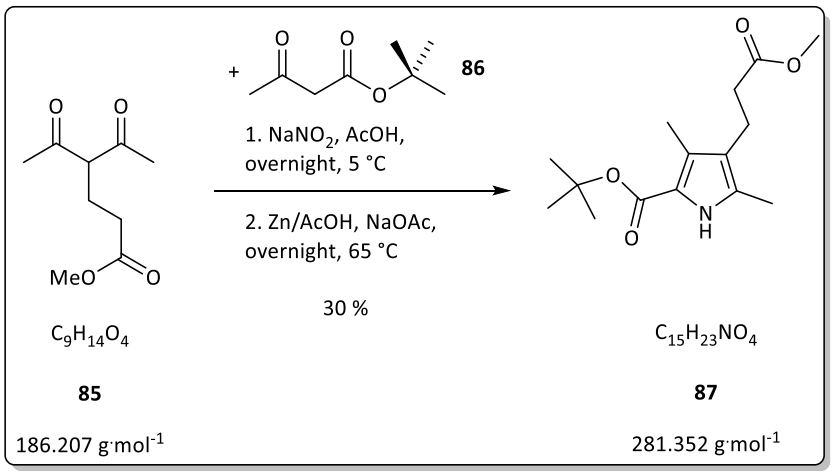

tert-Butyl acetoacetate (42.2 g, 44.2 mL, 267.0 mmol, 1.0 eq) was dissolved in glacial acetic acid (77 mL) and a solution of sodium nitrite (18.5 g, 267.0 mmol, 1.0 eq) in water (66 mL) was added dropwise over 2.5 hours, while the reaction mixture was kept at 5 °C. Subsequently the mixture was stirred at the same temperature for 5 hours and then the flask had to be stored in the fridge overnight. This solution was then added dropwise to a suspension of sodium acetate (54.18 g, 660.5 mmol, 2.48 eq), zinc (54.4 g, 764.4 mmol, 2.9 eq) and building block **85** (49.6 g, 266.0 mmol, 1.0 eq) in glacial acetic acid (60 mL). The temperature of the reaction mixture was kept between 60-80 °C using a salt/ice cooling bath. After the addition of this solution zinc power (54.1 g, 761.7 mmol, 2.9 eq) was added slowly to the reaction mixture and subsequently it was stirred overnight at 65 °C. The still warm solution was poured into ice water and the resulting precipitate was filtered off and washed with water to remove all salts. The solid was re-dissolved in ethanol to remove excess zinc by subsequent filtration. The filtrate was concentrated to 250 mL by evaporation of ethanol under reduced pressure. This highly concentrated solution was stored in the fridge overnight. The product precipitated from this solution and was filtered off and washed white with cold ethanol. The product **87** (22.5 g, 80.1 mmol) was obtained as a white solid substance with a yield of 30 %.

^{1}H-NMR (300 MHz, $CDCl_3$) δ = 1.55 (s, 9 H, *tert*-butyl ester-C*H*$_3$), 2.20 (s, 3 H, methyl-*CH*$_3$), 2.24 (s, 3 H, methyl-*CH*$_3$), 2.39 – 2.44 (t, ^3J = 7.41 Hz, 2 H, C*H*$_2$), 2.67 – 2.72 (t, ^3J = 7.42 Hz, 2 H, C*H*$_2$), 3.66 (s, 3 H, methyl ester-C*H*$_3$), 8.50 (bs, 1 H, pyrrole-N*H*) ppm.

Synthesis of the triester precursor – step 3 (88) – oxidation of methyl group to carboxylic acid

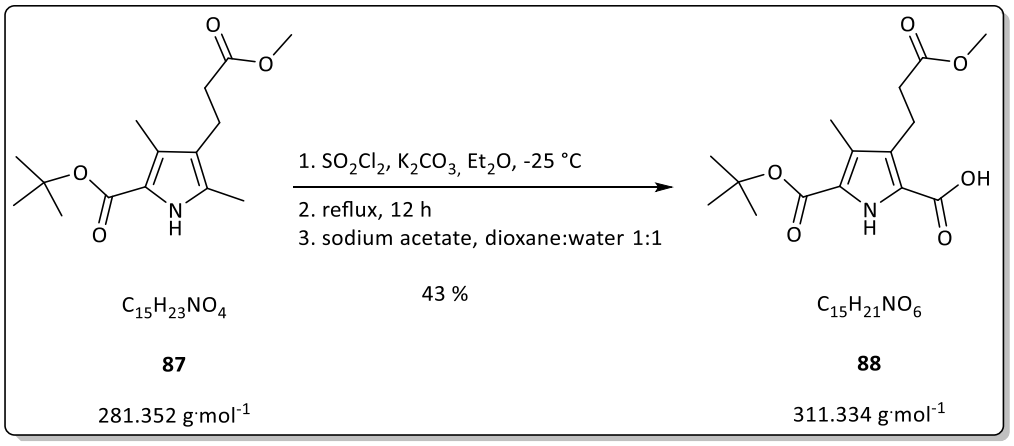

Pyrrole building block **87** (6.7 g, 23.8 mmol, 1.0 eq) and potassium carbonate (both substances need to be dried in a desiccator beforehand) were suspended in absolute diethyl ether (150 mL) under argon atmosphere. The mixture was cooled to -25 °C using an acetone/dry ice mixture and the flask was covered with tin foil to shade the flask from light. Sulfuryl chloride (10.9 g, 6.5 mL, 74.8 mmol, 3.15 eq) was added dropwise *via* a syringe over a time period of 60 minutes. The cooling bath was removed and the reaction mixture was allowed to slowly reach room temperature. Subsequently the reaction mixture was refluxed for 12 hours. The solvent was removed under reduced pressure and the resulting oily residue was hydrolyzed with a solution of sodium acetate in a mixture of water : 1,4-dioxane (400 mL, 1 : 1 ratio) and heated to 110 °C for 2 hours. Immediately after the mixture was cooled with an ice bath and the pH value was carefully set to a value of 2, the solution was extracted with diethyl ether (5 x 100 mL). The combined organic phases were then extracted with half-saturated sodium bicarbonate solution (8 x 100 mL). The aqueous fractions were separately cooled in an ice bath and the pH values were set to 1 under vigorous stirring using concentrated HCl. A white, slightly yellow substance precipitated from these solutions. These precipitates were filtered off and washed with cold water until the filtrates did not show acidic reaction against universal indicator pH paper anymore. The product **88** (3.2 g, 10.2 mmol) was obtained as a slightly yellow solid substance with a yield of 43 %.

^{1}H-NMR (300 MHz, DMSO-d_6) δ = 1.51 (s, 9 H, *tert*-butyl ester-C*H*$_3$), 2.15 (s, 3 H, methyl-*CH*$_3$), 2.38 – 2.45 (t, ^3J = 7.42 Hz, 2 H, C*H*$_2$), 2.86 – 2.92 (t, ^3J = 8.02 Hz, 2 H, C*H*$_2$), 3.56 (s, 3 H, methyl ester-*CH*$_3$), 11.28 (s, 1 H, COO*H*), 12.82 (bs, 1 H, N*H*) ppm.

Synthesis of the triester precursor – step 4 (90) – coupling with boc-guanidine

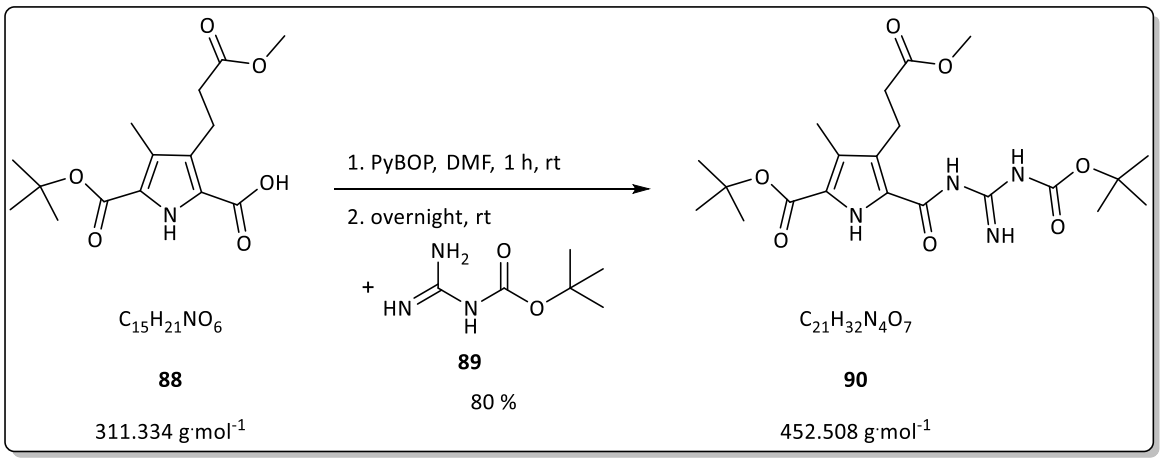

Pyrrole building block **88** (1.3 g, 4.2 mmol, 1.0 eq) was dissolved in DCM (30 mL) and DMF (8 mL). HCTU (2.1 g, 5.0 mmol, 1.2 eq) and DMAP (1.0 g, 8.3 mmol, 2.0 eq) were added. The mixture was stirred for 1 hour at room temperature. Subsequently Boc-guanidine (1.0 g, 6.3 mmol, 1.5 eq) was added and the reaction mixture was stirred overnight at room temperature. Afterwards DCM was evaporated under reduced pressure and the resulting oily residue was poured on ice water (80 mL). A light brown substance precipitated, which was then filtered off. The solid was re-dissolved in ethyl acetate and the solution was dried with $MgSO_4$. The crude product was purified *via* liquid chromatography (*n*-hexane : ethyl acetate - 4 : 1). The product **90** (3.7 g, 8.2 mmol) was obtained as a white solid substance with a yield of 80 %.

^{1}H-NMR (300 MHz, DMSO-d_6) δ = 1.47 (s, 9 H, boc-group-C*H*$_3$), 1.53 (s, 9 H, *tert*-butyl ester-C*H*$_3$), 2.16 (s, 3 H, methyl-*CH*$_3$), 2.44 – 2.48 (t, ^3J = 8.08 Hz, 2 H, C*H*$_2$), 2.93 – 2.98 (t, ^3J = 8.24 Hz, 2 H, C*H*$_2$), 3.56 (s, 3 H, methyl ester-*CH*$_3$), 8.50, 9.40, 10.14, 10.60 (bs, 1 H, N*H*) ppm.

Synthesis of the triester precursor – step 5 (91) – cleavage of the methyl ester

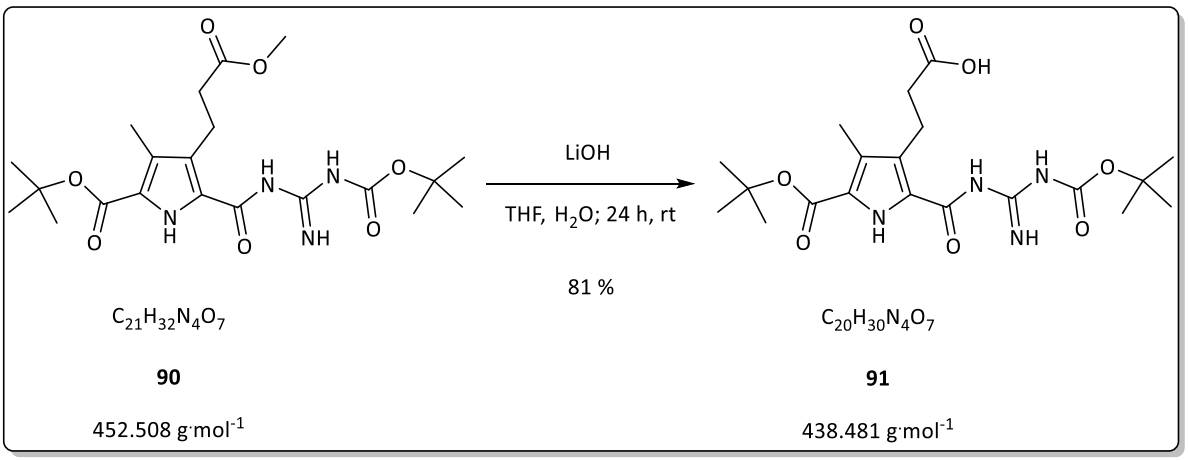

Building block **90** (1.4 g, 3.1 mmol, 1.0 eq) was dissolved in THF (48 mL). A solution of lithium hydroxide (149.0 mg, 6.2 mmol, 2.0 eq) in water (12 mL) was added and the mixture was stirred for 24 hours at room temperature. Subsequently THF was removed under reduced pressure and the resulting aqueous solution was diluted with water and neutralized with aqueous HCl (5 %). Part of the product precipitated and was filtered off. The aqueous phase was extracted with ethyl acetate (3 x 20 mL) to obtain the entire product from the aqueous phase. The combined organic phases were dried with $MgSO_4$ and ethyl ester was subsequently evaporated under reduced pressure. The product **91** (1.1 g, 2.5 mmol) was obtained as a white solid substance with a yield of 81 %.

^{1}H-NMR (300 MHz, $CDCl_3$) δ = 1.51 (s, 9 H, boc-group-C*H*$_3$), 1.56 (s, 9 H, *tert*-butyl ester-C*H*$_3$), 2.26 (s, 3 H, methyl-*CH*$_3$), 2.62 – 2.68 (t, ^3J = 8.01 Hz, 2 H, C*H*$_2$), 3.09 – 3.15 (t, ^3J = 8.12 Hz, 2 H, C*H*$_2$), 7.67, 8.59,8.65, 9.58 (bs, 1 H, N*H*), 9.81 (bs, 1 H, COO*H*) ppm.

Synthesis of the alkyne functionalized pyrrole building block 69

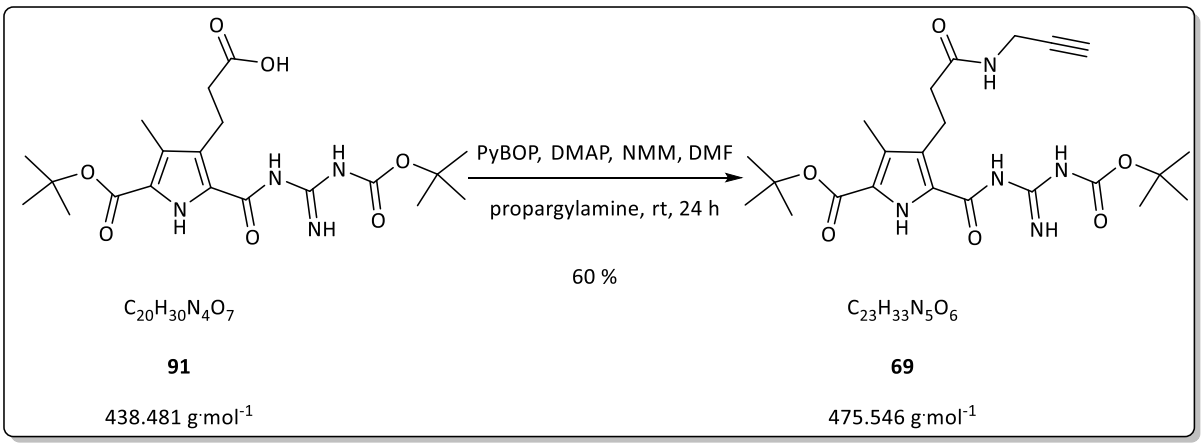

Triester building block **91** (1.1 g, 2.5 mmol, 1.0 eq) was dissolved under argon atmosphere in absolute DMF (5 mL). PyBOP (1.3 g, 2.7 mmol, 1.1 eq), DMAP (61.0 mg, 0.5 mmol, 0.2 eq), NMM (755.0 mg, 821.0 µL, 7.5 mmol, 3.0 eq) and propargylamine (151.0 mg, 175.0 µL, 2.7 mmol, 1.1 eq) were added to the solution and the reaction mixture was stirred for 24 hours at room temperature (TLC control). Subsequently the reaction mixture was poured on ice water; the precipitate was filtered off and dried. The crude product was purified *via* column chromatography (SiO_2, *n*-hexane : ethyl acetate - 7 : 3 + 1 % triethylamine). The product **69** (710.0 mg, 1.5 mmol) was obtained as a white solid substance with a yield of 60 %.

R_f-Value (*n*-hexane : acetate 7 : 3 + 1 % triethylamine) = 0.17

^{1}H-NMR (300 MHz, DMSO-d_6) δ = 1.47 (s, 9 H, CH_3), 1.52 (s, 9 H, CH_3), 2.15 (s, 3 H, methyl-CH_3), 2.23 – 2.28 (t, ^3J = 8.39 Hz, 2 H, CH_2), 2.90 – 2.95 (t, ^3J = 8.39 Hz, 2 H, CH_2), 3.05 – 3.06 (t, ^3J = 5.02 Hz, 1 H, C*H*), 3.80 – 3.83 (d-d, ^4J = 2.45 Hz and 2.93 Hz, 2 H, CH_2), 8.21 – 8.24 (t, ^3J = 5.61 Hz, 1 H, N*H*), 8.49, 9.39, 10.26, 10.68 (bs, 1 H, N*H*) ppm.

^{13}C-NMR (75.5 MHz, DMSO-d_6) δ = 9.81 (1 C, *C*H_3), 20.25 (4 C, *C*H_2), 27.71 (3 C, *C*H_3), 27.98 (3 C, *C*H_3), 35.94 (2 C, *C*H_2), 80.62 (1 C, C_q), 81.22 (1 C, C_q), 120.67, 124.51, 125.29, 128.51 (1 C, C_q), 157.88, 158.54, 160.18, 171.62 (1 C, *C*O/*C*N) ppm.

Synthesis of boc-guanidine 89

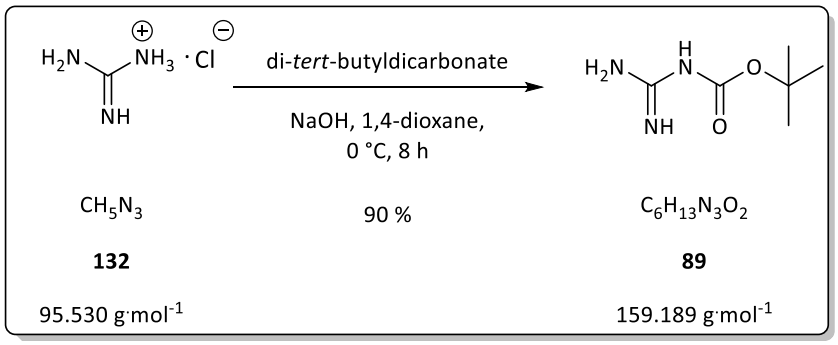

Guanidinium chloride **132** (26.5 g, 227.0 mmol, 4.1 eq) and NaOH (12.1 g, 303.0 mmol, 5.5 eq) were dissolved in water (50 mL). A solution of Di-*tert*-butyldicarbonate (12.0 g, 55.0 mmol, 1. eq) in 1,4-dioxane (100 mL) was added dropwise *via* a precision dropping funnel over time period of 8 hours. During this addition the reaction mixture was cooled to 0 °C using an ice bath. The resulting suspension was extracted with ethyl acetate (3 x 100 mL) and the combined organic fractions were subsequently dried with magnesium sulfate. After magnesium sulfate was filtered off, the solvent was evaporated under reduced pressure. The boc guanidine **89** (7.9 g, 49.5 mmol) was obtained s a white solid substance with a yield of 90 %.

^{1}H-NMR (300 MHz, DMSO-d_6) δ = 1.34 (s, 9 H, C*H*$_3$), 6.80 (bs, 3 H, N*H*), 7.46 (bs, 1 H, N*H*) ppm.

7.3.2 Trivalent zwitterionic core

Synthesis of 4-azidoacetophenone 112

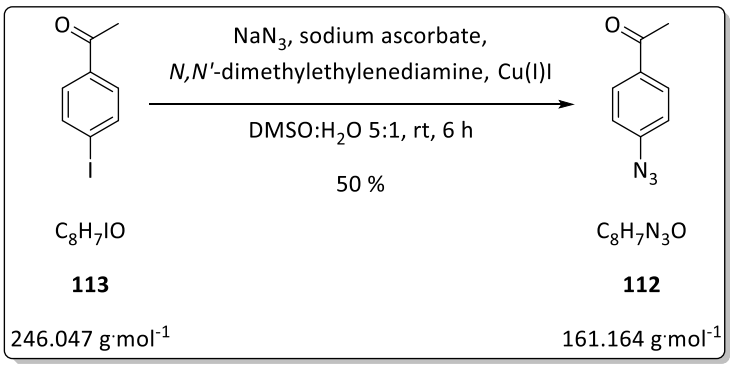

4-Iodoacetophenone **113** (2.0 g; 8.1 mmol; 1.0 eq), sodium azide (792.0 mg; 12.2 mmol; 1.5 eq.), sodium ascorbate (97.0 mg; 490.0 µmol; 0.06 eq) and copper iodide (155.0 mg; 812.0 mmol; 0.1 eq) were dissolved under argon atmosphere in a solvent mixture of THF and water (8 mL) in a 5 : 1 ratio. After the addition of *N,N'*-dimethyl ethylenediamine (142.0 µL; 1.3 mmol; 0.16 eq) the mixture was stirred for 6 hours at room temperature. After the reaction was completed the mixture was poured on ice water (20 mL), yielding a brownish green suspension. This suspension was extracted with ethyl acetate (3 x 50 ml) and the combined organic phases were dried with sodium sulfate. The solvent was removed in vacuum and the resulting crude product was purified *via* liquid chromatography (*n*-hexane : DCM – 1 : 1). The 4-azidoacetophenone **112** (660.0 mg, 4.1 mmol) was obtained as a brown solid substance with a yield of 50 %.

Mp. [°C] 40 – 44 °C

R_f-Value (*n*-hexane : dichloromethane; 1 : 1) = 0.10

^{1}H-NMR (300 MHz, $CDCl_3$) δ = 2.59 (s, 3 H, methyl-C*H*$_3$), 7.39 – 7.42 (m, 6 H, aromatic-C*H*), 7.07 – 7.10 (d, 2 H, aromatic-C*H*), 7.95 – 7.98 (d, 2 H, aromatic-C*H*), ppm.

^{13}C-NMR (75.5 MHz, $CDCl_3$) δ = 26.52 (1 C, *C*H$_3$), 119.04 (2 C, aromatic-*C*H), 130.34 (2 C, aromatic-*C*H), 133.93, 144.98 (C_q), 196.58 (*C*O) ppm

FT-IR ν [cm^{-1}] = 3112 (w), 2925 (w), 2091 (s), 1670 (s), 1505 (m), 828 (s).

Trimerization reaction of 4-azidoacetophenone to 1,3,5-tris-(4-azidophenyl)-benzene (73)

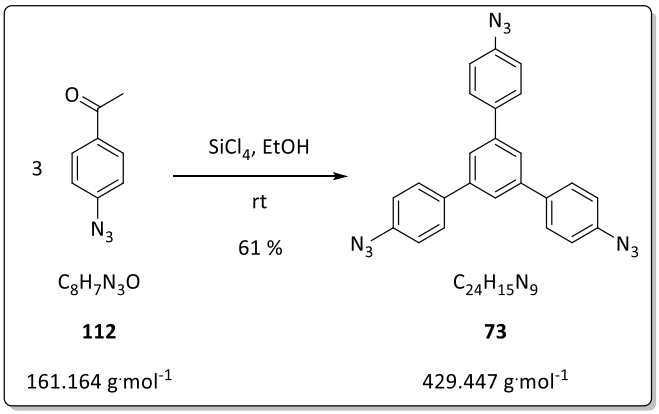

4-Azidoacetophenone **112** (230.0 mg; 1.4 mmol; 1.0 eq) was solved in dry ethanol (7 mL) under argon atmosphere. Silicon tetrachloride (0.5 mL; 4.3 mmol; 3.0 eq) was added slowly *via* a syringe. The reaction was stirred at room temperature and monitored with thin layer chromatography until no progress could be observed anymore, although the reaction was not complete. Thus, another 3 equivalents $SiCl_4$ (0.5 mL; 4.3 mmol; 3.0 eq) were added and the reaction was stirred for another two days. Finally another 1.5 equivalents $SiCl_4$ (250 µL; 2.2 mmol; 1.5 eq) were added and the mixture was stirred at room temperature for 12 hours. TLC control indicated a complete reaction. The reaction mixture was poured on ice water (200 mL) and a brownish substance precipitated. This suspension was extracted with toluene (3 x 70 ml) and the combined organic phases were washed with water (70 mL) and subsequently dried with $MgSO_4$. The drying agent was filtered off and the solvent was removed in vacuum. After a short filtration column (SiO_2, toluene : cyclohexane – 1 : 1) the 1,3,5-tris-(4-azidophenyl)-benzene **73** (125.0 mg, 290.0 µmol) could be obtained as a brown solid with a yield of 61 %.

Mp. [°C] 169 – 175 °C (decomposition)

R_f-Value (cyclohexane : toluene; 1 : 1) = 0.80

^{1}H-NMR (300 MHz, $CDCl_3$) δ = 7.13 – 7.16 (m, 6 H, aromatic-C*H*), 7.66 (m, 6 H, aromatic-C*H*), 7.68 – 7.69 (m, 3 H, aromatic-C*H*), ppm.

^{13}C-NMR (75.5 MHz, $CDCl_3$) δ = 119.69 (6 C, aromatic-*C*H), 124.78 (3 C, aromatic-*C*H), 128.80 (6 C, aromatic-*C*H) ppm.

FT-IR ν [cm^{-1}] = 2927 (w), 1500 (m), 813 (s).

Synthesis of the diazide pyrrole building block – step 1 (103) – Oxime

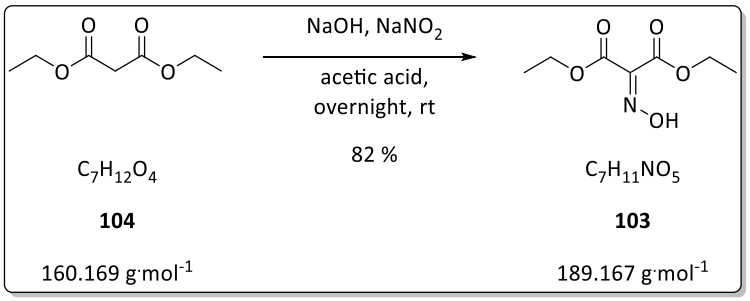

Sodium hydroxide (8.4 g; 206.0 mmol; 0.66 eq) was carefully dissolved in glacial acidic acid (68 mL), during this temperature reached 80 °C. After NaOH was dissolved completely and the temperature decreased to 40 °C, diethyl malonate (50.0 g; 312.0 mmol; 1.0 eq) was added. Subsequently a solution of sodium nitrite (45.8 g; 665.0 mmol; 2.13 eq) in water (63 mL) was added dropwise. After the reaction mixture was stirred overnight at room temperature, an ice cold aqueous solution of NaOH (20.8 g, 520.0 mmol, 1.7 eq, in 63 mL water) was added. The mixture was extracted with diethyl ether (3 x 250 mL). Water (250 mL) was added to the combined organic fractions and $NaHCO_3$ was added until it did not dissolve anymore. The organic phase was separated, washed with water (250 mL) and dried with $MgSO_4$. The solvent was evaporated under reduced pressure giving a colorless solid substance. The product **103** (48.6 g, 257.0 mmol) was obtained with a yield of 82 %.

^{1}H-NMR (300 MHz, $CDCl_3$) δ = 1.30 – 1.37 (m, 6 H, *CH_3*), 4.30 – 4.42 (m, 4 H, C*H_2*), 10.44 (bs, 1 H,O*H*) ppm.

This synthesis was performed according to literature protocol from the *Schmuck* group.[129] For additional data concerning the characterization of the respective molecule, which are not given in this experimental part, the cited literature can be consulted.

Synthesis of the diazide pyrrole building block – step 2 (102) – Synthesis of the pyrrole

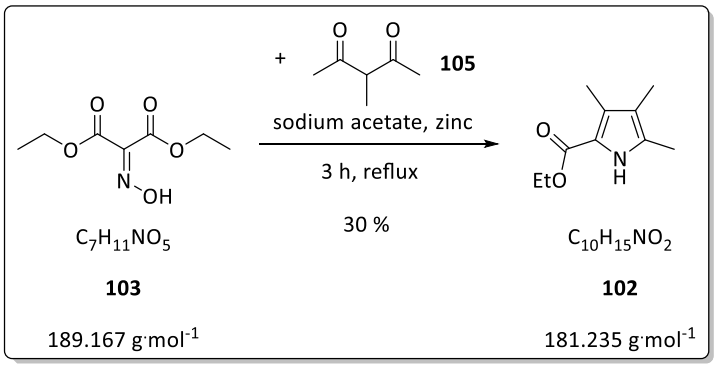

Sodium acetate (27.7 g, 338.0 mmol, 3.1 eq), diethyloximin malonate (23.0 g, 122.0 mmol, 1.1 eq) and 3-methylpentane-2,4dione (12.6 g, 110.0 mmol, 1.0 eq) were dissolved in glacial acetic acid (110 mL). The reaction mixture was heated to 90 °C and zinc dust was added slowly, whereas the temperature should not exceed 100 °C (ice bath if necessary). After the reaction mixture was refluxed foe 3 hours it was poured on ice water (100 mL). The resulting precipitate was filtered off and re-dissolved in hot ethanol and the excess zinc dust was filtered off. The ethanol solution was cooled in an ice bath, which led to the crystallization of the pyrrole building block **102**. The product **102** (6.0 g, 33.1 mmol) was obtained as a white solid substance with a yield of 30 %.

Mp. [°C] 128 °C

^{1}H-NMR (300 MHz, $CDCl_3$) δ = 1.33 – 1.37 (t, ^{3}J = 14.47 Hz, 3 H, ethyl ester-C*H*$_3$), 1.91 (s, 3 H, *C*H_3), 2.19 (s, 3 H, *CH*$_3$), 2.25 (s, 3 H, *CH*$_3$), 4.26 – 4.34 (q, ^{4}J = 21.25 Hz, 2 H, ethyl ester-*CH*$_2$), 8.93 (bs, 1 H, pyrrole-N*H*) ppm.

^{13}C-NMR (75.5 MHz, $CDCl_3$) δ = 8.83 (1 C, *C*H_3), 10.79 (1 C, *C*H_3), 11.49 (1 C, *C*H_3), 14.86 (1 C, *C*H_3), 59.72 (1 C, *C*H_2), 116.68, 117.17, 127.56, 129.84 (C_q), 162.11 (*C*O) ppm.

MS (ESI) m/z = 204.1 $[M + Na]^+$, calculated ($C_{10}H_{15}NNaO_2$) 204.11 g·mol^{-1}

This synthesis was performed according to literature protocol from the *Schmuck* group.[129] For additional data concerning the characterization of the respective molecule, which are not given in this experimental part, the cited literature can be consulted.

Synthesis of the diazide pyrrole building block – step 3 (101) – oxidation of methyl group to carboxylic acid

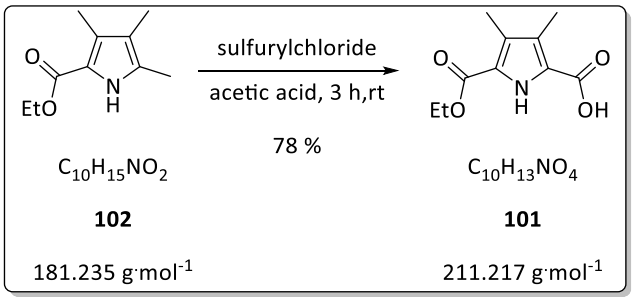

The pyrrole building block **102** (5.0 g, 27.6 mmol, 1.0 eq) was suspended in glacial acidic acid (30 mL) to give a yellow suspension. Sulfuryl chloride (11.2 g, 6.7 mL, 82.9 mmol, 3.0 eq) was mixed with glacial acidic acid. This mixture was added dropwise to the suspension over a time period of 2 hours, while the reaction mixture was kept at a temperature of 15 – 20 °C. The reaction mixture was stirred for 3 hours at room temperature, whereas the mixture turned into a red solution. This solution was treated with water (17 mL), which was added dropwise, while cooling the mixture with an ice bath. The crude product was precipitated by adding the reaction mixture on 30 mL ice water. The precipitate was filtered off and washed with cold water. The crude product was dissolved in ice cold aqueous sodium hydroxide solution (1.6 g NaOH in 260 mL water) and subsequently extracted with DCM (5 x 125 mL). The aqueous phase was acidified to pH 2 using concentrated aqueous HCl (37 %) resulting in a light brown precipitate. The precipitate was filtered off, washed with water and subsequently dried. The product **101** (4.5 g, 21.4 mmol) was obtained as a beige solid substance with a yield of 78 %.

^{1}H-NMR (300 MHz, DMSO-d_6) δ = 1.25 – 1.30 (t, ^3J = 7.16 Hz, 3 H, ethyl ester-C*H*$_3$), 2.17 (s, 3 H, *CH*$_3$), 2.18 (s, 3 H, *CH*$_3$), 4.19 – 4.26 (q, ^3J = 7.04 Hz, 2 H, ethyl ester-*CH*$_2$), 11.36 (bs, 1 H, pyrrole-N*H*) ppm.

This synthesis was performed according to literature protocol from the *Schmuck* group.[129] For additional data concerning the characterization of the respective molecule, which are not given in this experimental part, the cited literature can be consulted.

Synthesis of the diazide pyrrole building block – step 4 (100) – introduction of the *tert*-butyl ester

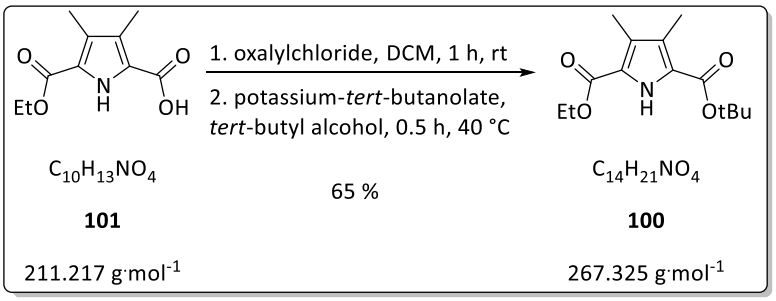

$C_{10}H_{13}NO_4$ — **101** — 211.217 g·mol^{-1}

65 %

$C_{14}H_{21}NO_4$ — **100** — 267.325 g·mol^{-1}

The pyrrole building block **101** (3.0 g, 14.2 mmol, 1.0 eq) was suspended in dry DCM (30 mL) and a few drops DMF were added. A solution of oxalyl chloride (5.6 g, 3.8 mL, 82.7 mmol, 5.8 eq) in DCM (7 mL) was added dropwise over a time range of 1 hour. The resulting red solution was stirred for 1 hour at room temperature. Subsequently the solvent was removed under reduced pressure and the residue was re-dissolved in *tert*-butanol (52 mL) and heated to 40 °C. Potassium *tert*-butanolate (2.8 g, 25.1 mmol, 1.8 eq) was added carefully in small portions to the solution and the mixture was subsequently stirred at 40 °C for approximately 30 minutes (TLC control). The solvent was removed under reduced pressure. The resulting brown residue was dissolved in DCM (70 mL) and was washed with aqueous sodium hydrogen sulfate solution (1 M, 35 mL), saturated sodium hydrogen carbonate solution (3 x 35 mL) and water (35 mL). The organic phase was dried with $MgSO_4$ and the solvent was removed under reduced pressure. The resulting crude product (brown oil) was purified *via* column chromatography (cyclohexane : ethyl acetate : triethylamine – 9 : 1 : 0.1). The product **100** (2.5 g, 9.2 mmol) was obtained as a colorless oil with a yield of 65 %.

R_f-Value (cyclohexane : ethyl acetate : triethylamine; 9:1:0.1) = 0.38

^{1}H-NMR (300 MHz, $CDCl_3$) δ = 1.34 – 1.39 (t, ^3J = 7.17 Hz, 3 H, ethyl ester-C*H*$_3$), 1.58 (s, 9 H, *tert*-butyl ester-C*H*$_3$), 2.23 (s, 2 H, *CH*$_2$), 2.25 (s, 2 H, *CH*$_2$), 4.30 – 4.37 (q, ^3J = 7.13 Hz, 2 H, ethyl ester-*CH*$_2$), 9.26 (bs, 1 H, pyrrole-N*H*) ppm.

This synthesis was performed according to literature protocol from the *Schmuck* group.[129] For additional data concerning the characterization of the respective molecule, which are not given in this experimental part, the cited literature can be consulted.

Synthesis of the diazide pyrrole building block – step 5 (106) – bromination

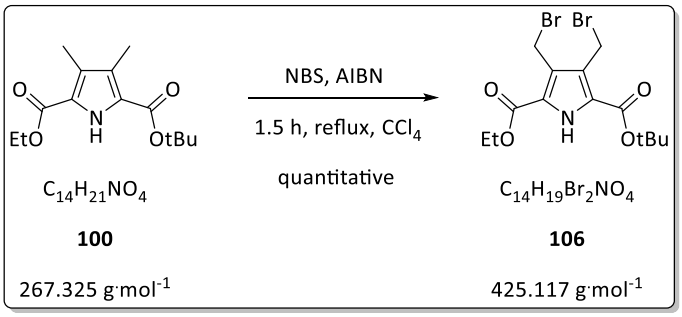

Pyrrole building block **100** (1.0 g, 3.7 mmol, 1.0 eq) was dissolved in carbon tetrachloride (30 mL). NBS (1.3 g, 7.5 mmol, 2.0 eq) and AIBN (amount of a spade point) were added and the mixture was refluxed for 1.5 hours until succinimide floated on top. The mixture was subsequently cooled to 0 °C and the succinimide was filtered off. The solvent was evaporated under reduced pressure. The product **106** (1.6 g, 3.7 mmol) was obtained as a yellow oil with quantitative yield.

^{1}H-NMR (300 MHz, $CDCl_3$) δ = 1.40 – 1.43 (t, ^{3}J = 6.98 Hz, 3 H, ethyl ester-CH_3), 1.62 (s, 9 H, *tert*-butyl ester-CH_3), 4.39 – 4.43 (q, ^{3}J = 7.13 Hz, 2 H, ethyl ester-CH_2), 4.81 (s, 2 H, CH_2), 4.84 (s, 2 H, CH_2), 9.62 (bs, 1 H, pyrrole-N*H*) ppm.

^{13}C-NMR (75.5 MHz, $CDCl_3$) δ = 14.41 (1 C, CH_3), 21.75 (1 C, CH_2), 21.88 (1 C, CH_2), 28.34 (3 C, CH_3), 61.68 (1 C, CH_2), 83.63, 121.71, 122.70, 123.79, 124.35 (C_q), 159.30, 159.90 (*C*O) ppm.

FT-IR ν [cm^{-1}] =3250 (m), 2975 (m), 1700 (s), 1668 (m), 1561 (m), 1473 (m), 1441 (m), 1391 (m), 1369 (m), 1298 (s), 1223 (m), 1124 (s), 1010 (m), 784 (m).

This synthesis was performed according to literature protocol from the *Schmuck* group.[129] For additional data concerning the characterization of the respective molecule, which are not given in this experimental part, the cited literature can be consulted.

Synthesis of the diazide pyrrole building block – step 6 (107) – substitution with sodium azide

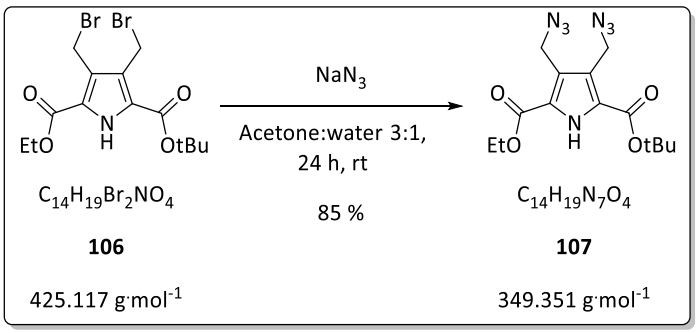

$C_{14}H_{19}Br_2NO_4$ — **106** — 425.117 g·mol^{-1}

$C_{14}H_{19}N_7O_4$ — **107** — 349.351 g·mol^{-1}

The dibromide **106** (500.0 mg, 1.2 mmol, 1.0 eq) was dissolved in a mixture of acetone and water (32 mL, 3 : 1 acetone : water ratio) and sodium azide (760.0 mg, 11.7 mmol, 10.0 eq) was added. The mixture was stirred for 24 hours. Subsequently acetone was removed under reduced pressure and the resulting aqueous solution was extracted with chloroform (3 x 10 mL). The combined organic phases were washed with brine (3 x 10 mL) and water (1 x 10 mL), and subsequently dried with $MgSO_4$. Chloroform was then removed under reduced pressure. The product **107** (350.0 mg, 1.0 mmol) was obtained as a yellow oil with a yield of 85 %.

^{1}H-NMR (300 MHz, $CDCl_3$) δ = 1.38 – 1.43 (t, ^3J = 7.20 Hz, 3 H, ethyl ester-C*H*$_3$), 1.61 (s, 9 H, *tert*-butyl ester-C*H*$_3$), 4.37 – 4.44 (q, ^3J = 7.20 Hz, 2 H, ethyl ester-*CH*$_2$), 4.52 (s, 2 H, *CH*$_2$), 4.56 (s, 2 H, *CH*$_2$), 9.77 (bs, 1 H, pyrrole-N*H*) ppm.

^{13}C-NMR (75.5 MHz, $CDCl_3$) δ = 14.39 (1 C, *C*H_3), 28.37 (3 C, *C*H_3), 43.59 (1 C, *C*H_2), 43.72 (1 C, *C*H_2), 61.68 (1 C, *C*H_2), 83.67, 123.01, 123.09, 124.08, 125.01 (C_q), 159.30, 160.00 (*C*O) ppm.

MS (ESI) m/z = 372.1 $[M + Na]^+$, calculated for ($C_{14}H_{19}N_7NaO_4$) 372.15 g·mol^{-1}

This synthesis was performed according to literature protocol from the *Schmuck* group.[129] For additional data concerning the characterization of the respective molecule, which are not given in this experimental part, the cited literature can be consulted.

Synthesis of alkyne functionalize pyrrole building block with short linker – step 1 (117) - pyrrole synthesis

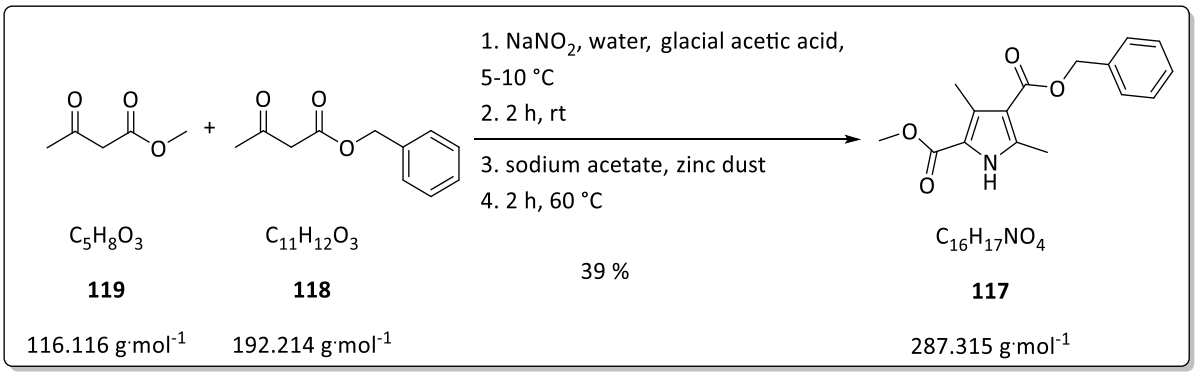

Methyl acetoacetate (20.0 g; 154.0 mmol; 1.0 eq) was dissolved in 60 mL glacial acetic acid and the mixture was cooled to 5-10 °C under rapid stirring. A solution of sodium nitrite (13.8 g 200.0 mmol; 1.3 eq) in water (40 mL) was added dropwise. The resulting yellow solution was stirred at 5 °C for 30 minutes. After the ice bath was removed the solution was stirred another 2 hours at room temperature, resulting in a color change to red. Sodium acetate (17.7 g; 215.0 mmol; 1.4 eq) and benzyl acetoacetate (29.5 g; 154.0 mmol; 1.0 eq) were added to the reaction mixture. Zinc dust (22.1 g; 338.0 mmol; 2.2 eq) was added carefully in small portions. During the addition of zinc dust the temperature of the mixture should not exceed70 °C. Subsequently the mixture was stirred at 60 °C for 2 hours, while strong foaming was observed. After cooling down to room temperature the mixture was poured on ice water (500 mL). The resulting precipitate was filtered and re-dissolved in DCM to be able to remove excess unreacted zinc powder by filtration. The solvent was removed in vacuum. The product **117** (12.2 g, 59.9 mmol) was obtained as a yellow solid substance with a yield of 39 %.

Mp. [°C] 170 – 172 °C

^{1}H-NMR (300 MHz, DMSO-d_6) δ = 2.50 (s, 3 H, methyl-C*H*$_3$), 2.56 (s, 3 H, methyl-C*H*$_3$), 3.85 (s, 3 H, methyl ester-*CH*$_3$), 5.29 (s, 2 H, *CH*$_2$), 7.31 – 7.44 (m, 5 H, aromatic-C*H*), 8.99 (bs, 1 H, pyrrole-N*H*) ppm.

^{13}C-NMR (75.5 MHz, DMSO-d_6) δ = 12.23 (1 C, *C*H$_3$), 14.64 (1 C, *C*H$_3$), 51.48 (1 C, *C*H$_3$), 65.63 (1 C, *C*H$_2$), 117.97 (*C*$_q$), 128.12 – 128.66 (6 C, aromatic-*C*H), 131.36, 136.71, 139.60 (*C*$_q$), 157.22, 162.17, 165.25 (*C*O) ppm.

MS (ESI) m/z = 310.1 $[M + Na]^+$, calculated ($C_{16}H_{17}NNaO_4$) 310.12 $g \cdot mol^{-1}$

FT-IR v [cm^{-1}] = 3268 (m), 1671 (s).

Synthesis of alkyne functionalized pyrrole building block with short linker – step 2 (116) – oxidation of methyl group to carboxylic acid

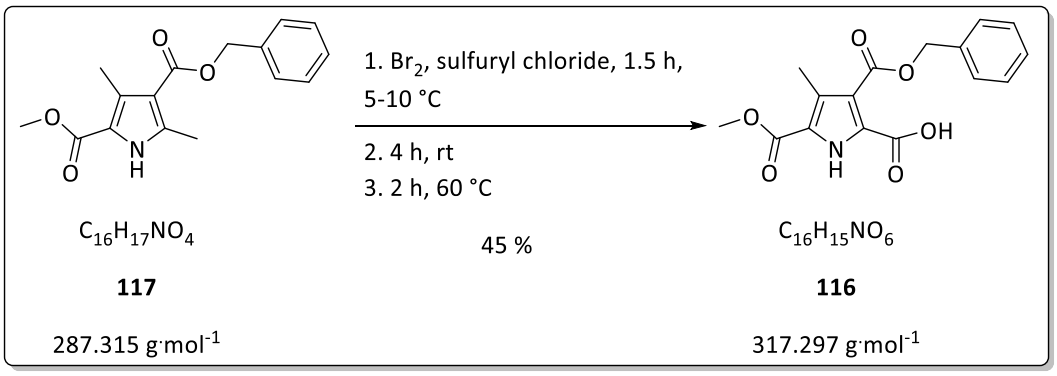

Pyrrole building block **117** (5.0 g; 17.4 mmol; 1.0 eq) was suspended in glacial acidic acid (50 mL), the temperature was set to 10 °C (ice bath) and bromine was added (870.0 µL; 17.1 mmol; 0.98 eq). Subsequently a solution of sulfuryl chloride (7.5 g, 4.5 mL; 55.7 mmol; 3.2 eq) in glacial acidic acid (3 mL) was added dropwise over a time range of 90 minutes, whereas the temperature should not exceed 15 °C (ice bath). After the resulting red solution was stirred for 4 hours at room temperature, water (15 mL) was added dropwise and the mixture was subsequently heated to 60 °C for 1 hour. The reaction mixture was then poured on ice water (200 mL) and the resulting yellow precipitate was filtered off, washed with water (2 x 100 ML) and cold diethyl ether (-20 °C, 150 mL). The product **116** (2.5 g, 7.8 mmol) was obtained as a white solid substance with a yield of 45 %.

Mp. [°C] 181 – 183 °C

R_f-Value (dichloromethane : methanol; 9.5:0.5) = 0.67

^{1}H-NMR (300 MHz, $CDCl_3$) δ = 2.58 (s, 3 H, methyl-C*H*$_3$), 3.91 (s, 3 H, methyl ester-C*H*$_3$), 5.46 (s, 2 H, *CH*$_2$), 7.38 – 7.46 (m, 5 H, aromatic-C*H*), 10.22 (bs, 1 H, pyrrole-N*H*) ppm.

^{13}C-NMR (75.5 MHz, $CDCl_3$) δ = 12.52 (1 C, *C*H_3), 52.21 (1 C, *C*H_3), 68.87 (1 C, *C*H_2), 115.62, 122.38 (*C*$_q$), 128.59 – 129.30 (6 C, aromatic *C*H), 131.59, 135.89 (*C*$_q$), 159.44, 160.34, 169.21 (*C*O) ppm.

MS (ESI) m/z = 340.08 $[M + Na]^+$, calculated ($C_{16}H_{15}NNaO_6$) 340.08 g·mol^{-1}

FT-IR ν [cm^{-1}] = 3256 (m), 2959 (w), 1708 (s).

Synthesis of alkyne functionalized pyrrole building block with short linker – step 3 (125) – introduction of *tert*-butyl ester

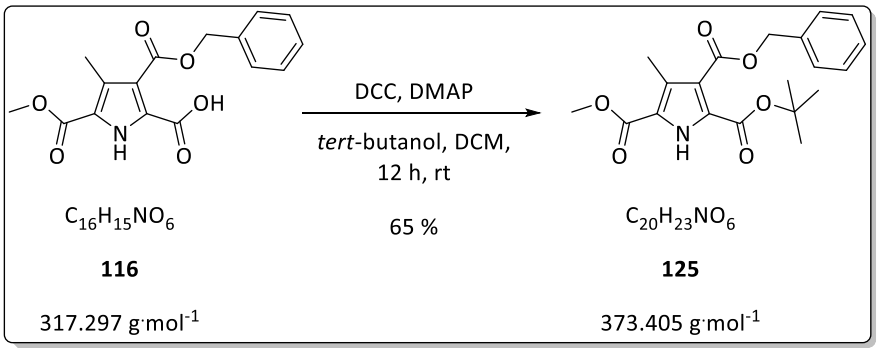

Pyrrole building block **116** (1.3 g; 3.9 mmol; 1.0 eq) was suspended in DCM (15 mL) and *tert*-butanol (30 mL), DCC (890.0 mg; 4.3 mmol; 1.1 eq) and DMAP (catalytic amount) were added. After the reaction mixture was stirred for 12 hours at room temperature, DCM (20 mL) was added and the mixture was extracted with water (3 x 50 mL) to remove the formed urea. The organic fraction was dried with magnesium sulfate and the solvent was evaporated under reduced pressure. The crude product was purified *via* liquid chromatography (SiO_2, ethyl acetate : cyclohexane 1 : 3 with 1 % triethylamine). The product **125** (950.0 mg, 2.5 mmol) was obtained as a white solid substance with a yield of 65 %.

Mp. [°C] 94 – 98 °C

R_f-Value (ethyl acetate : cyclohexane 1 : 3 with 1 % triethylamine) = 0.54

^{1}H-NMR (300 MHz, $CDCl_3$) δ = 1.50 (s, 9 H, *tert*-butyl ester-C*H*$_3$), 2.39 (s, 3 H, methyl-*CH*$_3$), 3.88 (s, 3 H, methyl ester-C*H*$_3$), 5.33 (s, 2 H, *CH*$_2$), 7.31 – 7.44 (m, 5 H, aromatic-C*H*), 9.56 (bs, 1 H, pyrrole-N*H*) ppm.

^{13}C-NMR (75.5 MHz, $CDCl_3$) δ = 11.05 (1 C, *C*H$_3$), 28.17 (3 C, *C*H$_3$), 51.96 (1 C, *C*H$_3$), 67.00 (1 C, *C*H$_2$), 83.04, 121.10, 121.23, 125.44 (*C*$_q$), 128.31 – 128.65 (6 C, aromatic-*C*H), 135.89 (*C*$_q$), 158.69, 161.08, 164.78 (*C*O) ppm.

MS (ESI) m/z = 396.14 $[M + Na]^+$, calculated ($C_{20}H_{23}NNaO_6$) 396.14 g·mol^{-1}

FT-IR ν [cm^{-1}] = 3234 (m), 2931 (w), 1706 (s).

Synthesis of alkyne functionalized pyrrole building block with short linker – step 4 (124) – cleavage of the benzyl ester

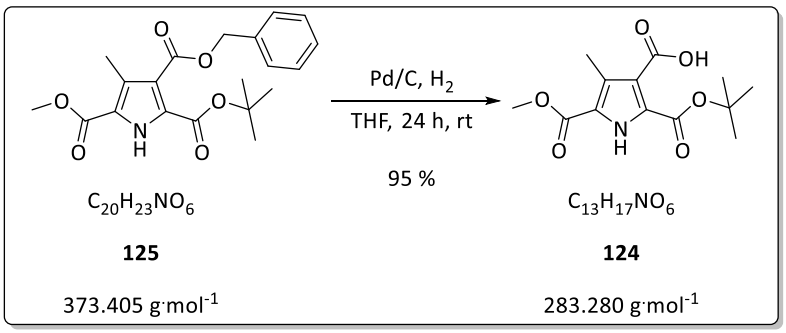

The pyrrole building block **125** (1.3 g; 3.5 mmol; 1.0 eq) was dissolved in THF (25 mL) under argon atmosphere. Subsequently palladium on charcoal (166.0 mg; 155.0 µmol; 0.045 eq) was added and the argon atmosphere was substituted by hydrogen atmosphere. The mixture was stirred for 24 hours and the Pd/C was filtered off using a nylon filter. After removing the solvent under reduced pressure, the product was obtained as a white solid substance **124** (946.0 mg, 3.3 mmol) with a yield of 95 %.

Mp. [°C] 117 °C

R_f-Wert (cyclohexane : ethyl acetate : triethylamine; 3 : 1 : 0.1) = 0.00

^{1}H-NMR (300 MHz, $CDCl_3$) δ = 1.64 (s, 9 H, *tert*-butyl ester-C*H*$_3$), 2.65 (s, 3 H, methyl-*CH*$_3$), 3.93 (s, 3 H, methyl ester-C*H*$_3$), 9.53 (bs, 1 H, pyrrole-N*H*) ppm.

^{13}C-NMR (75.5 MHz, $CDCl_3$) δ = 12.06 (1 C, *C*H_3), 28.27 (3 C, *C*H_3), 52.41 (1 C, *C*H_3), 87.48, 121.50, 122.71, 123.70, 134.14 (*C*$_q$), 161.12, 162.34, 162.71 (*C*O) ppm.

MS (ESI) m/z = 282.1 $[M-H]^-$, calculated for ($C_{13}H_{16}NO_6$) 282.106 g·mol^{-1}

FT-IR ν [cm^{-1}] = 3555 (m), 3447 (m), 3074 (w), 2962 (m), 2910 (w), 2571 (w), 2391 (m), 2285 (m), 1726 (s), 1620 (s), 1494 (m), 1424 (s), 1248 (s), 1150 (s), 1072 (s), 1016 (s), 833 (s), 798 (s).

Synthesis of alkyne functionalized pyrrole building block with short linker – step 5 (123) – coupling with propargylamine

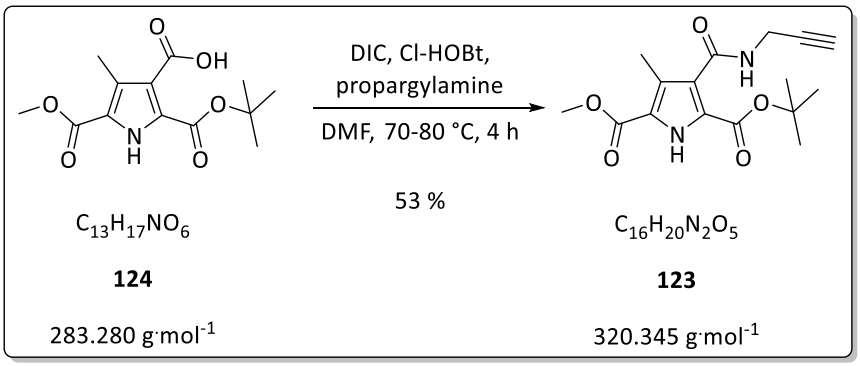

The pyrrole building block **124** (300.0 mg; 1.1 mmol; 1.0 eq) was dissolved in DMF (5 mL). Subsequently Cl-HOBt (360.0 mg, 2.1 mmol, 2.0 eq), DIC (268.0 mg, 2.1 mmol, 2.0 eq) and propargylamine (64.0 mg, 56.0 µL, 1.2 mmol, 1.1 eq) were added and the mixture was heated to 70 °C for 2 hours and then to 80 °C for another 2 hours. Afterwards the mixture was stirred overnight at room temperature. Then, the reaction mixture was poured on ice water and the resulting precipitate was filtered off and was washed with water. The resulting substance is lightly beige or white solid substance and did not require further purification. [In a second reaction attempt the precipitate showed a brownish color and required purification *via* liquid chromatography (SiO_2, cyclohexane : ethyl acetate 3 : 1 + 1 % triethylamine).] The product **123** (178.0 mg, 560.0 µmol) could be synthesized with a yield of 53 %.

Mp. [°C] 149 °C

R_f-Wert (cyclohexane : ethyl acetate : ; 3:1) = 0.15

^{1}H-NMR (300 MHz, $CDCl_3$) δ = 1.60 (s, 9 H, *tert*-butyl ester-C*H*$_3$), 2.22 – 2.24 (t, ^4J = 2.48 Hz, 1 H, C*H*), 2.57 (s, 3 H, methyl-*CH*$_3$), 3.90 (s, 3 H, methyl ester-C*H*$_3$), 4.17 -4.20 (d-d, ^4J = 2.50 Hz and 2.50 Hz, 2 H, *CH*$_2$), 8.83 (bs, 1 H, N*H*), 9.57 (bs, 1 H, pyrrole-N*H*) ppm.

^{13}C-NMR (75.5 MHz, $CDCl_3$) δ = 11.93 (1 C, *C*H$_3$), 28.31 (3 C, *C*H$_3$), 29.21 (1 C, *C*H$_3$), 52.10 (1 C, *C*H$_2$), 71.22(1 C, *C*H), 80.07, 84.52, 121.69, 123.07, 123.50, 131.60 (C_q), 160.01, 161.28, 163.73 (*C*O) ppm.

MS (ESI) m/z = 343.13 $[M + Na]^+$, calculated for ($C_{16}H_{20}N_2NaO_5$) 343.13 g·mol^{-1}

FT-IR ν [cm^{-1}] = 3495 (m), 3265 (m), 3211 (m), 3078 (w), 2954 (w), 2360 (m), 1714 (s), 1683 (s), 1617 (m), 1451 (m), 1254 (s), 1239 (s), 1136 (s), 1070 (m), 845 (m), 777 (m).

Synthesis of alkyne functionalized pyrrole building block with short linker – step 6 (122) – cleavage of the *tert*-butyl ester

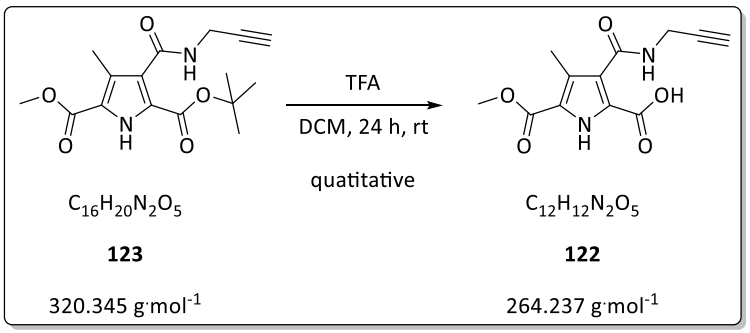

The pyrrole building block **123** (800.0 mg; 2.5 mmol; 1.0 eq) was dissolved in DCM (50 mL) and was treated with TFA (5.7 g; 37.0 mL, 50.0 mmol, 20.0 eq). The mixture was stirred for 24 hours at room temperature. After TLC (cyclohexane : ethyl acetate 3 : 1 + 1 % TFA) indicated complete reaction, solvent and acid were removed under reduced pressure and the product **122** (660.0 mg, 2.5 mmol) was obtained with a quantitative yield as a light brown solid substance.

Mp. [°C] 177 °C

R_f-Wert (cyclohexane : ethyl acetate : triethylamine; 3 : 1 : 0.1) = 0.08

^{1}H-NMR (300 MHz, DMSO-d_6) δ = 2.26 (s, 3 H, methyl-*CH*$_3$), 3.09 – 3.11 (t, ^4J = 2.60 Hz, 1 H, C*H*), 2.57, 3.78 (s, 3 H, methyl ester-C*H*$_3$), 3.97 -4.00 (d-d, ^4J = 2.42 Hz and 2.89 Hz, 2 H, *CH*$_2$), 8.73 – 8.76 (t, ^3J = 5.66 Hz, 1 H, N*H*), 12.14 (bs, 1 H, pyrrole-N*H*) ppm.

^{13}C-NMR (75.5 MHz, DMSO-d_6) δ = 10.70 (1 C, *C*H$_3$), 28.26 (1 C, *C*H$_3$), 51.36 (1 C, *C*H$_2$), 72.87 (1 C, *C*H), 80.87, 121.30, 123.71, 124.75, 126.31 (*C*$_q$), 160.57, 160.87, 164.20 (*C*O) ppm.

MS (ESI) m/z = 263.0 [M H]$^-$, calculated for ($C_{12}H_{11}N_2O_5$) 263.07 g·mol^{-1}

FT-IR ν [cm^{-1}] = 3566 (m), 3453 (m), 2955 (m), 2401 (s), 2389 (s), 1725 (s), 1613 (s), 1493 (s), 1421 (s), 1243 (s), 1141 (s), 1065 (s), 1010 (s), 812 (s).

Synthesis of alkyne functionalized pyrrole building block with short linker – step 7 (72) – coupling with boc-guanidine

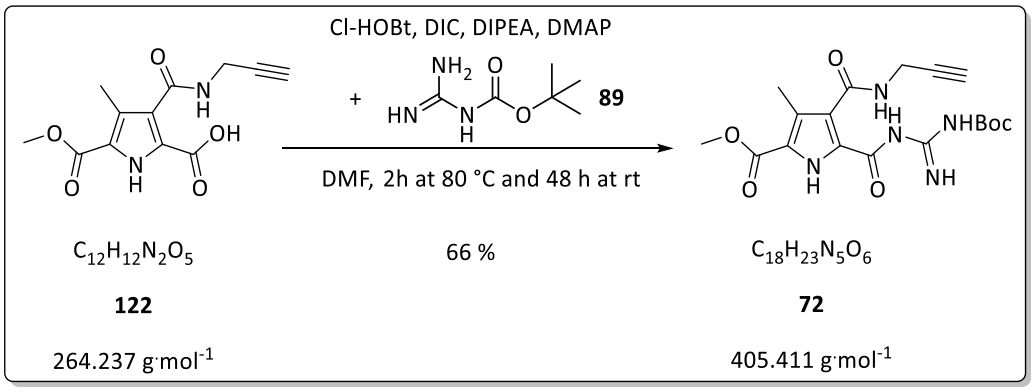

The pyrrole building block **122** (200.0 mg; 750.0 µmol; 1.0 eq) was dissolved in dry DMF (4 mL). Subsequently Cl-HOBt (254.0 mg, 1.5 mmol, 2.0 eq), DIC (189.0 mg, 234.0 µL, 1.5 mmol, 20 eq) and boc-guanidine **89** (361.0 mg, 2.3 mmol, 3.0 eq) were added and the reaction mixture was heated to 80 °C. After two hours at 80 °C the reaction mixture was cooled down to room temperature and stirred another 48 hours. After TLC (RP18, MeOH : H_2O 7 : 3) indicated complete reaction the mixture was poured on ice water and the resulting precipitate was filtered off and dried. The crude product was purified *via* reversed phase liquid chromatography (MPLC, RP18, 120 g column, flow 30 mL·min^{-1}, MeOH : $H_2$0 – 70 : 30 to 80 : 20 in 45 min, retention time 29 min). The product **72** (200.0 mg, 0.5 mmol) was obtained as a beige solid substance with a yield of 66 %.

Mp. [°C] 171 °C

R_f-Value (RP18; methanol : water; 7:3) = 0.55

^{1}H-NMR (300 MHz, $CDCl_3$) δ = 1.54 (s, 9 H, boc-group-C*H*$_3$), 2.29 – 2.31 (t, ^4J = 2.49 Hz, 1 H, C*H*), 2.64 (s, 3 H, methyl-*CH*$_3$), 3.89 (s, 3 H, methyl ester-C*H*$_3$), 4.21 -4.23 (d-d, ^4J = 2.73 Hz and 2.10 Hz, 2 H, *CH*$_2$), 8.54, 8.83, 9.34, 10.23, 10.80 (bs, 1 H, N*H*) ppm.

^{13}C-NMR (75.5 MHz, $CDCl_3$) δ = 12.15 (1 C, *C*H$_3$), 28.09 (3 C, *C*H$_3$), 29.23 (1 C, *C*H$_3$), 51.36 (1 C, *C*H$_2$), 71.64 (1 C, *C*H), 85.28, 107.51, 111.60, 122.00, 126.08 (*C*$_q$), 152.49, 161.24, 164.32 (*C*O) ppm.

MS (ESI) m/z = 406.18 $[M + H]^+$, calculated ($C_{18}H_{24}N_5O_6$) 406.41 g·mol^{-1}

FT-IR ν [cm^{-1}] = 3355 (m), 2945 (w), 1712 (s), 1625 (s).

Synthesis of the protected guanidiniopyrrole functionalized 1,2,5-trisphenylbenzene (92) – click reaction

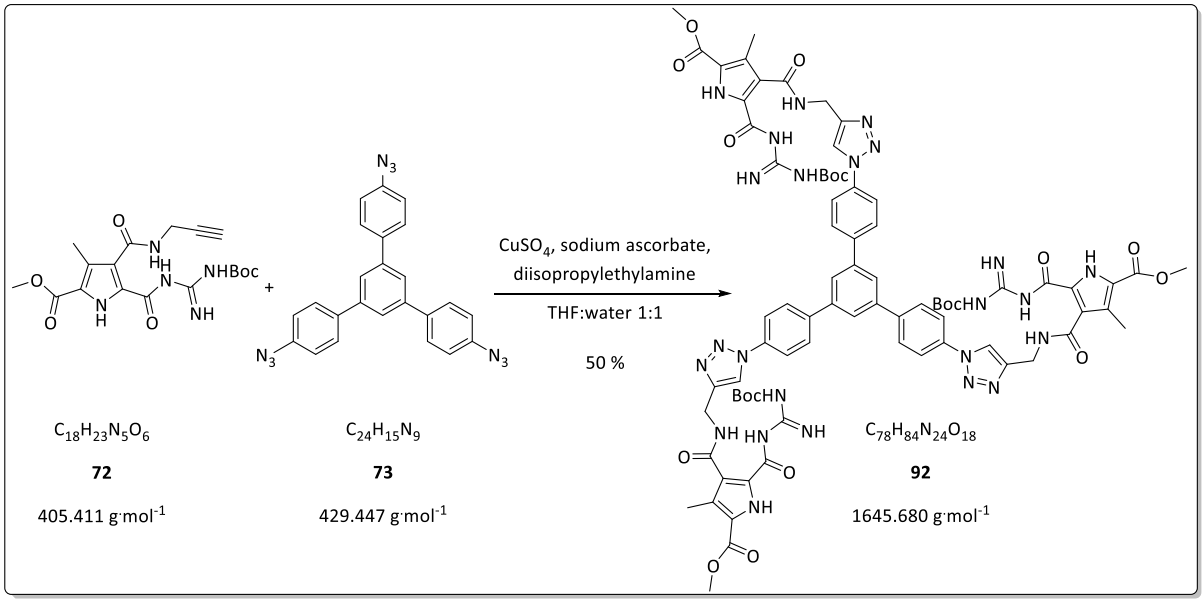

The alkyne functionalized pyrrole building block **72** (180.0 mg, 450.0 µmol, 3.1 eq) and the azide functionalized 1,3,5-trisphenylbenzene **73** (62.3 mg, 145.0 mmol, 1.0 eq) were dissolved in THF (5.2 mL). DIPEA (11.3 mg, 15.3 µL, 87.0 mmol, 0.6 eq), sodium ascorbate (17.2 mg, 87.0 mmol, 0.6 eq; dissolved in 1.0 mL water before the addition) and copper sulfate pentahydrate (10.9 mg, 43.5 µmol, 0.3 eq; dissolved in 1.0 mL water before the addition) were added to the solution and the water : THF ratio was set to 1 : 1. The resulting dark green mixture was stirred at room temperature and monitored by TLC (RP18, 1,4-dioxane : water 7 : 3) and HPLC (RP18, 1,4-dioxane : water 7 : 3 to 100 % 1,4-dioxane in 10 min). The reaction was monitored over 7 days and no further conversion was observed. Sodium ascorbate (17.2 mg, 87.0 µmol, 0.6 eq; dissolved in 1.0 mL water before the addition) and $CuSO_4$ (10.9 mg, 43.5 µmol, 0.3 eq; dissolved in 1.0 mL water before the addition) were again added another three times over a time span of ten days, while the reaction was continuously monitored. After 20 days in total, the reaction mixture was filled up with water and subsequently mixed with DCM intending to extract the product from the mixture. Instead, the product **92** precipitated and was filtered off and washed with DCM. The solubility of the obtained product was tested with a variety of solvents, which is shown in the following table.

DCM	x	Chloroform	x	MTBE	x	Acetonitile	x
Methanol	x	1,4-Dioxane	x	Isopropanol	x	THF	x
Toluene	x	Ethyl acetate	x	DMF	yes	DMSO	yes

The product **92** (119.0 mg, 72.0 µmol) was obtained with a yield of 50 % as a brown solid substance.

Mp. [°C] decomposition 320 °C

R_f-Value (RP18; 1,4-dioxane : water ; 7:3) = 0.68

^{1}H-NMR (500 MHz, DMSO-d_6) δ = 1.47 (s, 27 H, boc-C*H*$_3$), 2.54 (s, 9 H, methyl-*CH*$_3$), 3.84 (s, 9 H, methyl ester-C*H*$_3$), 4.61 -4.62 (d,^3J = 4.15 Hz, 6 H, *CH*$_2$), 7.99 – 8.19 (m, 15 H, aromatic-C*H*), 8.76 (bs, 3 H, N*H*), 8.83 (s, 3 H, C*H*), 9.41 (bs, 3 H, N*H*), 10.28 (bs, 3 H, N*H*), 10.65 (bs, 3 H, N*H*), 10.86 (bs, 3 H, N*H*) ppm.

Synthesis of the cationic form (126) – Boc deprotection

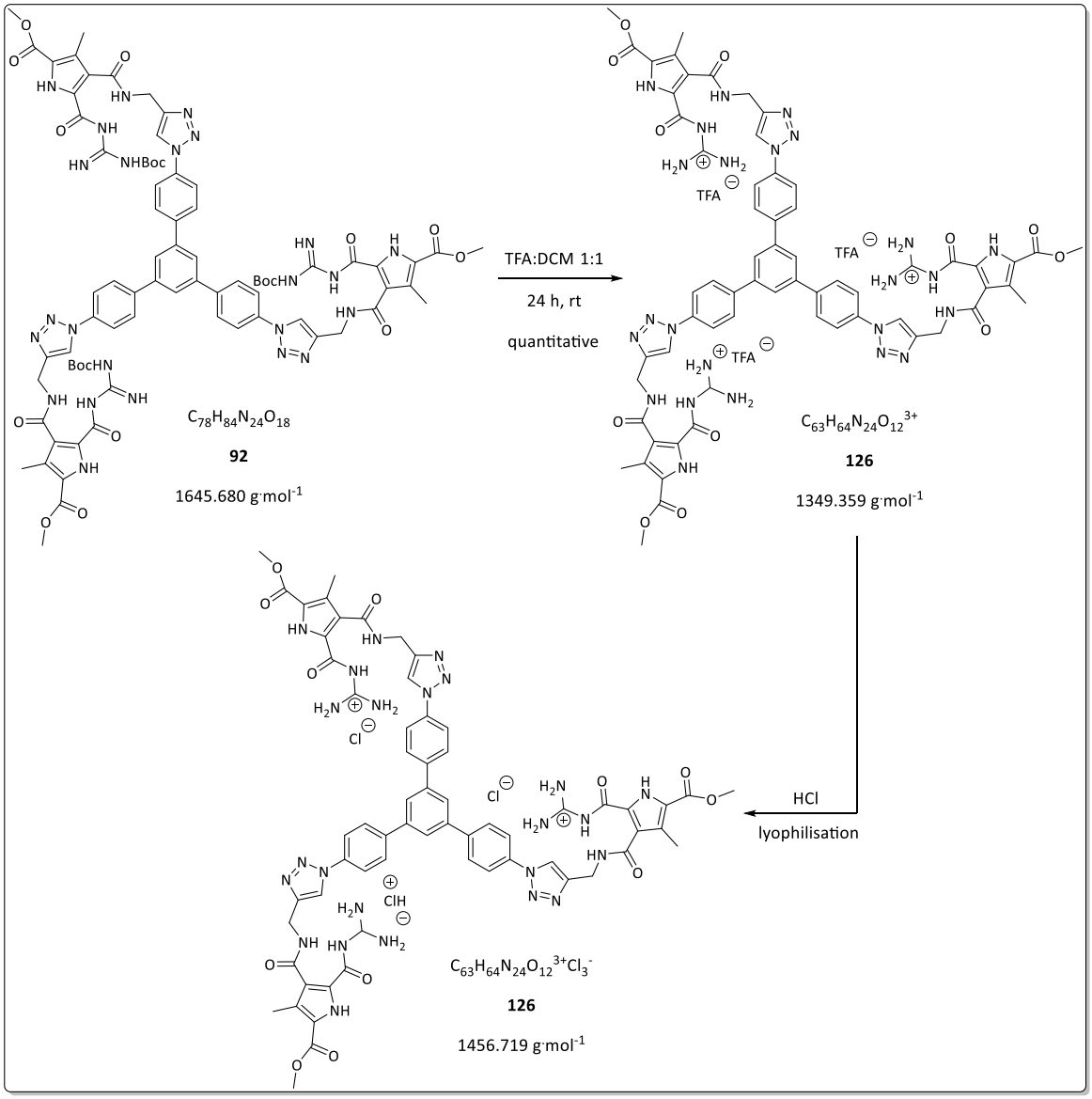

Building block **92** (60.0 mg, 36.5 µmol, 1.0 eq) was dissolved in TFA (5.9 g, 4.0 mL, 51.9 mmol). The mixture was diluted with DCM (8 mL) and stirred at room temperature for 24 hours (TLC control). TFA and DCM were removed under reduced pressure and the resulting brown residue was re-dissolved in aqueous HCl (5 %) and subsequently freeze dried. This procedure was repeated once more. The chloride salt of the product **126** (53.0 mg, 36.5 µmol) was obtained as a brown solid substance with quantitative yield.

Mp. [°C] decomposition 289 °C

R_f-Value (RP18; 1,4-dioxane : water ; 8:2) = 0.87

^{1}H-NMR (300 MHz, DMSO-d_6) δ = 2.37 (s, 9 H, methyl-*C*H_3), 3.84 (s, 9 H, methyl ester-C*H*$_3$), 4.63 -4.65 (d, ^{3}J = 5.12 Hz, 6 H, *C*H_2), 8.03 – 8.22 (m, 15 H, aromatic-C*H*), 8.49 (bs, 12 H, N*H*$_2$), 8.81 (s, 3 H, C*H*), 9.97 (bs, 3 H, N*H*), 12.32 (bs, 3 H, N*H*), 12.67 (bs, 3 H, N*H*) ppm.

^{13}C-NMR (75.5 MHz, DMSO-d_6) δ = 10.97 (3 C, methyl-*C*H_3), 35.08 (3 C, *C*H_2), 51.86 (3 C, methyl ester-*C*H_3), 120.31 (6 C, aromatic-*C*H), 121.32 (3 C, aromatic-*C*H), 122.58 (3 C, aromatic-*C*$_q$), 124.90 (3 C, *C*H), 125.41 (3 C, *C*$_q$), 125.47 (3 C, *C*$_q$), 126.48 (3 C, aromatic-Cq), 128.83 (6 C, aromatic-*C*H), 136.23 (3 C, *C*$_q$), 139.88 (3 C, *C*$_q$), 140.55 (3 C, *C*$_q$), 145.77 (3 C, *C*$_q$), 154.64 (3 C, *C*N), 159.39 (3 C, *C*O), 160.54 (3 C, *C*O), 164.68 (3 C, *C*O) ppm.

FT-IR ν [cm^{-1}] = 3328 (m), 3121 (m), 2392 (s), 2281 (s), 1992 (w), 1691 (s), 1561 (s), 1518 (s), 1442 (m), 1362 (m), 1258 (s), 1084 (s), 1053 (s), 990 (m), 819 (s), 777 (s).

Synthesis of the zwitterionic trisphenylbenzene core molecule 74 – methyl ester cleavage and pH 6

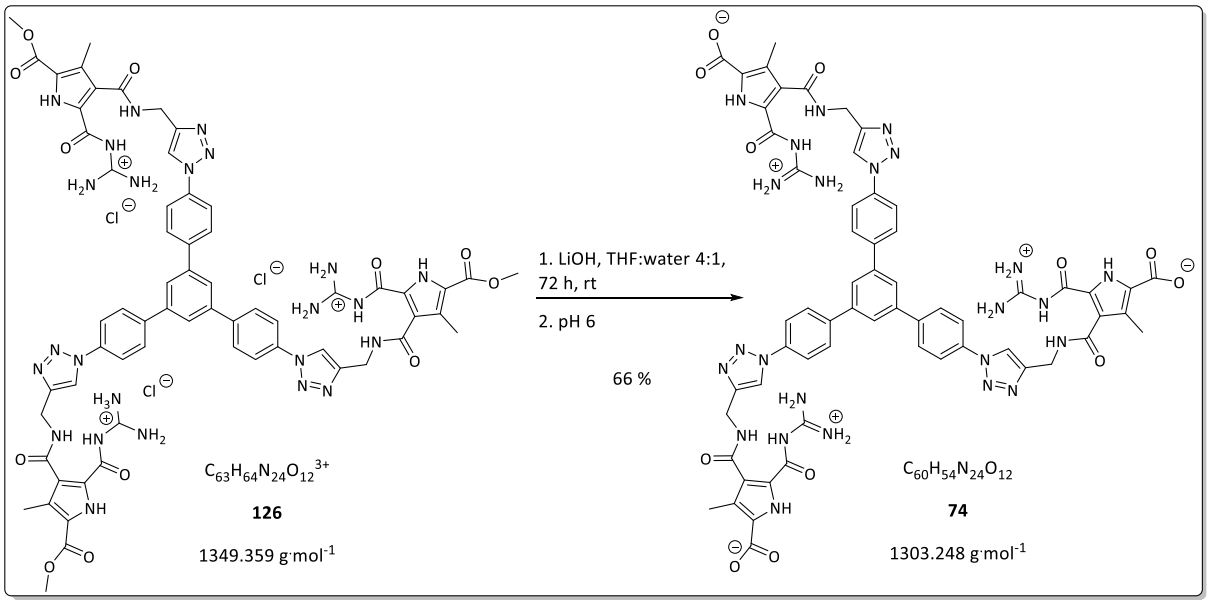

Building block **126** (53.0 mg, 36.5 µmol, 1.0 eq) was suspended in a mixture of THF and water (8 mL, 1 : 1 ratio) and lithium hydroxide ($LiOH \cdot 1H_2O$; 31.0 mg, 740.0 µmol, 20.0 eq) was added to this mixture. The resulting dark suspension was stirred for 72 hours (over the weekend) at room temperature. During the reaction the mixture turns into a solution, since the anion of building block **74** is water soluble. THF was evaporated under reduced pressure, the pH value of the aqueous solution was set to 5.8 and the resulting precipitate was filtered off (nylon membrane) and was washed with water. The zwitterionic tritopic core molecule **74** (36.0 mg, 27.6 µmol) was obtained as a black solid substance with a yield of 75 %.

Mp. [°C] no melting point measureable, no change until 410 °C (end of temperature range of the instrument)

^{1}H-NMR (300 MHz, DMSO-d_6) δ = 2.37 (s, 9 H, methyl-*CH*$_3$), 4.63 (bs, 6 H, *CH*$_2$), 8.03 – 8.17 (m, 15 H, aromatic-C*H*), 8.50 (bs, 12 H, N*H*$_2$), 8.81 (s, 3 H, C*H*), 8.93 (bs, 3 H, N*H*), 12.43 (bs, 3 H, N*H*), 12.63 (bs, 3 H, N*H*) ppm.

^{13}C-NMR (75.5 MHz, DMSO-d_6) δ = 10.85 (3 C, methyl-*C*H_3), 34.97 (3 C, *C*H_2), 120.14 (6 C, aromatic-*C*H), 121.21 (3 C, aromatic-*C*H), 123.78 (3 C, aromatic-C_q), 124.28 (3 C, *C*H), 125.05 (3 C, C_q), 125.89 (3 C, C_q), 126.46 (3 C, aromatic Cq), 128.63 (6 C, aromatic-*C*H), 136.12 (3 C, C_q), 139.83 (3 C, C_q), 140.46 (3 C, C_q), 145.71 (3 C, C_q), 154.40 (3 C, *C*N), 159.38 (3 C, *C*O), 161.55 (3 C, *C*O), 164.73 (3 C, *C*O) ppm.

MS (ESI) m/z = 652.92 $[M + 2H]^{2+}$, calculated ($C_{60}H_{56}N_{24}O_{12}$) 1304.23 $g \cdot mol^{-1}$

FT-IR v [cm^{-1}] = 3321 (m), 2774 (m), 2397 (s), 2285 (s), 2087 (w), 1590 (s), 1427 (s), 1334 (s), 1213 (s), 1096 (s), 1048 (m), 829 (m), 769 (m).

8 LITERATURE

(1) Buhleier, E.; Wehner, W.; Vogtle, F. *Synthesis* **1978**, 155.

(2) Tomalia, D. A. *Prog. Polym. Sci.* **2005**, *30*, 294.

(3) Astruc, D.; Boisselier, E.; Ornelas, C. *Chem. Rev.* **2010**, *110*, 1857.

(4) Wu, L. P.; Ficker, M.; Christensen, J. B.; Trohopoulos, P. N.; Moghimi, S. M. *Bioconjugate Chem.* **2015**, *26*, 1198.

(5) Liu, M. J.; Kono, K.; Frechet, J. M. J. *J. Control. Release* **2000**, *65*, 121.

(6) Newkome, G. R.; Yao, Z. Q.; Baker, G. R.; Gupta, V. K. *J. Org. Chem.* **1985**, *50*, 2003.

(7) Mintzer, M. A.; Grinstaff, M. W. *Chem. Soc. Rev.* **2011**, *40*, 173.

(8) Dong, R.; Zhou, Y.; Zhu, X. *Accounts of Chemical Research* **2014**, *47*, 2006.

(9) Guo, F.; Guo, Z. *RSC Advances* **2016**, *6*, 36623.

(10) Liu, R.; Fraylich, M.; Saunders, B. R. *Colloid and Polymer Science* **2009**, *287*, 627.

(11) Sun, L.; Huang, W. M.; Ding, Z.; Zhao, Y.; Wang, C. C.; Purnawali, H.; Tang, C. *Materials & Design* **2012**, *33*, 577.

(12) Song, Y. J.; Wei, W. L.; Qu, X. G. *Adv. Mater.* **2011**, *23*, 4215.

(13) Uhrich, K. E.; Cannizzaro, S. M.; Langer, R. S.; Shakesheff, K. M. *Chem. Rev.* **1999**, *99*, 3181.

(14) Fenske, T.; Korth, H. G.; Mohr, A.; Schmuck, C. *Chem.-Eur. J.* **2012**, *18*, 738.

(15) Schmuck, C. *Eur. J. Org. Chem.* **1999**, 2397.

(16) Schmuck, C. *Chem. Commun.* **1999**, 843.

(17) Schmuck, C. *Coord. Chem. Rev.* **2006**, *250*, 3053.

(18) Schmuck, C.; Wienand, W. *J. Am. Chem. Soc.* **2003**, *125*, 452.

(19) Rehm, T.; Schmuck, C. *Chem. Commun.* **2008**, 801.

(20) Schmuck, C.; Rupprecht, D. *Synthesis* **2007**, 3095.

(21) Schmuck, C.; Rupprecht, D.; Urban, C.; Walden, N. *Synthesis* **2006**, 89.

(22) Schmuck, C.; Bickert, V.; Merschky, M.; Geiger, L.; Rupprecht, D.; Dudaczek, J.; Wich, P.; Rehm, T.; Machon, U. *Eur. J. Org. Chem.* **2008**, 324.

(23) Groger, G.; Meyer-Zaika, W.; Bottcher, C.; Grohn, F.; Ruthard, C.; Schmuck, C. *J. Am. Chem. Soc.* **2011**, *133*, 8961.

(24) Merschky, M.; Wyszogrodzka, M.; Haag, R.; Schmuck, C. *Chem.-Eur. J.* **2010**, *16*, 14242.

(25) Fenske, M. T.; Meyer-Zaika, W.; Korth, H. G.; Vieker, H.; Turchanin, A.; Schmuck, C. *J. Am. Chem. Soc.* **2013**, *135*, 8342.

(26) Kamp, I. v., Universty of Duisburg-Essen, 2015.

(27) Rehm, T. H.; Schmuck, C. *Chem. Soc. Rev.* **2010**, *39*, 3597.

(28) Rehm, T. H.; Grohn, F.; Schmuck, C. *Soft Matter* **2012**, *8*, 3154.

(29) Hisamatsu, Y.; Banerjee, S.; Avinash, M. B.; Govindaraju, T.; Schmuck, C. *Angew. Chem.-Int. Edit.* **2013**, *52*, 12550.

(30) Fleischer, M.; Schmuck, C. *Chem. Commun.* **2014**, *50*, 10464.

(31) Schmuck, C.; Rehm, T.; Klein, K.; Grohn, F. *Angew. Chem.-Int. Edit.* **2007**, *46*, 1693.

(32) Rodler, F.; Linders, J.; Fenske, T.; Rehm, T.; Mayer, C.; Schmuck, C. *Angew. Chem.-Int. Edit.* **2010**, *49*, 8747.

(33) Bosman, A. W.; Janssen, H. M.; Meijer, E. W. *Chem. Rev.* **1999**, *99*, 1665.

(34) Vogtle, F.; Gestermann, S.; Hesse, R.; Schwierz, H.; Windisch, B. *Prog. Polym. Sci.* **2000**, *25*, 987.

(35) Tomalia, D. A.; Baker, H.; Dewald, J.; Hall, M.; Kallos, G.; Martin, S.; Roeck, J.; Ryder, J.; Smith, P. *Polym. J.* **1985**, *17*, 117.

(36) Grayson, S. M.; Frechet, J. M. J. *Chem. Rev.* **2001**, *101*, 3819.

(37) Vögtle F., R. G., Werner N *Dendrimer Chemistry*; WILEY-VCH: Weinheim.

(38) Vieyres, A.; Lam, T.; Gillet, R.; Franc, G.; Castonguay, A.; Kakkar, A. *Chem. Commun.* **2010**, *46*, 1875.

(39) Boris, D.; Rubinstein, M. *Macromolecules* **1996**, *29*, 7251.

(40) Tomalia, D. A.; Baker, H.; Dewald, J.; Hall, M.; Kallos, G.; Martin, S.; Roeck, J.; Ryder, J.; Smith, P. *Macromolecules* **1986**, *19*, 2466.

(41) Bock, V. D.; Hiemstra, H.; van Maarseveen, J. H. *Eur. J. Org. Chem.* **2006**, 51.

(42) Joralemon, M. J.; O'Reilly, R. K.; Matson, J. B.; Nugent, A. K.; Hawker, C. J.; Wooley, K. L. *Macromolecules* **2005**, *38*, 5436.

(43) Hawker, C. J.; Frechet, J. M. J. *J. Am. Chem. Soc.* **1990**, *112*, 7638.

(44) Jayaraman, M.; Frechet, J. M. J. *J. Am. Chem. Soc.* **1998**, *120*, 12996.

(45) Grayson, S. M.; Frechet, J. M. J. *Org. Lett.* **2002**, *4*, 3171.

(46) Hawker, C. J.; Frechet, J. M. J. *Macromolecules* **1990**, *23*, 4726.

(47) Wooley, K. L.; Hawker, C. J.; Frechet, J. M. J. *J. Chem. Soc.-Perkin Trans. 1* **1991**, 1059.

(48) Aida, T.; Meijer, E. W.; Stupp, S. I. *Science* **2012**, *335*, 813.

(49) De Greef, T. F. A.; Smulders, M. M. J.; Wolffs, M.; Schenning, A.; Sijbesma, R. P.; Meijer, E. W. *Chem. Rev.* **2009**, *109*, 5687.

(50) Wang, F.; Han, C. Y.; He, C. L.; Zhou, Q. Z.; Zhang, J. Q.; Wang, C.; Li, N.; Huang, F. H. *J. Am. Chem. Soc.* **2008**, *130*, 11254.

(51) Smith, D. K.; Hirst, A. R.; Love, C. S.; Hardy, J. G.; Brignell, S. V.; Huang, B. Q. *Prog. Polym. Sci.* **2005**, *30*, 220.

(52) Zeng, F. W.; Zimmerman, S. C.; Kolotuchin, S. V.; Reichert, D. E. C.; Ma, Y. G. *Tetrahedron* **2002**, *58*, 825.

(53) Zimmerman, S. C.; Zeng, F. W.; Reichert, D. E. C.; Kolotuchin, S. V. *Science* **1996**, *271*, 1095.

(54) Ma, Y.; Kolotuchin, S. V.; Zimmerman, S. C. *J. Am. Chem. Soc.* **2002**, *124*, 13757.

(55) Freeman, A. W.; Vreekamp, R.; Frechet, J. M. J. *Abstr. Pap. Am. Chem. Soc.* **1997**, *214*, 128.

(56) Plevoets, M.; Vogtle, F.; De Cola, L.; Balzani, V. *New J. Chem.* **1999**, *23*, 63.

(57) Yamaguchi, N.; Hamilton, L. M.; Gibson, H. W. *Angew. Chem.-Int. Edit.* **1998**, *37*, 3275.

(58) Yan, J.; Zhang, X.; Zhang, X.; Liu, K.; Li, W.; Wu, P.; Zhang, A. *Macromolecular Chemistry and Physics* **2012**, *213*, 2003.

(59) Franz, A.; Bauer, W.; Hirsch, A. *Angew. Chem.-Int. Edit.* **2005**, *44*, 1564.

(60) Grimm, F.; Hartnagel, K.; Wessendorf, F.; Hirsch, A. *Chem. Commun.* **2009**, 1331.

(61) Eckelmann, J.; Dethlefs, C.; Brammer, S.; Dogan, A.; Uphoff, A.; Luning, U. *Chem.-Eur. J.* **2012**, *18*, 8498.

(62) Martin, A. L.; Li, B.; Gillies, E. R. *J. Am. Chem. Soc.* **2009**, *131*, 734.

(63) Mammen, M.; Choi, S. K.; Whitesides, G. M. *Angew. Chem.-Int. Edit.* **1998**, *37*, 2755.

(64) Brinkmann, N.; Giebel, D.; Lohmer, G.; Reetz, M. T.; Kragl, U. *J. Catal.* **1999**, *183*, 163.

(65) Montilla, F.; del Rio, D.; Pastor, A.; Galindo, A. *Organometallics* **2006**, *25*, 4996.

(66) Li, C. F.; Li, D. X.; Zhang, Z. J.; Feng, S. Y. *Chin. Chem. Lett.* **2005**, *16*, 1389.

(67) Liu, L.; Breslow, R. *J. Am. Chem. Soc.* **2003**, *125*, 12110.

(68) Liang, C.; Frechet, J. M. J. *Prog. Polym. Sci.* **2005**, *30*, 385.

(69) Mizugaki, T.; Hetrick, C. E.; Murata, M.; Ebitani, K.; Amiridis, M. D.; Kaneda, K. *Chem. Lett.* **2005**, *34*, 420.

(70) Markham, J. P. J.; Lo, S. C.; Magennis, S. W.; Burn, P. L.; Samuel, I. D. W. *Appl. Phys. Lett.* **2002**, *80*, 2645.

(71) Chen, C. Z. S.; Beck-Tan, N. C.; Dhurjati, P.; van Dyk, T. K.; LaRossa, R. A.; Cooper, S. L. *Biomacromolecules* **2000**, *1*, 473.

(72) Calabretta, M. K.; Kumar, A.; McDermott, A. M.; Cai, C. Z. *Biomacromolecules* **2007**, *8*, 1807.

(73) O'Loughlin, J.; Millwood, I. Y.; McDonald, H. M.; Price, C. F.; Kaldor, J. M.; Paull, J. R. A. *Sex. Transm. Dis.* **2010**, *37*, 100.

(74) Mumper, R. J.; Bell, M. A.; Worthen, D. R.; Cone, R. A.; Lewis, G. R.; Paull, J. R. A.; Moench, T. R. *Drug Dev. Ind. Pharm.* **2009**, *35*, 515.

(75) Joshi, N.; Grinstaff, M. *Curr. Top. Med. Chem.* **2008**, *8*, 1225.

(76) Upadhyaya, L.; Singh, J.; Agarwal, V.; Tewari, R. P. *J. Control. Release* **2014**, *186*, 54.

(77) Chan, J. C. Y.; Burugapalli, K.; Naik, H.; Kelly, J. L.; Pandit, A. *Biomacromolecules* **2008**, *9*, 528.

(78) Wiener, E. C.; Brechbiel, M. W.; Brothers, H.; Magin, R. L.; Gansow, O. A.; Tomalia, D. A.; Lauterbur, P. C. *Magn.Reson.Med.* **1994**, *31*, 1.

(79) Rudovsky, J.; Botta, M.; Hermann, P.; Hardcastle, K. I.; Lukes, I.; Aime, S. *Bioconjugate Chem.* **2006**, *17*, 975.

(80) Nguyen, Q. T.; Olson, E. S.; Aguilera, T. A.; Jiang, T.; Scadeng, M.; Ellies, L. G.; Tsien, R. Y. *Proc. Natl. Acad. Sci. U. S. A.* **2010**, *107*, 4317.

(81) Olson, E. S.; Jiang, T.; Aguilera, T. A.; Nguyen, Q. T.; Ellies, L. G.; Scadeng, M.; Tsien, R. Y. *Proc. Natl. Acad. Sci. U. S. A.* **2010**, *107*, 4311.

(82) Hashemi, M.; Tabatabai, S. M.; Parhiz, H.; Milanizadeh, S.; Farzad, S. A.; Abnous, K.; Ramezani, M. *Mater. Sci. Eng. C-Mater. Biol. Appl.* **2016**, *61*, 791.

(83) Dehshahri, A.; Sadeghpour, H. *Colloid Surf. B-Biointerfaces* **2015**, *132*, 85.

(84) He, D. S.; Wagner, E. *Macromol. Biosci.* **2015**, *15*, 600.

(85) Khandare, J.; Calderon, M.; Dagia, N. M.; Haag, R. *Chem. Soc. Rev.* **2012**, *41*, 2824.

(86) Fang, J.; Nakamura, H.; Maeda, H. *Adv. Drug Deliv. Rev.* **2011**, *63*, 136.

(87) Papasani, M. R.; Wang, G. K.; Hill, R. A. *Nanomed.-Nanotechnol. Biol. Med.* **2012**, *8*, 804.

(88) Panyala, N. R.; Pena-Mendez, E. M.; Havel, J. *J. Appl. Biomed.* **2009**, *7*, 75.

(89) Ahmad, M. Z.; Akhter, S.; Rahman, Z.; Akhter, S.; Anwar, M.; Mallik, N.; Ahmad, F. J. *J. Pharm. Pharmacol.* **2013**, *65*, 634.

(90) Rimoli, M. G.; Rabaioli, M. R.; Melisi, D.; Curcio, A.; Mondello, S.; Mirabelli, R.; Abignente, E. *Journal of Biomedical Materials Research Part A* **2008**, *87A*, 156.

(91) Amorim, R.; Vilaça, N.; Martinho, O.; Reis, R. M.; Sardo, M.; Rocha, J.; Fonseca, A. M.; Baltazar, F.; Neves, I. C. *The Journal of Physical Chemistry C* **2012**, *116*, 25642.

(92) Mintova, S.; Jaber, M.; Valtchev, V. *Chem. Soc. Rev.* **2015**, *44*, 7207.

(93) Kordel, C.; Popeney, C. S.; Haag, R. *Chem. Commun.* **2011**, *47*, 6584.

(94) Soussan, E.; Cassel, S.; Blanzat, M.; Rico-Lattes, I. *Angew. Chem.-Int. Edit.* **2009**, *48*, 274.

(95) Higashi, S.; Setoguchi, T. *Adv. Drug Deliv. Rev.* **2000**, *45*, 57.

(96) Li, Y. L.; Maciel, D.; Rodrigues, J.; Shi, X. Y.; Tomas, H. *Chem. Rev.* **2015**, *115*, 8564.

(97) Kabanov, A. V.; Vinogradov, S. V. *Angew. Chem.-Int. Edit.* **2009**, *48*, 5418.

(98) Ma, M. F.; Xing, P. Y.; Li, S. Y.; Chu, X. X.; Wang, B.; Hao, A. Y. *Prog. Chem.* **2014**, *26*, 1317.

(99) van der Meel, R.; Fens, M.; Vader, P.; van Solinge, W. W.; Eniola-Adefeso, O.; Schiffelers, R. M. *J. Control. Release* **2014**, *195*, 72.

(100) Duncan, R. *Nat. Rev. Drug Discov.* **2003**, *2*, 347.

(101) Gillies, E. R.; Frechet, J. M. J. *Drug Discov. Today* **2005**, *10*, 35.

(102) Pourianazar, N. T.; Mutlu, P.; Gunduz, U. *J. Nanopart. Res.* **2014**, *16*, 38.

(103) Kesharwani, P.; Jain, K.; Jain, N. K. *Prog. Polym. Sci.* **2014**, *39*, 268.

(104) Frey, H.; Haag, R. *Journal of biotechnology* **2002**, *90*, 257.

(105) Kainthan, R. K.; Mugabe, C.; Burt, H. M.; Brooks, D. E. *Biomacromolecules* **2008**, *9*, 886.

(106) Jansen, J.; Debrabandervandenberg, E. M. M.; Meijer, E. W. *Science* **1994**, *266*, 1226.

(107) Jansen, J.; Meijer, E. W.; Debrabandervandenberg, E. M. M. *J. Am. Chem. Soc.* **1995**, *117*, 4417.

(108) Beezer, A. E.; King, A. S. H.; Martin, I. K.; Mitchell, J. C.; Twyman, L. J.; Wain, C. F. *Tetrahedron* **2003**, *59*, 3873.

(109) Morgan, M. T.; Carnahan, M. A.; Immoos, C. E.; Ribeiro, A. A.; Finkelstein, S.; Lee, S. J.; Grinstaff, M. W. *J. Am. Chem. Soc.* **2003**, *125*, 15485.

(110) Jansen, J.; Meijer, E. W.; deBrabandervandenBerg, E. M. M. *Macromol. Symp.* **1996**, *102*, 27.

(111) Baars, M.; Kleppinger, R.; Koch, M. H. J.; Yeu, S. L.; Meijer, E. W. *Angew. Chem.-Int. Edit.* **2000**, *39*, 1285.

(112) Wyszogrodzka, M.; Haag, R. *Chem.-Eur. J.* **2008**, *14*, 9202.

(113) Gupta, U.; Agashe, H. B.; Asthana, A.; Jain, N. K. *Biomacromolecules* **2006**, *7*, 649.

(114) Morgan, M. T.; Nakanishi, Y.; Kroll, D. J.; Griset, A. P.; Carnahan, M. A.; Wathier, M.; Oberlies, N. H.; Manikumar, G.; Wani, M. C.; Grinstaff, M. W. *Cancer Res.* **2006**, *66*, 11913.

(115) Ooya, T.; Lee, J.; Park, K. *Bioconjugate Chem.* **2004**, *15*, 1221.

(116) Ooya, T.; Lee, J.; Park, K. *J. Control. Release* **2003**, *93*, 121.

(117) Wyszogrodzka, M.; Mows, K.; Kamlage, S.; Wodzifiska, J.; Plietker, B.; Haag, R. *Eur. J. Org. Chem.* **2008**, 53.

(118) Wyszogrodzka, M.; Möws, K.; Kamlage, S.; Wodzińska, J.; Plietker, B.; Haag, R. *Eur. J. Org. Chem.* **2008**, *2008*, 53.

(119) Barraza, L. F.; Jimenez, V. A.; Alderete, J. B. *Macromolecular Chemistry and Physics* **2016**, *217*, 605.

(120) Wang, H.; Huang, Q.; Chang, H.; Xiao, J. R.; Cheng, Y. Y. *Biomater. Sci.* **2016**, *4*, 375.

(121) Calderón, M.; Quadir, M. A.; Strumia, M.; Haag, R. *Biochimie* **2010**, *92*, 1242.

(122) Thota, B. N. S.; Urner, L. H.; Haag, R. *Chem. Rev.* **2016**, *116*, 2079.

(123) Liu, G.; Zhang, G.; Hu, J.; Wang, X.; Zhu, M.; Liu, S. *J. Am. Chem. Soc.* **2015**, *137*, 11645.

(124) Haag, R. *Angew. Chem.-Int. Edit.* **2004**, *43*, 278.

(125) Calderon, M.; Quadir, M. A.; Sharma, S. K.; Haag, R. *Adv. Mater.* **2010**, *22*, 190.

(126) Xu, S. J.; Luo, Y.; Graeser, R.; Warnecke, A.; Kratz, F.; Hauff, P.; Licha, K.; Haag, R. *Bioorg. Med. Chem. Lett.* **2009**, *19*, 1030.

(127) Grayson, S. M.; Jayaraman, M.; Frechet, J. M. J. *Chem. Commun.* **1999**, 1329.

(128) Merschky, M., University of Duisburg-Essen, **2010**.

(129) Walden, N., Bayerische Julius-Maximilians-Universität Würzburg 2009.

(130) Cohen, Y.; Avram, L.; Frish, L. *Angew. Chem.-Int. Edit.* **2005**, *44*, 520.

(131) Prokop, A.; Riepl, H.; Wieder, T.; Google Patents: **2004**.

(132) Greenspan, P.; Fowler, S. D. *Journal of Lipid Research* **1985**, *26*, 781.

9 ABBREVIATIONS

AFM	Atomic force microscopy
AIBN	Azo-bis-(isobutyronitrile)
°C	Degree centigrade
$CDCl_3$	Chloroform-d
Cl-HOBt	6-Chloro-1-hydroxybenzotriazole
d	Duplett
DCM	Dichlormethane
DIC	*N,N'*-Diisopropylcarbodiimide
DIPEA	Diisopropylethylamine
DLS	Dynamic light scattering
DMAP	Dimethylaminopyridine
DMF	Dimethylformamide
DMSO	Dimethyl sulfoxide
DOSY	Diffusion-ordered spectroscopy
eq	Equivalent(s)
ESI	Electrospray-Ionization
g	Gram
[G*n*]	Dendron of n^{th} generation
HCl	Hydrochloric acid
HPLC	High pressure liquid chromatography
Hz	Hertz
IR	Infrared
m	Multiplett (NMR); Medium (IR)
MDC	Methallyl dichloride

mg	Milligram
mL	Milliliter
mM	Millimolar
mmol	Millimole
MPLC	Medium pressure liquid chromatography
NaOH	Sodium hydroxide
NBS	*N*-Bromosuccinimide
nm	Nanometer
NMM	*N*-Methylmorpholine
NMR	Nuclear magnetic resonance
NR	Nile red
R_f	Retention factor
rt	Room temperature
PyBOP	Benzotriazol-1-yl-oxytripyrrolidinophosphonium-
q	Quartett
s	Singulett (NMR); strong (IR)
t	Triplett
TEM	Transmission electron microscopy
TFA	Trifluoroacetic acid
THF	Tetrahydrofuran
UV	Ultra violet light
Vis	Visible light
w	weak
µL	Microliter